Geology and Geochemistry of Sedimentary Ferromanganese Ore Deposits,

Woodstock, New Brunswick, Canada

by

Bryan C. Way

B.A. University of Maine at Farmington, 2007

A Thesis submitted in Partial Fulfillment of the Requirements for the Degree of

Master of Science

in the Graduate Academic Unit of Earth Sciences

Supervisors: David R. Lentz, Ph D., Department of Earth Sciences

David G. Keighley, Ph D., Department of Earth Sciences

Examining Board: David R. Lentz, Ph D., Department of Earth Sciences
David G. Keighley, Ph D., Department of Earth Sciences
Les Fyffe, MSc., NB Geological Surveys Branch
Graham Forbes, Department of Forestry and Environmental
Management PhD

This thesis, dissertation or report is accepted by the
Dean of Graduate Studies

THE UNIVERSITY OF NEW BRUNSWICK

October, 2012

ABSTRACT

The Early-Silurian Woodstock Fe-Mn Deposits are a series of six, northeast-trending, low grade manganiferous-iron deposits in western New Brunswick that collectively represent the largest Mn resource in North America (194,000,000 tonnes; 13% Fe and 9% Mn). Recent expansion of Route 95 has allowed a more detailed local stratigraphy, mineralogy, and geochemistry of the Fe-Mn deposits within the context of the regional stratigraphy to ascertain the genesis of these deposits. Geological mapping during the field seasons of 2008 and 2009 has revealed six Lithofacies Associations (O, I, II, III, IV, V) within the area, that, generally, are lying conformably on top of each other. However complications due to folding and interbedding have resulting in juxtaposition of the lithofacies associations so they are not always in stratigraphic order. These lithofacies associations are composed of a turbidite-rich section of blue grey calcareous sandstone (O) overlain by black pyritic mudstone (I), associated mineralized and nonmineralized green (II) and red siltstone (III), and laminated to massive grey green calcareous sandstone (IV and V).

Na/Mg ratios, chondrite-normalized REE patterns, and mineralogical evidence of rapid changes in ocean redox conditions suggest the Fe-Mn mineralized lithofacies were formed in the offshore zone of a continental shelf on a stable cratonic margin. Al-Fe-Mn ternary and SiO_2/Al_2O_3 binary plots developed from archived drill core data indicate the Fe-Mn mineralization was initially derived from hydrogenous-detrital sources without any indication of a hydrothermal input as a source of Fe and Mn.

TABLE OF CONTENTS

LIST OF EQUATIONS

CHAPTER 1

INTRODUCTION AND HISTORY OF THE WOODSTOCK FE-MN DEPOSITS

1.1   GENERAL STATEMENT

The Woodstock iron-manganese (Fe-Mn) deposits are a series of near

vertically dipping, Lower Silurian sedimentary manganiferous iron deposits that are

located west of the town of Woodstock, in western New Brunswick, Canada (Fig.

1.1). These deposits represent the largest Mn resource in North America

(194,000,000 tonnes; 13% Fe and 9% Mn) and consist of six major ore bodies

(Sidwell, 1957; Potter, 1983; DesRoches, 2004) several of which were mined from

1848 to 1884, principally to produce iron-armour plating on British naval frigates

(Sidwell, 1964; Potter, 1983).

1.2   PURPOSE OF STUDY AND METHODS

The purpose of this study was to describe the detailed mineralogy and

geochemistry of the Fe-Mn deposits within the context of the regional stratigraphy

to ascertain the formation conditions of these deposits. At the time of this study the

primary concern was to determine the formation conditions of these deposits so as

to aid in exploration and location of similar Fe-Mn deposits that might have

economic potential.

In the Woodstock area there has been geological mapping ever since 1836

by government based geological surveys and private exploration companies.

However, within the Route 95 study area there were only 7 out of the 16 mapped
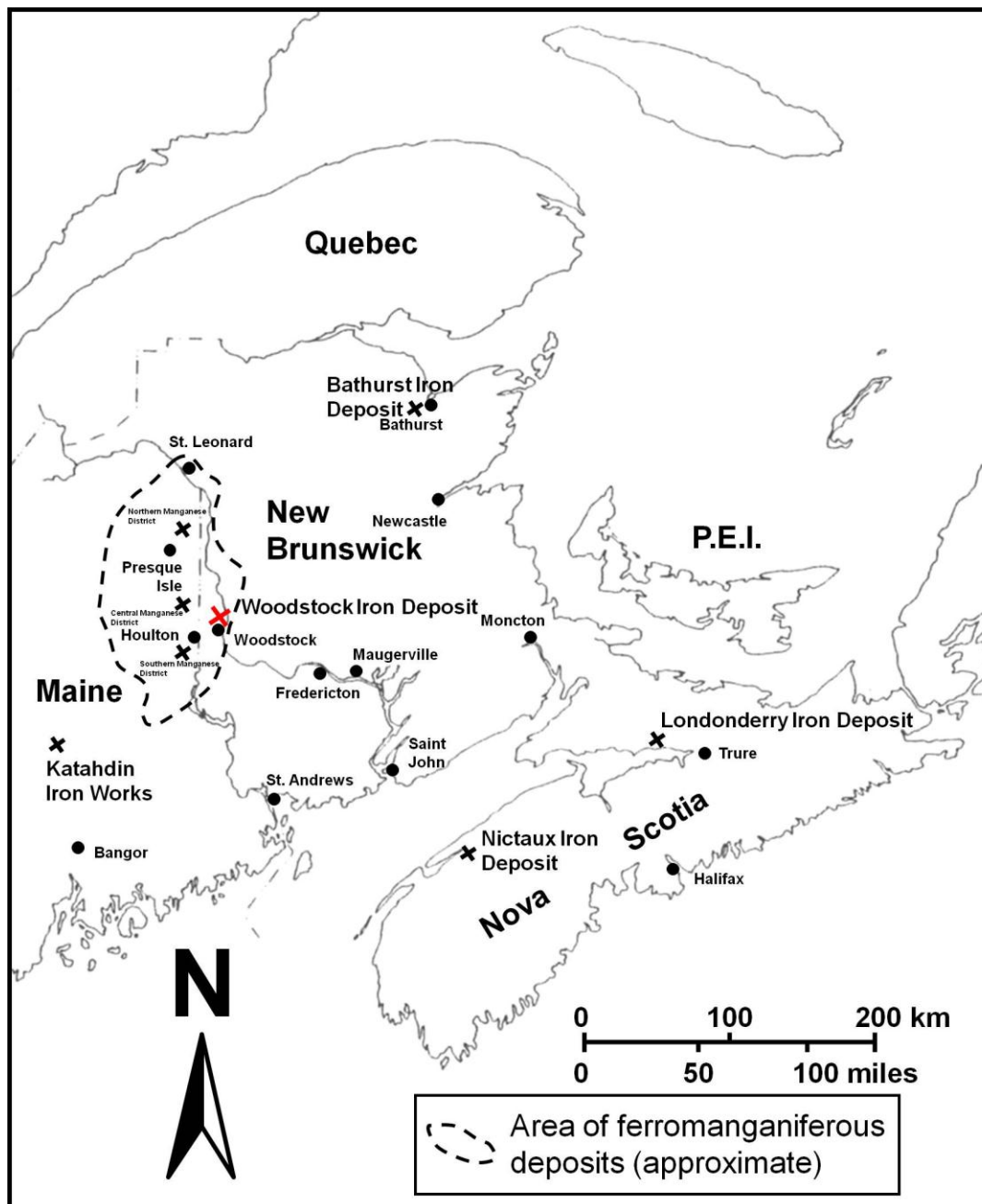
Fig. 1.1: Regional map of the Maritimes showing the location and regional extent of the ferromanganiferous deposits in western New Brunswick and Maine, USA. The x's on the map indicate known iron deposits (modified from Potter, 1983).

sites were visible as outcrops prior to this study. Most of these previous sites were small (< 30 m in length), irregularly spaced, and offered very little exposure of bedrock in the area. This left a majority of the local stratigraphy and mineralogy unexposed, except in drill core, so generalized and up to interpretation. The local stratigraphy of the area was also very incomplete, and often entire lithofacies associations were absent from exposed bedrock. Currently, there has been no definitive study on the genesis of the Woodstock Fe-Mn deposits in the context of the regional stratigraphy. In particular, how these deposits formed and where the Fe and Mn within the deposits originated from, which was done by assessing the mineralogy and archived geochemical data.

Recent expansion of NB Route 95 from Woodstock, New Brunswick, to Houlton, Maine, USA, has led to new road cuts exposing outcrop nearly perpendicular to the general northeast strike of the bedrock. These new exposures have presented an opportunity to further study the stratigraphic and petrologic relationships of the Fe-Mn mineralized zones and surrounding sedimentary rocks within the Woodstock area. Together with a re-examination of the archived drill core, and lithogeochemical data from the Plymouth deposit, the new stratigraphic and petrological data and context is used here to reassess the origin of the Fe-Mn deposits in the Woodstock area.

Within the study area on Route 95 and surrounding area each outcrop was mapped by recording the strike and dip orientation using a geological compass and a GPS to determine the global position (located on a georeferenced map) of each measurement. There were a total of 82 samples that were taken from outcrops.

3

Some of the samples were selected from each of the observed facies as an overall representative sample. Others were taken along the contacts of the facies to aid in determining sedimentological and mineralogical differences between facies along the contacts. Each of the 82 samples were then cut by a diamond saw and made into polished rock slabs. Sections of each of these samples were also made into polished thin sections for detailed optical microscopy using a petrographic microscope to determine the mineralogy of rock. Some of the samples were followed up with UNB's JEOL733 Scanning Electron Microscopy (SEM) for imagining by Backscatter Electron (SEM-BSE) contrast imaging and Energy Dispersive Spectrometry (SEM-EDS) study of the complex mineralogy. Powder X-Ray Diffractometry (XRD) (UNB's D8 Advance) was also done to analyze the mineralogy in detail, especially on the complex Fe-Mn mineral-rich beds. There were also 196 geochemical data samples archived from the Roberts and Prince (1990) exploration project used in this study to determine geochemistry of several of the facies. These samples were taken from four drill holes and two trenches and analyzed for major oxides, trace elements, and rare earth elements (see Roberts and Prince, 1990 for analytical details) that will be described later in Chapter 5.

1.3   LOCATION AND ACCESS

The Woodstock Fe-Mn deposits are located approximately 7.2 km (4.5 miles) northwest of Woodstock, between the towns of Jacksontown and Plymouth (Fig. 1.2). Minor Fe-Mn occurrences are also found within the strata southwest of Plymouth, as far south as Union Corner (Sidwell, 1954). Similar Fe-Mn deposits
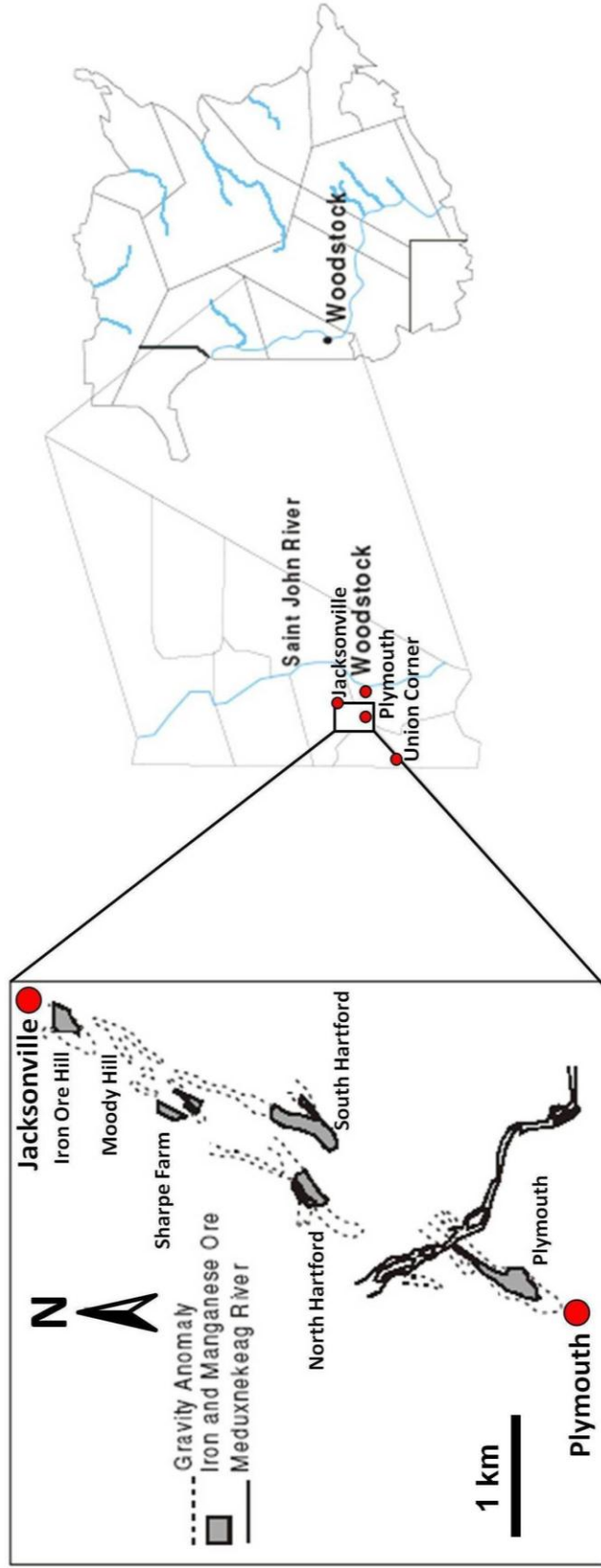
Fig. 1.2: General location map displaying the known iron-manganese deposits in western New Brunswick associated with the Woodstock Fe-Mn Deposits (modified from DesRoches, 2004).

occur across the US border in Aroostook County, Maine, hosted in Silurian metasedimentary rocks (White, 1943).

1.4 HISTORY OF THE WOODSTOCK FE-MN DEPOSITS

The Woodstock Fe-Mn deposits have a history that first dates back to the early nineteenth century. Since their discovery by early settlers in the 1820's Woodstock Fe-Mn deposits have been sporadically explored over the past 190 years with much of the exploration of these deposits has been governed by the economics at the time. The first detailed account of the iron formations in the Woodstock area of New Brunswick was written by Professor Charles T. Jackson of Boston, Massachusetts, in 1836, and commissioned by the Maine Geological Survey. The deposits were described by Jackson (1837) as dense rocks with a blocky cleavage and composed primarily of red hematite (Fe_2O_3) with a surface crust of manganese oxide covering the iron-ore beds. The beds were reported in the original write-up as having a thickness of almost 274.3 m (900 ft) and unknown in length, with the greatest thickness of the beds and accessibility in Jacksontown, near Jacksonville, NB (Jackson, 1837). Over the next twelve years, the Iron Ore Hill and Moody Hill deposits were mapped out and assayed for major elements by wet chemical analysis by the York and Carleton Mining Company (Fig 1.2; Table 1.1). Several smaller unmarked deposits northeast of the Meduxnekeag River were also identified. The Jacksonville mines (notably at Iron Ore Hill and Moody Hill) opened in 1848, and employed approximately 40 men to quarry the iron ore. The ore was then transported approximately 5 km southeast to a blast furnace by ten to twelve pairs of horses with wagons and sleds (Gardiner, 2003; Fig. 1.3). The first blast furnace

6

Silica	Carbonate of Lime	Alumina	Peroxide of iron	Oxide of Manganese	Water
17.80 %	4.00%	2.16%	52.50%	18.90%	5.70%

Modern Chemical formula

SiO_2	$CaCO_3$	Al_2O_3	Fe_2O_3	MnO	H_2O
17.80 %	4.00%	2.16%	52.50%	18.90%	5.70%

Table 1.1: Initial major oxide contents from the Fe-Mn deposits near Woodstock from the early 19th century.

Fig. 1.3: Remains of one of the ore wagons (circa 1848 – 1864) in one of the pits at Iron Ore Hill, Jacksonville, New Brunswick.

was also built in 1848, with the capacity of 7 tonnes per day of raw ore, on the west side of the St. John River near Sheriff's Hill (Sidwell, 1964; Potter, 1983). The exact location of Sheriff's Hill has not been located.

Early problems resulted in the furnace being rebuilt in 1849. The newer 1849 design consisted of a circular hearth producing a more even heating that in turn produced a more consistent quality of pig iron (Gardiner, 2003). Around this time the Katahdin Ironworks in north central Maine was also established west of the Woodstock Fe-Mn deposits (Fig. 1.1). Initial results stated that the iron from Iron Ore Hill and Moody Hill was of excellent quality (Gardiner, 2003). High amounts of manganese within the iron ore combined with excess sulfur during smelting to produce a quality of iron that was fibrous, silver grey in colour, high density, extremely hard (a similar ring to steel when struck), but not brittle like cast iron, and had a tensile strength of 24.80 tonnes per square inch (Hind, 1865; Sidwell, 1964; Potter, 1983). However, elevated amounts of phosphorus, often an undesirable impurity that can lead to hard brittle steel if present in large amounts, were also noted (Marmontov et al., 1969; Potter, 1983; Carr, 1994).

In December of 1853, the Carleton Sentinel (Gardiner, 2003) depicted a written schematic of the blast furnace built by the Woodstock Iron and Charcoal Company and the process involved in preparing the iron ore for smelting that was later described by Ells (1876). Once the iron ore was brought from the Jacksonville mines to the smelting facility, it was first stacked on skids with alternating layers of wood or charcoal and iron ore to allow air flow so the ore could be roasted and then broken into pieces suitable for the blast furnace (Fig. 1.4). Ells (1876) described the

8
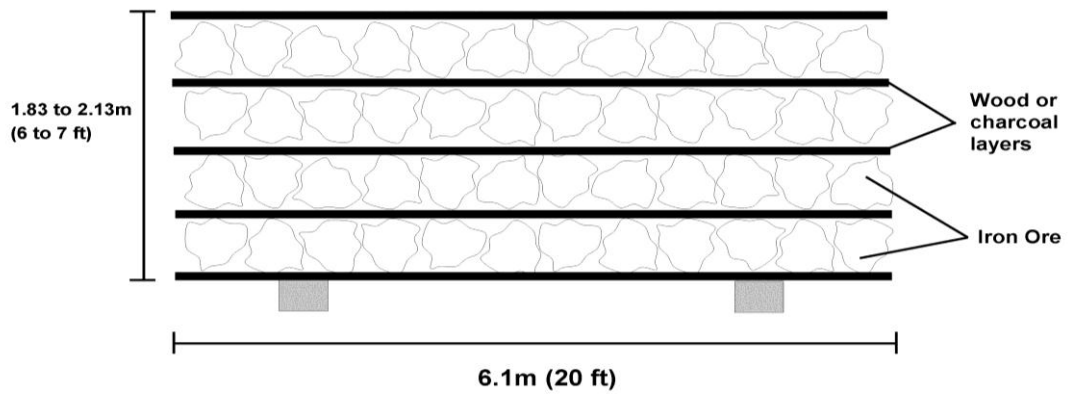
Fig. 1.4: Palettes for roasting Fe ore from Jacksontown (ca. 1853) in preparation for blast furnace (modified from Ells, 1876).

blast furnaces (Fig. 1.5) and charcoal kilns (Fig. 1.6) in further detail, as well as the costs, at that time, of producing both the iron and charcoal:

 "The first furnace erected was thirty-seven feet high and thirty-three feet square at its base, having three twyer arches, built of Gulquac sandstone with Stourbridge lining. The size of the crucible was three feet six inches by four feet, and six feet high; boshes, and the twyers were two feet above the bottom of the crucible. The capacity of this furnace was seven tons per day. Later a smaller one was built, enclosed in boiler plate, having a circumference of forty feet, and a capacity of five and a half tons per day. This is lined with Stourbridge bricks. There were two high-pressure engines, with cylinders sixteen inches in diameter and four feet stroke, of twenty-six nominal horsepower; two blowing cylinders, six feet by five, with an air receiver, twenty-eight feet by four feet ten inches. Steam was generated in five boilers, twenty-eight feet in length by three feet three inches in diameter, and was maintained by the waste gas from the head of the furnace. The fuel used was chiefly hardwood charcoal, from maple, birch and beech, yielding at the kilns, forty-five bushels of charcoal to the cord of wood."

"The cost of the wood at the kilns is about $2 or $2.50 per cord. There were ten charcoal kilns, with an average capacity of seventy-five cords of wood, and a production of 2,800 to 3,200 bushels of coal. The quantity of ore used was, on an average, three tons to the ton of pig, and the cost at the furnace $1.20 per ton. One hundred and twenty-six bushels of charcoal were required per ton, at a cost of seven cents per bushel, and the cost of pig produced was $20 to $22 per ton. Much delay and expense has occurred by the frequent stoppage of the furnace for repairs, which
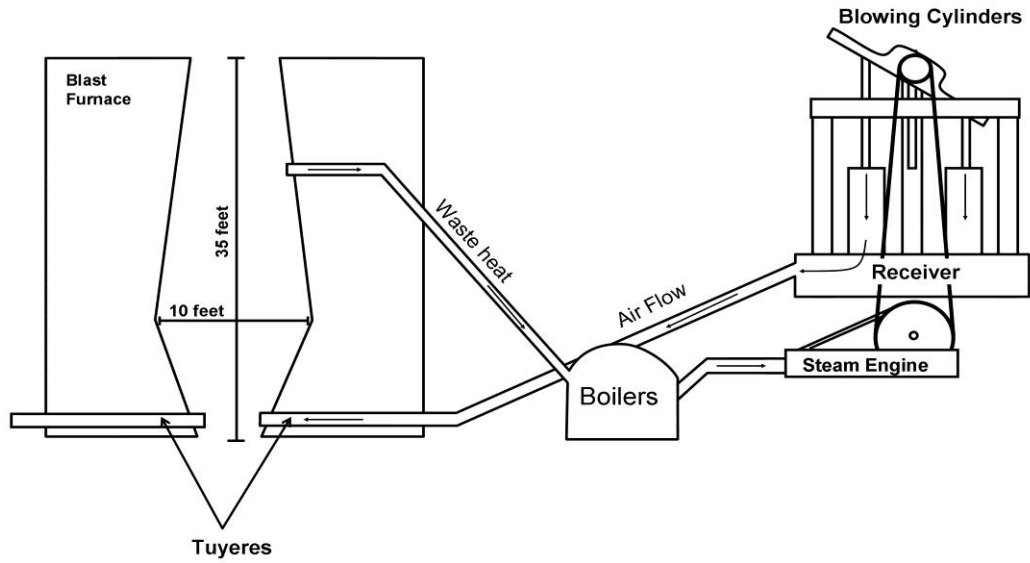
Fig. 1.5: Layout of the Woodstock iron blast furnace (ca. 1853) (modified from Ells, 1876).

Fig. 1.6: Brick laid beehive charcoal kilns near the Katahdin Ironworks (ca.1843 to 1890) similar to the design and layout of the ones used for the Woodstock Charcoal and Iron Company (ca. 1848 to 1889) (Maine Geological Survey, 2005).

were deemed necessary every four or five months, keeping the furnace idle about two months in the year."

The manager of the Woodstock Charcoal and Iron Company, Mr. Norris Best, described that each charge for the blast furnace was 612 kg of iron ore, 32 kg of limestone, and 317.5 kg (700 lb (20 bushels)) of charcoal (Bailey, 1864; Sidwell, 1964; Potter, 1983). The limestone was initially mined 11 kilometres to the northeast on the Becaguimec River and later from Sheriff's Hill approximately 600 yards from the blast furnace. The charcoal was produced in 10 kilns with four of the beehive kilns set onsite near the blast furnace (Fig. 1.6); the wood was harvested locally from maple, beech, and birch trees (Ells, 1876). Approximately 25 to 50 men were employed at the first blast furnace.

By 1853 the iron production at the Woodstock Charcoal and Iron Company smelter was already directed towards producing armoured plating on British navy ships. During testing by the British Admiralty in Shoeburyness, England, 230-lb shot from an Armstrong gun shattered every iron plate tested, except for a triple plate produced from Woodstock iron. The plates themselves were seen to have indented slightly during the test, but were not pierced and therefore received immediate interest. Accordingly, several Royal Navy ships were plated in Woodstock Iron (Bailey, 1864, 1898; Sidwell, 1964; Potter, 1983). Annual capacity was enough to plate two British naval frigates (approximately 2150 tonnes). Although the mines at Iron Ore Hill and Moody Hill shut down in 1864, production continued sporadically until 1884. Constant production was often impossible because of fires and quality control. The high phosphorus content of the iron ore,

limited extent of the deposits and hardwood for charcoal, and high transportation costs eventually made the deposits uneconomic to mine and smelter. It was also at this time that the massive banded iron formations (BIFs) were discovered in Ontario near Lake Superior.

In total, approximately 70,000 tonnes of ore were mined and smelted from the Iron Ore Hill and Moody Hill deposits (Sidwell, 1964; Anderson, 1968; Potter, 1983). The smelting facility was torn down on June 10th, 1889 and the brick was used for future buildings in the town of Woodstock (Gardiner, 2003).

Subsequently, the Woodstock Fe-Mn deposits were often ignored as a source of Fe as it seemed to be an unprofitable endeavour and a thing of the past, as explained by Bailey (1898). However he suggested that the Woodstock Fe-Mn deposits might be profitable in future years if more cost effective methods of smelting were to be adopted.

World War II depleted much of the world of its supply of metal and revived a lot of interest in mineral resources that had proven to be profitable in the past. Many mineral localities including the Woodstock Fe-Mn deposits were kept confidential by exploration and mining companies because they had the potential of providing large quantities of metals. In 1943 Noranda Mines Limited re-evaluated the Woodstock Fe-Mn deposits as a potential resource of manganese and attempted to extract iron-manganese concentrates by floatation methods. In 1951, commissioned by Fundy Bay Copper Mines Limited, a confidential survey of the area was undertaken by F.D. Anderson and John G. McCombe who re-mapped Iron Ore Hill and Moody Hill and discovered the North Hartford and South Hartford

deposits. Seventeen samples were analyzed, with assays ranging from 11.31% to 33.73% Fe and 7.50% to 19% Mn (McCombe, 1952; Anderson, 1968). Due to the importance of the metal in steel production and the lack of any domestic production of manganese, the property containing the Fe-Mn deposits was obtained by the New Brunswick Resources Development Board in 1952 (Potter, 1983; Roberts and Prince, 1990).

In 1953 the area was staked by Stratmat Limited, totalling 77 claims and approximately 760 acres, in attempts to determine remaining extent, grade, and tonnage (Sidwell, 1957; Atkinson, 1960; Potter, 1983). John G. McCombe's request for further work of the Moody Hill and Iron Ore Hill deposits resulted in gravimetric surveys and diamond drilling to be done on areas surrounding the known Fe-Mn deposits by National Management Limited in 1954 (Sidwell, 1954). Several gravimetric anomalies were drilled by Stratmat Limited that confirmed four new Fe-Mn deposits that were named Plymouth, North Hartford, South Hartford, and Sharpe Farm (Sidwell, 1954, 1957, 1964; Potter, 1983; Roberts and Prince, 1990; DesRoches, 2004). Fifty-four diamond drill holes (DDHs) were sunk, totalling 10,369.6 m (34,021 ft), within the anomalies. Most of the attention was directed towards a gravimetric anomaly just south of the Meduxnekeag River near Plymouth (Sidwell, 1957; Roberts and Prince, 1990) with 34 DDHs located at 42.7 m centres (140 feet) and spaced out every 122 m (400 feet) along the strike of the deposit. A second set of DDHs were set midway in between the 122 m (400 foot) intervals with centres of 85.3 m (280 feet). Many of the DDHs were drilled to a depth of 122 m (400 feet) at 45° inclination, but there were also a few shallow

vertical DDHs, two 30° DDHs, and two 60° DDHs (with a maximum depth of 267 m (876 ft) totalling 5300 m (17,388 ft) of drilling (Sidwell, 1957; Roberts and Prince, 1990). This drilling program determined that the six ore bodies were stratigraphically separate units and that there were two major ore assemblages associated with the Woodstock Fe-Mn deposits, namely a Fe-Mn oxide facies and a Fe-Mn carbonate facies. The Woodstock Fe-Mn deposits were determined to be approximately 194,000,000 tonnes with an average grade of 13% Fe and 9% Mn (Sidwell, 1957; Roberts and Prince, 1990).

Samples of the ore were shipped from the Plymouth deposit by truck to Woodstock where the grade was improved by sink-float methods. The sink product was then shipped by rail to Niagara Falls, Ontario, where it was subject to pyrometallurgical processes (the Udy process within an electric-arc furnace) to separate out metallic iron and ferromanganese by differential reduction (Zyryanov, 1960). However, these methods were found not to be cost effective.

Exploration for Fe-Mn deposits within the Woodstock area continued into the mid-1960's and included further mapping and tonnage/grade calculations of the deposits and layouts for potential open-pit mines. However, rising energy costs prevented mining operations from taking place (Potter, 1983). Much of the information about the drill cores surrounding and within the Fe-Mn ore bodies was kept confidential by the exploration companies during this time and much of the information regarding the drill core data from the 1950's and 1960's has apparently been lost.

Geologic mapping resumed in the Woodstock area, primarily by F. D. Anderson in 1968, and T. Hamilton-Smith in 1972. In 1969, John Wark of the Mandate Refining Limited looked at a more cost-effective method of separating the iron and manganese by co-roasting the Woodstock Fe-Mn ore with waste pyrite tailings from base-metal mines (particularly from Heath Steele Mines Limited in northern New Brunswick). The process produced soluble iron and manganese sulfates and remaining base-metals were retrieved by electrolysis. Unfortunately, metallurgical problems arose during the process and the project and the claims were abandoned in the early 1970's (Wark, 1970; Potter, 1983; Roberts and Prince, 1990).

From 1976 to 1980, Minuvar Limited held claims over the Woodstock area and completed geological and geophysical work on the Fe-Mn deposits. In 1984, Maritime Resource Research Limited (which later became GEODAT), headed by G.C. Roberts, staked 57 claims over the extent of the Woodstock Fe-Mn deposits and in the following year performed a geological survey of the Plymouth deposit. The Plymouth deposit is the largest Fe-Mn deposit of the six deposits that form the Woodstock Fe-Mn deposits. A preliminary geologic map of the Plymouth deposit was constructed and one drillhole was drilled at this site to a depth of 108.8 m (357 feet). Also in 1985, Tim Webb and Don Barnett of the New Brunswick Department of Natural Resources collected samples from the Plymouth Fe-Mn deposit and performed some mineralogical work on the deposit. The following year, Atlantic Analytical Services and the Research and Productivity Council (R.P.C.) collected samples from the Plymouth and South Hartford deposits for mineralogy and grade

determination of the deposits. Then, in 1987, Maritime Resource Research Limited

(MRR) undertook an extensive mapping and sampling program for the Plymouth

deposit. This included a Proton Ground Magnetometer Survey over the initial 1954

gravimetric anomaly that was successful in outlining the extent of the Plymouth

deposit. In addition, two trenches were made perpendicular to the strike

approximately 152 m (500 ft) long and placed 164 m (540 ft) apart. In order to

produce a cross-section of the deposit and to re-examine the grade and potential

tonnage, MRR drilled four successful drillholes within the trenches (two drill holes

per trench) to a maximum depth of 190m (622 feet) and a total of 196 analytical

samples were taken and analyzed for bulk composition and rare earth elements

(REEs). The four drill holes intersected almost continuous low-grade Fe-Mn

mineralization in the thickest section of the Plymouth Fe-Mn deposit. Large 68.04

kg (150 lb) samples were also taken every 20 feet (6.1 m) within the trenches for

additional metallurgical analysis. Tonnage and grade estimates of the Plymouth Fe-

Mn deposit were also recalculated by the aid of bulk sampling, drill cores, and

geochemical data (Roberts and Prince, 1990). These analyses done by Roberts and

Prince (1990) are the only geochemical data used in this thesis and will be

discussed in greater detail in chapters 5 and 6.

The Roberts and Prince (1990) study on the Plymouth Fe-Mn deposit was

until very recently the last exploration project associated with the Woodstock Fe-

Mn deposits. The New Brunswick Department of Natural Resources has continued

geologic mapping the Woodstock area and produced new compilation maps

displaying the extent of the bedrock units in the Woodstock area (Smith and Fyffe,

2006). Then in August of 2010 the mineral claims of the Plymouth, North Hartford, and South Hartford deposits in conjunction with several properties southwest of Woodstock were acquired by Buchans Minerals Corporation. In the summer of 2011, Buchans Minerals Corporation initiated and undertook a five drillhole project on the Plymouth deposit. The scope of this project was to recreate the drilling program performed by Roberts and Prince (1990) and use the 2011 drill holes (with the aid of the 1987 drill holes) to produce a NI-43-101 compliant resource report for the Plymouth deposit. The author of this thesis was fortunate enough to partake in the drilling and core logging of the 2011 Plymouth Fe-Mn exploration program. Globex Minerals has acquired the claims on the Moody Hill and Iron Ore Hill and drilled three drill holes within the area during the summer of 2011. One of the drill holes was set in an area near Irish Settlement whereas the second and third drill holes were set into different areas of Iron Ore Hill. Further work involving an in-house economic model for hydrometallurgical leaching has been completed in May of 2012 for the Plymouth deposit by Buchans Minerals Corporation.

Each chapter in this thesis is designed to look at each of the various aspects of the Woodstock Fe-Mn deposits in context with the regional stratigraphy. The deposits are first looked at in relation to the regional stratigraphy. The local stratigraphic context of the deposits is then assessed by use of stratigraphic logs constructed by the author. Then the Fe-Mn deposits themselves are observed in a petrographic context, assessing the mineralogical aspects of deposits and further subdividing the deposits into their Fe-Mn mineralized units. The geochemistry of one of the Woodstock Fe-Mn deposits (Plymouth) is looked at in detail to assess the

geochemical similarities and differences between the lithofacies associations in the

local stratigraphy. The geochemical data of the Plymouth deposit is then looked at

further through use of geochemical discrimination diagrams to identify the likely

origin for the Woodstock Fe-Mn deposits.

GEOLOGY OF WOODSTOCK, NB AND ASSOCIATED FE-MN STRATA

2.1   STUDY AREA

The area of study lies along Route 95 from the Woodstock, New

Brunswick/Houlton, Maine border crossing station to Woodstock, New Brunswick

in York County in west-central New Brunswick (Fig. 2.1). Each of the Woodstock

Fe-Mn deposits lie just west of the Saint John River (Fig. 2.2). The Woodstock Fe-

Mn mineralized zones are hosted in Lower Silurian strata of the Perham Group that

form part of the Matapedia-Aroostook Belt in western New Brunswick and

northeastern Maine (Fig. 2.1). This chapter presents the regional and local geology

of the area that has been compiled from previous research and current research by

the author.

2.2   REGIONAL STRATIGRAPHY

2.2.1   GENERAL

The stratigraphy of the Woodstock area (Fig. 2.2) consists predominantly of

deformed quartzite, quartz wacke, and silty shale of the Cambrian to Ordovician

Woodstock Group that are intruded by the Ordovician Gibson Granodiorite and

Benton Granite. The Woodstock Group is disconformably overlain by the Meductic

Group that comprises Lower Ordovician felsic and mafic volcanic and

volcaniclastic rocks exposed east of the Woodstock Fault (van Staal, and Fyffe,

1991; Fyffe, 2001). Only part of the volcanic succession of the Meductic Group is
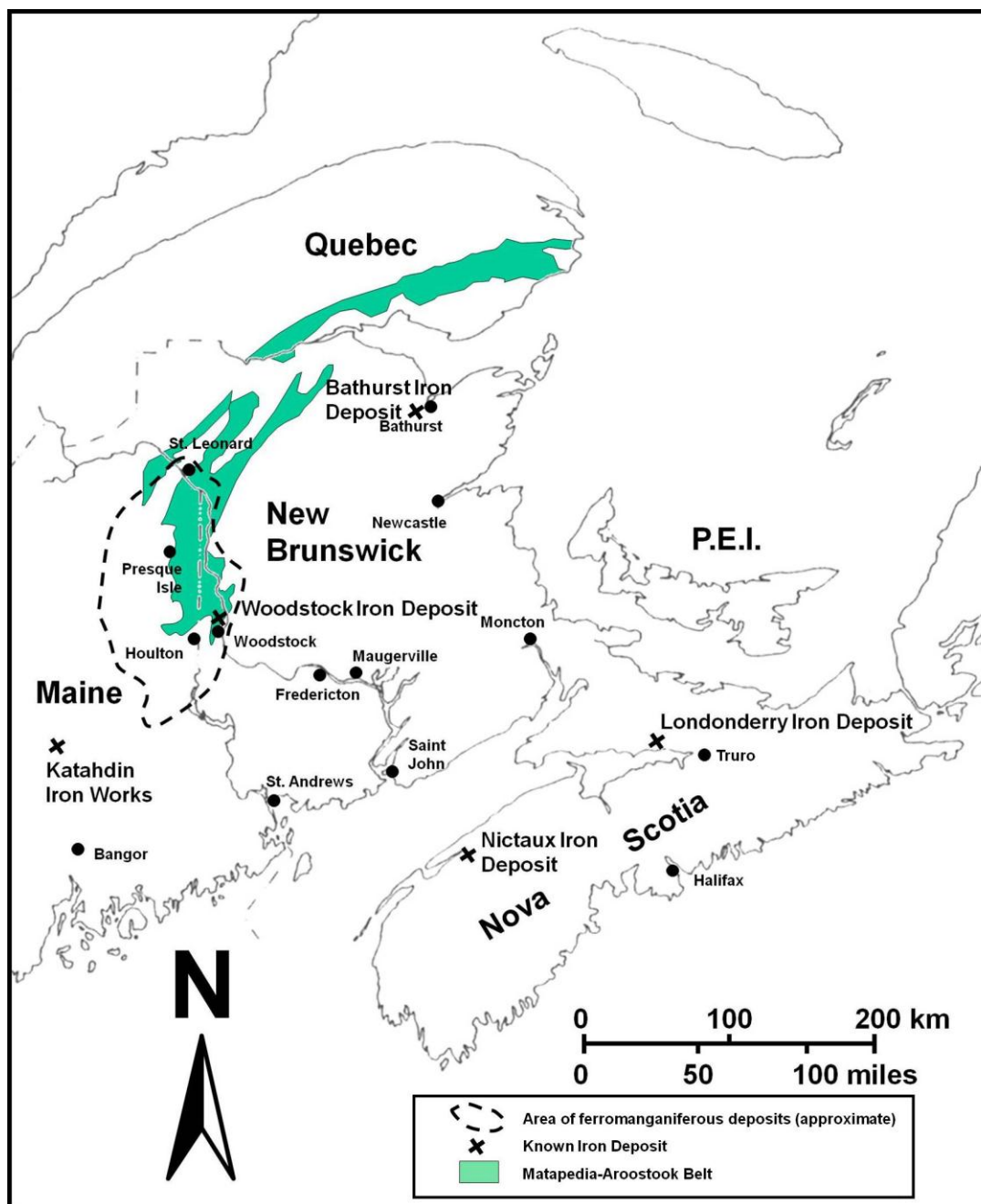
Fig. 2.1: Regional Map of the Maritimes displaying the extent of the Matapedia-Aroostook belt (in green) and the extent of the ferromanganiferous deposits (modified from Potter, 1983; Reed et al., 2005).
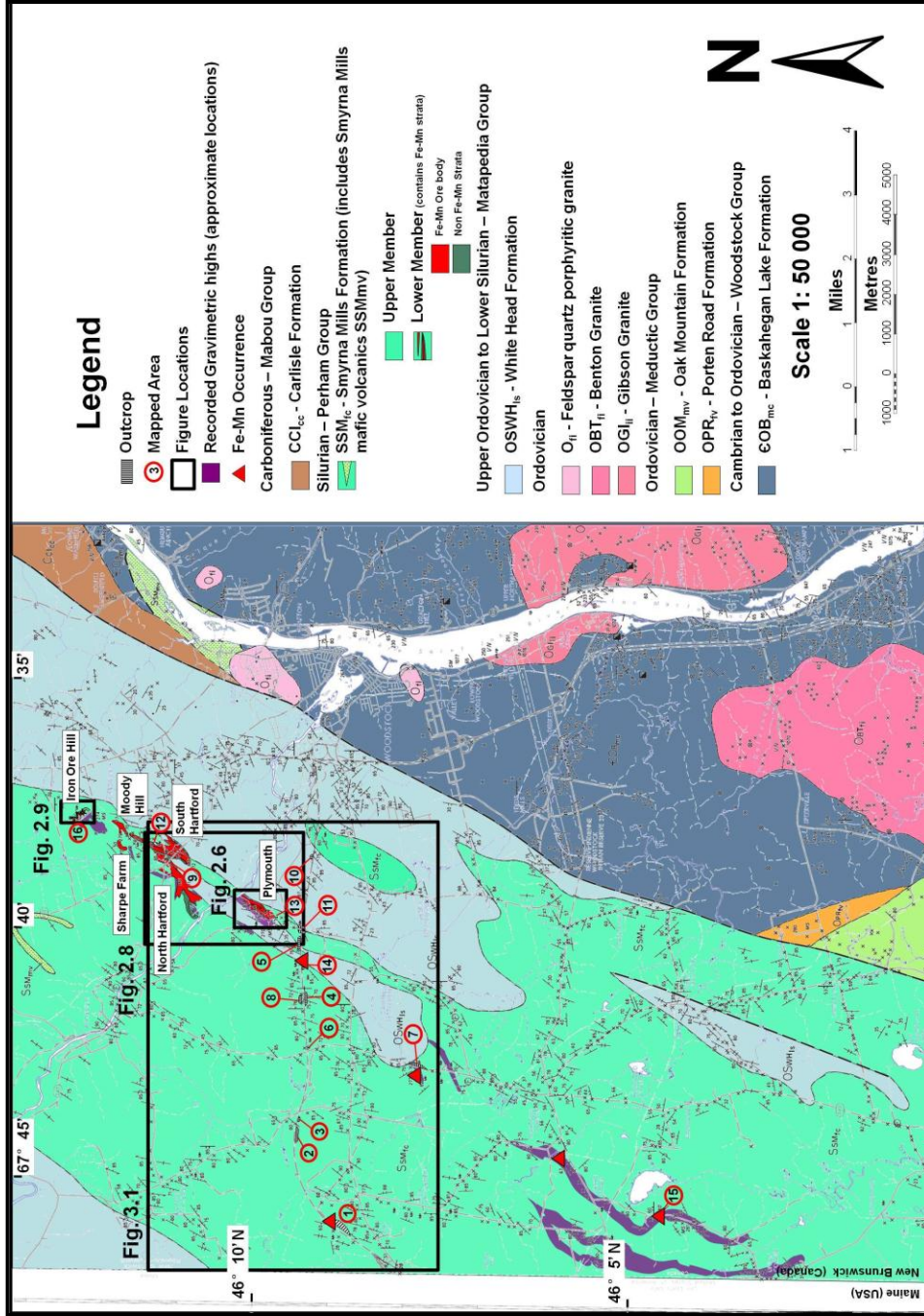
Fig. 2.2: Bedrock Geology Map of the Woodstock Area displaying areas of Fe-Mn mineralization west of the Woodstock Fault, as well as the underlying and overlying formations within the area (modified from Sidwell, 1954; Gliders, 1976; Potter, 1983; Roberts and Prince, 1990; Smith and Fyffe, 2006).

22

exposed in the study area. To the west of the Woodstock Fault, structurally separate, and unconformable on the Woodstock Group, lies the argillaceous limestone and calcareous shale of the Upper Ordovician to Lower Silurian Matapedia Group (Fyffe, 1982; Ludman, 1988; Smith and Fyffe, 2006). This area west of the Woodstock Fault exposes none of the Meductic Group, Woodstock Group, or the base of the Matapedia Group. It can only be assumed that the Matapedia Group lies unconformably on the Meductic Group in this area. Conformable on top of the Matapedia Group is the Perham Group, which is dominated by siltstone, noncalcareous and calcareous sandstone, and associated ferromanganiferous siltstone. The Lower Carboniferous Carlisle Formation, which comprises red sedimentary rock, lies unconformably on top of the Woodstock Group east of the Woodstock Fault and is terminated sharply on the western side by the Woodstock Fault (Fig. 2.2).

2.2.2 WOODSTOCK GROUP

Baskahegan Lake Formation

The basal unit in the Woodstock area is the Cambrian to Ordovician Baskahegan Lake Formation that comprises light grey and green, medium to thickly bedded quartzite, thin to medium bedded quartz wacke, with dark green siltstone and minor red sandstone and shale. The quartz wacke beds display graded bedding with ripple marks, load casts, and flame structures (Ludman, 1988; Fyffe, 2001; Smith and Fyffe, 2006). The base of this unit is not exposed within New Brunswick or Maine and due to the complexity of the deformation of the sequence and lack of

exposure its general thickness is unclear (Ludman, 1988). However, Anderson
(1968) suggests the formation is not any less than 900 m thick, but may be as much
as 1200 m in certain areas.

2.2.3 MEDUCTIC GROUP

Porten Road Formation

The Lower Ordovician Porten Road Formation is composed of greyish
green rhyolite that is locally porphyritic rhyolite. The unit occurs as a small wedge-
shaped unit approximately 10 km southwest of Woodstock. It is terminated on its
western side by the Woodstock Fault (Fig. 2.2) (Smith and Fyffe, 2006). The
formation thickness is estimated to be around 750 m. Local Fe-Mn mineralization is
observable separated by beds of dark grey shale (Fyffe, 2001). The Fe-Mn
mineralization associated with the Lower Ordovician volcanic rocks of the Porten
Road Formation is distinct from the Silurian Fe-Mn mineralization occurring in the
Woodstock Fe-Mn sedimentary deposits and will not be discussed further in this
thesis.

Oak Mountain Formation

The Lower Ordovician Oak Mountain Formation lies in fault contact with
the Porten Road Formation and consists of dark green porphyritic, amygdaloidal
basalt flows with clinopyroxene phenocrysts. Minor pillow lavas also occur within
this formation, as well as basalt breccia, bedded hyaloclastite, and red chert. An
estimated thickness of 300 m is observed southwest of Woodstock (Fig. 2.2) (Fyffe,
2001; Smith and Fyffe, 2006).

2.2.4   *MATAPEDIA GROUP*

White Head Formation

Within the Woodstock area, the Upper Ordovician to Lower Silurian White Head Formation (formerly the Cary Mills Formation) lies unconformably on top of the Cambrian to Ordovician Baskahegan Lake Formation to the northwest of the study area (Fyffe, 1982). These two formations are structurally separated by the south southwest-trending Woodstock Fault in the study area (Anderson, 1968; Fyffe, 1982; Smith and Fyffe, 2006). The White Head Formation occurs locally as a series of tightly folded antiforms and synforms associated with local D_1 and D_2 events and is conformably underlying the lower member of the Silurian Smyrna Mills Formation (Fig. 2.3). The White Head Formation consists of dark grey to blue-grey, massive and laminated argillaceous limestone, and interbedded calcareous shale and medium-grained calcareous sandstone and siltstone with a thickness of over 750 m in areas west of Woodstock (Hamilton-Smith, 1972).

2.2.5. *Perham Group*

Smyrna Mills Formation

As identified in outcrop and drill core, the Smyrna Mills Formation lies conformably on the White Head Formation (Fig. 2.3). The Smyrna Mills Formation of eastern Maine and western New Brunswick is a near vertically dipping interbedded siltstone and sandstone sequence with a northeast strike (Pavlides and Berry, 1966; Hamilton-Smith, 1972; Fyffe, 1982; Roberts and Prince, 1990; Smith and Fyffe, 2006). Slivers of locally abundant interbedded mafic volcanic rocks and felsic tuffs are present within the formation north of Woodstock (Venugopal, 1981;
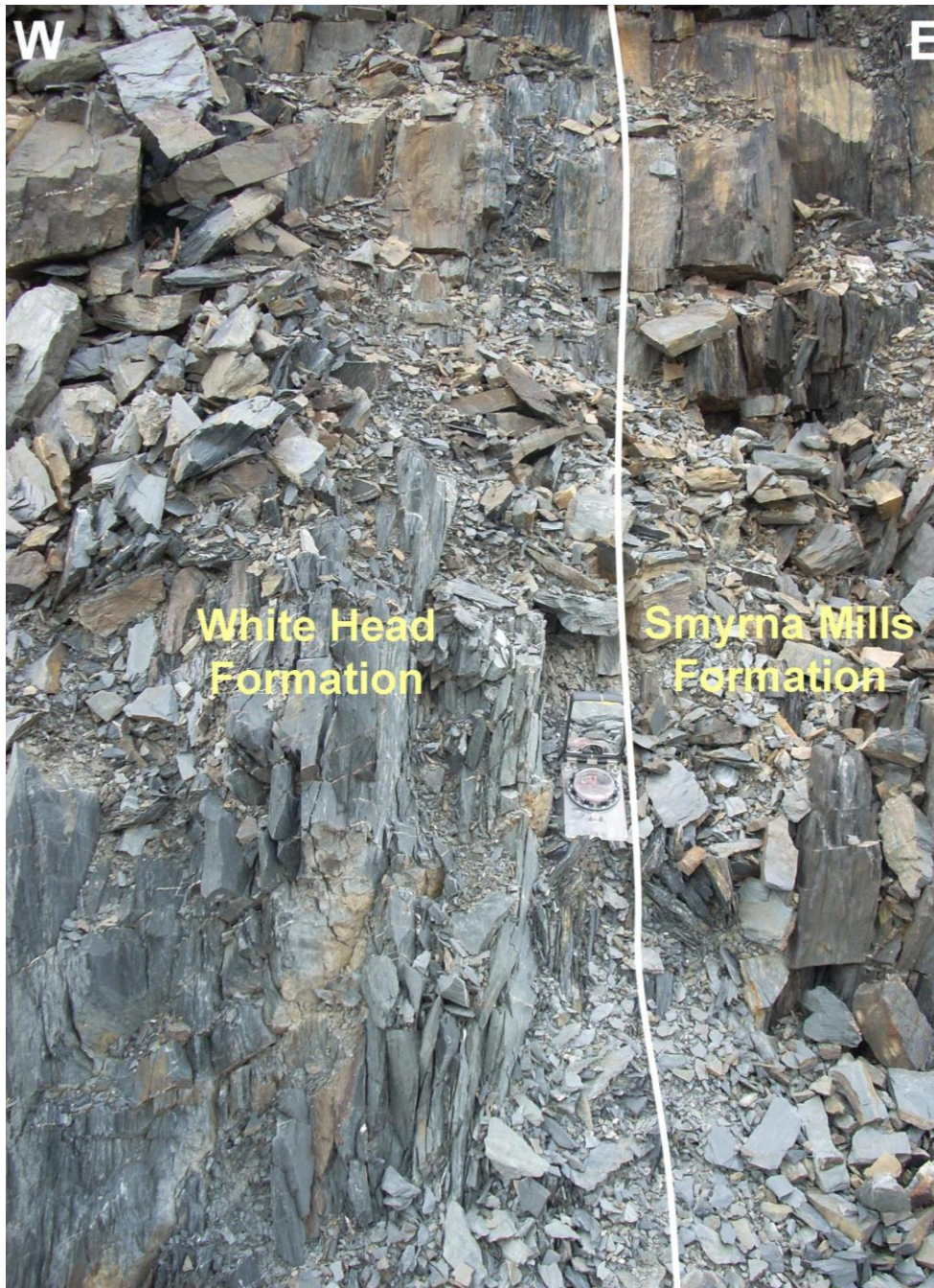
Fig. 2.3: Outcrop displaying the conformable boundary between the lower member of the Silurian Smyrna Mills Formation and the Upper Ordovician to Lower Silurian White Head Formation in Plymouth, New Brunswick. The White Head Formation here is composed of calcareous medium-grained sandstone and siltstone, whereas the lower member of the Smyrna Mills Formation is composed of noncalcareous siltstone. Compass for scale.

Fyffe, 1982; Smith and Fyffe, 2006). The Smyrna Mills Formation also exhibits one of the most complete Silurian graptolite sequences in North America and has been biostratigraphically dated as late Wenlockian to Ludlovian in age (Pavlides and Berry, 1966) (Fig. 2.4).

Hamilton-Smith (1972) subdivided the Smyrna Mills Formation into lower and upper members. The lower member comprises dark grey noncalcareous siltstone and shale with minor green and red siltstone and associated Fe-Mn siltstone that have been collectively measured to be 200 to 450 m thick (Hamilton-Smith, 1972; St. Peter, 1982). The conformable upper member is composed of dark grey calcareous shale and siltstone with interbedded with grey, calcareous, quartzose sandstone displaying flute and load casts. The thickness of individual sandstone beds varies from 2.5 to 15 cm, whereas the overall thickness attains 600 to 900 m in the McKenzie Corner area of New Brunswick (Fig. 2.2) proximal to the area of study. Elsewhere, the upper member can reach thicknesses of more than 1500 m into the Glassville area of New Brunswick approximately 40 km northeast of Woodstock (Pavlides and Berry, 1966; Pavlides, 1968; Hamilton-Smith, 1972; St. Peter, 1982; Smith and Fyffe, 2006).

2.2.6   *MABOU GROUP*

Carlisle Formation

A minor fault wedge of Lower Carboniferous Carlisle Formation occurs just north of Woodstock, along the Woodstock Fault, where it lies unconformably on top of the Cambrian to Ordovician Baskahegan Lake Formation (Fig. 2.2). The Carlisle Formation comprises red polymictic conglomerate with interbedded lithic

British Standard Section			Graptolitic zones	McKenzie Corner Area		Thickness (m)	Fossil Ages
				Name	Lithology		
Silurian	Upper	Ludlow	36	Smyrna Mills Formation	Upper Member	Dark grey Calcareous Slate, siltstone, and sandstone. Minor Limestone and conglomerate	1524+	
			35					
			34					
			33					
			32					
		Wenlock	31		Lower Member	Dark grey Noncalcareous Siltstone with minor green and red siltstones and associated Fe-Mn siltstone	213 – 457	
			30					
			29					
			28					
			27					
			26					
	Lower	Llandovery	25					
			24					
			23					
			22					
			21					
			20					
			19		White Head Formation	Blue-grey Calcareous siltstone and limestone with interbedded sandstone	762+	
			18					
			17					
			16					
Ordovician	Upper	Ashgill	15					
		Cardadoc	14					
	Middle		13					
			12					

Fig. 2.4: Thickness and fossil ages of the Smyrna Mills Formations and the White Head Formation present within McKenzie Corner, NB (modified from Pavlides and Berry, 1966; Hamilton-Smith, 1972).

sandstone; red mudstone, with grey arkose is present at the base of the unit. The overall thickness of the formation is 150 to 200 m (St. Peter, 1982; Smith and Fyffe, 2006).

2.3   THE WOODSTOCK FE-MN DEPOSITS

Within the regions of western New Brunswick and eastern Maine several Fe-Mn localities have also been reported in Silurian bedrock near Woodstock, New Brunswick and in Aroostook County, Maine (Pavlides, 1962). West of the Woodstock Fault in the Woodstock area (Fig. 2.2), there are six low-grade Fe-Mn deposits (average grade of 13% Fe and 9% Mn; Table 2.1) that are located near Jacksonville, and run south-westward to Plymouth, NB (Fig. 2.2). These Fe-Mn deposits form part of the lower member of the Smyrna Mills Formation. These Fe-Mn deposits occur parallel to the strike of the bedrock where the orientation of the Fe-Mn deposits and host stratigraphic units are governed by F1 and F2 folds (Sidwell, 1957; Roberts and Prince, 1990). The F1 and F2 folds were generated by deformation and associated with D_1 and D_2 events of Devonian Acadian Orogeny and may also be attributed to the Salinic Orogeny (Fyffe et al., 2011); regional metamorphism accompanying deformation was subgreenschist grade (Roberts and Prince, 1990). The Woodstock Fe-Mn deposits are devoid of volcanic rocks, whereas Fe-Mn localities within northeastern Maine locally contain slivers of mafic and felsic metavolcanic rocks. Gravimetric data (c. 1954) from Fig. 2.2 displays several large gravimetric anomalies southwest of the Woodstock deposits indicating that study area is only part of a much larger system.

Fe-Mn mineralization is observable in outcrop as jet-black rocks with a high specific gravity and a blocky cleavage (Fig. 2.5). The colour is due to surface weathering comprising Fe-Mn hydroxide and is localized only to siltstone enriched in Fe and Mn (Fig. 2.5). The Fe-Mn-rich beds are in conformable contact with intercalated red and green siltstone and rarely with grey siltstone with a general strike direction of 022°. Commonly, beds of Fe-Mn siltstone are crosscut by quartz-carbonate, quartz-chlorite-sulfide, and sulfide veinlets with minor base-metal mineralization.

Tonnages and grades of the six major, lenticular-shaped, Fe-Mn deposits have been identified, (Fig. 2.2, Table 2.1) have been estimated, from drilling of gravimetric anomalies (Sidwell, 1954, 1957, 1959; Potter, 1983; Table 2.1). Stratigraphic lensing of the Fe-Mn mineralization and geochemical variation within Fe-Mn deposits suggests that these are separate mineralized zones and not one continuous horizon (Roberts and Prince, 1990).

2.3.1   PLYMOUTH DEPOSIT

The Plymouth deposit has received the most attention by exploration companies since its discovery by gravimetric surveys in 1954 (Sidwell, 1954). Currently, it is the largest of the Woodstock Fe-Mn deposits in both tonnage and grade (Table 2.1). In the early to mid 1950's, a total of 23 drill holes were sunk into the deposit. Drilling indicated that the extent of Fe-Mn deposit was continuous for a length of 945 m (3100 ft) southwest of the Meduxnekeag River (Figs. 2.6, 2.7, 2.8) with an average width of 99 m (325 ft) and to a depth of about 200 m (700 ft) of continuous Fe-Mn mineralization (Sidwell, 1957). The western side of the orebody

Fig. 2.5: Photograph of an outcrop displaying layers of Fe-Mn mineralization within red and green siltstone located in an abandoned quarry along the edge of the South Hartford deposit. Hammer for scale.

Deposit	Tonnage	Average Fe %	Average Mn %
Plymouth	51,000,000	13.3	10.9
North Hartford	50,000,000	12.0	8.0
South Hartford	50,000,000	12.0	8.0
Moody Hill	10,000,000	N/A	9.5
Iron Ore Hill	25,000,000	14.0	10.0
Sharpe Farm	8,000,000	N/A	9.0
Total	194,000,000	13.0	9.0

Table 2.1: Tonnage and grade of each of the Woodstock Fe-Mn deposits (Sidwell, 1957; Potter 1983)

Fig. 2.6: Geologic map of the Plymouth deposit displaying the two different mineralized zones in relation to the surrounding bedrock. Both Fe-Mn mineralized zones were found within Treench 1 and 2 (modified from Roberts and Prince, 1990). (See Fig. 2.2 for location)
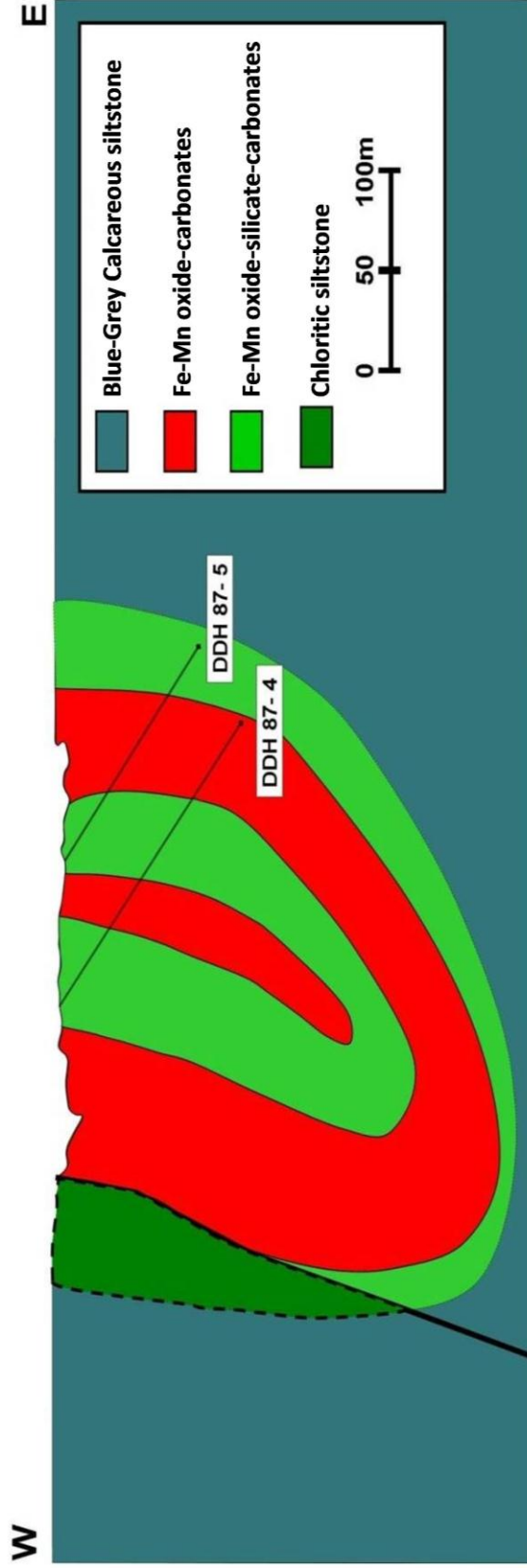
Fig. 2.7: East-West cross section of the Plymouth deposit through Trench 2 (modified from Sidwell, 1957; Roberts, 1985; Roberts and Prince, 1990). (See Fig. 2.6).

33
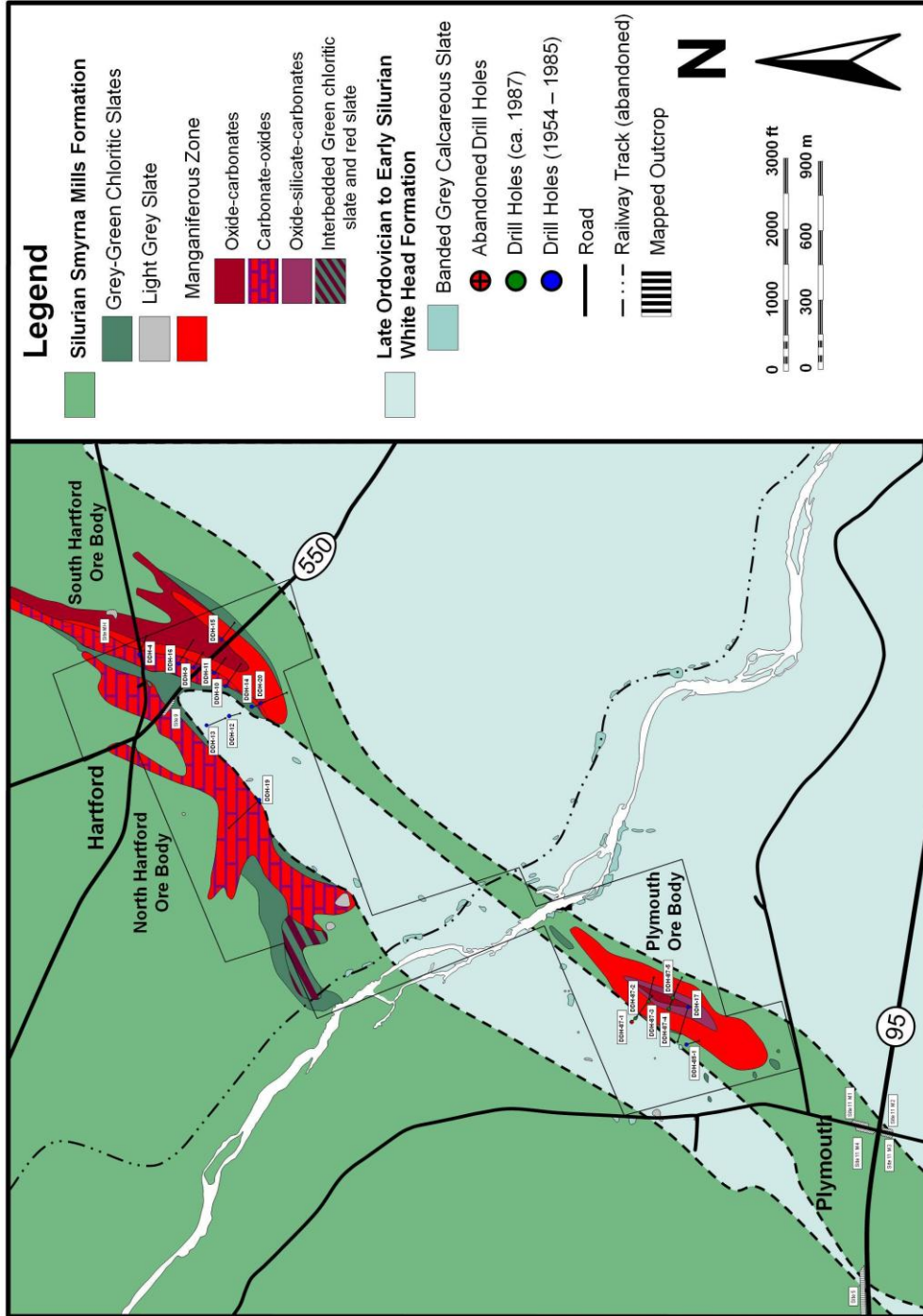
Fig. 2.8: Geologic Map of the Plymouth, North Hartford, and South Hartford deposits in relation to the surrounding bedrock Site 9 and Site 12 are marked on this map near Route 550 (modified from Gilders, 1976; Roberts and Prince, 1990). (See Fig. 2.2 for location).

Legend

Silurian Smyrna Mills Formation
- Grey-Green Chloritic Slates
- Light Grey Slate
- Manganiferous Zone
- Oxide-carbonates
- Carbonate-oxides
- Oxide-silicate-carbonates
- Interbedded Green chloritic slate and red slate

Late Ordovician to Early Silurian White Head Formation
- Banded Grey Calcareous Slate

- Abandoned Drill Holes
- Drill Holes (ca. 1987)
- Drill Holes (1954 – 1985)

- Road
- Railway Track (abandoned)
- Mapped Outcrop

1000 2000 3000 ft
300 600 900 m

South Hartford Ore Body
North Hartford Ore Body
Plymouth Ore Body
Hartford
Plymouth
550
95

is terminated by a small local fault that is characterized by highly chloritized rocks (Figs. 2.6, 2.7) (Roberts, 1985; Roberts and Prince, 1990). The relatively large size of the deposit set initial plans for open-pit mining with a single elongated pit about 690 m (2267 ft) long, 240 m (797.6 ft) at its widest, and 60 m (200 ft) at its maximum depth (Sidwell, 1957, 1960; Gliders, 1976; Roberts and Prince, 1990).

Fe-Mn mineralization within the Plymouth deposit is composed of Fe-Mn oxide-carbonates that occur in red siltstone, and Fe-Mn oxide-silicates-carbonates that occur within green siltstone (Fig. 2.6) (Nickel, 1957; Sidwell, 1957; Heinrich, 1962; Roberts and Prince, 1990). Roberts and Prince (1990) reported high anomalous concentrations of copper and cobalt within areas of Fe-Mn mineralization at this deposit. Copper was reported of having a maximum concentration of 410 ppm, whereas Co had a maximum concentration of 250 ppm.

2.3.2 *NORTH HARTFORD DEPOSIT*

The North Hartford Deposit (Fig. 2.8) is the second largest of the Woodstock Fe-Mn deposits. It is estimated at 50,000,000 tonnes (12% Fe and 8% Mn) based on 13 diamond drill holes, totalling 1640 m (5381 ft). Although there is very little Fe-Mn mineralization observed in outcrop, drill holes indicate the presence of Fe-Mn carbonates with a general strike of 045° and dipping 80° SE with a thickness of 152 m (500 ft). The bedding is overturned on the southwestern tip of the North Hartford deposit. The Fe-Mn mineralization is exposed as a jet black outcrop (~ 4 m wide) with a blocky cleavage that contains layers of ellipsoidal rhodochrosite ([Ca, Fe, Mn]CO_3) concretions 1 cm in diameter with minor interbedded hematite and Fe-Mn carbonate beds, locally in conformable

contact with green siltstone (Site 9). Euhedral sulfides (0.5 to 1 cm in diameter) are present within some of the mineralized talus at the outcrop; however the sulfide mineralization seems to be localized to this particular outcrop (Site 9) (Figs. 2.1 & 2.8), which is the only bedrock exposure of the North Hartford Deposit.

2.3.3   *SOUTH HARTFORD DEPOSIT*

The South Hartford Deposit (Figs. 2.5 & 2.8) lies approximately 0.25 km southeast of the North Hartford Deposit and extends northeast towards the Moody Hill Deposit (Fig. 2.2). It also exhibits a tonnage and grade (50,000,000 tonnes; 12% Fe and 8% Mn) similar to the North Hartford Deposit, but predominantly comprised of manganiferous hematite. Nine drill holes were sunk into the deposit during the 1950's and indicated a highly folded and contorted ore body that consists of red siltstone, maroon interbedded manganiferous hematite siltstone, and minor green siltstone (Sidwell, 1957). A section of this deposit, along the edge of the Fe-Mn mineralization is exposed extensively in an abandoned quarry that was probably worked during the 1950's.

2.3.4   *IRON ORE HILL DEPOSIT*

The Iron Ore Hill Deposit, the northernmost Fe-Mn deposit in the area, (Fig. 2.2) is located in Jacksonville (Fig. 2.9). This deposit was extensively mined during the mid-1850's and served as the main supply of iron ore for the Woodstock Iron and Charcoal Company (Sidwell, 1957). The initial trenches were dug from 1848 to 1864 and for the most part were restricted to the extent of the Fe-Mn mineralization with the base of the trench more or less level with the surrounding road. Although it is graded at only half the tonnage of the North and South Hartford deposits, it
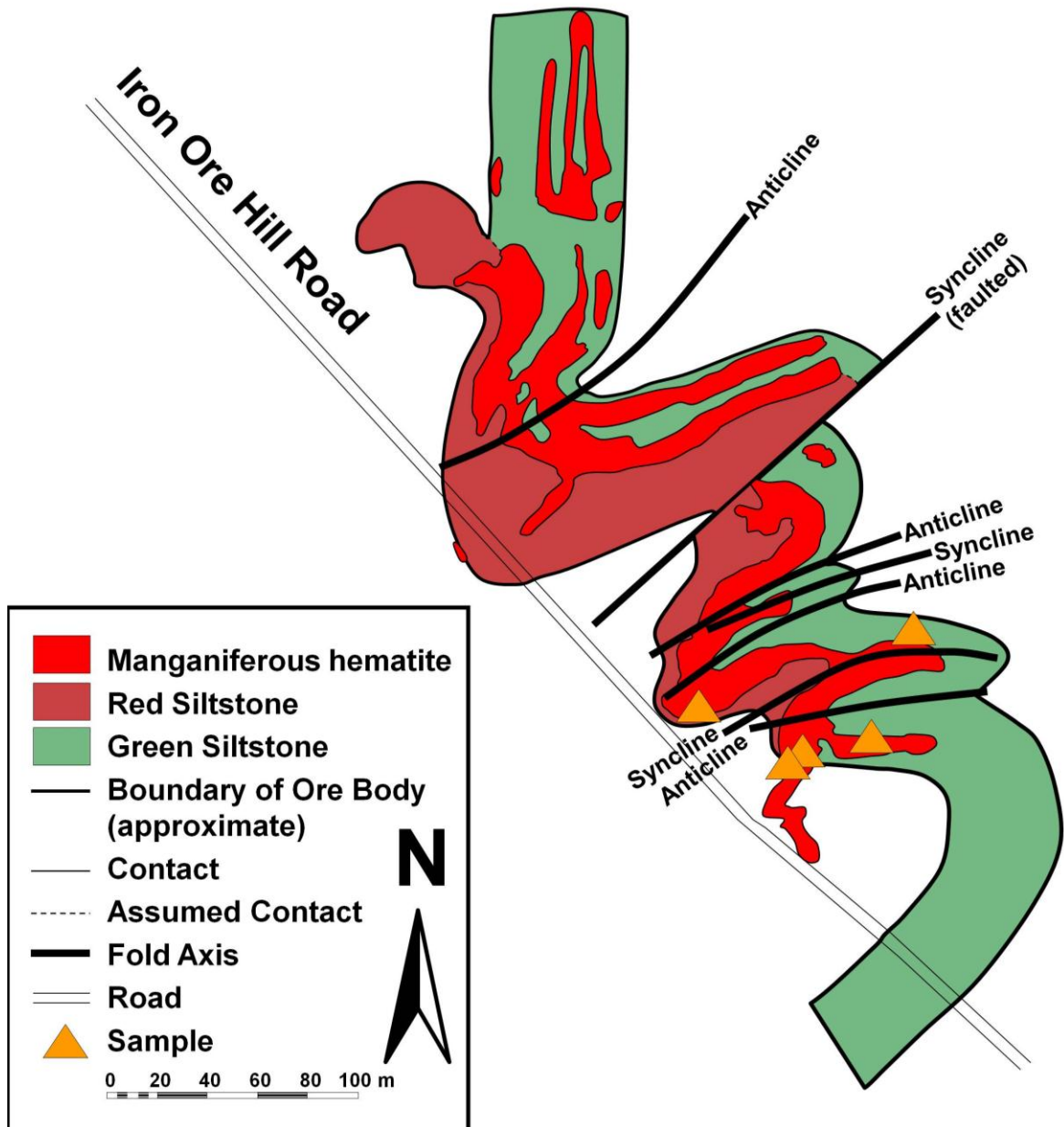
Fig. 2.9: Geologic map of Iron Ore Hill deposit (modified from Baldwin, 1954). Trenches from the mid 1800's generally follow the strike of the manganiferous hematite mineralization. These areas generally constitute narrow beds of manganiferous hematite with interbedded red and green siltstone (Baldwin, 1954; Anderson, 1968). (See Fig. 2.2 for location).

contains the highest grade of Fe (14%) and the second highest Mn content (10.0%).

Two drill holes were sunk into the gravimetric anomaly during the 1950's southwest of the old trenches dug between 1848 and 1864. The first drill hole intersected a Fe-Mn mineralized section composed of silicified siltstone, zones of manganiferous hematite, and red siltstone over a length of 225 m (738 ft). The second drill hole (122 m), southwest of the first drill hole, intersected the same mineralized section over a length of 53 m (175 ft) indicating that the mineralization thins considerably to the southwest in this area. A large portion of the bedrock exposed at this locality is red and green siltstone with interbedded layers of manganiferous hematite. Robb (1870) noted the presence of pyrite (FeS_2) and chalcopyrite ($CuFeS_2$), which are locally present within the hinges of folded manganiferous hematite layers. Within the trenches at Iron Ore Hill, Fe-Mn mineralization is dominantly inbedded hematite, Mn-silicate (possibly rhodonite; ($MnSiO_3$)) and rhodochrosite (Sidwell, 1957).

2.3.5   MOODY HILL DEPOSIT

Three holes were drilled in 1954 into the Moody Hill Deposit (Fig. 2.2) indicating 10,000,000 tonnes of low-grade ore averaging 9.5 % Mn with an unknown percent of Fe and a width of 252 m (825 ft) and unknown strike length. Sixty percent of the deposit is composed of red, green, and grey siltstone where the Fe-Mn mineralization is found as lenticular beds of manganiferous hematite hosted in red siltstone and green siltstone (Sidwell, 1957). Although Moody Hill served as one of the sources of Fe between 1848 and 1864 (Sidwell, 1964; Anderson, 1968; Potter, 1983), outcrop is currently exposed at the deposit.

2.3.6 *SHARPE FARM DEPOSIT*

The Sharpe Farm Deposit, which lies midway between the Moody Hill and Iron Ore Hill deposits (Fig. 2.2), is the smallest of the six Fe-Mn deposits with approximately 8,000,000 tonnes of ore with an average grade of 9% Mn and an unknown grade of Fe. Two holes drilled in 1954 intersected the mineralized zone within a gravimetric anomaly of 46 m (150 ft) width. The deposit occurs as manganiferous silicified siltstone within a sequence of grey siltstone (Sidwell, 1957; Anderson, 1968). No outcrop is currently exposed at this location.

2.4 MINOR FE-MN OCCURRENCES

Although a bulk of the major Fe-Mn mineralization occurs northeast of Route 95, several minor occurrences are known south of the highway. Sidwell (1954) first noted two large gravimetric anomalies 18 km southwest of Woodstock and proximal to the US/Canada border (Fig. 2.2). Early geologic maps (c. 1936; Baldwin, 1954) have identified occurrences of ferromanganiferous beds, but drilling of the gravimetric anomalies suggests that these are areas with only minor Fe-Mn mineralization.

2.4.1 *UNION CORNER*

The Union Corner Fe-Mn occurrence, although largely hidden by dense overgrowth, is a 4.7 m wide roadcut composed largely of heavily Fe-hydroxide stained manganiferous green and brown siltstone (Fig. 2.10) that is composed largely of interbedded oligonite ($[Fe,Mn]CO_3$) and rhodochrosite with cross-cutting quartz-carbonate-sulfide, quartz-chloride-sulfide, and sulfide veinlets. The brown

Fe-Mn-bearing siltstone beds were observed to be in conformable contact with Fe-Mn-rich green siltstone. The extent of the Fe-Mn mineralization is unclear within this area due to the lack of exposure.

2.4.2 IRISH SETTLEMENT

Approximately 1 km east of the US/Canada border on Route 95 lies a large roadcut approximately 430 metres in length (Fig. 2.11). Although a large portion of the exposure is unmineralized siltstone, the northeast corner of the roadcut contains minor Fe-Mn bearing siltstone beds that are stratigraphically underlain with white carbonate and pyrite beds. The southwest section of the outcrop also reveals the presence of Fe-Mn mineralization with the large amount of wad concentrated in a 2 m section that is parallel to strike of the Fe-Mn beds.

2.5 FE-MN DEPOSITS IN EASTERN MAINE

Several Fe-Mn deposits are also found in Upper Ordovician and Silurian strata of Aroostook County, Maine (Figs.1.1 and 2.1). These are divided into Northern, Central and Southern Manganese Districts (Fig. 1.1).

2.5.1 MAPLE AND HOVEY MOUNTAIN DEPOSIT

The Maple and Hovey Mountain Deposit is one of the Fe-Mn deposits that forms part of the Central Manganese District. Pavlides (1962) reports that the Fe-Mn deposit is located about 1.5 km southeast of Number Nine Lake in Aroostook County, Maine. Sixty-one drill holes were sunk into this deposit between 1949 and 1952 and revealed beds of magnetite (Fe_3O_4) and rhodochrosite (Fig. 2.12). The main exposed outcrop displays heavily folded ferromanganiferous strata that are

Fig. 2.10: Photograph of an exposure of ferromanganiferous siltstone at Union Corner. The main area of mineralization is seen as a black Fe-Hydroxide stained area with a high specific gravity.

Fig. 2.11: A composite photograph of a section of the Irish Settlement roadcut looking northeast displaying areas of Fe-Mn mineralization in relation to the surrounding bedrock.

Figure 2.12: Photograph of a magnetite-rhodochrosite-bearing siltstone from the Maple and Hovey Mountain Deposit (46° 24' 03.0" N, 68° 02' 18.7") displaying interbedded layers of magnetite and rhodochrosite.

locally unweathered and composed of interbedded magnetite-rhodochrosite-bearing siltstone beds that are in sharp conformable contact with green siltstone. Flame structures were observed in the Fe-Mn siltstone allowing the tops direction to be traced within the folds.

2.5.2   *AROOSTOOK (DUDLEY) DEPOSIT*

The Aroostook (Dudley) Fe-Mn Deposit is part of the Northern Manganese District in Aroostook County, Maine (Pavlides, 1962). The Fe-Mn mineralization is hosted by greenish argillite in the Silurian Ashland Shale, and by slate and calcareous slate in the Ordovician Aroostook Limestone (White, 1943). Devonian and Mississippian felsic volcanic rocks are observable within the stratigraphy and intrude the sedimentary rocks. The Fe-Mn mineralization occurs as manganiferous hematitic siltstone and as Fe-Mn silicate-carbonate siltstone (Twenhofel, 1941; White, 1943; Pavlides, 1962).

2.5.3   *HOULTON SOUTH DEPOSIT*

The Houlton South Deposit is part of the Southern Manganese District that was discovered by magnetic surveys and prospecting. Lenses of manganiferous siltstone are hosted in grey slate that occurs in Upper Ordovician and Early Silurian strata. Deformation in this area was found to be more complex than in the Aroostook Fe-Mn Deposit, but the Houlton South Fe-Mn Deposit lacks the overlying Devonian felsic volcanic rocks noted in the Northern Manganese District (Pavlides, 1962). The mineralization is likely to be similar to the Union Corner Fe-Mn occurrence that is located approximately 5 km to the east in New Brunswick,

due to the similarities in the surrounding green siltstone associated with the Smyrna

Mills Formation.

CHAPTER 3

SEDIMENTOLOGY ALONG ROUTE 95 HIGHWAY

3.1   INTRODUCTION

Bedrock exposure within western New Brunswick and eastern Maine is often limited to small irregularly situated outcrops and roadcuts. Hamilton-Smith (1972) was the first to map this area in detail (Figs. 3.1, 3.2). A recent expansion of Route 95 from the Woodstock, New Brunswick/Houlton, Maine border-crossing station to Woodstock, New Brunswick, has led to several large new roadcuts exposing strata west of the Woodstock Fe-Mn ore bodies that are perpendicular to the general northeast strike of bedrock. Geologic mapping and sampling was done on a series of several outcrops and roadcuts, many of which spanned over several hundred metres.

Sedimentological examination of the outcrops resulted in the identification of fourteen lithofacies (Table 3.1). A majority of these lithofacies were classified by subtle changes in colour and mineralogy since many of the rocks had the same grain size and a general lack of bedding features. Based on the methodology of Miall (1978), some of lithofacies listed in Table 3.1 could be grouped together into six lithofacies associations (Table 3.2). Although resolution of the succession is complicated by folding and interbedding of individual lithofacies, in general the lithofacies associations lie in stratigraphic succession. In the Smyrna Mills Formation, lithofacies associations can range from tens to hundreds of metres in thickness.
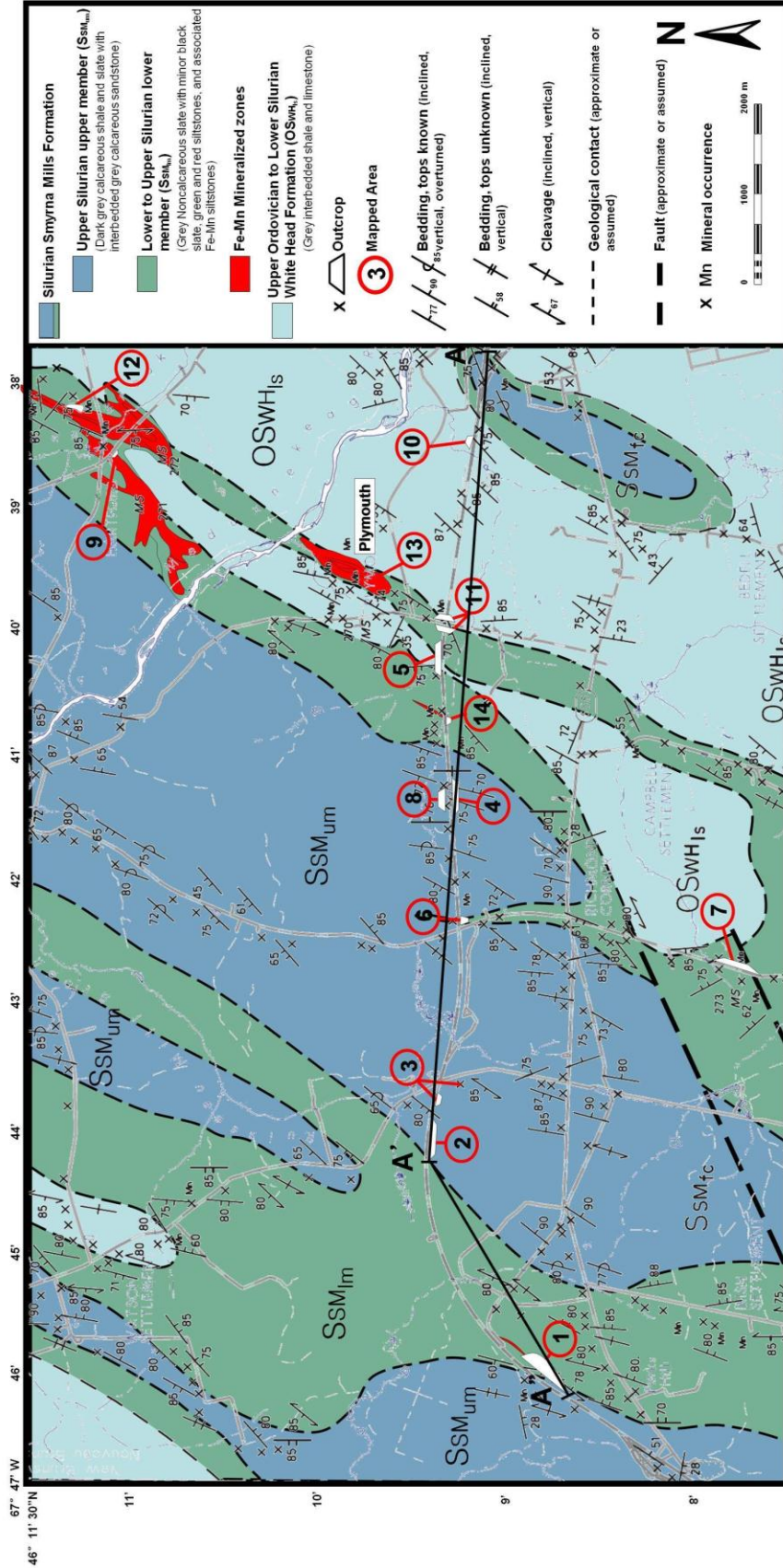
Fig. 3.1: Detailed geologic map of Route 95 area displaying the distribution of the lower and upper members of the Silurian Smyrna Mills Formation and the underlying Upper Ordovician to Lower Silurian White Head Formation. Numbers refer to sites mapped during this study. Sites 1, 4, 5, 8, 10, and 11 were not exposed during previous mapping (larger map modified from Hamilton-Smith, 1972; Gliders, 1976; Roberts and Prince, 1990; Smith and Fyffe, 2006). (See Fig. 2.2 for location).
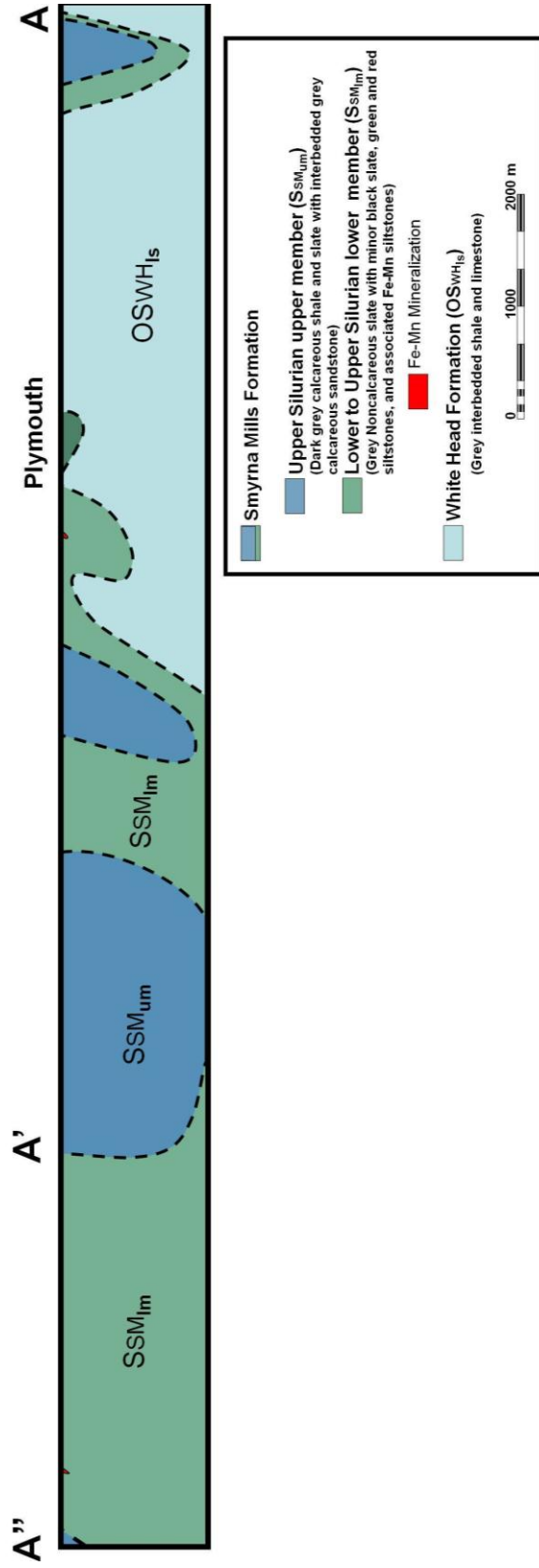
Fig. 3.2: Cross-section along Route 95 (see Fig. 3.1) displaying the placement and distribution of the lower and upper members of the Silurian Smyrna Mills Formation and the underlying Upper Ordovician to Lower Silurian White Head Formation (modified from Hamilton-Smith, 1972; Gliders, 1976; Roberts and Prince, 1990; Smith and Fyffe, 2006).

Lithofacies Description	Code	Interpretation of sedimentary process(es)	Lithofacies Association(s)
Blue-grey laminated calcareous sandstone. May contain calcareous concretions	Sbuc	Deeper marine environment possibly associated with turbidity flows.	O
Blue-gray calcareous laminated siltstone. May contain calcareous concretions	Fbuc	Deeper marine environment possibly associated with turbidity flows.	O
Blue-grey limestone	Lbu	Deeper marine biogenic environment	O
Green calcareous siltstone	Fgnc	Anoxic marine environment	I
Green and grey interbedded laminated siltstone (tiger-striped)	Fgngyib	Marine anoxic environment with minor organic input	I
Black to grey laminated mudstone with authigenic pyrite	Fbkpl	Marine stagnant organic-rich anoxic environment.	I, II
Grey and minor greenish laminated siltstone	Fgyl	Marine anoxic marine organic environment with less sulfur.	I, II, V
Greyish green siltstone	Fgygn	Marine anoxic environment with minor organic input	I,II, IV, V
Green laminated siltstone with rare white microspheroidal limestone	Fgnl	Marine anoxic environmental with less sulfur with rare possible biogenic limestone	I, II, III, IV, V
Dark green to black laminated mineralized siltstone	Fgnz	(detailed further in Ch 4)	II, rare III
Green to greyish green and tan calcareous and noncalcareous massive or laminated sandstone	Sgnl	Shallow marine environment.	II, III, IV
Red and maroon, variably arenaceous siltstone. Massive or with asymmetric cross-laminations	Frml	Oxic marine environment.	III, rare II
Red and maroon mineralized siltstone	Frmz	(detailed further in Ch 4)	III
Grey laminated, asymmetrically cross-laminated, cross-bedded, or massive sandstone. Locally bioturbated, locally with crinoids hash. Bases may be intruded with flame structures	Sgyce	Shallow marine environment with macroscopic organisms present.	IV, V

Table 3.1: Tabulation of observed lithofacies along the Route 95 study area. The codes of each lithofacies coincide with the following descriptions based on Miall (1978). S = Sandstone, F = Siltstone, L = Limestone, bu = blue-grey, bk = black, gy = grey, gn = green, rm = red and maroon, wh = white, c = calcareous concretions, p = pyritic, z = mineralized, l = laminated, o = microspheriodal, e = cross-bedded or massive, m = massive, ib = interbedded.

Lithofacies Associations	Component Lithofacies	Bed Thickness	Bed Geometry	Bed bases	Sedimentary Structures	Fe-Mn Mineralization	Outcrop locations	Associated Formation and (or) Member
V	Fgyl, Fgnl, and Sgyce	>90 m	Tabular bedding with some lensing	Sharp, conformable	Finely parallel laminated bedding, minor cross bedding	None	Sites 3, 4, 8	Smyrna Mills Formation upper member
IV	Sgyce, Sgnl, and Fgnl	>280 m	Tabular bedding with some lensing	Sharp, conformable	Massive and parallel laminated sandstone, asymmetrical ripples, laminated bedding, flame structures, minor cross-bedding	None	Sites 2, 3, 4, 8	Smyrna Mills Formation upper member
III	Frml, Fgyl, Fgnl, Sgnl, Frmz, and rare Fgnz	~15 m	Tabular bedding with some lensing	Sharp, conformable	Finely parallel laminated bedding, minor cross-bedding	Fe-Mn oxides with minor Fe-Mn silicates and Fe-Mn carbonates	Sites 6, 9, 12	Smyrna Mills Formation lower member
II	Fbkpl, Fgyl, Fgnl, Fgnz, Sgnl, and rare Frmz	>279 m	Tabular bedding with some lensing	Sharp, conformable	Finely parallel laminated, concretions, minor asymmetrical ripples	Fe-Mn carbonates and minor Fe-Mn silicates	Sites 1, 5, 7, 11, 13, 14	Smyrna Mills Formation lower member
I	Fgnc, Fgngyib, Fbkpl, Fgyl, and Fgnl	~253 m	Tabular bedding with some lensing	Sharp, conformable	Finely parallel laminated beds, concretions	Fe sulfide mineralization	Sites 1, 5, 11, 13	Smyrna Mills Formation lower member
O	Sbuc, Fbuc, and Lbu	>43.3 m	Tabular bedding with some lensing	Sharp, conformable	Finely laminated beds with coarsening upward sequences	None	Sites 5,10, 11	White Head Formation

Table 3.2: A summary of characteristics of the six sedimentary lithofacies associations present in the study area. Thicknesses are measured in outcrops on Route 95 and can vary in areas proximal to the area of study.

3.2   LITHOFACIES ASSOCIATION O

3.2.1 Description:

Lithofacies Association O (Figs. 3.1, 3.3, Tables 3.1, 3.2) is predominantly of lithofacies *Sbuc* (blue-grey calcareous sandstone) interbedded with lithofacies *Fbuc* (blue-grey calcareous siltstone) with lesser lithofacies *Lbu* (limestone) and differs from Lithofacies Associations I, II, III, IV, and V in appearance, component lithofacies, and absence of Fe-Mn mineralization (Tables 3.1 and 3.2). It is measured to be at least 43.3 m in thickness and is observed in outcrop at Sites 5, 10, and 11. Commonly this lithofacies association contains abundant fining up beds and calcareous concretions (Fig. 3.3) that are more abundant near to the contact of the overlying Lithofacies Association I. A predominance of lithofacies *Fbuc* near the base, overlain by predominantly lithofacies *Sbuc* above 30 m results in an overall coarsening upward succession at least 40 m thick (Fig 3.3). This feature is also observable outside the study area in outcrop on Route 95 at its intersection with Route 2 (Fig. 3.1).

A roadcut (Site 10; Fig. 3.4) located on Route 95 approximately 3.4 km east from the intersection of Route 95 and Route 2 exposes lithofacies *Fbuc* that is highly folded and displays several crosscutting veins of calcite ($CaCO_3$) and quartz (SiO_2) (Fig. 3.5). Petrographic analysis of a polished thin section reveals that lithofacies *Fbuc* largely comprises quartz, feldspar ($NaAlSi_3O_8$), calcite, and minor muscovite ($KAl_2(AlSi_3O_{10})(OH)_2$. Opaque minerals include minor subhedral pyrite and hematite (Fig. 3.5). No Fe-Mn mineralization was associated within the outcrops of Lithofacies Association O.
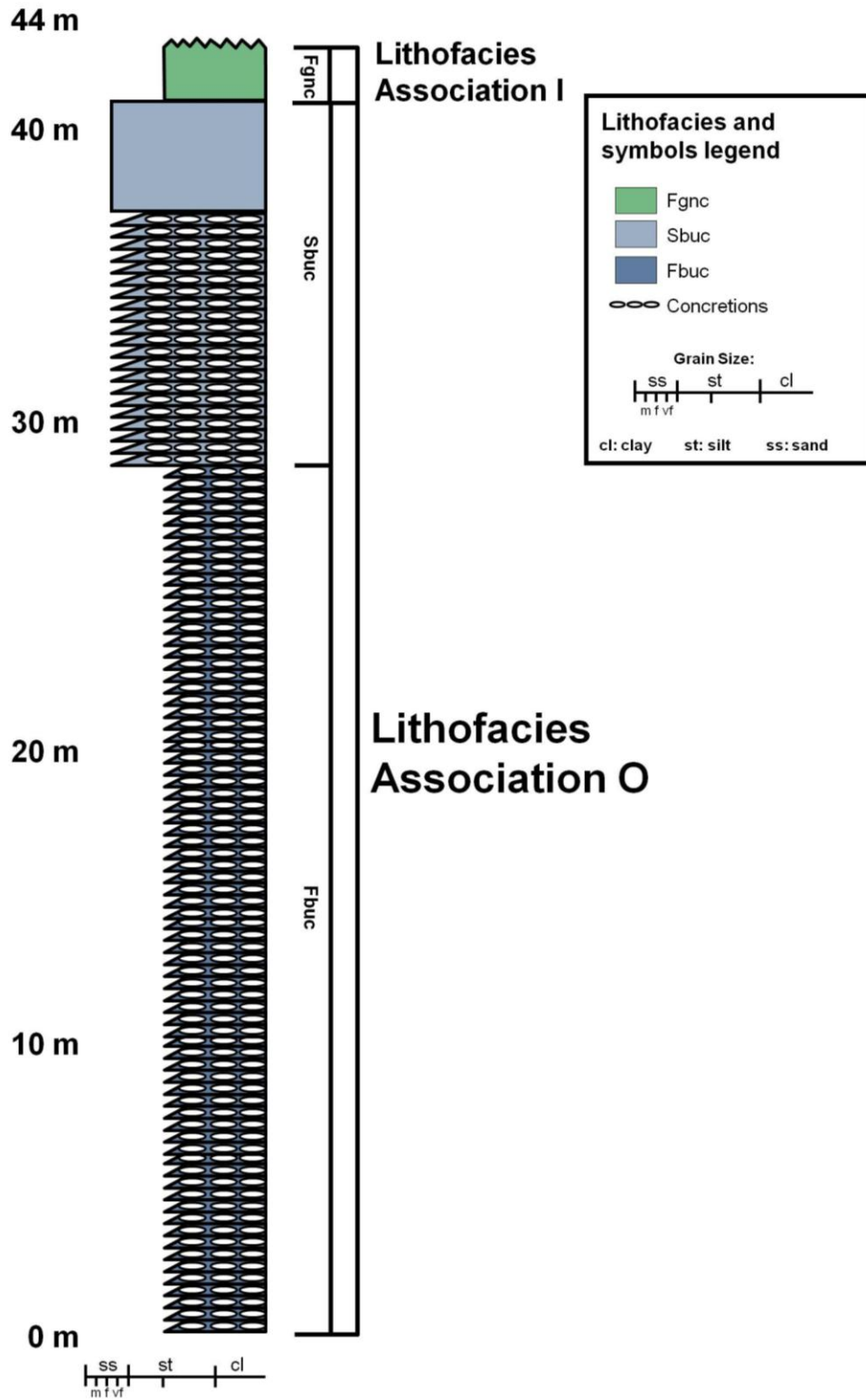
Fig. 3.3: Stratigraphic column of Lithofacies O. This depositional contact of Lithofacies Association O with overlying Lithofacies Association I is visible in several outcrops (e.g., Site 11).

Fig. 3.4: Photograph of an outcrop of the Lithofacies Association O displaying secondary calcite crystallization within the cavities of the blue grey calcareous siltstone layers (Lithofacies *Fbuc*). Euhedral calcite crystals were found to be up to 5 cm in diameter. Located at Site 10. Pencil for scale.

0.4 mm
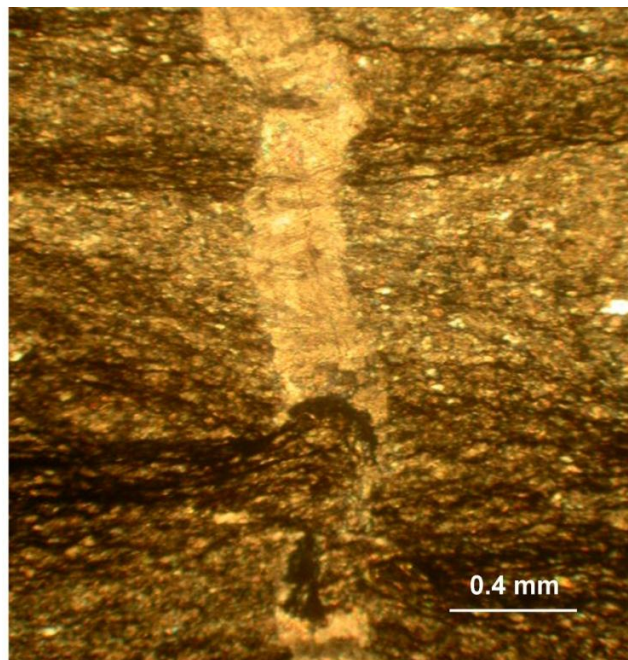
Fig. 3.5: Photomicrograph of the Lithofacies Association O under cross-polarized transmitted light displaying layers of altering layers of fine-grained sandstone and siltstone. Cross-cutting veins of calcite are particularly common within this unit and commonly produced large euhedral calcite crystals within cavities (Fig. 3.1; Site 10) Sample 10-17-S2.

3.2.2 Interpretation:

The general calcareous composition, interbedded nature, abundant turbidite beds, and blue-grey colour of lithofacies *Sbuc, Fbuc,* and *Lbu* are likely associated with the White Head Formation. The White Head Formation, a predominant formation within the study area, is described previously by Pickerill (1980) and St. Peter (1982) as being composed of calcareous, interbedded blue-grey sandstone and siltstone with lesser limestone containing coarsening and fining upward units. Pickerill (1980) and St. Peter (1982) concluded that the fining upward sequences within the White Head Formation were the result of turbidity flows associated with a submarine fan. These turbidite beds, observed in outcrop (Sites 5, 10, 11), are abundant within Lithofacies Association O. The overall coarsening upward could be associated with deposition from a series of progressively more energetic turbidity currents that are related to a more proximal source and may be related to a regression in sea level. It is likely this lithofacies association was located on the outskirts of the continental shelf of the ocean at the time of deposition (Pickerill, 1980; St. Peter, 1982). The stratigraphic column of Lithofacies Association O (Fig. 3.3) displays an increase in grain size at 30 m that may suggest a more energetic environment of deposition associated with a regression in sea level. The lack of Fe-Mn beds suggests the environment was not saturated in Fe^{2+} ions and (or) not subject to changes in ocean redox potential. In the regional context, Lithofacies Association O was accreted on the Laurentian margin during the uplift of the Popelogan terrane within a late Taconic tectonic event that marked the complete closure of the Iapetus Ocean (Fyffe et al., 2011).

3.3 Lithofacies Association I

3.3.1 *Description*:

Lithofacies *Fgnc* (Green calcareous siltstone)*, Fgngyib* (Green and grey interbedded laminated siltstone), *Fbkpl* (Black to grey laminated mudstone), *Fgyl* (Grey and minor greenish laminated siltstone), *Fgygn* (Greyish green siltstone), and *Fgnl* (Green laminated siltstone with rare white microspheroidal limestone) comprise the Lithofacies Association I (Fig. 3.6). Upsection from the contact with the underlying Lithofacies Association O is lithofacies *Fgnc* that was only visible in drillcore sections from the Plymouth Fe-Mn deposit. Elsewhere, the first 130 m of Lithofacies Association I comprises predominately lithofacies *Fgngyib* with increasing interbeds of *Fgyl* and *Fbkpl* upsection along with minor occurrences of lithofacies *Fgygn* and lithofacies *Fgnl.* Continuing upsection a small 11 m thick section of lithofacies *Fgygn* occurs at 133 m and then interbeds of lithofacies *Fgyl* and *Fbkpl* increase in thickness until about 177 m. Further upsection, interbeds of lithofacies *Fgyl* generally decrease in thickness and interbeds of lithofacies *Fbkpl* continue to increase in thickness until about 253 metres, which is the calculated thickness of Lithofacies Association I at Site 5 (Fig. 3.1) near Plymouth (Fig. 3.6). Lithofacies Association I was found in outcrop at Sites 1, 5, 11, and 13.

Lithofacies *Fgnc* is the marker bed that designates the transition between Lithofacies Associations O and I in drill core (Site 13). Lithofacies Fgnc does not appear to be interbedded with any of the other lithofacies coupled with Lithofacies Association I; however Roberts and Prince (1990) noted that the contact between lithofacies *Fgnc* and the overlying lithofacies *Fgygnib* appears to be a gradational
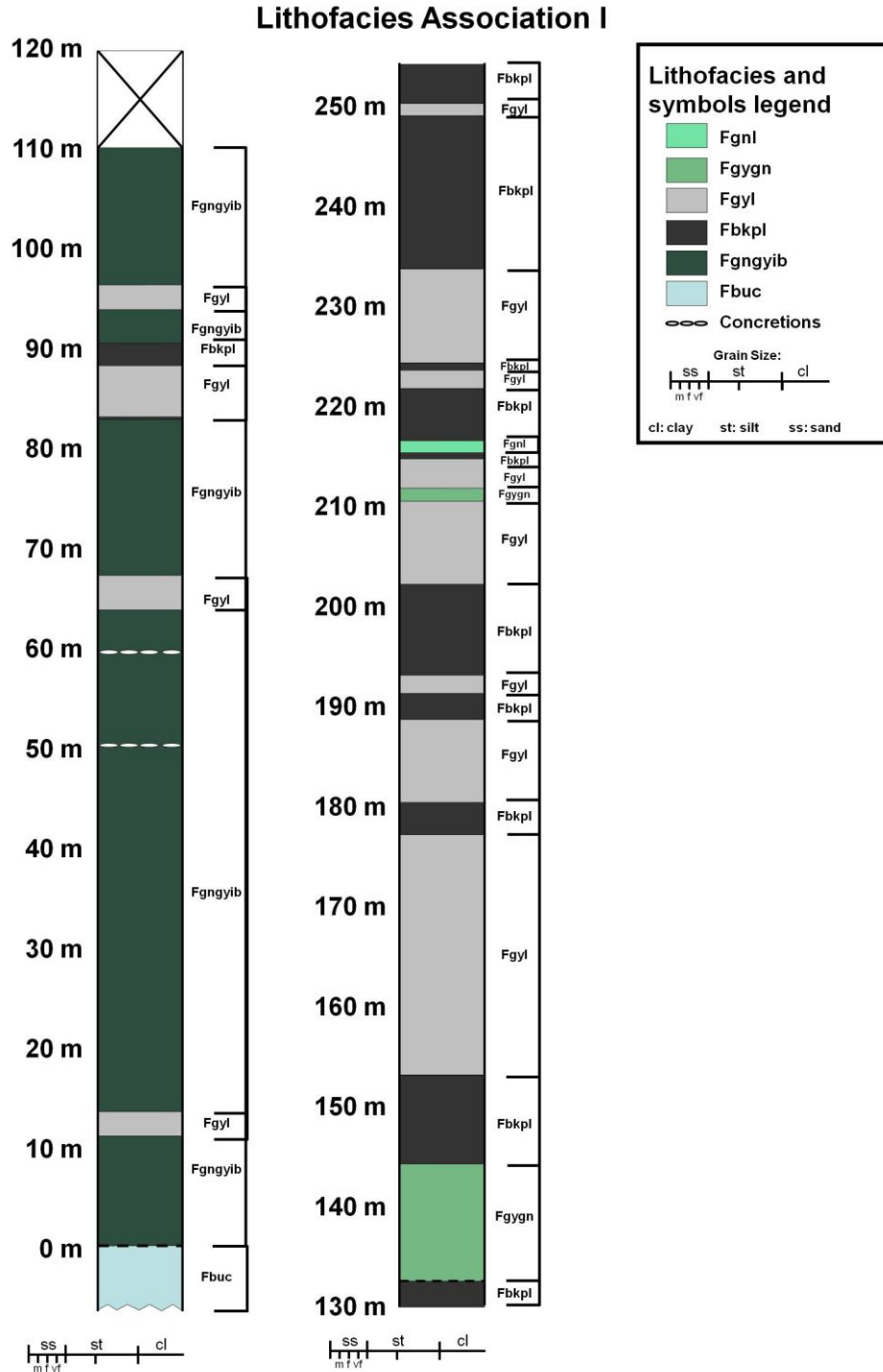
Fig. 3.6: Stratigraphic column of Lithofacies Association I (Site 5). Large exposure of this lithofacies association allowed a near complete section of Lithofacies Association I that was observed to be in conformable contact with Lithofacies Association II. This stratigraphic column was constructed from only Site 5 and did not contain any occurrence of lithofacies *Fgnc*. Other occurrences of Lithofacies Association I were also located at Sites 1, 11, and 13.

contact as observed in drill core from the Plymouth Fe-Mn deposit. Roberts and

Prince (1990) identified the mineralogy of lithofacies *Fgnc* as chlorite

($[Fe,Mg_5Al][AlSi_3]O_{10}[OH]_8$), muscovite, and epidote

($(Ca_2)(Al_2Fe)(Si_2O_7)(SiO_4)O(OH)$) with secondary, overprinting, replacement

calcite, and minor fine-grained disseminated pyrite.

Lithofacies *Fgngyib* is largely composed of interbedded laminated

noncalcareous green siltstone and dark grey mudstone that has, by appearance, a

tiger-striped pattern that is easily identified in both outcrop and drill core (Sites 1, 5,

11, and 13). Locally it contains rare occurrences of concretions. The green siltstone

beds are composed of silt-sized chlorite, muscovite, and quartz, whereas the dark

grey siltstone beds are composed of mud-sized muscovite, quartz, and clay-sized

framboidal pyrite.

Upsection, lithofacies *Fgyl* is composed of grey noncalcareous silt-sized

quartz, feldspar, muscovite, and clay-sized framboidal pyrite. *Fbkpl* is composed of

black, pyritic mudstone beds that contain disseminated framboidal pyrite and

overprinting euhedral pyrite-chalcopyrite (Figs. 3.7, 3.8, 3.9). The black mudstone

contains lenticular bedding, local parallel lamination, and concretions ranging from

a few millimetres to several decimetres in diameter, but no biogenic structures are

present.

Greyish-green siltstone (lithofacies *Fgygn*) is composed of finely laminated

layers of mud-sized quartz and minor interbedded framboidal pyrite and

overprinting euhedral pyrite crystals. Locally, trace amounts of overprinting

disseminated subhedral and euhedral pyrite grains occur within beds and within quartz veinlets (Fig. 3.10).

Near Plymouth, New Brunswick (Fig 3.1; Site 5, Site 11), Lithofacies Association I displays at least two episodes of folding (Figs. 3.9, 3.10) that equate to the F_1 and F_2 events discussed in Chapter 2. The first episode of folding is present as S_1 fabrics that are parallel to bedding (S_0 fabrics). The second episode of folding is the S_2 fabrics that appear as kink banding, perpendicular to the S_1 fabrics. These features are visible at both the micro- and macroscale (Fig. 3.9). Locally, kink banding is visible within this lithofacies association, a feature that is observable on larger scale outcrops.

3.3.2   Interpretation:

Hamilton-Smith (1972) described the lower member of the Smyrna Mills Formation to be almost entirely composed of black and grey noncalcareous siltstone with minor green, red, and associated ferromanganiferous siltstone. This statement suggests Lithofacies Association I, recognized in this study, forms part of the lower member of the Smyrna Mills Formation. Although the grain size of this Lithofacies Association remains largely unchanged, the large diversity of lithofacies present suggests an environment that is changing geochemically at the time of deposition. Upsection from Lithofacies Association O, the transition from lithofacies *Sbuc* to lithofacies *Fgnc* suggests a gradual change in the environment of deposition from a carbonate-rich continental shelf to a silicate-rich anoxic shelf environment with occasional high organic input as observed by the amount of grey, black, minor green siltstone beds and lack of oxide-rich red beds.

Fig. 3.7: Photograph of Lithofacies Association I (lower member, Smyrna Mills Formation) in outcrop at Site 5 displaying lithofacies *Fbkpl* in gradual and sharp conformable contacts with lithofacies *Fgyl* and minor *Fgnl*. Hammer for scale.
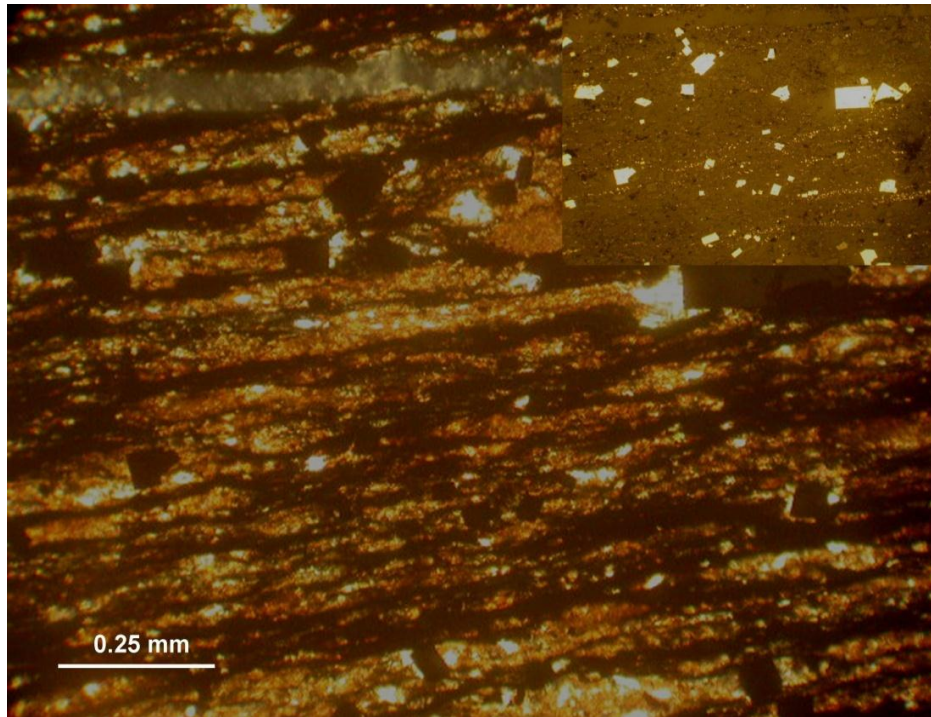
Fig. 3.8: Photomicrograph of lithofacies *Fbkpl* within the Lithofacies Association I (lower member, Smyrna Mills Formation) in transmitted cross polarized light. The top right insert displays the same image within reflected light displaying the distribution of framboidal and euhedral sulfides within the mudstone layers. Located at Site 5; Sample 5-14-S3.
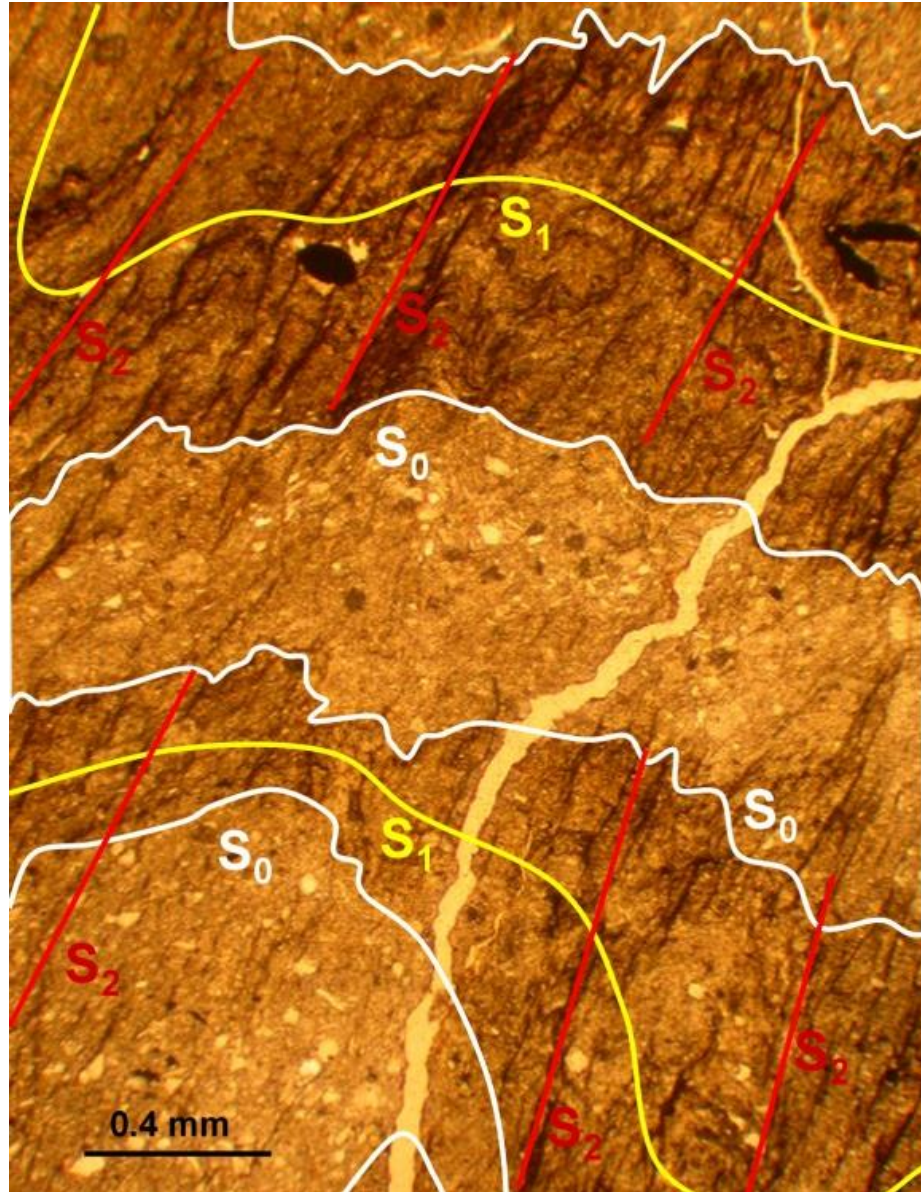
Fig. 3.9: Photomicrograph of the lithofacies *Fgngyib* under transmitted plane polarized light. The green siltstone layers are comprised of fine-grained quartz and muscovite with clasts of quartz and feldspar. S_0, S_1, S_2 fabrics are present within the polished thin section. Minor sulfide mineralization was also associated within this unit that was comprised of diagenetic framboidal pyrite and epigenetic chalcopyrite. Located at Site 5, Sample 5-13-S1.
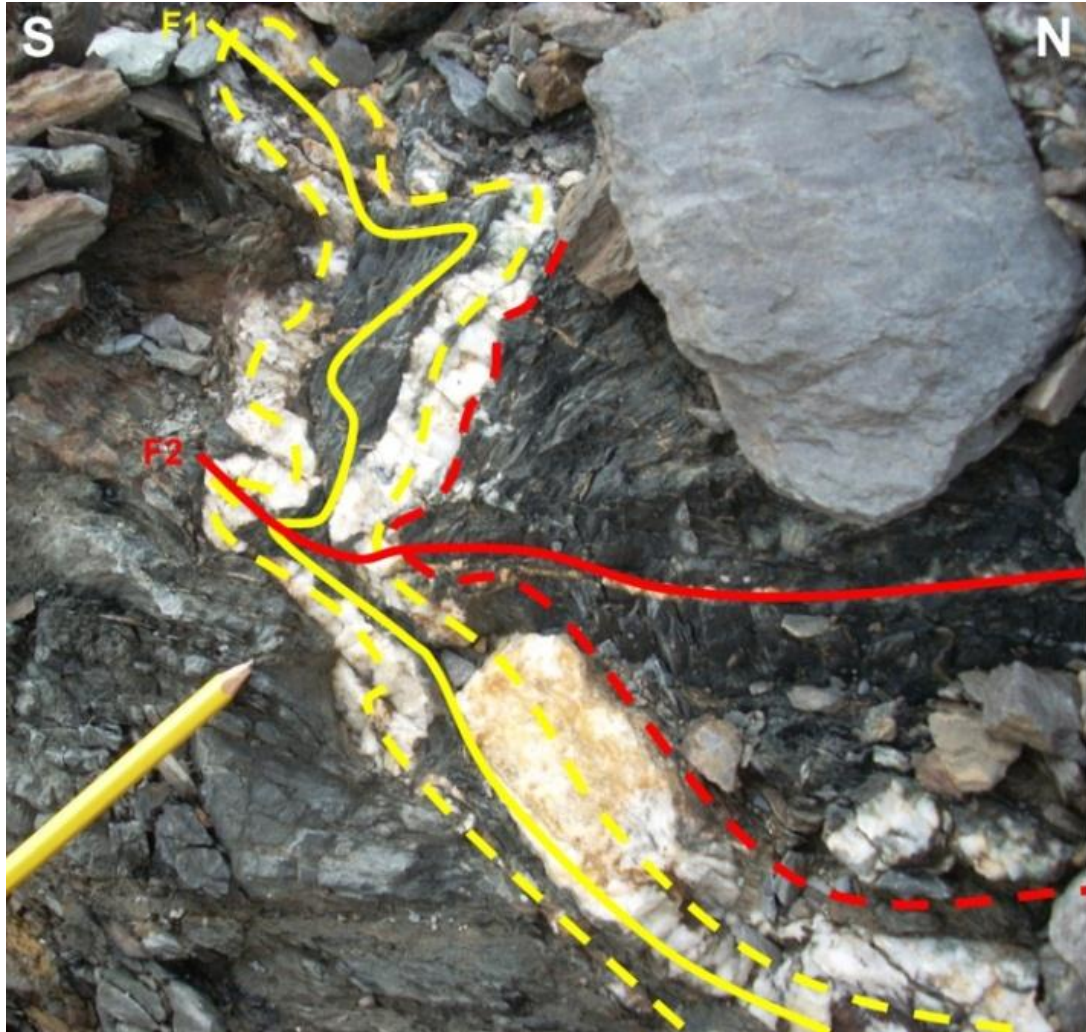
Fig. 3.10: F1 and F2 folds visible within quartz veins present in deformed section of Lithofacies Association I. The largest quartz vein is conformable to the bedding in the dark grey and green siltstone. Located at Site 11. Pencil for scale.

Continuing upsection, the environment of deposition is then largely clay-rich and anoxic with occasional high organic input that resulted in the interbedded green and grey siltstone. The increasing abundance of organic matter and pyrite upsection suggests the organic-rich matter was subject to degradation in sulfate- and iron-reducing conditions. The framboidal pyrite is suggestive of Fe fixation with SO_4^{-2} produced by sulfate-reducing bacteria usually at or below the sediment-water interface during early diagenesis (Berner, 1974; Wilkin and Barnes, 1997). This reaction will be discussed in detail in later chapters. The evidence is consistent with the regional context at the time of deposition where the closure of the Iapetus Ocean would have resulted in restricted ocean circulation allowing for localized ocean anoxia (Fyffe et al., 2011). Massive quantities of organic matter would collect within this continental-shelf environment and be deposited in the form of grey siltstone (*Fgyl*) and black pyritic mudstone (*Fbkpl*).

The deformation of Lithofacies Association I within the Plymouth Fe-Mn deposit is associated with regional subgreenschist grade metamorphism related to the Devonian Acadian Orogeny (Hamilton-Smith, 1972). The quartz veins, which from observation appear to be associated with the D_1 events, are likely associated with some of the Cu and Co anomalies that will be discussed in further detail in Chapter 4.

3.4   Lithofacies Association II

3.4.1 *Description*:

Lithofacies *Fgygn* (Greyish green siltstone), *Fgnl* (Green laminated siltstone

with rare white microspheroidal limestone), *Sgnl,* (Green to grayish green and tan calcareous and noncalcareous massive or laminated sandstone) and minor *Fgnz* (Dark green to black mineralized siltstone), *Fgyl* (Grey and minor greenish laminated siltstone), *Fbkpl* (Black pyritic mudstone) and *Frmz* (Red and maroon mineralized siltstone), collectively comprise Lithofacies Association II (Fig. 3.11). Lithofacies *Fgygn* dominates, with increasing interbeds of lithofacies *Fgyl* and *Fgnl* and minor increase in interbeds of *Sgnl, Fbkpl,* and *Fgnz* upsection. Collectively, Lithofacies Association II in the Route 95 study area is estimated to be at least 279 m thick.

Lithofacies *Fgygn* and *Fgnl* are more common than in Lithofacies Association I. Both locally contain interlaminations of greyish green to green siltstone. Their mineralogy is largely composed of composite and single grains of quartz, muscovite clasts with minor amounts of calcite, detrital hematite and trace framboidal pyrite. Lithofacies *Fgnl* overall contains more chlorite and less pyrite than lithofacies *Fgygn* (Fig. 3.12). Minor calcite associated with lithofacies *Fgnl* appears to only be localized as white, non-fossiliferous, microspheroidal carbonate laminae (Figs. 3.13, 3.14, and 3.15) and is found stratigraphically beneath beds of Fe-Mn mineralization that are discussed in later chapters. The white carbonate laminae are often interbedded with zoned pyrite (Figs. 3.16A & B) and are found in outcrop at Sites 1, 12, and 14, and in drill core from the Plymouth Fe-Mn deposit. These beds of carbonate laminae are approximately 1 to 3 cm-thick with a grain-size ranging from 0.05 to 1.0 mm.
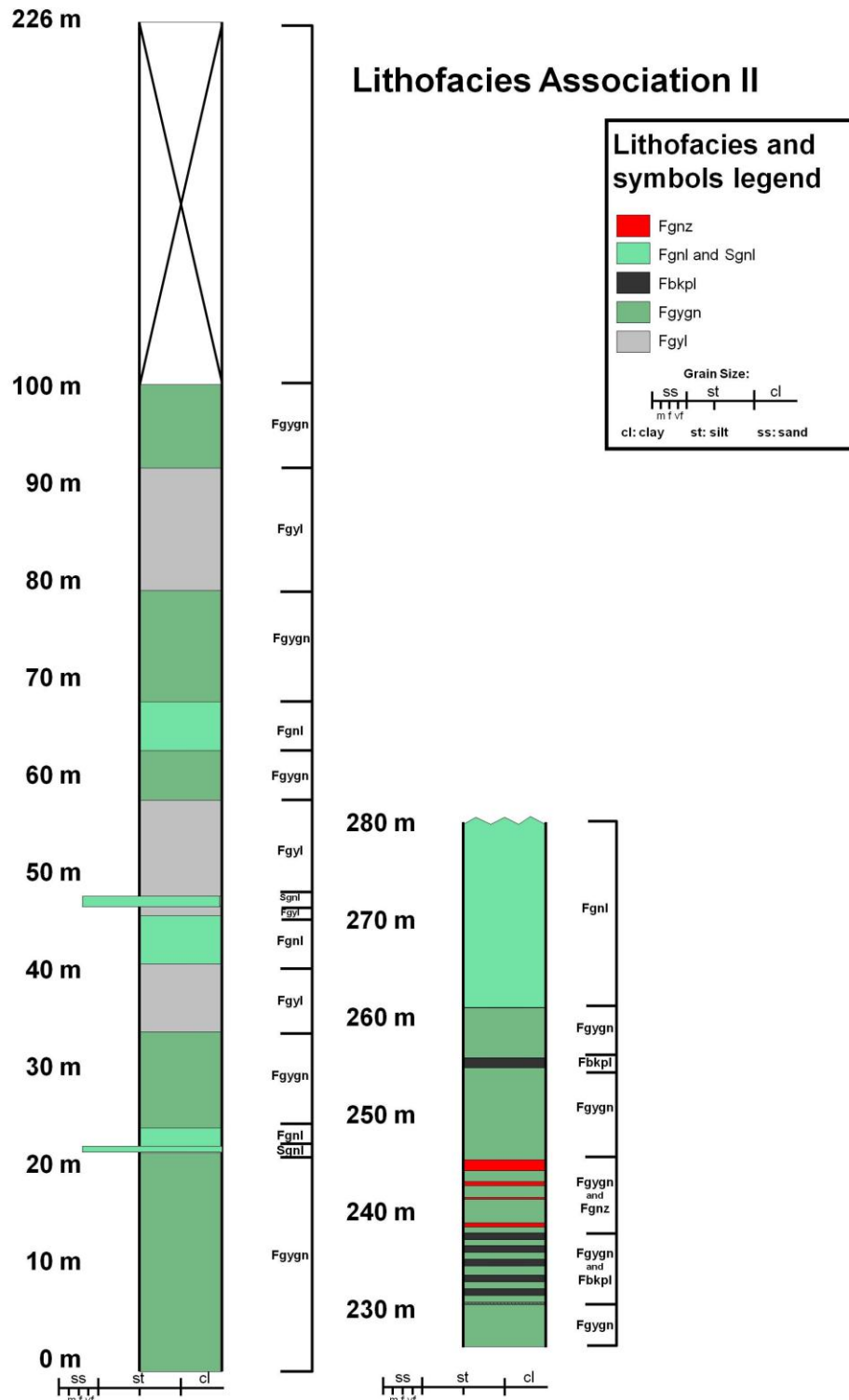
Fig. 3.11: Stratigraphic section of Lithofacies Association II (lower member, Smyrna Mills Formation) present within the Route 95 study area that is a composite section of Sites 5 and 14. The leftmost column is Site 5 and the rightmost column Site 14. Some areas of Fe-Mn mineralization were present within this Lithofacies Association.

Fig. 3.12: Green siltstone beds associated with lithofacies *Fgnl* of Lithofacies Association II (lower member, Smyrna Mills Formation) present in an outcrop 1 km southeast of Plymouth, New Brunswick (Site 5). Hammer for scale.

Fig. 3.13: Photograph of a lithofacies *Fgnz* (Fe-Mn oxide-silicate-carbonate mineralized beds) present within Lithofacies Association II (lower member, Smyrna Mills Formation) approximately 1.5 km southeast of Plymouth, NB at Site 14. Field notebook for scale.
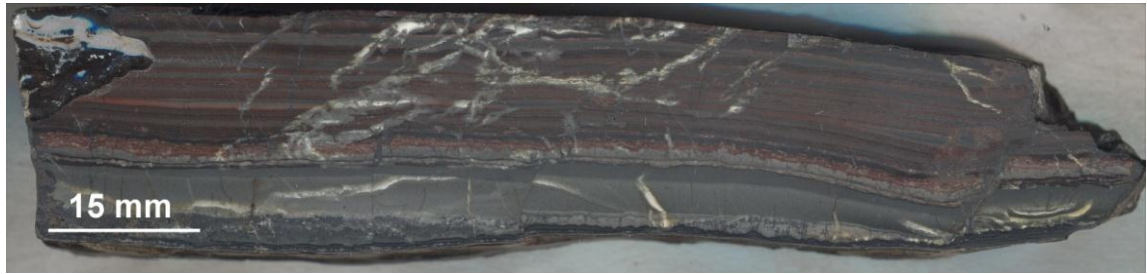
Fig. 3.14: Photograph of a polished slab of lithofacies *Fgyl* in sharp conformable contact with lithofacies *Fgnz* (Fe-Mn-oxide-silicate-carbonate) approximately 1.5 km southwest of Plymouth, New Brunswick. This is a sample from the lower member of the Smyrna Mills Formation at Site 14. Sample 5X-2.
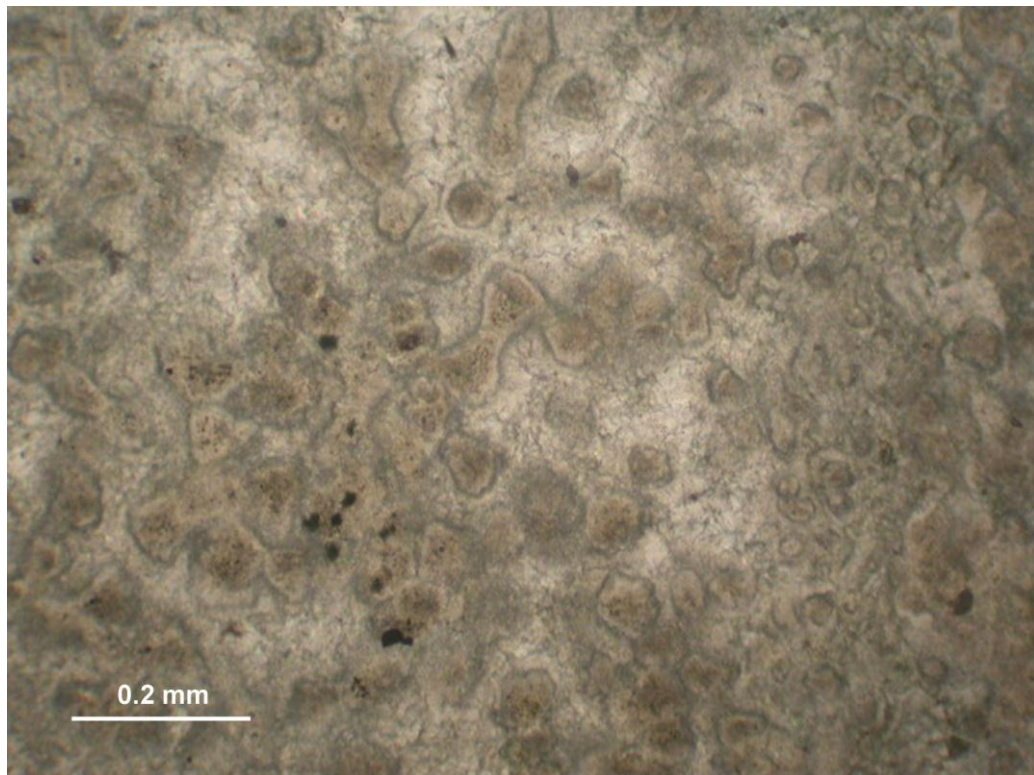
Fig. 3.15: Photomicrograph of a microspheroidal limestone bed in lithofacies *Fgnl* from the South Hartford deposit in transmitted plane polarized light. This sample was taken from Site 12, but similar samples were also found at Sites 1, and 14. Sample 1-SH-5.
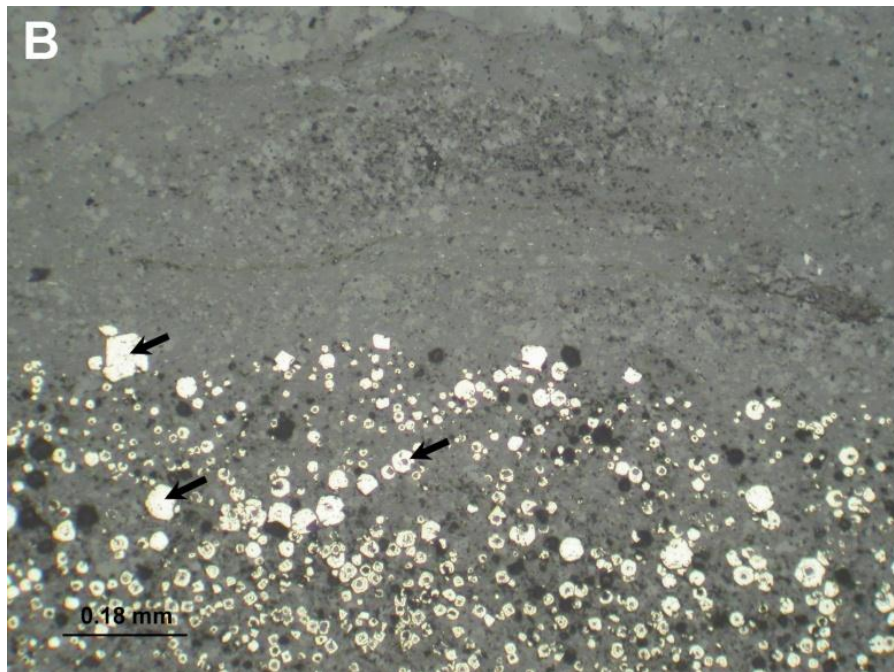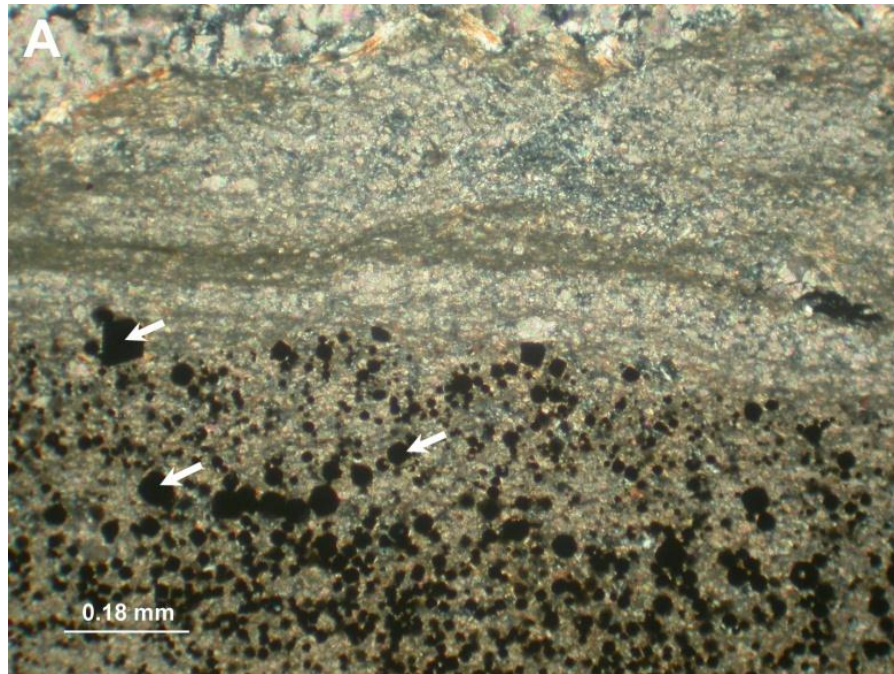
Figs. 3.16A & B: Photomicrographs of zoned pyrite crystals in a matrix of calcite from a rare carbonate-rich section of lithofacies *Fgnl* in Lithofacies Association II (lower member, Smyrna Mills Formation) in transmitted cross-polarized light (A) and under reflected light plane-polarized light (B). These microspheriodal limestone beds are located stratigraphically below beds of Lithofacies *Fgnz* (Fe-Mn oxide-silicate-carbonate). Arrows are pointing to the same corresponding pyrite crystals in both photomicrographs. Located at Site 1; Sample 1-4-S9.

Lithofacies *Fgnz* is a dark green to black Fe-Mn oxide-silicate-carbonate mineralized siltstone and represents the first of the two Fe-Mn mineralized lithofacies associated with the Woodstock Fe-Mn deposits. In general, this Fe-Mn mineralized siltstone occurs only within Lithofacies Association II. However, in both outcrop (Sites 9, 12, 13 and 16) and drill core occasionally lithofacies *Fgnz* is found interbedded with lithofacies *Frmz* (Red and maroon Fe-Mn-oxide-carbonates), in Lithofacies Associations II and III (lithofacies *Frmz* is much more common in Lithofacies Association III). The Fe-Mn mineralized beds in lithofacies *Fgnz* are commonly composed of silt-sized magnetite, chlorite, Fe-Mn silicates, and rhodochrosite (Fig. 3.11, Table 3.1) and will be discussed in further detail in Chapter 4.

Lithofacies *Sgnl* is composed of green sandstone locally with parallel-laminated bedding and appears only as a minor lithofacies with increasing thickness upsection. Compositionally it contains sand-sized grains of chlorite, quartz, and muscovite, with minor dolomite ($CaMg(CO_3)_2$), and pyrite, similar to lithofacies *Fgnl*.

3.4.2   *Interpretation*:

Lithofacies Association II is generally found to occur on top of Lithofacies Association I within the study area. The presence of lithofacies *Fgnz* (Fe-Mn oxide-silicate-carbonate) interbedded with *Fgygn* and rarely with *Frmz* (Fe-Mn oxide-carbonate) suggests that Lithofacies Association II forms part of the lower member of the Smyrna Mills Formation as described by Hamilton-Smith (1972). A stratigraphic section of Lithofacies Association II displays an increase in thickness

of lithofacies *Fgyl, Fgnl, Fbkpl* and *Sgnl* with a decrease in *Fgygn* upsection. The increased thickness of grey and green, compared to grayish green fine-grained lithofacies may be associated with rapid changes in organic content of the sediment, while an anoxic environment of deposition prevailed. The appearance and subtle increase in the coarser lithofacies *Sgnl* upsection until 47 m within the 279 m stratigraphic section may be associated with a change in the strength of the transporting medium that in turn may be related to greater storm-wave depth, or near proximity to a river mouth, and thus a nearer to shore setting than Lithofacies Association I. However, the lack of green sandstone beds continuing upsection in Lithofacies Association II could also suggest that environment of deposition does not continue getting shallower. The minor occurrences of lithofacies *Fbkpl* interbedded with lithofacies *Fgygn,* exclusive of areas proximal to ferromanganiferous strata, suggests much lower relative rates of organic matter input or preservation and only minor fractionation of Fe^{2+} from the water column or pore waters took place compared to that in Lithofacies Association I.

The green colour in many of the siltstone beds (lithofacies *Fgnl, Fgygnl,* and *Fgnz)* is caused by chlorite that forms as pore-fillings and as grain coatings (Grigsby, 2001). At Sites 1, 12, and 14, the presence of zoned euhedral pyrite, where the centre existed initially as organic carbon (Lougheed, 1983), within microspheroidal carbonate laminae suggests bacterial breakdown of pre-existing organic matter in the substrate prior to the deposition of the overlying Fe-Mn oxide-silicate-carbonate mineralized zone (Lougheed, 1983). The breakdown of organic matter would have strongly influenced the Eh and pH of the seawater producing a

more anoxic environment. Although the microspheroids are observed to be non-fossiliferous, these might be the remains of organic-rich carbonates that were chelated by bacteria and associated with the changes in redox responsible for precipitation of Fe-Mn mineralization. An SEM and carbon isotope analysis is recommended for these microspheriodal carbonate laminae, if further research on the origin of the Fe-Mn deposits is pursued.

Within the regional setting of Lithofacies Association II, the closure of the Iapetus Ocean may have first resulted in localized ocean anoxia that was accelerated by the input of organic matter (Fyffe, et al., 2011).

3.5   Lithofacies Association III

3.5.1 Description:

Lithofacies Association III (Fig. 3.17) is comprised predominately of lithofacies *Frml* (Red and maroon siltstone) with increasing interbeds of *Sgnl* (Green to greyish green and tan calcareous and non calcareous massive or laminated sandstone) that increase in thickness from 5 to 15 m (Fig. 3.17), and decreasing interbeds of *Fgnl* (Green laminated siltstone with rare white microspheroidal limestone) upsection. Lithofacies *Frmz* (Red and maroon mineralized siltstone) is also present as local Fe-Mn mineralized zones. Only one outcrop (Fig. 3.1; Site 6) of Lithofacies Association III is located on Route 95 (Fig. 3.18) with a long lateral cross-section that runs a length of 73 m within a tight anticline (Hamilton-Smith, 1972; Figs. 3.1 & 3.2). Overall, the outcrop has a calculated thickness of 15 metres along Route 95. To the northeast of the Route 95
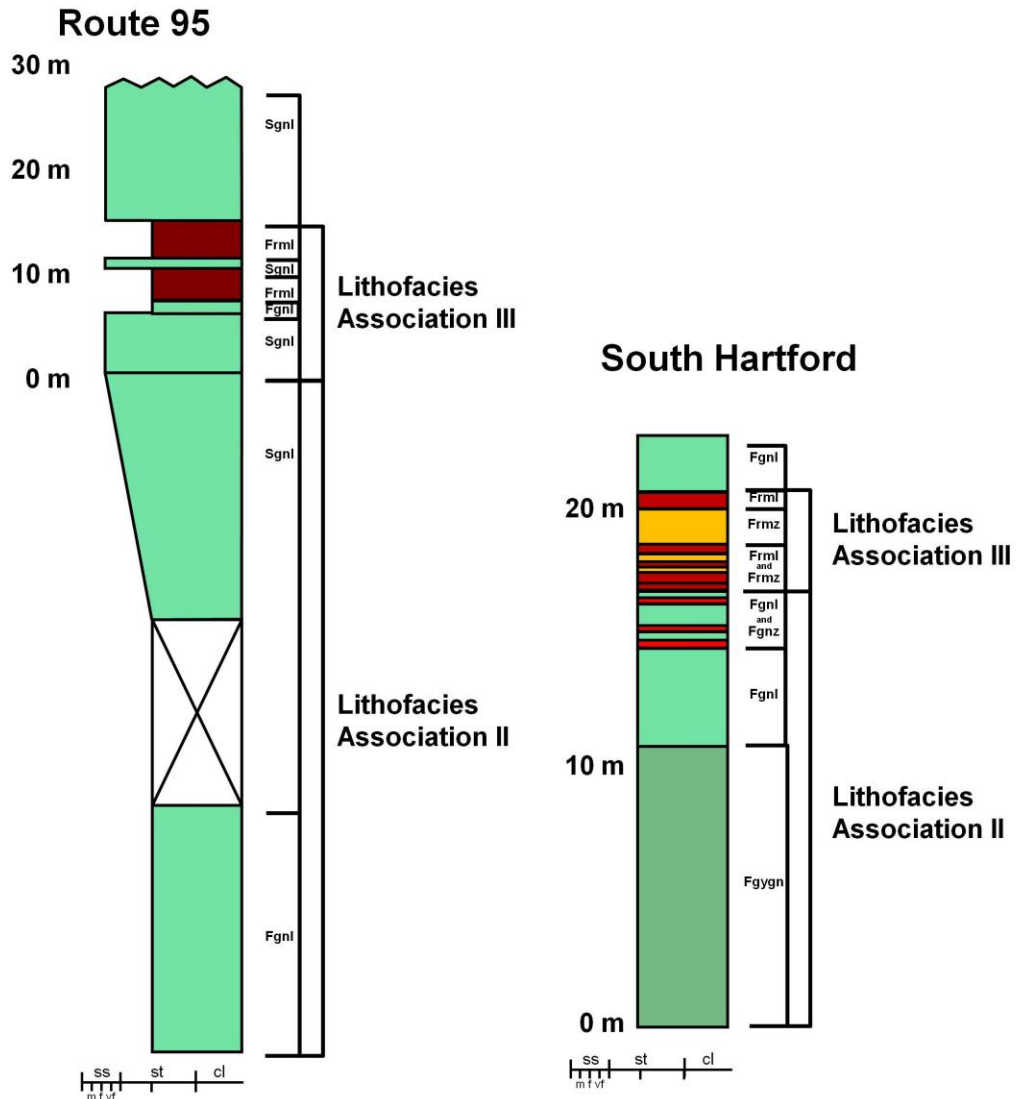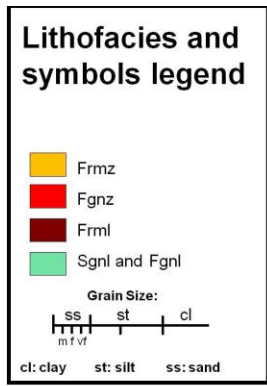
Fig. 3.17: Example stratigraphic section of Lithofacies Association III (lower member, Smyrna Mills Formation) from the Route 95 (Site 6) study area and from a Fe-Mn mineralized section from the South Hartford Fe-Mn deposit (Site 12). Fe-Mn mineralization was also present outcrops northeast of Plymouth (Sites 9, 13 and 14).

Fig. 3.18: Lithofacies *Frml* at Site 6 forming part of Lithofacies Association III (lower member, Smyrna Mills Formation). Hammer for scale.

study area, it is observable at several outcrop localities (Sites 6, 9, 12, 13, 16). These are proximal to areas of major Fe-Mn mineralization and are associated with Plymouth, North Hartford, South Hartford, and Iron Ore Hill deposits (Figs. 2.2, 3.1) (Sidwell, 1957, 1964; Hamilton-Smith, 1972; Roberts and Prince, 1990).

Lithofacies *Frml* is composed of arenaceous red and maroon siltstone that is locally massive, rarely amorphous, with locally parallel and lenticular laminations and small-scale asymmetrical cross-bedding indicating tops to the northeast. The groundmass of lithofacies *Frml* is dominated by grains of quartz, muscovite, and feldspar (Figs. 3.19 & 3.20A & B).

Lithofacies *Frmz* is composed of red and maroon microbanded Fe oxides and Fe-Mn carbonates and forms part of the Fe-Mn mineralized sequence that will be discussed further in Chapter 4. While a majority of outcrops that expose lithofacies *Frmz* are encrusted in a surface coating Fe-Mn hydroxide (Sites 9, 12, 13, 14), some of lithofacies *Frmz* remains relatively unweathered. Although similar to lithofacies *Frml*, lithofacies *Frmz* differs somewhat in appearance and mineralogy and occurs within several outcrops outside of Route 95 at Sites 9 and 12 northeast of Plymouth (Fig. 3.1). It is possible that this unweathered section of lithofacies *Frmz* also forms part of the Fe-Mn mineralization sequence that will be discussed further in Chapter 4. Under transmitted light samples 9-16-S2 and IRH-01 (Sites 9 and 16) contain generally higher concentrations of opaque minerals that are mostly comprised of finely disseminated hematite. Locally, near Hartford, New Brunswick (Fig. 3.1; Site 9) red, very fine crystalline beds contain clasts of coarse silt-sized feldspar and coarse sand-sized clasts of composite quartz (Figs. 3.20A &
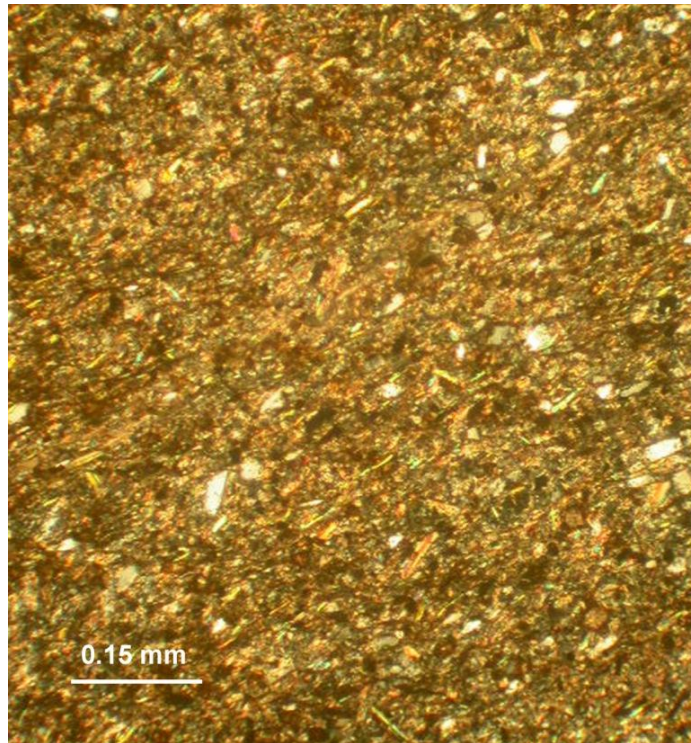
Fig. 3.19: Photomicrograph arenaceous siltstone of lithofacies *Frml* under transmitted cross polarized light from Richmond Corner, NB (Site 6). The mineralogy within these lithofacies is dominated by quartz and muscovite, with minor hematite. The red and maroon colour within the siltstone associated with Lithofacies Association III (lower member, Smyrna Mills Formation) is caused by the presence of the finely disseminated hematite. Located at Site 6; Sample 6-10-S6.
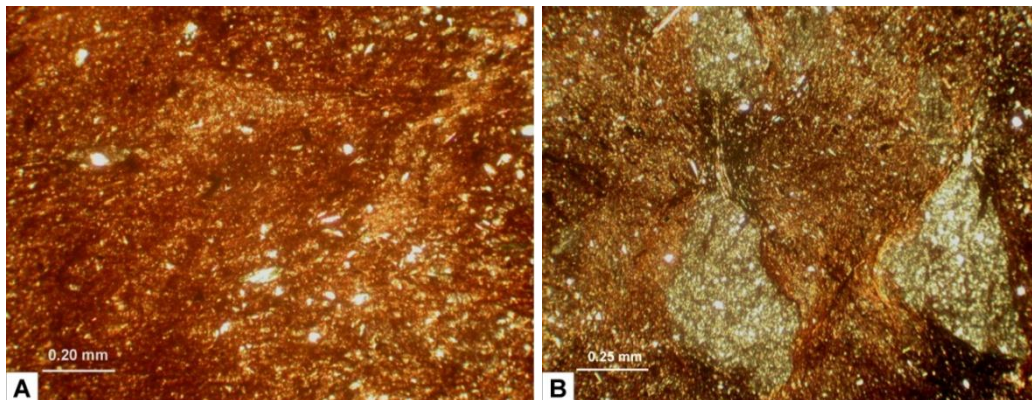
Fig. 3.20: (A) Photomicrograph very fine crystalline beds from lithofacies *Frmz* under transmitted cross polarized light displaying fine-grained manganiferous siltstone within coarse silt-sized clasts of feldspar. (B) Coarse sand-sized clasts of composite quartz within maroon red very fine crystalline beds. These very fine crystalline beds are proximal to areas of Fe-Mn oxide-carbonate mineralization within the North Hartford Fe-Mn Deposit at Site 9. Sample 9-16-S2.

73

B). Beds of massive red siltstone and 1 to 1.5 m thick beds of manganiferous hematite are also present at this location that will be discussed further in Chapter 4.

3.5.2 Interpretation:

Lithofacies Association III, in general, is found to occur stratigraphically on top of Lithofacies Association II, but this is not always apparent in core and outcrop due to folding. Interbedding of Lithofacies Associations II and III also occurred during deposition. The presence of lithofacies *Frml* and *Frmz* with occasional lithofacies *Fgnz* in the Plymouth area suggests that this association is part of the lower member of the Smyrna Mills Formation (Hamilton-Smith, 1972). Hamilton-Smith (1972) indicated Fe-Mn mineralization proximal to the location of the outcrop on Route 95 (Fig. 3.1; Site 6), but no Fe-Mn mineralization was recognized in the roadcut other than finely disseminated hematite mineralization that contributes to the colour of the red and maroon siltstone. The small-scale asymmetrical cross-bedding in the red and maroon siltstone indicates a tops direction to the northeast that is consistent with previous measurements taken by Sidwell (1957) and Hamilton-Smith (1972).

The increasing abundance of sand upsection may relate to increased strength of the transporting medium than previously, and associated with either greater storm-wave depth, lowered sea-level, or closer proximity to the base of a delta or fan slope and (or) river mouth. The large thickness, high Mn content, and microbanding of Fe oxides and Fe-Mn carbonates of lithofacies *Frmz* further suggests a shallower setting, it being the most oxygenated environment of deposition of the Lithofacies Associations (van der Weijden, 1992).

The interbedding of lithofacies *Sgnl* and *Frml* (Sidwell, 1957; Anderson, 1968; Roberts and Prince, 1990) also suggests an intermittently oxic environment. The silt-sized grains associated with lithofacies *Frmz, Frml,* and *Fgnl* suggests that the sediment is derived from either a distal source or a proximal source containing fine-grained sediment (Roberts and Prince, 1990). In the regional context, an early Salinic regression (Fyffe et al., 2011) would have exposed more offshore parts of the continental shelf to mixing by waves, allowing for increased oxygenation of the shelf.

3.6   Lithofacies Association IV

3.6.1   *Description:*

Lithofacies Association IV (Fig. 3.21) is predominately composed of lithofacies *Fgygn* (Greyish green siltstone), but becomes increasingly interbedded with lithofacies *Sgnl* (Green to grayish green and tan calcareous and noncalcareous massive or laminated sandstone), and *Sgyce* (Grey laminated, asymmetrically cross-laminated, bioturbated, or massive sandstone) and decreasing interbedded Fgnl (Green laminated siltstone with rare white microspheroidal limestone) upsection. It also has a generally calcareous composition in particular within lithofacies *Sgyce*. bioturbated sediments.

This Lithofacies Association differs from Lithofacies Associations II, and III by the absence of a Fe-Mn mineralized lithofacies, lack of lithofacies *Fbkpl*, generally calcareous composition, and an increase in observed bedding features and
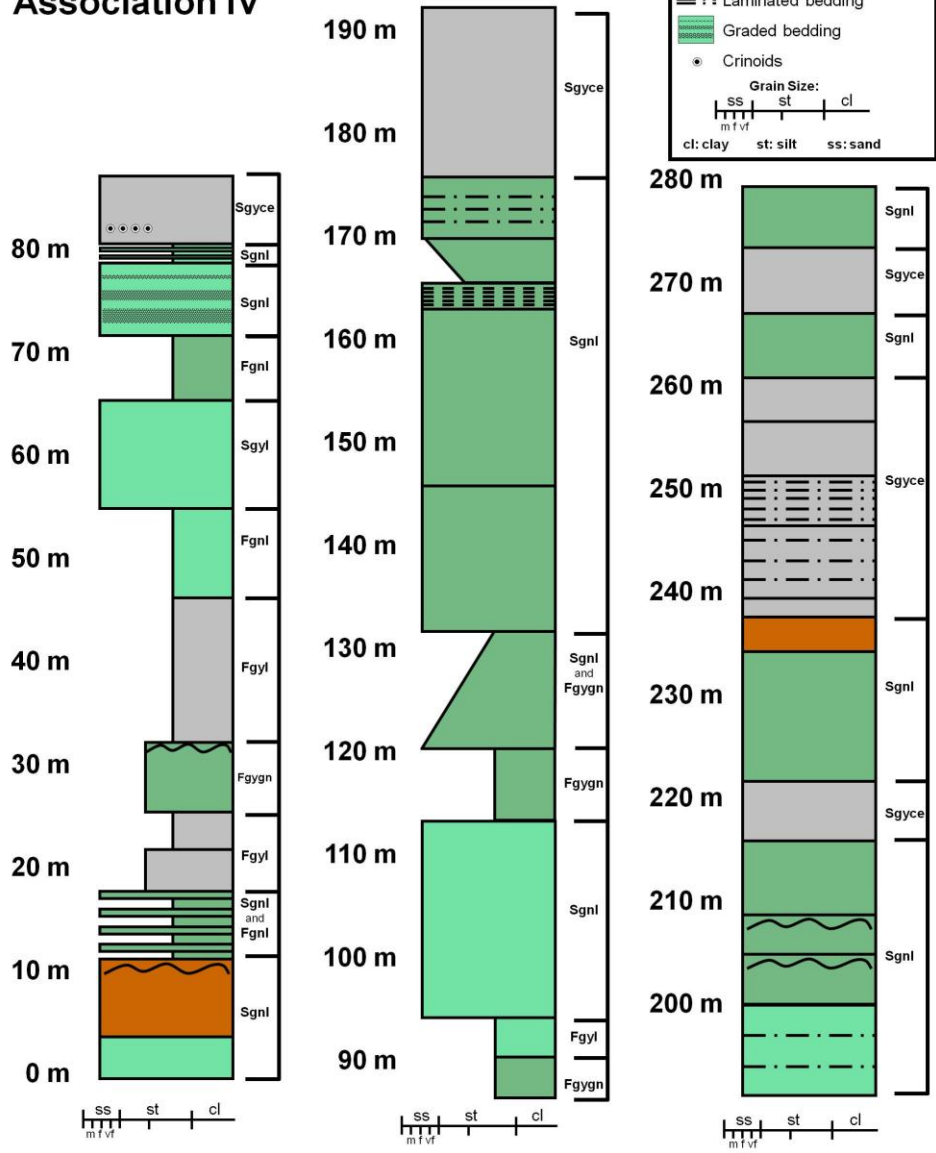
Fig. 3.21: A composite stratigraphic section of Lithofacies Association IV composed of Sites 4 and 8 as present within the Route 95 study area. This Lithofacies Association located at Sites 2, 4, 8) and was largely composed of lithofacies *Sgyce, Sgnl, Fgnl,* and *Fgygn* that occasionally contained asymmetrical ripple marks, graded and laminated bedding and minor cross-bedding with rare fossil and trace fossil horizons. The trace fossil horizons were found in the talus piles and not in outcrop.

Lithofacies *Sgyce* is composed of calcareous grey to grayish green parallel laminated, asymmetrically cross-laminated (ripple marked), cross-bedded, or massive sandstone beds with bases that may be intruded with flame structures (Fig. 3.21). Locally it is bioturbated and locally contains macrofossil hash (Fig. 3.22). In the talus (and locally in outcrop) of lithofacies *Sgyce* are rare crinoid stems and *Helminthopsis isp.* that were observed by the author (Fig. 3.22). It is composed of composite and monomictic quartz, muscovite, chlorite, carbonate, and detrital hematite with rare carbonate ghost structures present in the carbonates (Fig. 3.23).

Lithofacies *Sgnl* within Lithofacies Association IV is calcareous to noncalcareous in composition and is composed of massive and laminated green and locally tan coloured (possibly dolomitic) sandstone beds with local asymmetrical ripple marks preserved (Fig. 3.21), and flame structures with occasional crinoidal hash. It is composed of quartz, chlorite, calcite, dolomite, with trace pyrite and hematite.

Lithofacies *Fgnl* and *Fgygn* within Lithofacies Association IV appear to be noncalcareous in composition and do not contain the white carbonate beds that were observed in Lithofacies Association II.

3.6.2   *Interpretation:*

The presence of crinoidal stems within lithofacies *Sgyce* (Fig. 3.22) and *Sgnl* confirms that Lithofacies Association IV was deposited in a marine environment. The increase in thickness of 10 to 20 m thick interbeds of lithofacies *Sgyce* and *Sgnl* upsection from 55 to 280 m suggests a more predominantly high energy transporting medium. The increase in local bioturbated sandstones, and general

Fig. 3.22: Photograph of crinoid stems visible within an outcrop of lithofacies *Sgyce* in upper member, Smyrna Mills Formation near Richmond Corner, NB. Pencil for scale.
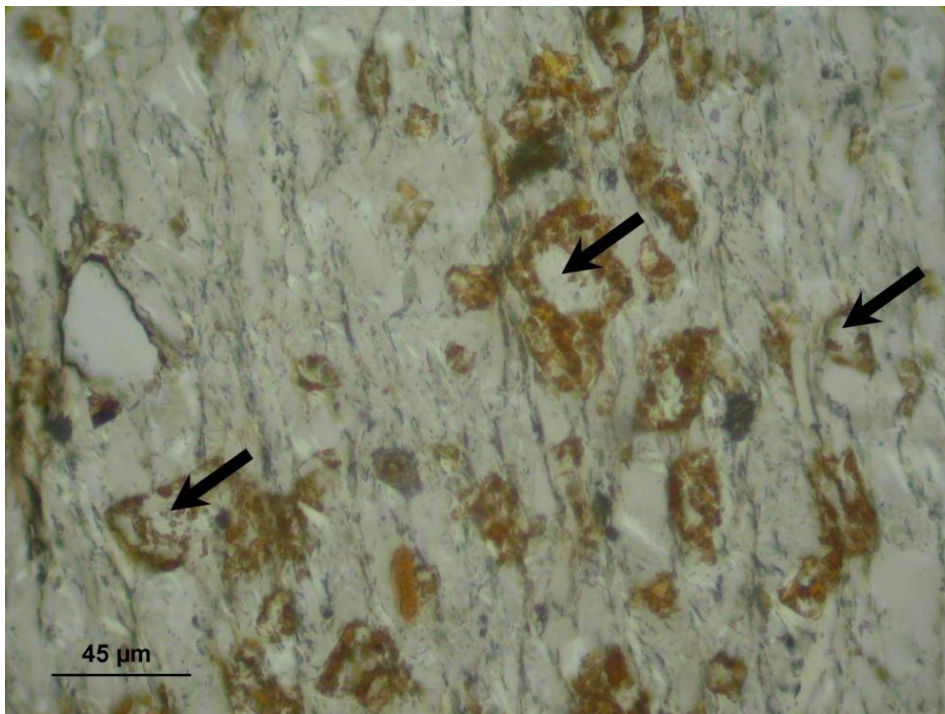
Fig. 3.23: Photomicrograph of ghost structures present in carbonate minerals present in Lithofacies Association IV in plane polarized light (upper member, Smyrna Mills Formation). Site 2; Sample 2-5-S5.

calcareous composition are characteristic of the upper section of the offshore zone on the continental shelf (Nichols, 2009).

Asymmetrical ripple marks and minor centimetre-scale cross-bedding within fine-grained sedimentary rocks that contain marine fossils are associated with unidirectional currents which may be associated with ocean currents, turbidites, and (or) at the base of a delta front. The fining-up beds, which are abundant in lithofacies *Sbuc* and *Fbuc* of Lithofacies Association O (Fig. 3.3), do not occur within Lithofacies Association IV suggesting that the asymmetrical ripple marks are not caused by turbidites. Since the sediment within these lithofacies is well sorted, with no angular-shaped boulders, these primary sedimentary structures are likely associated with unidirectional marine currents, or waning fluvial currents beyond a river mouth.

Lithofacies *Sgyce* and *Sgnl* may suggest Lithofacies Association IV was deposited in an offshore shelfal marine environment. This is also consistent with the presence of microbanded Fe-Mn mineralized lithofacies Fgnz and Frmz in Lithofacies Associations II and III. In marine environments Fe-Mn deposits are known to occur only in depositional environments associated with a continental shelf, volcanic centres, or deep-sea abyssal plains that will be discussed further in Chapter 6. The increase in lithofacies *Sgyce* and *Sgnl* is characteristic of and is only associated with Lithofacies Associations IV and V of the upper member of the Smyrna Mills Formation (Hamilton-Smith, 1972). The upper member of the Smyrna Mills Formation is interpreted by Fyffe et al. (2011) to have formed during the late Salinic regression.

Ghost structures of microspheroidal carbonates are present in several of the carbonate crystals within Lithofacies Association IV. This suggests these were initially deposited as microspheroids of carbonate (Fig. 3.23). The euhedral carbonate crystals that form a crystal mosaic within Lithofacies Association IV suggest that these were the primary cements at the time of deposition. Similar diagenetic euhedral carbonate minerals are locally present in carbonate-rich iron formations within Precambrian continental shelf deposits (Lougheed, 1983). This may suggest a similar continental shelf setting for the Woodstock Fe-Mn deposits.

3.7   Lithofacies Association V

3.7.1   Description:

Lithofacies Association V (Fig. 3.24) is predominantly of *Fgyl* (Grey and minor greenish laminated siltstone) with minor interbedded lenticular 10 cm-thick beds of *Sgyce* (Grey laminated, asymmetrically cross-laminated, bioturbated, or massive sandstone) and increasing interbeds of *Fgygn* (Greyish green siltstone) upsection and a calculated thickness of at least 90 m. Lithofacies *Sgyce* comprises angular to subangular fragments of feldspar and quartz (Fig. 3.25). Calcite and other carbonate minerals are mostly confined to quartz-carbonate veins and veinlets. Lithofacies *Fgyl* and *Fgygn* are the same compositions as described earlier within this chapter.

Overall Lithofacies Association V is similar in appearance to Lithofacies Association II, but differs in the lithofacies present since it does not contain lithofacies *Fgnz.* This lithofacies association also displays a general fining-up

Lithofacies Association V
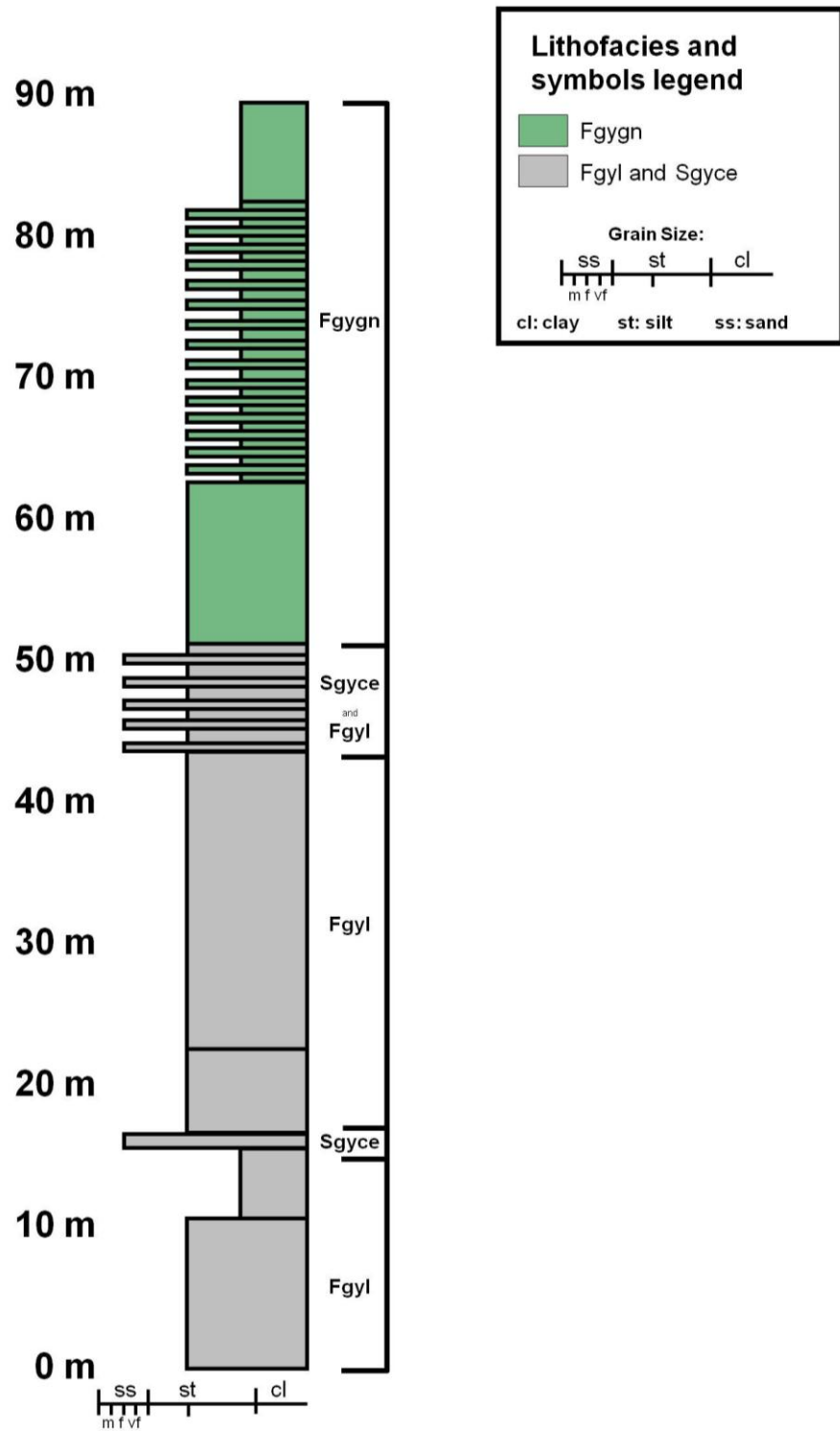
Fig. 3.24 Stratigraphic section of Lithofacies Association V as present within the Route 95 study area (Site 3).
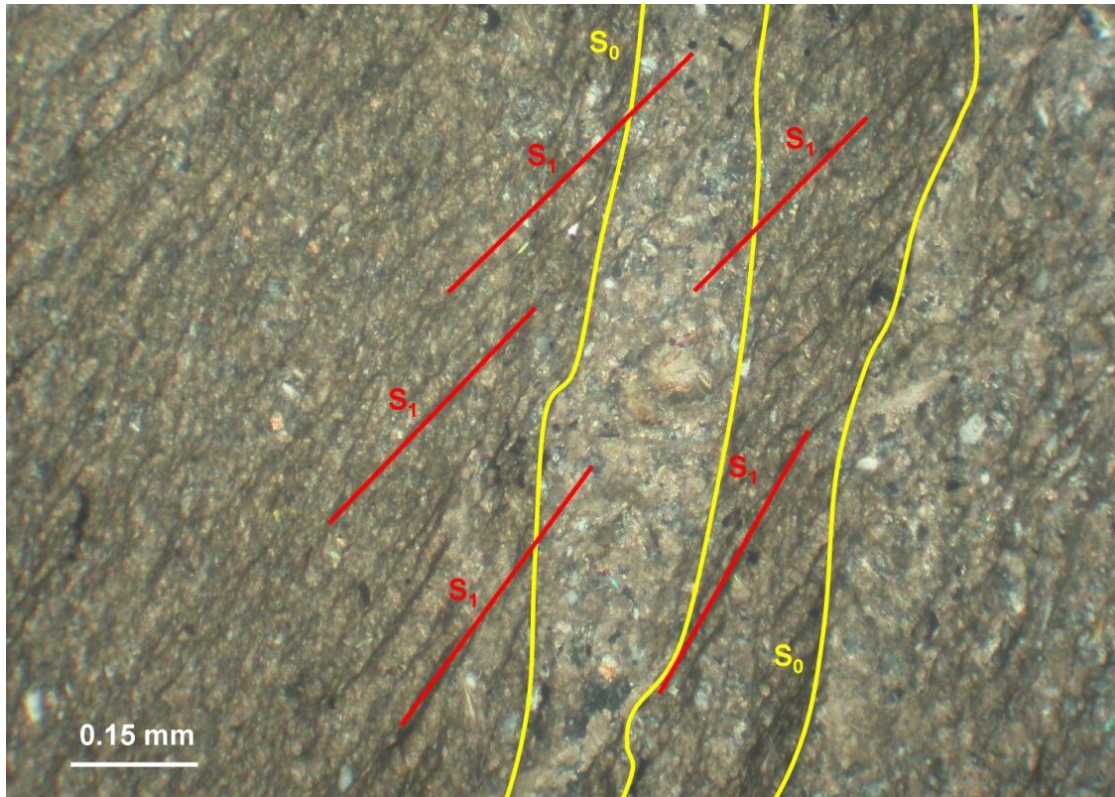
Fig. 3.25: Photomicrograph of interbedded lithofacies *Fgyl* and *Sgyl* within Lithofacies Association V under cross polarized light. Lithofacies *Sgyl* is dominantly composed of clasts of quartz and feldspar. The feldspar clasts often contained crystalline mafic minerals and euhedral feldspar suggesting the source of sand-sized material was highly immature and derived from an igneous provenance. Two S fabrics were present within this sample. Sample 1-2-S6 (upper member, Smyrna Mills Formation).

succession (Fig. 3.24).

3.7.2   Interpretation:

The increase in interbeds of lithofacies *Fgygn* upsection suggests a decrease in both the energy of the transporting medium and in organic content. This could relate to an increase in water depth upsection. The lack of lithofacies *Frml* and *Frmz* suggest that it was an anoxic environment. Many of the feldspar fragments contain inclusions of euhedral quartz and mafic minerals suggesting that these sedimentary layers are derived from an igneous provenance. The general fining-up succession present with this lithofacies association in contrast to the coarsening-upward sequence of Lithofacies Association IV suggests that this is a deepening sequence within the Smyrna Mills Formation (Howard, 1978).

3.8   SUMMARY

In outcrops along Route 95, and west of Woodstock, there are six identified lithofacies associations (Tables 3.1 and 3.2). The first five lithofacies associations, which generally occur sequentially with each other in the study area, are interpreted as an overall general shallowing-upward marine sequence on a cratonic margin (Appendix I).

CHAPTER 4

MINERALIZATION OF FERROMANGANIFEROUS STRATA AND ASSOCIATED MINOR

BASE METALS WITHIN THE WOODSTOCK FE-MN ORE BODIES

4.1   INTRODUCTION

Drilling on the Woodstock Fe-Mn deposits during July of 2011, along with

the archived drill core from Roberts and Prince (1990) and prior mapping by the

author in the Woodstock area, allowed an assessment of the stratigraphic

relationships of the Fe-Mn mineralization and its association with unmineralized

strata. Certain sections of Lithofacies Associations II and III from the lower

member of the Smyrna Mills Formation are observable as jet black Fe-Mn-rich

strata that have a surface coating of amorphous Fe-Mn hydroxide, with minor

pyrolusite (MnO_2), barite ($BaSO_4$), chalcopyrite, and cobaltite (CoAsS) (Figs. 2.5,

4.1, and 4.2). The high specific gravity of the Fe-Mn mineralized bedrock is due to

the high abundance of ferromanganiferous minerals (hematite, rhodochrosite,

magnetite, with minor Fe-Mn silicates). All observed sections with Fe-Mn

mineralization are sharply or gradationally conformable with intercalated

noncalcareous red and green siltstone and rare grey siltstone (Sidwell, 1957;

Gilders, 1976; Roberts and Prince, 1990).

4.2   MINERALIZED LITHOFACIES

As described in Chapter 3, the study area is comprised of six lithofacies

associations; the Fe-Mn mineralization (lithofacies *Fgnz, Frmz*) is observed to

occur only within Lithofacies Associations II and III. With the aid of outcrops, drill

core, and previous reports by Sidwell (1957), Anderson (1968), Gilders (1976), and

Fig. 4.1: Photograph of an outcrop at the North Hartford deposit displaying the Fe-Mn hydroxide coating of the interbedded lithofacies *Fgnz* and *Frmz*, separated in part by lithofacies *Fgnl* (Site 9; hammer for scale).
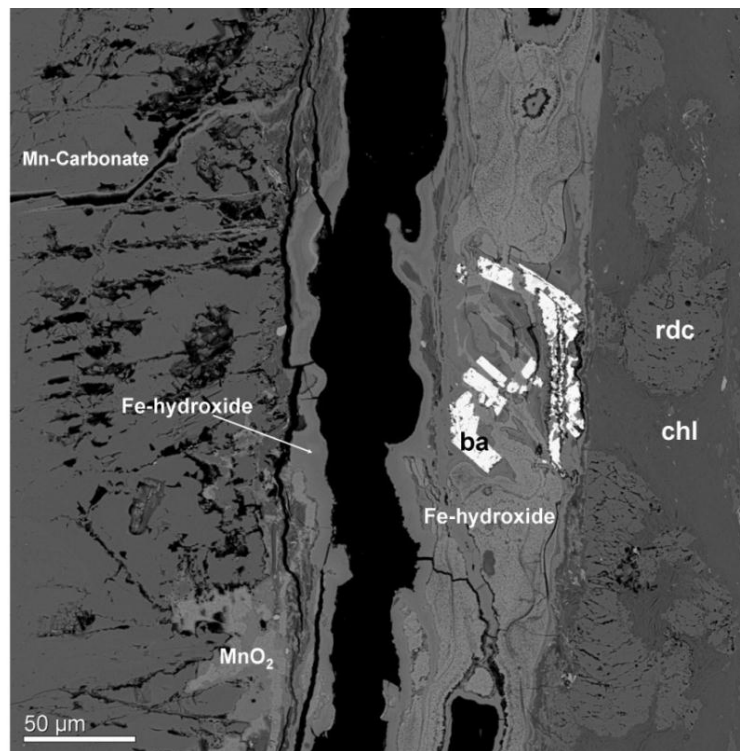
Fig. 4.2: SEM-BSE image of the surface coating along a fracture plane of Fe-Mn-rich laminae at the North Hartford deposit. SEM-EDS analysis reveals a coating of interwoven amorphous Fe and Mn hydroxides. The Fe/Mn of the hydroxide crust typically reflects the Fe-Mn concentrations of the bedrock. Site 9; Sample 9-15-S1.

Roberts and Prince (1990) that relate mainly to the Plymouth deposit, the Fe-Mn mineralized lithofacies *Fgnz* and *Frmz* were each subdivided into three separate mineralization units on the basis of their petrography and appearance. Under petrographic analysis, they are found to have dominant hematite, magnetite, rhodochrosite, and chlorite particles of a euhedral shape. This imparts a crystalline (rather than a granular, clastic) fabric to samples, and their resulting classification is of a mineralized siltstone.

A total of 26 samples of the Fe-Mn mineralized lithofacies were also collected from areas of Fe-Mn mineralization along roadcuts and outcrops on Route 95 and localities west of Woodstock (Table 4.1). All of the samples were examined by petrographic microscope. Seven of the samples were analyzed by XRD, and 6 samples were analyzed by SEM–EDS (Appendix II**).**

4.2.1 PETROGRAPHIC DESCRIPTIONS

4.2.1.1 LITHOFACIES FGNZ (FE-MN OXIDE-SILICATE-CARBONATES)

Lithofacies Association II contains a Fe-Mn mineralized, very finely crystalline lithofacies (lithofacies *Fgnz*) with an average crystal size of about 15 µm. that were identified within the Woodstock Fe-Mn deposits and surrounding Fe-Mn localities. Fig. 4.3 demonstrates that lithofacies *Fgnz* (Fe-Mn oxide-silicate-carbonate) can be separated into three mineralization units (A, B, and C) that, in general, form stratigraphically on top of each other. However, exceptions are found due to complexities associated with folding and (or) interbedding of the Fe-Mn mineralized units, in both outcrops and drill cores.

Overall the Fe-Mn mineralization associated with lithofacies *Fgnz* contains

86

DDH 87-2

1.5 m

Fbuc
Fgygn

14 m
17.1 m

Frmz (Units F and E)

DDH 87-3

56.7 m

Fgnz (Unit A)
Fgygn and minor Frmz (Unit F)

6.1 m

Frmz (Unit E) and Fgygn

67.1 m
70.1 m
71.3 m
73.2 m

Fgygn and Frmz (Unit E)
Frmz (Unit E)
Fgygn and minor Frmz (Unit E)
Fgygn and Frmz (Unit E)

28 m

Frmz (Unit E)

79.3 m

Fgygn and Frmz (Unit E)

38.7 m

Fgnz (Unit B)
Fgnz (Unit C)
Fgygn

Frmz (Unit E) and Fgnz (Unit A)

Frmz (Units F and E)

98.8 m

Frmz (Unit E) and Fgnz (Unit A)
shear zone present

53 m

Frmz (Unit E) and Fgnz (Unit C)

Frmz (Unit E)
Fgnz (Unit C)

Frmz (Unit E)

103.6 m
108.5 m
111.3 m

Fgnz (Unit C) and minor Frmz (Unit E)

Frmz (Unit E)
Frmz (Unit E)

Frmz (Unit E)

Frmz (Unit D) and Fgnz (Unit C)

ss   st   cl

Frmz (Unit F)

m f vf

95.1 m

Frmz (Unit B and C)

102.4 m

Frml

Fgnz (Unit B)

Lithofacies and symbols legend

Frmz (Unit D) and Fgnz (Unit C)
Frmz (Unit F)
Fgnz (Unit C)
Frmz (Unit F)

Frmz (Unit D) and Fgnz (Unit C)
Faulting present

Frmz

Fgnz (Unit B)

Fgnz

Frml

140.2 m

Fgygn
Fgnz (Unit B)
Fgygn

Fgygn

149.4 m

Fgnz (Unit A)

Fgngyib

Fgnz (Unit A)

Fgnc

Fgygn

Fbuc

179.2 m
182.9 m

Fgngyib

Grain Size:

ss   st   cl

Fgnc

m f vf

193.6 m

cl: clay   st: silt   ss: sand

ss   st   cl

m f vf

Fig. 4.3: Drill core logs DDH 87-2 and DDH 87-2 from Trench 1 of the Plymouth deposit displaying the various distribution of Fe-Mn mineralized lithofacies (*Fgnz* and *Frmz*). Lithofacies *Fgnz* can be subdivided into Units A, B, and C, and lithofacies Frmz can be subdivided into Units D, E, and F.

87

Areas of Fe-Mn Mineralization

	Plymouth	South Hartford	North Hartford	Iron Ore Hill	Union Corner	Richmond Corner	Site 14
Hematite	Major	Major	Major	Major	Minor	Minor	Minor
Magnetite	Major	Minor	Minor	Minor	n/a	n/a	n/a
Rhodochrosite	Major	Major	Major	Major	Major	Minor	Minor
Oligonite	n/a	n/a	n/a	n/a	Major	n/a	n/a
Pyroxmangite	Minor	n/a	n/a	Minor	n/a	n/a	n/a
Apatite	Minor	Trace	Trace	Minor	n/a	n/a	n/a
Rhodonite	Minor	n/a	n/a	Minor	n/a	n/a	n/a
Calcite	Minor	Minor	Minor	Minor	Trace	Minor	Trace
Stilpnomelane	Major	Trace	Trace	n/a	n/a	Minor	Minor
Mn-Clinochlore	Trace	Trace	Trace	n/a	n/a	Major	Major
Chlorite	Major	Trace	Minor	Minor	Minor	Minor	Minor
Pyrite	Trace	Trace	Trace	Trace	Minor	Trace	n/a
Cobaltite	Trace	n/a	Trace	Trace	n/a	n/a	Trace
Chalcopyrite	Trace	n/a	Trace	Trace	Trace	n/a	Trace

Table 4.1: Mineral abundances within sampled Fe-Mn deposits and occurrences within the Woodstock area. This table includes only the minerals observed in this study and not those observed in previous studies.

40 – 80% Mn carbonate that includes rhodochrosite, Mn-calcite ([Ca,Mn]CO_3), and Mn-siderite ([Mn,Fe]CO_3). In thin section, the silicate minerals were identified by Roberts and Prince (1990) to be Mn-chlorite, Mn-mica, and axinite ($Ca_2MgAl_2BO_3Si_4O_{12}$[OH]) and constitute 10 – 20% of the lithofacies. The oxide minerals were identified to be braunite ($MnMn_6$[O_8SiO_4]), hematite, pyrolusite, manganite (MnO(OH)), and magnetite.

Mineralization Unit A

This type of mineralization is visible in drill cores from the Plymouth and Iron Ore Hill deposits and also in outcrop at Sites 1, 7, 9, 12, 14, 16. Unit A is a dark green chloritic mineralized, very finely crystalline layer with an average crystal size of about 15 μm with minor occurrences of pink ellipsoidal rhodochrosite nodules (Fig. 4.4), Fe-Mn silicate, Fe-Mn carbonate, and white microspheroidal calcite. Other minerals include Mn-clinochlore ($Mg_3Mn_2AlSi_3AlO_{10}(OH)_8$), stilpnomelane ($K(Fe,Mg,Fe)_8(Si,Al)_{12}(O,OH)_{27} \cdot n(H_2O)$), minor pyrite, and trace chalcopyrite and cobaltite. The unit appears in contact with lithofacies *Fgygn* but is also found to occur alongside Unit E of lithofacies *Frmz*.

Mineralization Unit B

The next unit is found in drill cores from the Plymouth and Iron Ore Hill deposits and also in outcrop at Sites 9, 12, 14, 15, 16 where it is observed as weakly magnetic, dark green, and very finely crystalline with an average particle size of about 15 μm (Fig. 4.5) and magnetite crystals with a particle size of 30 μm. The mineralogy is composed of magnetite, chlorite, rhodochrosite, oligonite, with minor quartz, calcite, and trace pyrite, chalcopyrite, cobaltite, and monazite
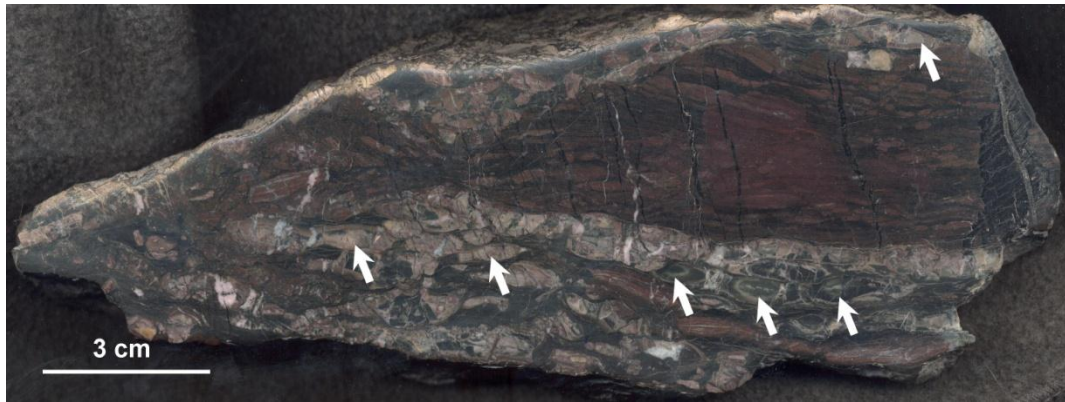
Fig. 4.4: Photograph of a polished slab of the chloritic Fe-Mn oxide-silicate-carbonate siltstone from (Unit A) from the North Hartford deposit (Site 9) with white arrows pointing at pink Fe-Mn carbonate ellipsoidal nodules. Sample 9-NH-S1.
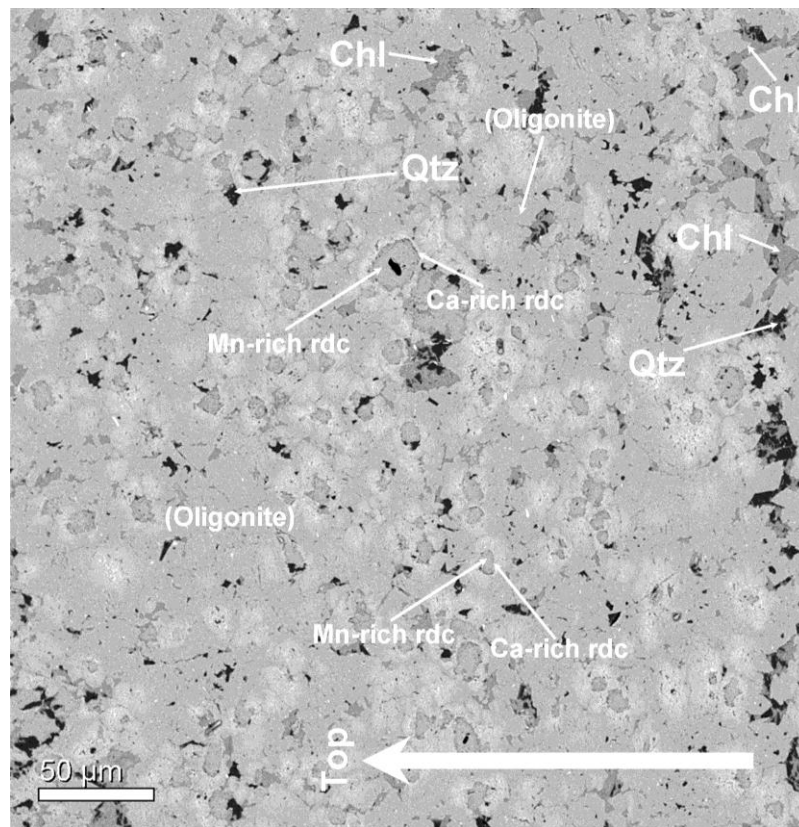
Fig. 4.5: SEM-BSE image of a Fe-Mn carbonate-rich section of Unit B from Union Corner, NB. The image displays the crystalline oligonite with occasional ghost structures that are present as microspheroids of rhodochrosite. Sample GR-S13-01. See glossary for abbreviations.

([La,Ce,Nd](PO_4)). This unit is comprised of almost entirely of Fe-Mn carbonate

with minor pyrite and trace chalcopyrite as observed in outcrops at the Union

Corner Fe-Mn locality (Site 15). Rhodochrosite is observed largely as

microspheroids and devoid of inclusions (Fig. 4.5). In contrast, oligonite is

subhedral to euhedral in shape and often peppered with inclusions of quartz,

chlorite, and $1 - 2$ μm trace inclusions of manganiferous ilmenite ($MnTiO_3$) and

monazite (Fig. 4.6). Unit B is found to occur generally on top of Unit A, but also

occurs in outcrop (Site 13 and 16) and drill cores with lithofacies *Fgygn, Frml, and*

Frmz (Units C, D, E, and F) possibly by either folding and (or) interbedding.

Mineralization Unit C

This mineralization is observable as a strongly magnetic, black to dark

green, and very finely crystalline with an average crystal size of about 15 μm.

Magnetite crystals have a particle size of 30 μm. Unit C is often in drill cores from

the Plymouth and Iron Ore Hill deposits and rarely in outcrop at both of these Fe-

Mn localities. The mineralogy of Unit C comprises euhedral magnetite, chlorite,

rhodochrosite, with minor Fe-Mn silicates, and trace cobaltite, and chalcopyrite.

This magnetite-rich mineralization in general is the uppermost part of Lithofacies

Fgnz and is associated with Lithofacies Association II, but is found to occur in drill

cores (Fig. 4.3) alongside lithofacies *Frmz* (Units D and E).

4.2.1.2 LITHOFACIES FRMZ (FE-MN OXIDE-CARBONATES)

Three types of Fe-Mn mineralization occur in this lithofacies that forms part

of Lithofacies Association III (Fig. 4.3) that was described by earlier workers

(Sidwell, 1957; Roberts and Prince, 1990) as a Fe-Mn oxide facies. Lithofacies
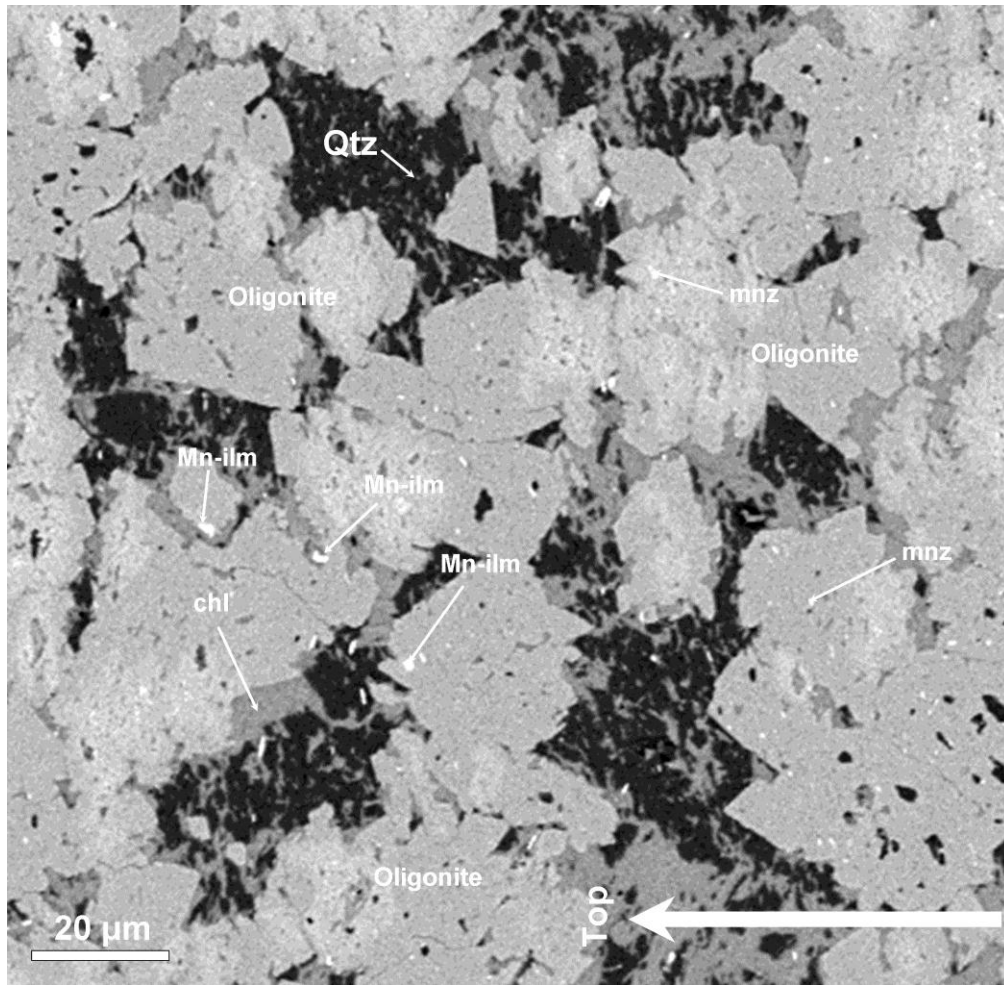
Fig. 4.6: SEM-BSE image of the Fe-Mn mineralization present at Union Corner, NB. Subhedral crystal grains of oligonite with inclusions of manganiferous ilmenite and monazite in a quartz groundmass with chlorite cement. Sample GR-S13-01. See glossary for abbreviations.

Frmz (Fe-Mn oxide-carbonate lithofacies) is often maroon to red in colour in contrast to the dark green to black coloured lithofacies *Fgnz* associated mainly with Lithofacies Association II. Observation by petrographic microscope and SEM-EDS of thin sections indicates lithofacies *Frmz* is composed of finely laminated, very finely crystalline layers, again with an average particle size of about 15 µm and magnetite crystals with a particle size of 30 µm. It is composed of acicular hematite and subhedral to anhedral rhodochrosite, and euhedral magnetite, with minor occurrences of chlorite, acicular rhodonite, Mn-clinochlore, stilpnomelane, calcite, quartz, and trace sulfides (Table 4.1). Roberts and Prince (1990) described their "Fe-Mn oxide-carbonate lithofacies" of the Plymouth deposit containing 30 – 80% Fe-and Mn-bearing oxides. The major oxide minerals are hematite, magnetite, minor braunite, bixbyite ($[Mn,Fe]_2O_3$), and trace ilmenite ($FeTiO_3$). Thirty to 50% of the oxide-carbonate lithofacies is composed of carbonate minerals, chiefly rhodochrosite, and minor calcite. The remaining 5 to 20% is composed of manganiferous silicates that are identified as Mn-chlorite ($[Mn,Mg_5Al][AlSi_3]O_{10}[OH]_8$), Mn-mica ($KMnAl(AlSi_3O_{10})(OH,F,Cl)_2$), pyroxymangite ($[Fe,Mn]SiO_3$), rhodonite, tephroite ($Mn_2[SiO_4]$), and knebelite ($(Fe,Mn)_2SiO_4$). The Fe-Mn mineralized strata within lithofacies *Frmz* are locally crosscut by veins of chlorite, rhodochrosite, and minor veins of sursassite ($Mn_2Al_3[(OH)_3(SiO_4)Si_2O_7]$; Heinrich, 1962; Roberts and Prince, 1990) (Fig. 4.7).

Mineralization Unit D

Fe-Mn mineralized unit D is associated with Lithofacies Association III and occurs with lithofacies *Fgnz* and Unit E and F of lithofacies *Frmz*. is a magnetic,
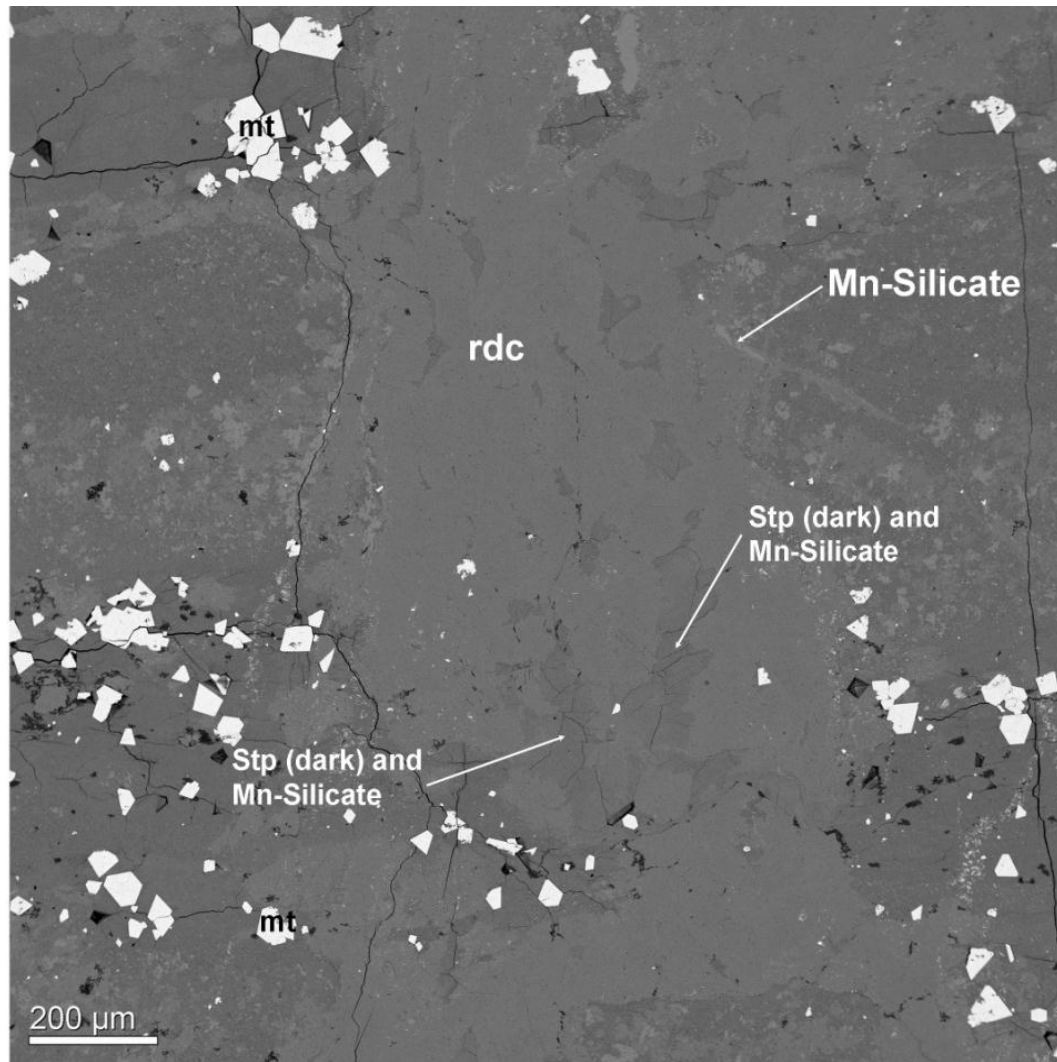
Fig. 4.7: SEM-BSE of Unit D (Fe-Mn oxide-carbonate lithofacies *Frml*) at the Plymouth Fe-Mn deposit displaying a crosscutting rhodochrosite veinlet with surrounding magnetite, and Mn-silicates. Sample PLY-002. See glossary for abbreviations.

dark maroon, very finely crystalline layer with an average particle size of about 15 μm and magnetite crystals with a particle size of 30 μm (Unit D; Fig. 4.7), occasionally encountered in drill cores from the Plymouth Fe-Mn deposit and rarely in outcrop at Site 12 and 13. This unit is mineralogically composed of magnetite, hematite, and rhodochrosite, with minor rhodonite, pyroxmangite, chlorite, apatite $((Ca_5[PO_4]_3[OH,F,Cl])$ and trace pyrite, chalcopyrite, and cobaltite. Unlike the dark green to black magnetite-rich lithofacies *Fgnz*, the groundmass is composed of rhodochrosite with only minor chlorite.

Mineralization Unit E

Unit E is a mineralized sequence and is a maroon to red hematite-rhodochrosite-rich very finely crystalline series of layers with an average particle size of about 15 μm (Figs. 4.8, 4.9). It is commonly observed in several outcrops (Figs 2.2, 3.1, 4.3; Sites 9, 12, 13, and 16) and in drill cores from the Plymouth and the Iron Ore Hill deposits. Unit E is observed to make up a majority of the Fe-Mn mineralization within lithofacies *Frmz* and comprises hematite, rhodochrosite, minor magnetite, chlorite, apatite, and trace Mn-clinochlore, pyrite, chalcopyrite, and cobaltite.

The hematite is commonly present as acicular needles that occur parallel to bedding within a groundmass of rhodochrosite, chlorite, and minor quartz and Mn-clinochlore (Fig. 4.8). In rare occurrences it is also present as 1 to 10 mm-thick cryptocrystalline bands within minor interbedded rhodochrosite. The cryptocrystalline hematite beds are usually brecciated, with the surrounding matrix composed of chlorite and Fe-Mn carbonate (Fig. 4.9). Minor, coarse-silt-sized

95
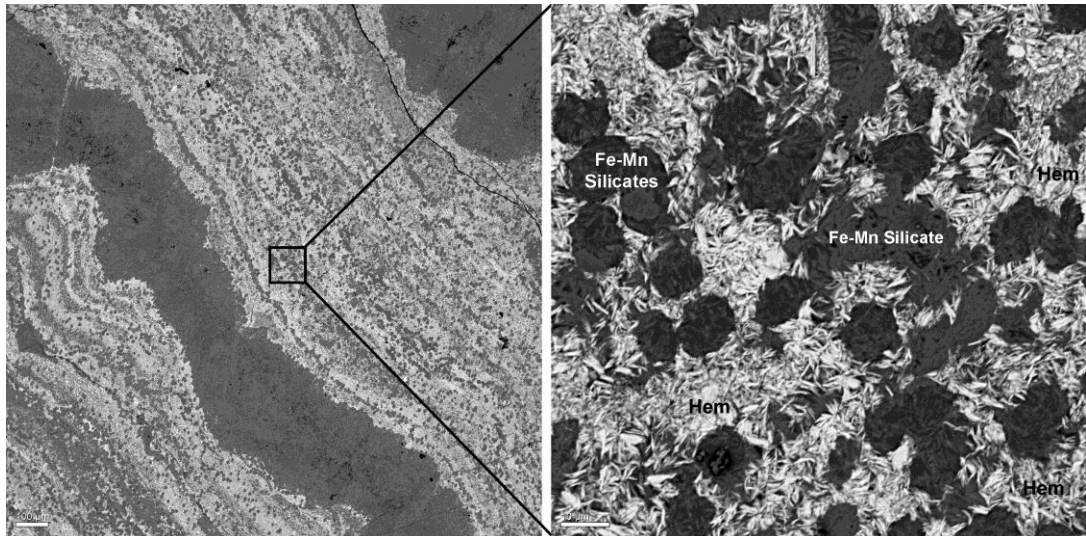
Fig. 4.8: SEM-BSE images of acicular hematite and spherical clusters of Fe-Mn silicates (possibly pyroxmanganite) in layers separated by beds of interwoven rhodochrosite and apatite. Sample IRH-01. See glossary for abbreviations.
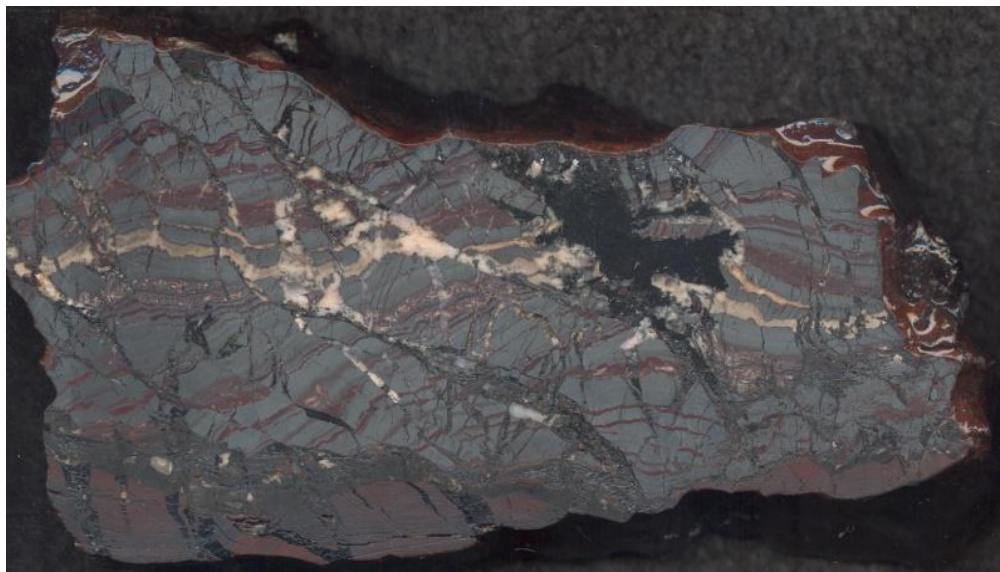
Fig. 4.9: Polished slab of a brecciated hematite-rich section of Fe-Mn mineralization from the South Hartford deposit. This sample occurs in a tight, late forming, synform. This is possibly related to the fracturing the layers of cryptocrystalline hematite and the injection of the quartz-carbonate and chlorite veins. Sample 3-SH-1.

euhedral magnetite (~30 μm grain size) is also present in thin sections sampled

from the North Hartford, South Hartford, Plymouth, and Iron Ore Hill deposits.

Manganiferous clinochlore and minor pyroxmangite are two particular manganese

silicates associated within Unit E that are identified by SEM and XRD analysis. The

latter silicate appears to form as 15 μm-sized spherical clusters of interwoven

acicular Fe-Mn silicate crystals (possibly pyroxmanganite) in surrounding layers of

acicular hematite (Fig. 4.8). Within the samples taken from Iron Ore Hill, unit E

contains higher amounts of various minor minerals, such as apatite and

pyroxmanganite. Apatite exists as a microcrystalline skeletal-shaped groundmass

that is interwoven amongst anhedral rhodochrosite that is easily identified under

chroma SEM-cathodoluminescence by a yellowish-white hue (Figs. 4.10A and

4.10B). The term skeletal is often used in igneous petrography to describe minerals

that have an amorphous shape that, by appearance, resembles a skeleton. The

yellowish tint of the skeletal apatite is likely caused by the abundance of Mn^{+2}

cations as a substitution for Ca^{+2} present in the apatite (Mariano and Ring, 1975;

Filippelli and Delaney, 1993; Barbarand and Pagel, 2001). Apatite also occurs as

subhedral grains within a groundmass of stilpnomelane as observed in the Plymouth

Fe-Mn deposit (Fig. 4.11). The higher apatite content (up to 1%) appears to be

limited to lithofacies *Frmz*.

Mineralization Unit F

The final observed type of Fe-Mn mineralization, which is observed in drill

core from the Plymouth deposit is Unit F (Fig. 4.12). Generally it occurs on top of

Unit E but it is also found to occur with lithofacies *Fgygn*, and *Fgnz* (Units A, B, C
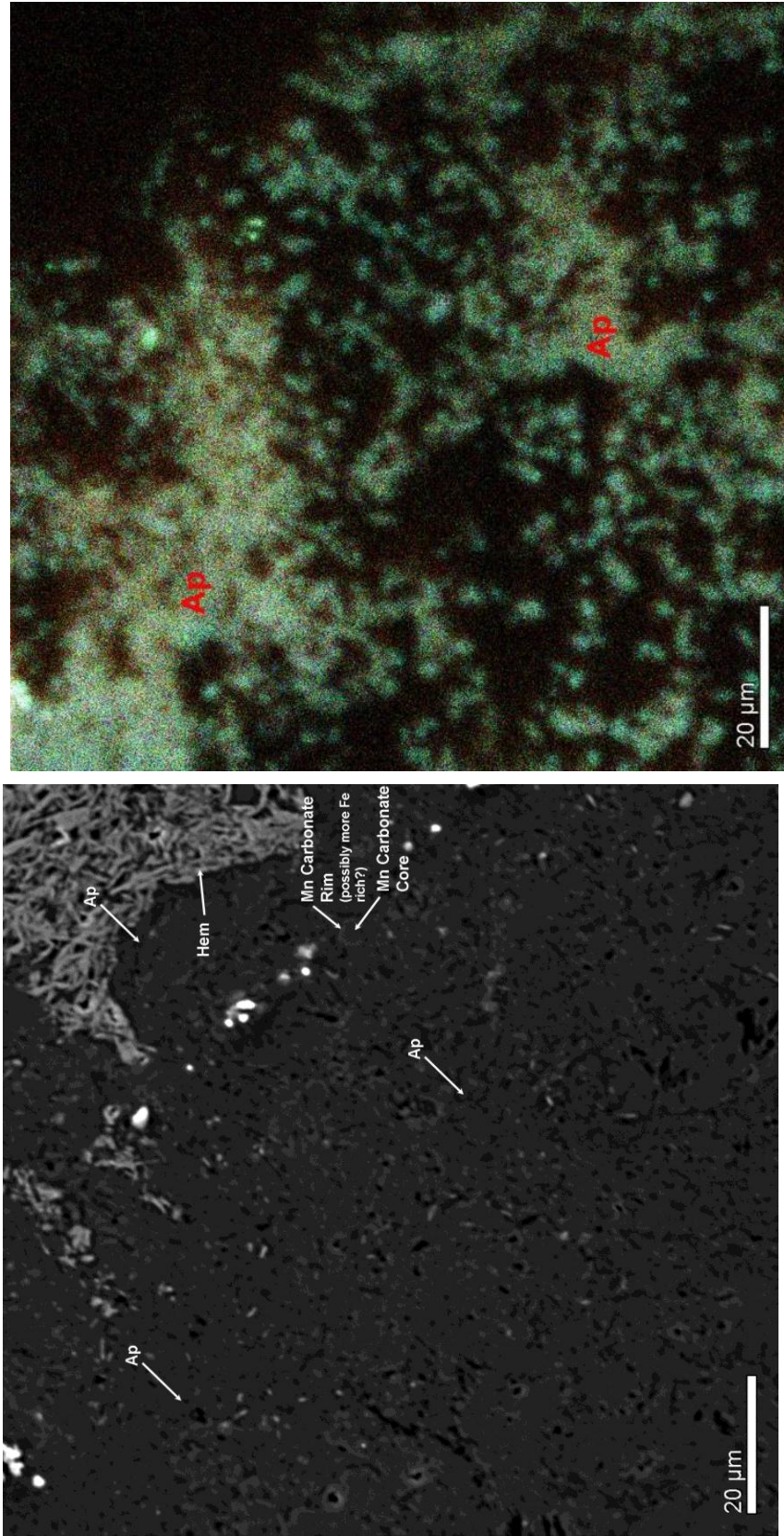
Fig. 4.10A: SEM-BSE image of interwoven apatite and rhodochrosite at Iron Ore Hill. The similarities in molecular mass make it difficult to distinguish differences between the anhedral apatite and anhedral rhodochrosite. Sample IRH-01. Fig. 4.10B Chroma SEM-CL image of the same area in Fig. 5.9a displaying yellowish-white anhedral apatite grains under cathodoluminescence. Sample IRH-01. See glossary for abbreviations.
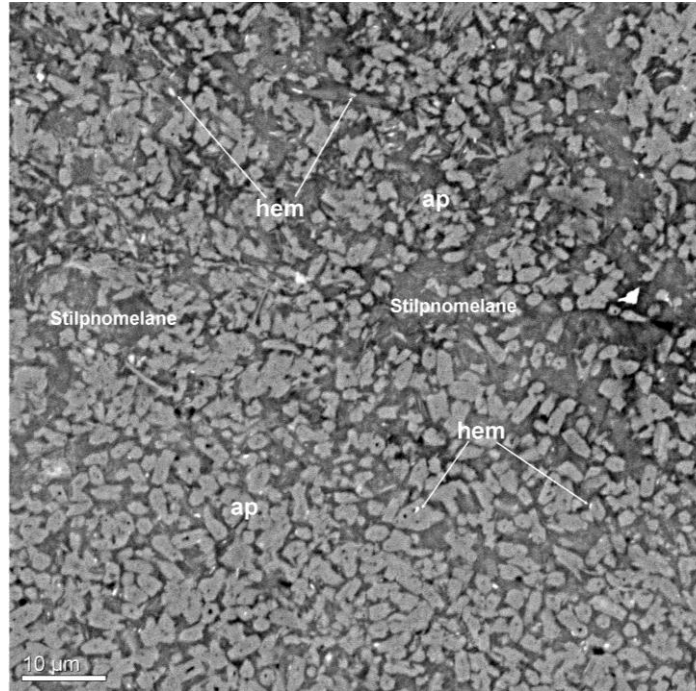
Fig. 4.11: SEM-BSE image of subhedral to anhedral apatite crystals within a groundmass of stilpnomelane with trace amounts of hematite occurring both in the stilpnomelane groundmass and as inclusions in the apatite. Sample PLY-001. See glossary for abbreviations.

Fig. 4.12: Outcrop of Unit F displaying cryptocrystalline red layers at the Iron Ore Hill deposit.

and Unit D in lithofacies *Frmz.* It is composed of a laminated to cryptocrystalline,

brick red, (average particle size of about 15 µm) beds that was observable in

outcrops at the Plymouth, North Hartford, South Hartford, and Iron Ore Hill

deposits. Unlike all of the underlying Fe-Mn mineralized units in Lithofacies

Associations II and III, Unit F does not have a Fe- Mn hydroxide surface crust. The

cryptocrystalline nature of the siltstone makes determining the mineralogy difficult.

Roberts and Prince (1990) concluded that the mineralogy of this siltstone is of

hematite, rhodochrosite, with minor Fe-Mn silicates, apatite, quartz, and calcite.

4.2.2 MINERALOGIC RELATIONSHIPS

4.2.2.1 PREDIAGENETIC FEATURES

Many marine sedimentary Fe-Mn deposits often form when seawater,

saturated in Fe^{2+} and Mn^{2+} ions, is subject to changes in the ocean redox conditions.

This results in Fe and Mn minerals precipitating from the seawater and collecting

on the seafloor. Depending on the redox conditions and dissolved anions present,

the Fe and Mn can precipitate out as oxyhydroxides, oxides, carbonates, and (or)

sulfides. Seasonal changes in the dissolved Fe^{2+} and Mn^{2+} ions often result in

amicrobanding of the layers (Maynard, 1983). As observed in thin section (Fig.

4.7), lithofacies *Fgnz* and *Frmz* contain Fe-Mn mineralization that occurs as

alternating layers of iron-rich minerals (hematite and (or) magnetite) with layers of

manganese-rich and silicate-rich minerals (rhodochrosite, Mn-clinochlore,

pyroxmanganite, and stilpnomelane). Many depositional features in the six Fe-Mn

mineralized units has been subject to later diagenesis and subgreenschist metamorphism, and so persists in only a handful of samples.

Rare, localized, ghost structures of microspheroidal rhodochrosite in crystalline oligonite (Fig. 4.5) suggest that the microspheroidal texture is prediagenetic in origin and not caused by later diagenetic processes. A similar feature in oolitic calcite was described by de Villiers (1971) within the Kalahari Manganese Field where iron hydroxide gel (FeO(OH) $\cdot$ n(H$_2$O)), siderite (FeCO$_3$), and rhodochrosite were also present. In lithofacies *Frmz* the microspheroids of zoned rhodochrosite are typically within a groundmass of acicular hematite.

Aside from a surface coating of amorphous Fe-Mn hydroxides, all samples from the Woodstock Fe-Mn deposits appear to be devoid of any Fe-Mn hydroxides. It is possible that some of the Fe precipitated out originally as Fe-oxyhydroxides and the Mn as rhodochrosite, but the only remaining evidence of them are the hematite and magnetite layers in lithofacies *Fgnz* and *Frmz*.

4.2.2.2 DIAGENETIC FEATURES

LITHOFACIES FGNZ

In Fe-Mn localities such as Union Corner (Fig. 2.2 Site 15), the bands of oligonite form as finely crystalline minerals with minor occurrences of quartz and chlorite. In thin section, crystalline oligonite contains ghost structures of rhodochrosite microspheroids (Fig. 4.14). The ghost structures are a characteristic that is often more common in the jet-black sections (lithofacies *Fgnz*) of the Union Corner Fe-Mn occurrence (Fig. 4.5). Magnetite that is found to occur in Units B, and C always appears to overprint the interlaminated acicular hematite, Fe-Mn
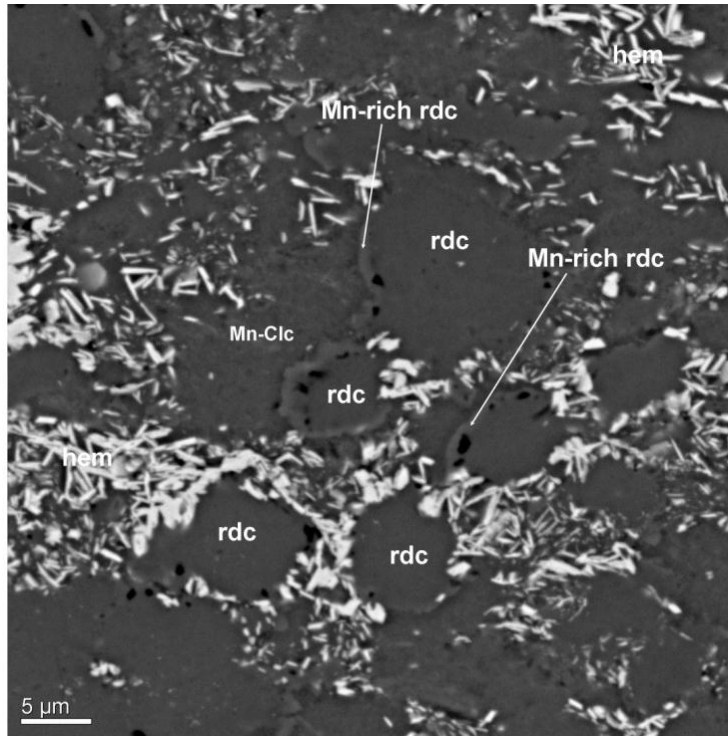
Fig. 4.13: SEM-BSE image of the microspheroids of rhodochrosite from lithofacies *Frmz* (Unit E) of the North Hartford deposit as present as microspheroids of rhodochrosite. The image also displays several of the rhodochrosite microspheroids with Fe-rich centres and Mn-rich rims. Sample 9-15-S2. See glossary for abbreviations.
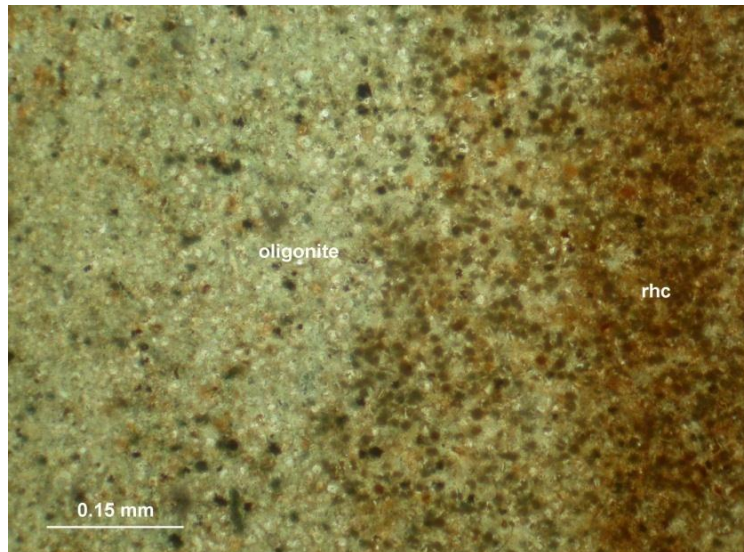
Fig. 4.14: Photomicrograph of a Fe-Mn carbonate-rich section of the Fe-Mn oxide-silicate-carbonate lithofacies (Unit B) present at Union Corner, NB displaying the gradation of crystalline oligonite and microspheroidal rhodochrosite. See glossary for abbreviations.

102

silicates, and Fe-Mn carbonate crystals (Figs. 4.15A & B), which is consistent with magnetite being a high-relief mineral. As a consequence, it is unclear if magnetite post dates the other minerals. In some Precambrian iron formations magnetite crystallization is the result of Fe^{3+} oxyhydroxides undergoing diagenesis and reduced to magnetite crystals (Pufahl and Fralick, 2004).

In localities that display the Units B and C, base-metal concentrations are generally higher. Locally, euhedral magnetite crystals sporadically contain inclusions of chalcopyrite and cobaltite (Figs. 4.15A & B) alongside overprinting euhedral to subhedral chalcopyrite and cobaltite.

LITHOFACIES FRMZ

Although rare occurrences of microspheroidal minerals do exist within these Woodstock Fe-Mn deposits, a majority of the mineralogy is present as crystalline minerals. Some of these crystalline minerals are found to contain ghost structures of microspheroidal minerals (Fig. 4.5). In localities where lithofacies *Frmz* is present (Sites 9, 12, 13, and 16) Fe-oxide minerals are observed to be acicular crystals with rare cryptocrystalline bands of hematite and minor euhedral magnetite (Figs. 4.8 and 4.9). In localities where these are subject to weathering along fracture planes and exposed surfaces the Fe-oxide minerals are now present as unidentified Fe and Mn-hydroxide minerals (Fig. 4.2). Fe-Mn carbonates, which appear to be the primary manganese mineral within lithofacies *Frmz*, are observed as anhedral to euhedral crystalline rhodochrosite.

Fe-Mn silicates and various clay minerals that were initially deposited as fine-grained clastics between the layers of hematite would be recrystallized during
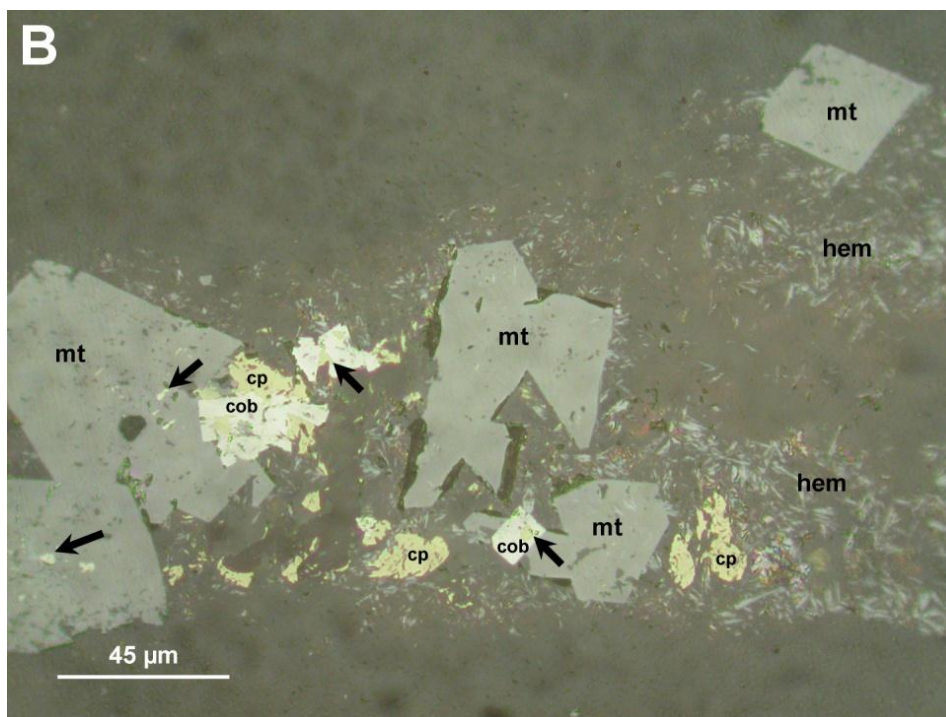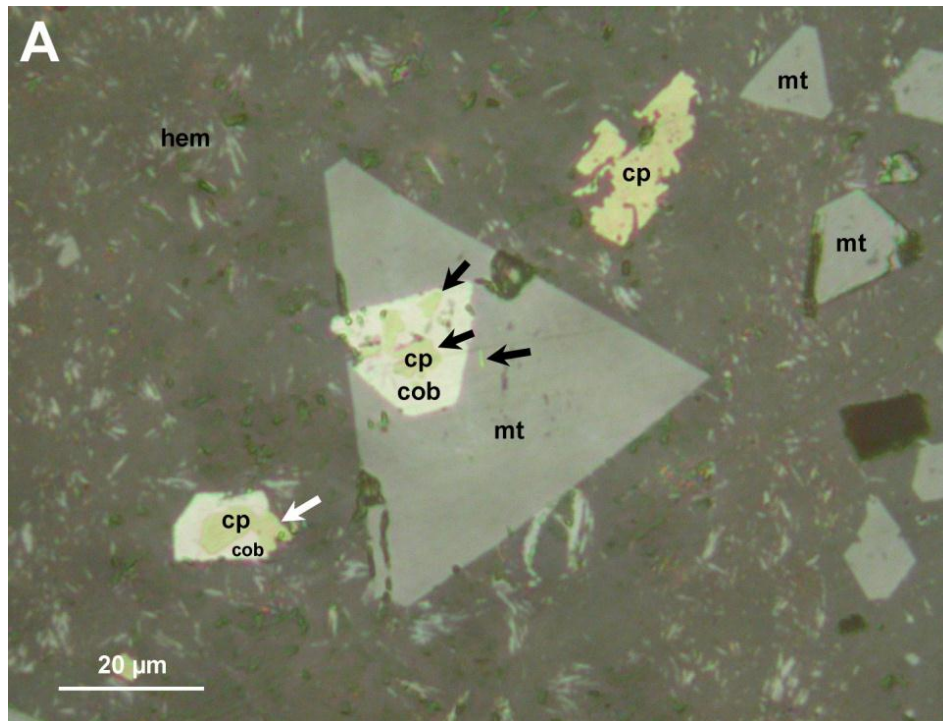
Fig. 4.15A & B: Photomicrographs of Fe-Mn in Unit C at Iron Ore Hill in plane polarized reflected light displaying euhedral magnetite crystals with inclusions of cobaltite and chalcopyrite. Locally subhedral chalcopyrite crystals overprint grains of euhedral cobaltite (white arrows), but typically the chalcopyrite is present as inclusions within the cobaltite and magnetite grains (black arrows). Sample IRH-03. See glossary for abbreviations.

104

diagenesis and formed chlorite, Mn-clinochlore, stilpnomelane, and minor pyroxmanganite. The silicate minerals are occasionally present between crystals of hematite and are likely diagenetic in origin (Fig. 4.8). Thin, laminated beds of Fe-Mn mineralization within lithofacies *Frmz* display thin bands of acicular hematite with alternating bands of rhodochrosite and minor apatite.

Locally, subhedral chalcopyrite crystals overprint grains of chlorite, and stilpnomelane that will be discussed later on in this chapter. Minor silicic and potassic alteration was also observed with archived drill core from the Plymouth Fe-Mn deposit within lithofacies *Fgnz* and *Frmz*.

4.3   INTERPRETATION OF THE MINERALOGIC RELATIONSHIPS

4.3.1 LITHOFACIES FGNZ (FE-MN OXIDE-SILICATE-CARBONATE)

With variations in the mineralogy and appearance of lithofacies *Fgnz* and *Frmz* it is clear that the two Fe-Mn mineralized lithofacies had at some stage been exposed to environments with different redox potential. In the depositional environment associated with lithofacies *Fbkpl* and *Fgyl* the seawater was above the saturation point for S^{2-} ions to fixate as pyrite and resulting in seawater saturated with a greater ratio of dissolved Mn^{2+} to Fe^{2+} ions. The higher abundance of magnetite and rhodochrosite suggests that the lithofacies *Fgnz* was deposited within an anoxic environment that was below the saturation point for Fe^{2+} to precipitate as FeS_2. The Fe^{2+} would precipitate out as an amorphous Fe^{2+} hydroxide gel and also with Mn^{2+} and dissolved CO_2 to form microspheroidal rhodochrosite. Many of the silicates that are now present in the Woodstock Fe-Mn deposits were likely clay

105

minerals at the time of deposition, some of which reacted to the Fe^{2+} and Mn^{2+} ions within the Fe^{+2} hydroxide gel and microspheroidal rhodochrosite resulting in Fe- and Mn-rich silicates such as chlorite, Mn-clinochlore, and stilpnomelane.

Units B, C that are rich in magnetite also display gradual changes in magnetite content that increase upsection within lithofacies *Fgnz*. Microlayering of magnetite with alternating bands of rhodochrosite, chlorite, Mn-clinochlore, and stilpnomelane within lithofacies *Fgnz* further suggest that a Fe^{2+} hydroxide gel (that later diagenetically recrystallized as magnetite) was precipitated in the water column. Within an anoxic setting that is devoid of circulation of currents it is possible that the seawater was at very low Eh and higher pH conditions for lithofacies *Fgnz* and below the saturation point for FeS_2 to form, making it more ideal for precipitating out Fe^{2+} hydroxides rather than pyrite. The thick, overlying, magnetite-rich lithofacies *Fgnz* may suggest that Fe^{2+} oxyhydroxide gel forming instead of FeS_2.

During diagenesis, the amorphous Fe^{2+} hydroxide gel would be compacted and recrystallize to form magnetite (Fig. 4.16). Most of the microspheroidal rhodochrosite would also be recrystallized simultaneously with the Fe^{2+} hydroxide gel during diagenesis which is observable in most thin sections. Some of the rhodochrosite would also be crystalline oligonite leaving rare remnant ghost structures of original, depositional, microspheroidal rhodochrosite (Fig. 4.5; Lougheed, 1983).

Some of the cobaltite and chalcopyrite, which crosscut euhedral magnetite crystals, are also seen as inclusions within the magnetite (Figs. 4.15A & B). This

106

suggests cogenesis of the Cu-Fe-S and Co-As-S base-metal mineralization occurred at the same time as the formation of magnetite. This cogenesis of the base-metal mineralization is apparent in all of the sampled locations where magnetite is present and is observable in various thin sections. Cobaltite and chalcopyrite are present as inclusions and overprinting crystals within the lithofacies *Fgnz* (Units B and C) suggesting minor Cu-Fe-S and Co-As-S mineralization occurred at the time of deposition. Base-metal mineralization is not uncommon in marine Fe-Mn deposits. Deep-sea Fe-Mn nodules which occur in areas of high biogenic activity are often richer in base-metal concentrations, a process that will be discussed further in Chapter 6. It is possible that sections of lithofacies *Fgnz* that had higher rates of biological productivity at the time of deposition or within the Fe^{2+} hydroxide gel could have resulted in higher overall base-metal concentrations.

4.3.2 LITHOFACIES FRMZ (FE-MN OXIDE-CARBONATES)

Lithofacies *Frmz* is interpreted to have formed in an oxic marine environment of deposition. When seawater saturated in Fe^{2+} and Mn^{2+} is subject to increases in ocean redox in an oxic environment, the more redox sensitive Fe^{2+} would precipitate out first as an amorphous Fe^{3+} hydroxide gel. Then with a majority of the Fe precipitated out as insoluble Fe^{3+} the remaining redox sensitive Mn^{2+} and residual Fe^{2+} in the remaining seawater will combine to dissolved CO_2 and form microspheroids of rhodochrosite (Hem, 1972; Roy, 1981; Force and Cannon, 1988). The zonation of the microspheroids with iron-rich centre with a more Mn-rich outer rim further suggests this (Fig. 4.13). Like with Fe-Mn nodules, the rhodochrosite could also readily react with any free floating matter within the

seawater, which at the time of deposition, would likely be some of the previously precipitated Fe-hydroxide gel that has not yet been deposited on the seafloor (Roy, 1981). These newly formed rhodochrosite microspheroids would have eventually settled out of the water column and maybe deposited with previously or syndepositionally precipitated hydroxide.

In the present-day Bahamas, Fe and Mn oxyhydroxides and hydroxides are currently precipitated out of the seawater by a seasonal increase in oxidation (Lougheed, 1983; Torres-Ruiz, 1983). Higher Eh conditions allow Fe^{2+} to oxidize to Fe^{3+} precipitate out as $Fe(OH)_3$ forming ferric hydroxide laminae on the seafloor. Ferric hydroxide, which would have served as the initial Fe-rich syn-depositional precipitate, has all been converted to crystals of hematite (Equation 4.1) with rare magnetite by diagenesis (Figs. 4.16, 4.17 and 4.18).

$$2Fe(OH)_3 \rightarrow Fe_2O_3 + 3H_2O$$
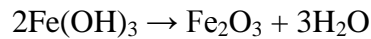
Equation 4.1: Reaction of ferric hydroxide to form hematite and water. Prior to diagenesis much of the mineralogy of the Lithofacies *Frmz* would have existed as amorphous Fe^{3+} hydroxides, microspheroidal Fe-Mn carbonates, and various clay minerals. Upon the advent of subsurface diagenesis, many of the previously mentioned minerals would then be recrystallized to the euhedral to anhedral minerals observed in thin section. The Fe^{3+} hydroxides would have likely recrystallized as hematite with minor magnetite. The Fe-Mn carbonates (mostly rhodochrosite) would start to deform from microspheroidal to subhedral and anhedral in shape.
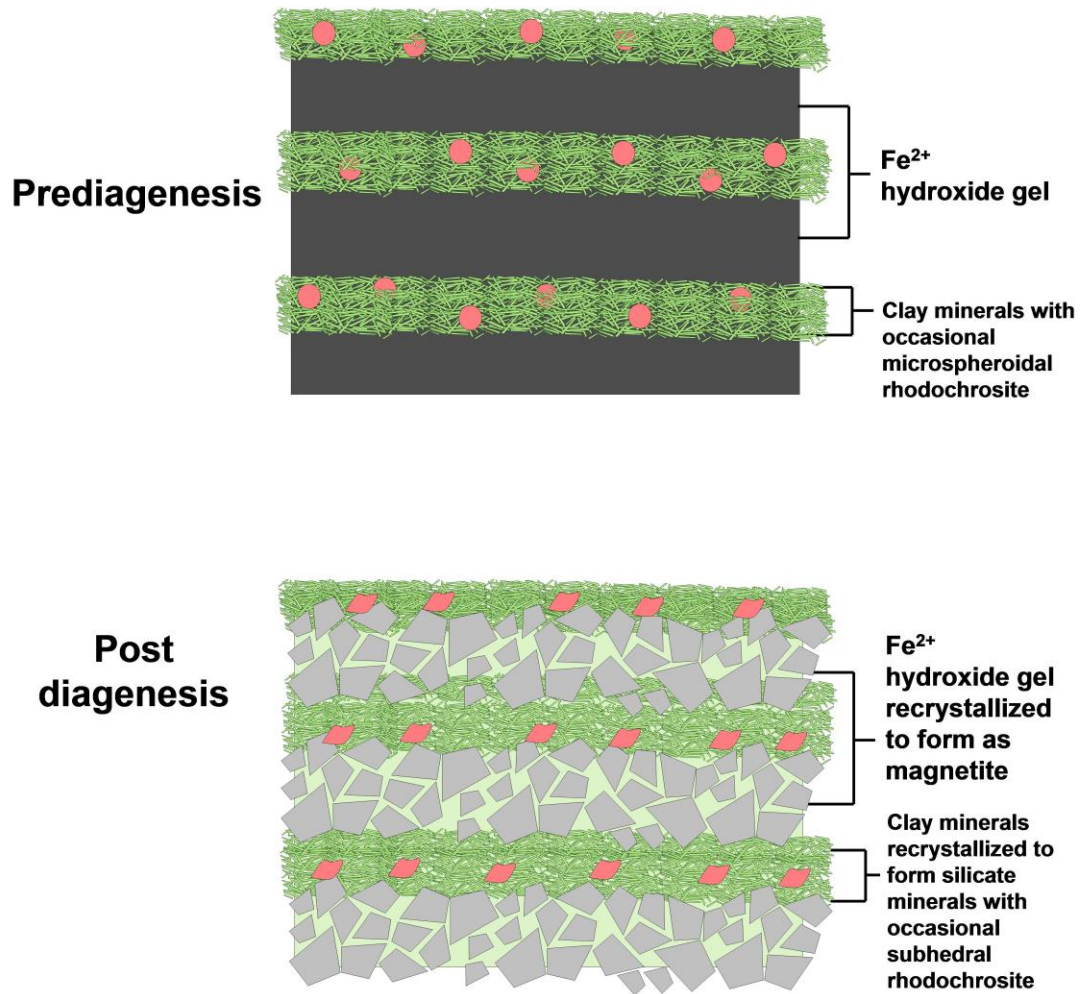
Fig. 4.16: Diagram displaying the changes in the Fe-Mn mineralized bands in lithofacies *Fgnz* prior to diagenesis and after diagenesis.
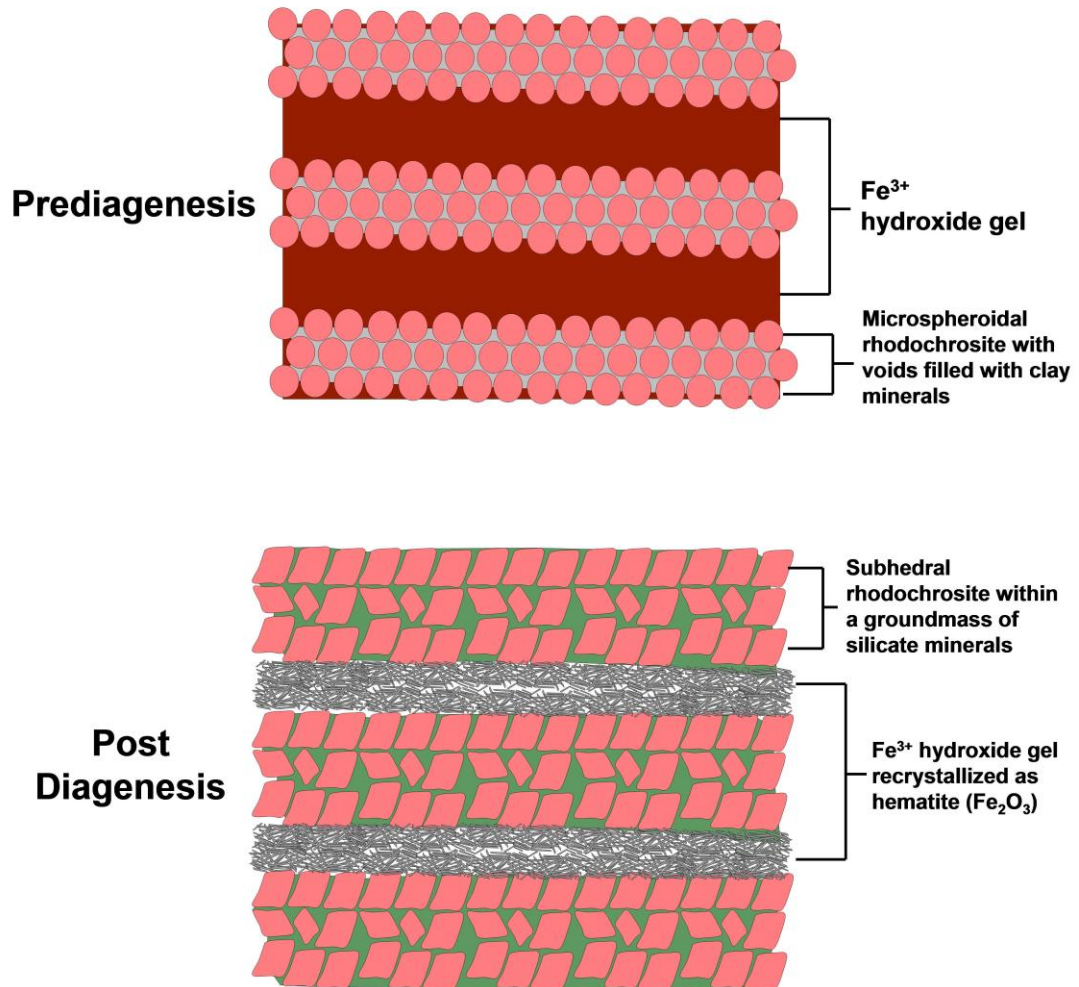
Fig. 4.17: Diagram displaying the changes in the Fe-Mn mineralized bands in lithofacies *Frmz* prior to diagenesis and after diagenesis.
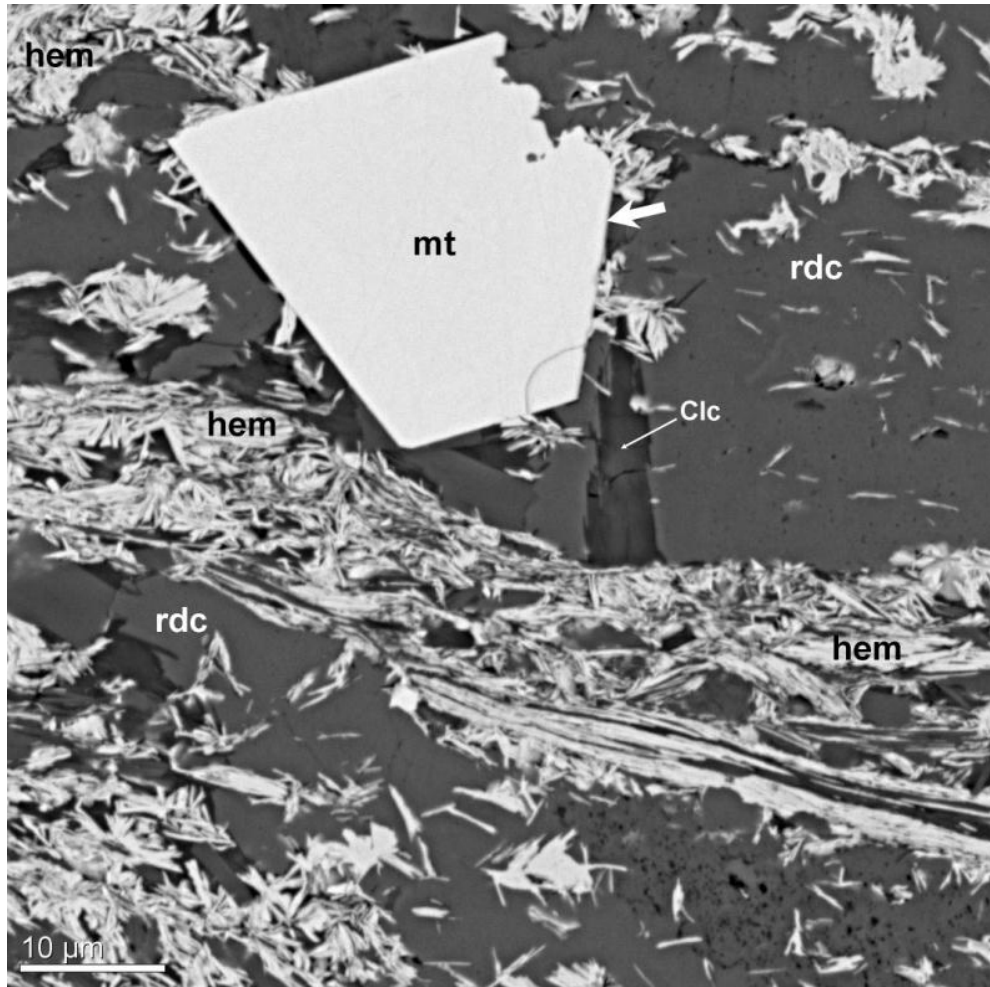
Fig. 4.18: SEM-BSE image of a rare magnetite crystal (porphyroblast) in Unit E. The magnetite crystal appears to be overprinting beds of acicular hematite and subhedral rhodochrosite. Sample 9-15-S2. See glossary for abbreviations.

During diagenesis the original Fe^{3+} hydroxide gel formed at the time of deposition appears to have all been converted to hematite with some magnetite (Fig. 4.17). The rhodochrosite microspheres would then be deformed to subhedral to anhedral rhodochrosite and occasionally recrystallized as oligonite with minor silicates, such as chlorite, Mn-clinochlore, stilpnomelane, and minor pyroxmanganite that were deposited on the seafloor (Fig. 4.17). Varying degrees of diagenesis depending on pressure and temperature (all of which occur below 20 km depth and 200°C) may cause some areas of Fe-Mn mineralization to contain the original rhodochrosite microspheroids that were at the shallowest depths and lowest pressures. In contrast, areas of higher temperature and pressure during diagenesis would have other areas would cause the rhodochrosite to recrystallize in the form of oligonite with the rare remnant ghost structures (Fig. 4.5).

Minerals such as apatite within lithofacies *Frmz* (Fig. 4.11) likely existed as amorphous phosphates at the time of deposition and would readily absorb onto the surfaces themselves to the Fe^{3+} oxyhydroxides within lower pH and oxygen-rich settings. In contrast, higher pH conditions (such as those present during the deposition of lithofacies *Fbkpl*) would cause FeS_2 to precipitate and phosphate to remain soluble. Reduction of the Fe(OOH) during diagenesis would cause the absorbed phosphate to release from the Fe(OOH) possibility due to OH^- ions replacing the absorbed phosphates, an anaerobic process that depends on the pH conditions and P/Fe ratio (Maine et al., 1992). The isolated amorphous phosphates would then begin to crystallize to form apatite as further heat and pressure from diagenesis occurred. The presence of phosphates in the seawater would have also

stimulated growth in microorganisms and also led to further fixation of Fe^{2+} ions into Fe^{3+} hydroxides through biogenic processes.

The presence of rare, coarse sand-sized granules of composite quartz (Fig. 3.21), microspheroidal textures (Figs. 4.12, and 4.13), and an oxic and anoxic Fe-Mn mineralized lithofacies (*Fgnz* and *Frmz*) are typically indicators of a continental shelf environment (Gross, 1972), where the sand-sized granules of quartz are derived from a continental provenance. Changes from anoxic to highly oxic conditions in the seawater, which is also an observable by two mineralogically different lithofacies (*Frmz* and (*Fgnz*), that in general are underlain by Lithofacies Association I are also characteristic of continental shelf environment.

In summary, Lithofacies Association I has been interpreted as forming in an anoxic reducing environment on the continental shelf, that, in general, underlies the two Fe-Mn mineralized lithofacies: *Fgnz* (Fe-Mn oxide-silicate-carbonates) and *Frmz* (Fe-Mn oxide-carbonates). These lithofacies with gradual changes in mineral composition and microbanding of Fe-Mn minerals (Maynard, 1983) suggest a change in redox conditions that have allowed precipitation and deposition of Fe-Mn minerals. The microbanding of the Fe- and Mn-rich minerals are likely attributed to seasonal fluctuations of dissolved Fe^{2+} and Mn^{2+} within the seawater. This cycle of Fe and Mn precipitation would occur as long as Fe and Mn remained dissolved within the water column and oxidizing conditions persisted (Maynard, 1983).

4.4 METAMORPHISM AND SECONDARY BASE-METAL MINERALIZATION

4.4.1. DESCRIPTION

The presence of base-metal sulfides within the study area was first recorded by Robb (1870), who observed chalcopyrite and pyrite hosted in quartz veinlets in the crests of numerous folds that are repeated on both a macro-and micro-scale (Fig. 4.19). The Fe-Mn mineralized lithofacies, as described by Roberts and Prince (1990), contain features such as quartz-carbonate, quartz-chlorite-sulfide, and quartz-sulfide veins and veinlets that crosscut the beds of Fe-Mn mineralized and unmineralized siltstone with minor low grade base-metal mineralization (Fig. 4.20). Roberts and Prince (1990) also noted that the presence of the Fe-Mn oxide-silicate-carbonate assemblage within the Woodstock deposit suggests an interaction of Fe-Mn-rich carbonates that reacted with the surrounding silicates at subgreenschist-grade metamorphism according to Equation 4.2.

$$2(\text{Fe, Mn})CO_3 + SiO_3{}^{2-} \rightarrow (\text{Fe, Mn})SiO_3 + (\text{Fe,Mn})CO_3 + CO_3{}^{2-}$$

Equation 4.2: Reaction of Fe-Mn carbonates with surrounding unmineralized silicates.

Petrographic and SEM-EDS analysis identifies several samples of minor Cu-Fe-S and Co-As-S mineralization that crosscuts the precursor interlamination of hematite, Mn silicate, and Mn carbonate. This base-metal mineralization is present in both Fe-Mn mineralized lithofacies *Fgnz* and *Frmz* present in the Woodstock Fe-Mn deposits. Several of chalcopyrite crystals hosted in the folds with the North Hartford Fe-Mn deposit contain rims of covellite (CuS) (Fig. 4.21). As described earlier in the chapter, Cu-Fe-S and Co-As-S mineralization was also found to occur

Fig. 4.19: Photograph of minor occurrences of sulfides within a with the Fe-Mn oxide-carbonate lithofacies of a tightly folded Fe-Mn siltstone bed at Iron Ore Hill. The minor sulfide mineralization was not restricted to any particular lithofacies.
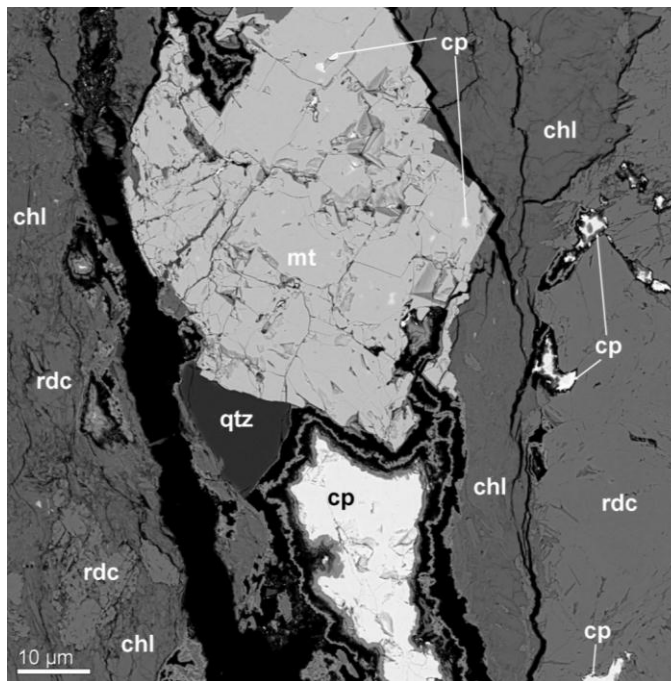
Fig. 4.20: SEM-BSE image of a subhedral magnetite crystal within a quartz-sulfide veinlet within the North Hartford deposit. Magnetite crystals within the Woodstock Fe-Mn mineralized zones locally contain inclusions of chalcopyrite. Sample 9-15-S1. See glossary for abbreviations.
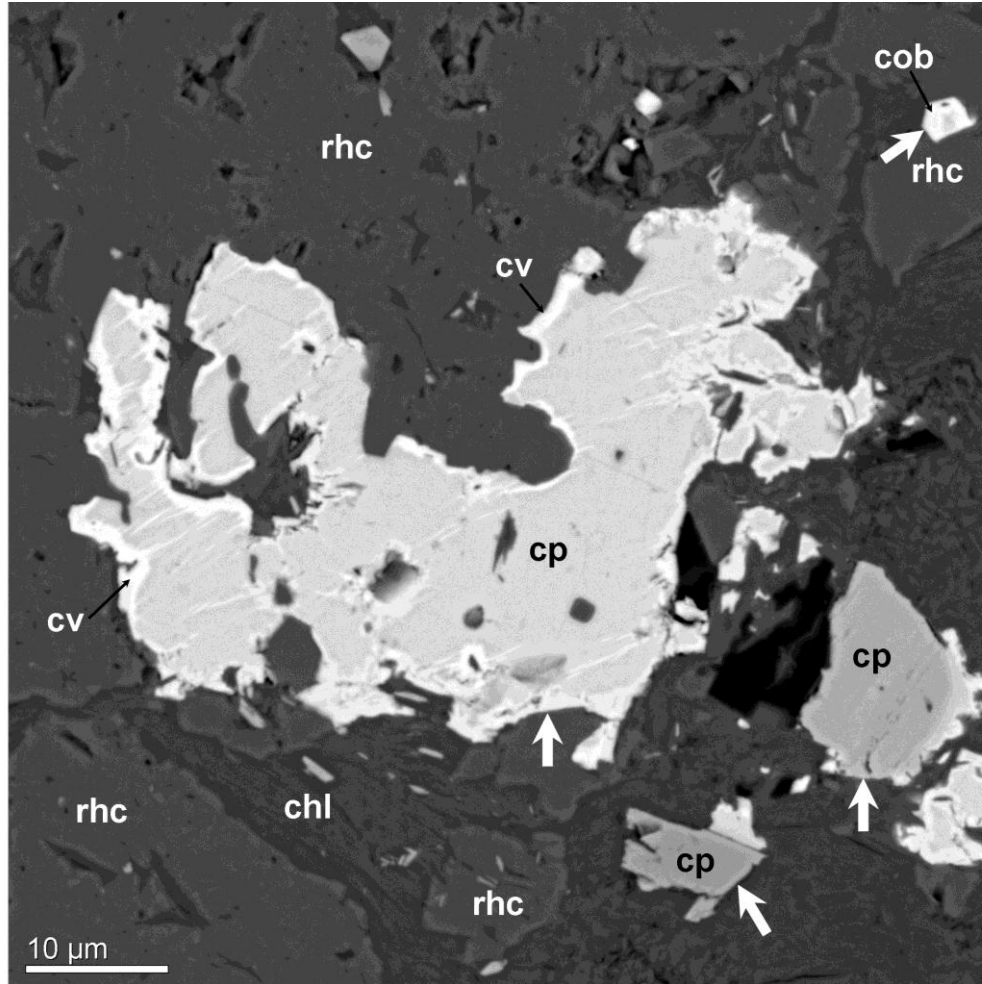
Fig. 4.21: SEM-BSE image of covellite-rimmed anhedral chalcopyrite crystals associated with microfaults in the groundmass composed of rhodochrosite precipitates and chlorite. Sample 9-15-S1. See glossary for abbreviations.

in sections of Units B and C. It was present in these units as crystals and inclusions of chalcopyrite and cobaltite alongside euhedral magnetite crystals. The cobaltite crystals range from euhedral to anhedral in shape and are found to have anhedral inclusions of chalcopyrite and trace inclusions of galena (PbS) (Figs. 4.22, and 4.23). All observable areas of Fe-Mn mineralization that contain minor chalcopyrite, cobaltite, and trace covellite base-metal mineralization in veins and veinlets display an overprinting of sulfides relative to Fe-Mn mineralization (Figs. 4.20). Union Corner was found to display the best example of crosscutting minor Cu-Fe-S mineralization that forms perpendicular of the bands hematite, Fe-Mn carbonate, and Fe-Mn silicate. The chalcopyrite within this area is hosted in the near perpendicular crosscutting quartz-chlorite-sulfide, quartz-sulfide, and sulfide veinlets (Figs. 4.24 and 4.25).

4.4.2 *INTERPRETATION OF BASE-METAL MINERALIZATION*

The metamorphism likely occurred during the Acadian Orogeny in the Early Devonian (Roberts and Prince, 1990). The chlorite-rich mineralization (Units A, and B) and minor silicic and potassic alteration has also raised the hypothesis of the Fe and Mn associated with the Woodstock Fe-Mn deposits being derived from a hydrothermal input (Roberts and Prince, 1990). The alteration of the Fe-Mn mineralized beds is also a characteristic that is seen in hydrothermal Fe-Mn deposits in active tectonic areas. These crosscutting veins and veinlets are likely associated with the low-grade regional metamorphism. Occurrences of the quartz-chlorite-sulfide, quartz-sulfide, and sulfide veinlets at Union Corner suggest these veinlets are late epigenetic in origin (Lovering, 1963) and formed sometime after the
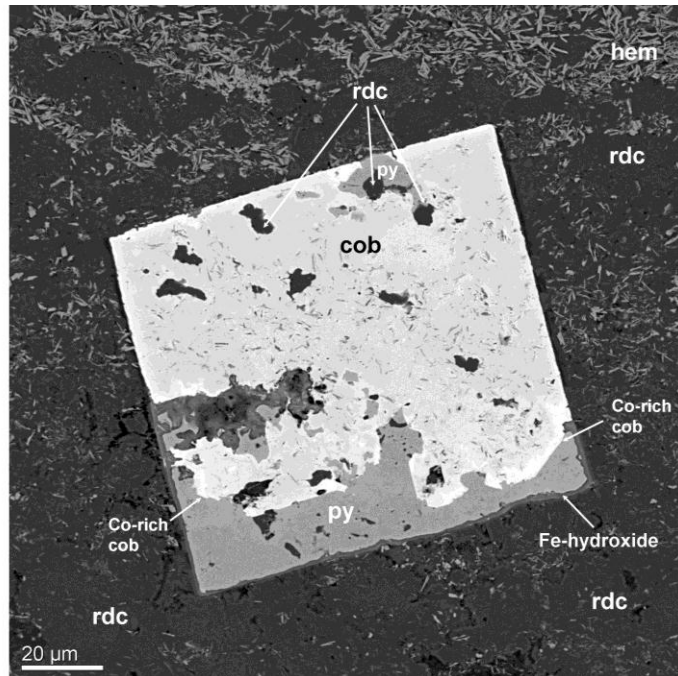
Fig. 4.22: SEM-BSE image of a hetrogenous euhedral cobaltite with inclusions of pyrite and trace hematite from the North Hartford deposit with a more Co-rich composition along the outer rim of the crystal (bright white). Sample 9-15-S1. See glossary for abbreviations.
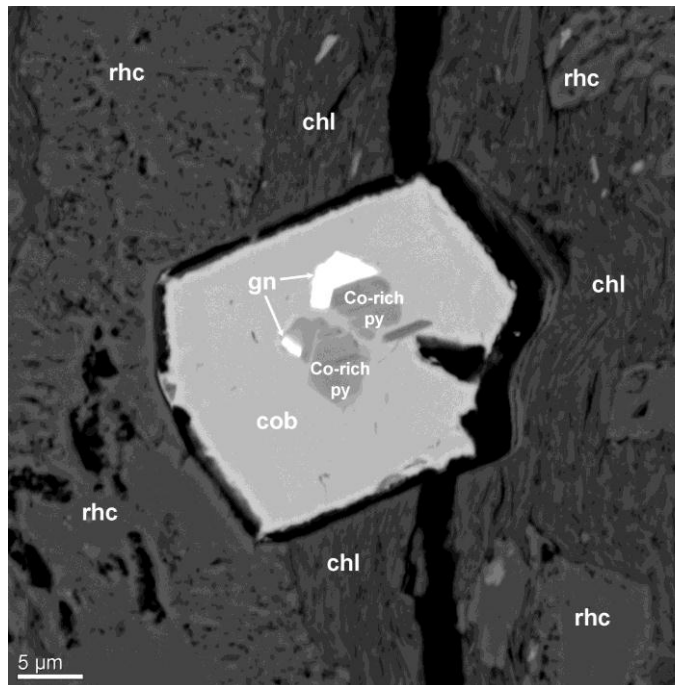
Fig. 4.23: SEM-BSE image of a subhedral cobaltite crystal from the North Hartford deposit with inclusions of euhedral galena and Co-rich pyrite. Sample 9-15-S1. See glossary for abbreviations.

118
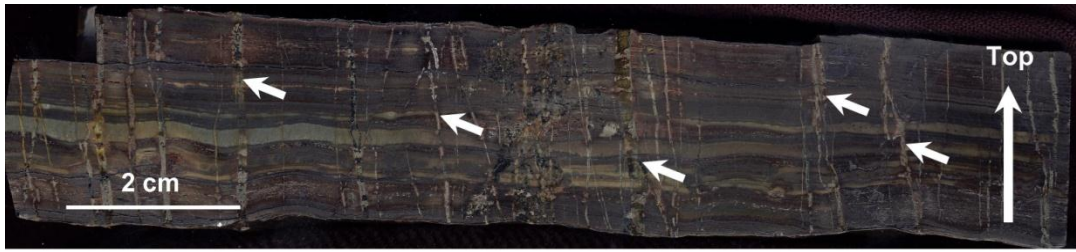
Fig. 4.24: Photograph of a polished slab of interbedded layers of oligonite (green), and rhodochrosite (dark grey) and crosscutting quartz-carbonate, quartz-chlorite-sulfide, and sulfide veinlets, which host minor Cu-Fe-S mineralization. Sample GR-S13-02.
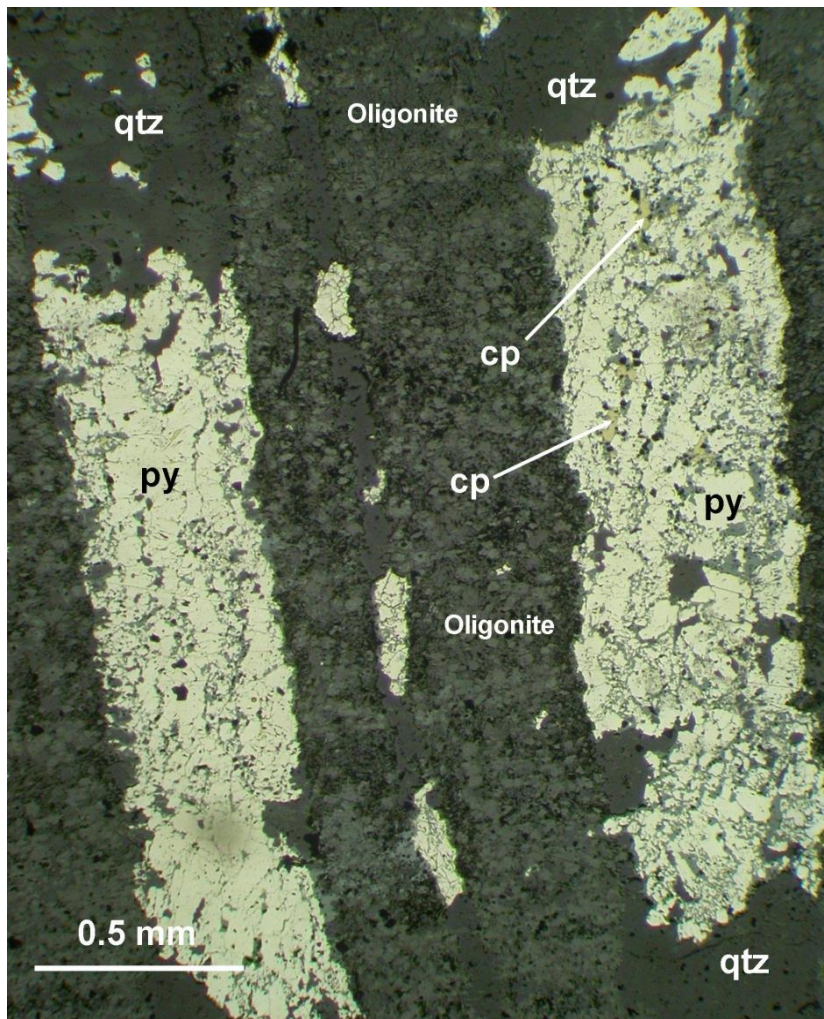
Fig. 4.25: Photomicrograph of sulfide veinlets in a groundmass of subhedral oligonite, in plane polarized reflected light. Minor chalcopyrite is present as inclusions within pyrite. All observed chalcopyrite is confined to the quartz-chlorite-sulfide, and sulfide, veinlets and does not occur outside of the veinlets. Sample GR-S13-02. See glossary for abbreviations.

119

primary, depositional major Fe-Mn, with minor Cu-Fe-S and Co-As-S

mineralization. This evidence suggests that there were two periods of minor Cu-Fe-

S and Co-As-S mineralization within the Woodstock Fe-Mn deposits. It is possible

that some of the original depositional base-metals were remobilized by the

introduction of fluids during the late epigenetic mineralization. Deformation is

present within the sulfide mineralization of Unit B (Figs. 4.14, 4.21) and suggests

that the Cu-Fe-S mineralization within this area occurred before the advent of the

D_2 deformation.

CHAPTER 5

GEOCHEMISTRY OF THE WOODSTOCK FE-MN DEPOSITS

5.1 INTRODUCTION

All geochemical data presented within this current thesis was obtained from archived geochemical data from the project spearheaded by Roberts and Prince (1990). These authors attempted to categorize and analyze only the Plymouth deposit by calculating the potential grade and tonnage, producing a three dimensional model of the deposit, and determining the concentrations of other previously recorded anomalous metals, such as Ga, Ge, Cu, Co, and Au. This archived data has been reassessed to aid in determining the origin of the Plymouth deposit. Roberts and Prince (1990) selected 196 samples from four drill holes and two trenches. Samples during this exploration project were then ground to a -200 mesh using an agate mill to avoid contamination. Major elements (measured as oxides) were analyzed by XRF (X-Ray Fluorescence) where the samples were fused into a glass disk in the presence of air with lithium borates converting all salts (including sulfides, sulfates, and carbonates) and free metals into oxides. Trace elements and rare earth elements (REEs) were measured by Fire Assay Direct Coupled Plasma (FADCP), Directly Coupled Plasma (DCP), Inductively Coupled Plasma Mass Spectrometry (ICPMS), Graphite Furnace Atomic Absorption (GFAA), Atomic Absorption (AA), and Fire Assay Atomic Absorption (FAA). The initial geochemical reports of the bulk geochemical analyses undertaken by XRAL (X-ray Assay Labs Ltd, Don Mills, Ontario) did not include the amount of sample

used for analysis and (or) digestion procedures. The raw geochemical data for the drill holes and associated trenches are presented in Appendix III; sample locations and drill holes logs are present in Appendix IV and on Figure 3.4.

In years prior to 1987, several other samples from the other Woodstock Fe-Mn deposited were assayed, but only for common elements such as Fe, Mn, S, P, as well as insoluble material (McCombe, 1952; Gliders, 1976). This data has not been reassessed for this project.

5.2   GEOCHEMISTRY OF THE LITHOFACIES ASSOCIATIONS

Major oxides and trace metals from four drill holes from the Plymouth deposit (Appendix III) are displayed in relation to Lithofacies Associations O, I, II, and III. Lithofacies IV and V are not present in the Plymouth area (Fig. 3.1). To recap, Lithofacies Association O from the White Head Formation forms the basal part of the section in the area. The three remaining lithofacies associations are only present in the lower member of the Smyrna Mills Formation. Lithofacies Association I contains no Fe-Mn mineralized lithofacies. Lithofacies Association II in general hosts lithofacies *Fgnz* (Fe-Mn oxide-silicate-carbonate) that is occasionally interbedded with lithofacies *Frmz* (Fe-Mn oxide-carbonate). Lithofacies Association III hosts lithofacies *Frmz* (Fe-Mn oxide-carbonate) that is occasionally interbedded with lithofacies *Fgnz* (Fe-Mn oxide-silicate-carbonate).

5.2.1   *LITHOFACIES ASSOCIATION O (WHITE HEAD FORMATION)*

Only eight samples from Lithofacies Association O were analyzed for major oxides, trace elements, and REEs (Fig. 5.1) due to the limited exposure of this

122
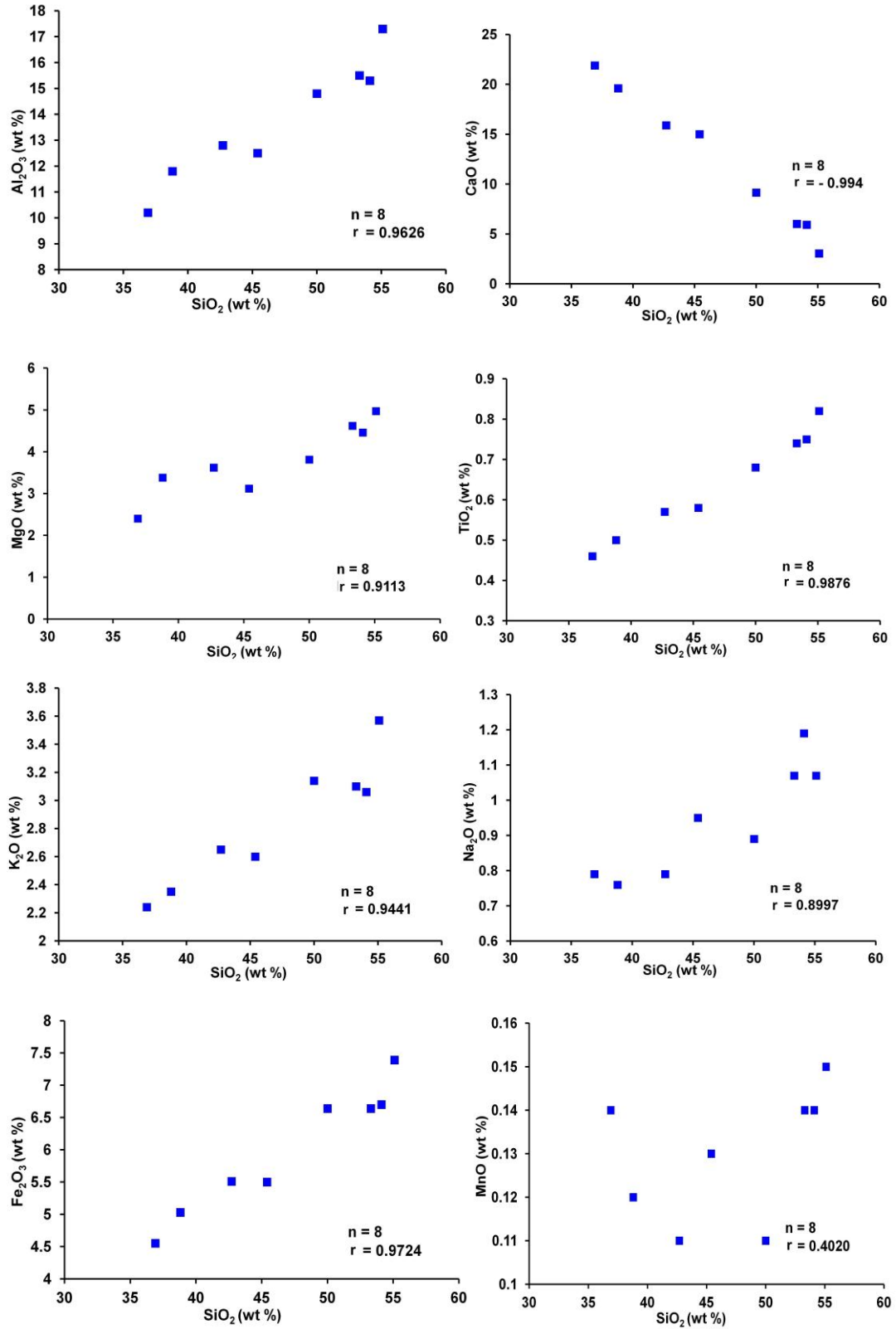
Fig. 5.1: Harker Diagrams for various major oxides and trace elements plotted against SiO_2 within the Lithofacies Association O.
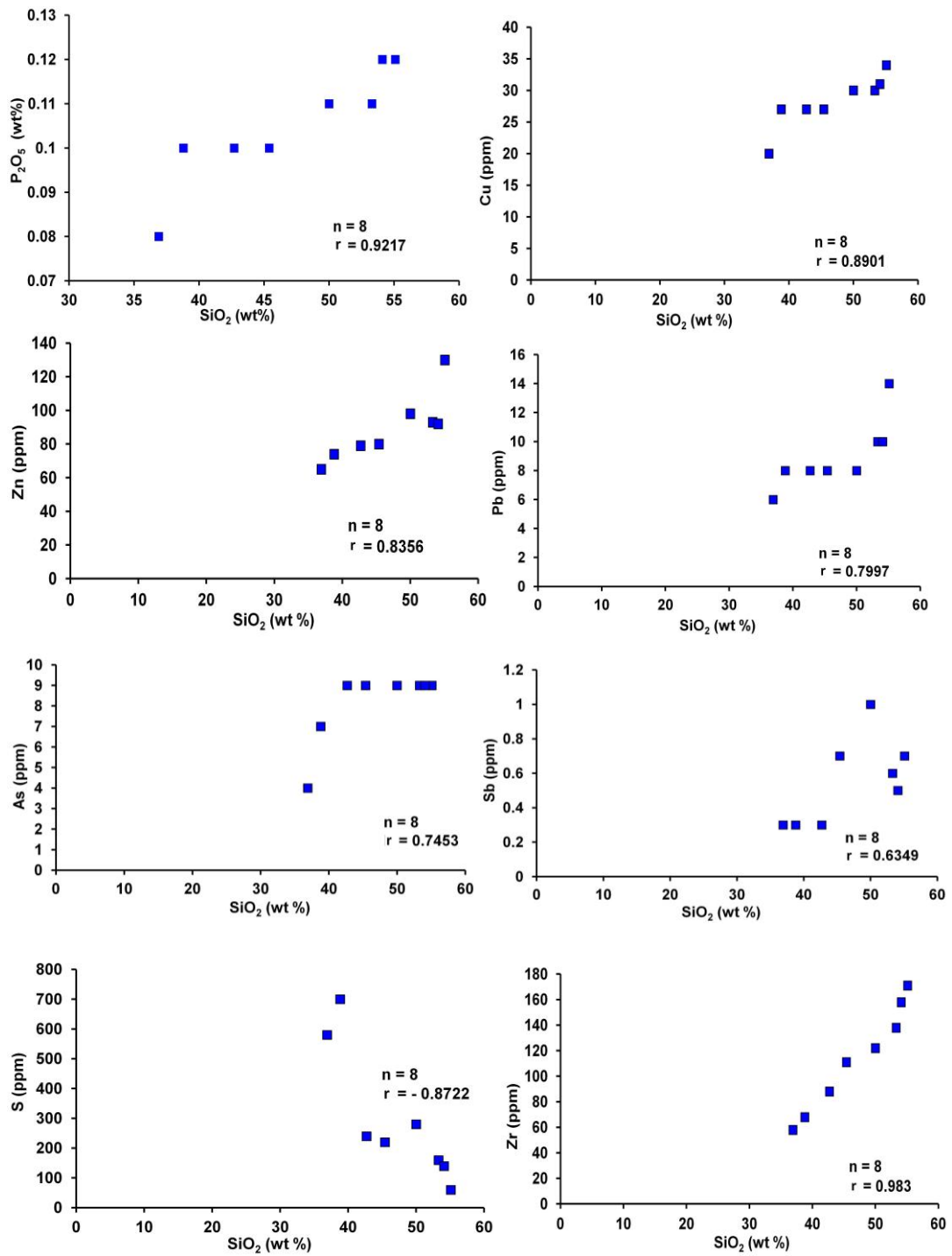
Fig. 5.1: (continued).
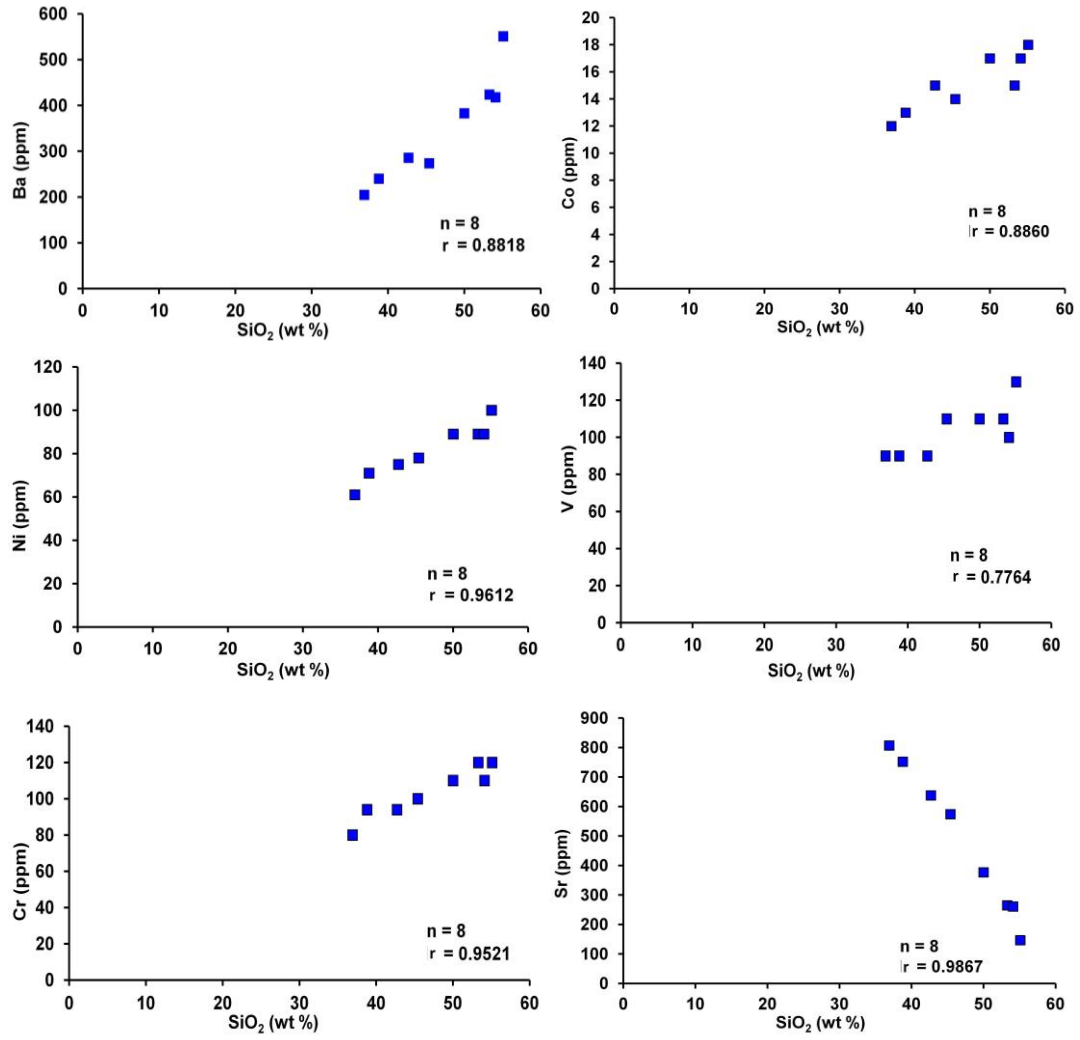
Fig. 5.1: (continued).

lithofacies association at the selected drill and trench sites. Two of the samples were taken from DDH 87-2 (Fig. 5.1) and six samples were extracted from Trench 1 and Trench 2 (Fig. 2.6; Roberts and Prince, 1990). These samples were composed of lithofacies *Sbuc* and *Fbuc* that were described in Chapter 3. Major oxides plotted against SiO_2, with the exception of CaO, MnO, and P_2O_5 show strong positive linear trends with increasing SiO_2 (Fig. 5.1). MnO and P_2O_5 display weaker linear trends that contain several outlying data points, but no high MnO values are present. CaO (mean ± stdev; 12 ± 7%) in contrast displays a strong negative slope in comparison to SiO_2. Al_2O_3 was found to have an average concentration of 13 ± 2% and K_2O had an average concentration of 2.8 ± 0.4%.

As the SiO_2 content of Lithofacies Association O increases, the mean ± standard deviation values of trace metals, such as Cu (28 ± 4 ppm), Zn (88 ± 19 ppm), Pb (9 ± 2 ppm), Ba (347 ± 116 ppm), Co (15 ± 2 ppm), As (8 ± 1 ppm), Ni (81 ± 12 ppm), Cr (103 ± 14 ppm), V (104 ± 14 ppm), and Zr (114 ± 40 ppm) also increase (Fig. 5.1). Only elements such as S (297 ± 224 ppm) and Sr (477 ± 247 ppm) (Fig. 5.1) were found to decrease with increasing SiO_2. The samples within Lithofacies Association O were found to have Fe_2O_3 (6.0 ± 0.9%) and MnO (0.13 ± 0.01%) values that were uniformly below the mean Fe and Mn values in the Plymouth deposit (13.3%, and 10.9%). Uranium has an average concentration of 1.5 ± 0.2 ppm with a maximum concentration of 2.0 ppm in Lithofacies Association O. No high anomalous metals were found with the sampled lithofacies *Sbuc, Fbuc,* and *Lbu* of this formation.

5.2.2 LITHOFACIES ASSOCIATION I (LOWER MEMBER SMYRNA MILLS FORMATION)

Six samples ascribed to Lithofacies Association I were obtained from DDH 87-2, DDH 87-3, Trench 1 and Trench 2 at the Plymouth deposit (Appendix III) by Roberts and Prince (1990) and are representative of lithofacies *Fgngyib, Fgyl*, and *Fbkpl*. Harker diagrams display positive linear trends between Al_2O_3, TiO_2, K_2O, and Na_2O in comparison to SiO_2; whereas CaO, MgO, Fe_2O_3, MnO, and P_2O_5 decreased with SiO_2 content (Fig. 5.2). These trends are strongly influenced by outliers within the dataset. Overall major oxide contents (mean ± stdev) of Al_2O_3 (16 ± 5%), K_2O (4 ± 2%), Fe_2O_3 (12 ± 4%), MnO (4 ±1%), and P_2O_5 (0.3 ± 0.5%) were higher in Lithofacies Association I in comparison to Lithofacies Association O [Al_2O_3 (13 ± 2%), K_2O (2.8 ± 0.4%), Fe_2O_3 (6.0 ± 0.9%), MnO (0.13 ± 0.01%), and P_2O_5 (0.11 ± 0.01%)]. In contrast, mean ± stdev values of CaO (1 ± 1%) were lower in Lithofacies Association I in comparison to Lithofacies Association O that contained a limestone lithofacies [CaO (12 ± 7%)]. The increase in MnO content may be associated with minor Fe-Mn carbonates in the bedrock.

Trace elements such as Cu, Zn, Pb, As, Ba, Cr, V, and Zr display positive linear trends with increased SiO_2 content, whereas Sb, Co, and Sr show negative linear trends (Fig. 5.2). Overall higher mean ± stdev values of Cu (77 ± 13 ppm), Pb (18 ± 6 ppm), S (3683 ± 2916 ppm), As (13 ± 5 ppm), Ba (786 ± 197 ppm), Co (52 ± 17 ppm), and V (140 ± 50 ppm) with lower Sr (73 ± 45 ppm) in relation to SiO_2 mean values occur in Lithofacies Association I compared to Lithofacies Association O. Higher Cu and Co concentrations are observable in thin-section as minor base-metal mineralization.
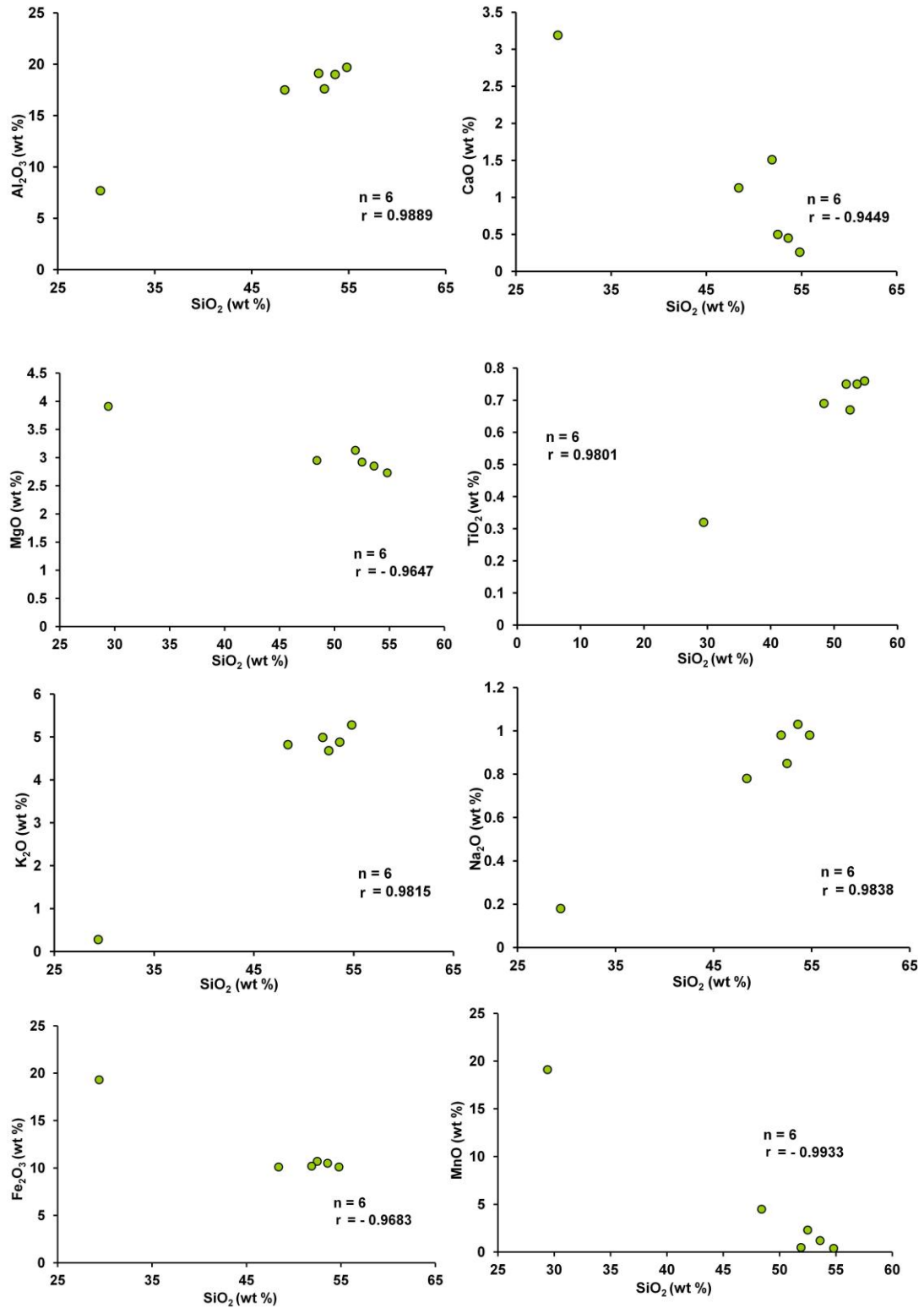
Fig. 5.2: Harker Diagrams for various major oxides and trace elements plotted against SiO_2 within Lithofacies Association I.

128
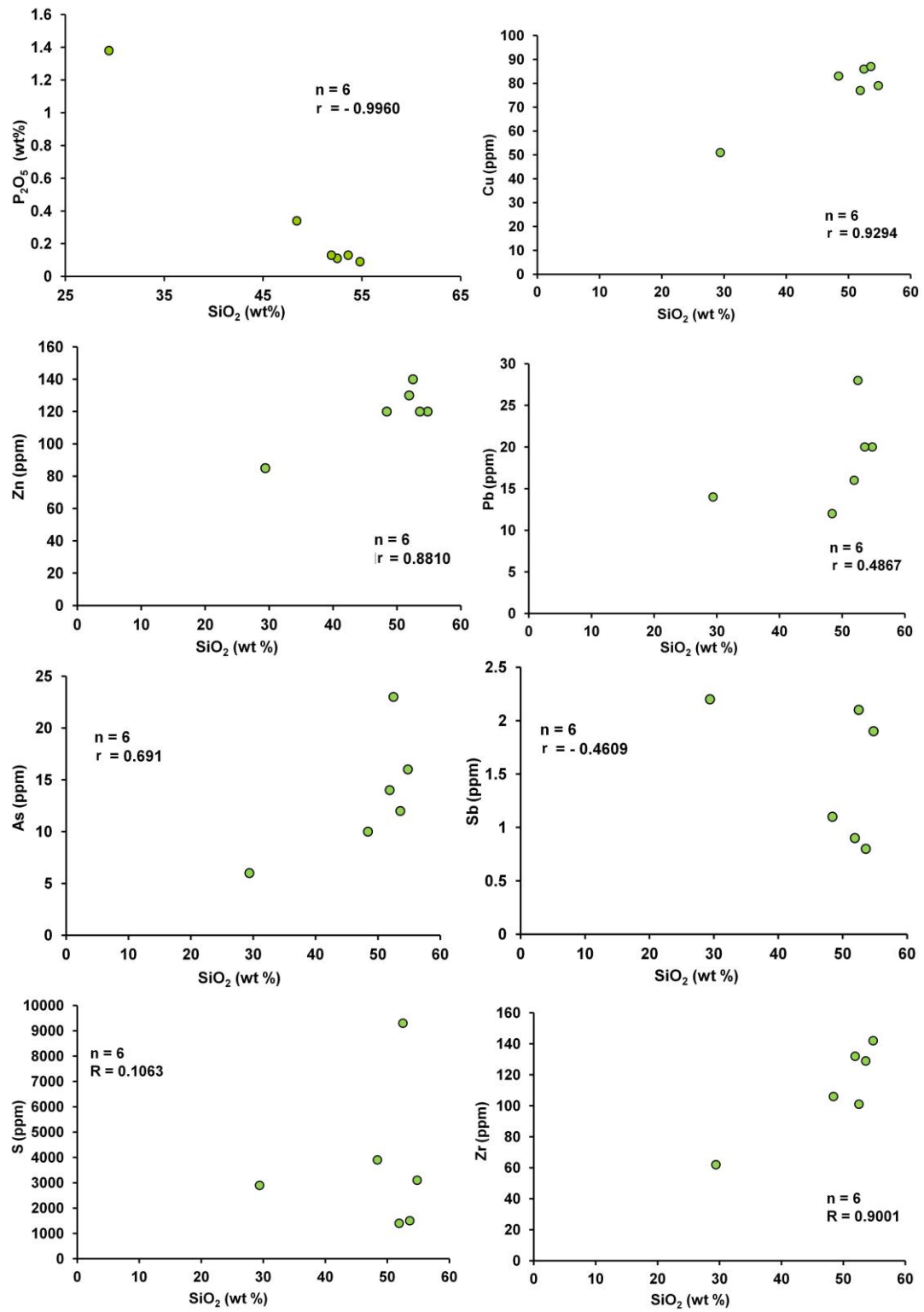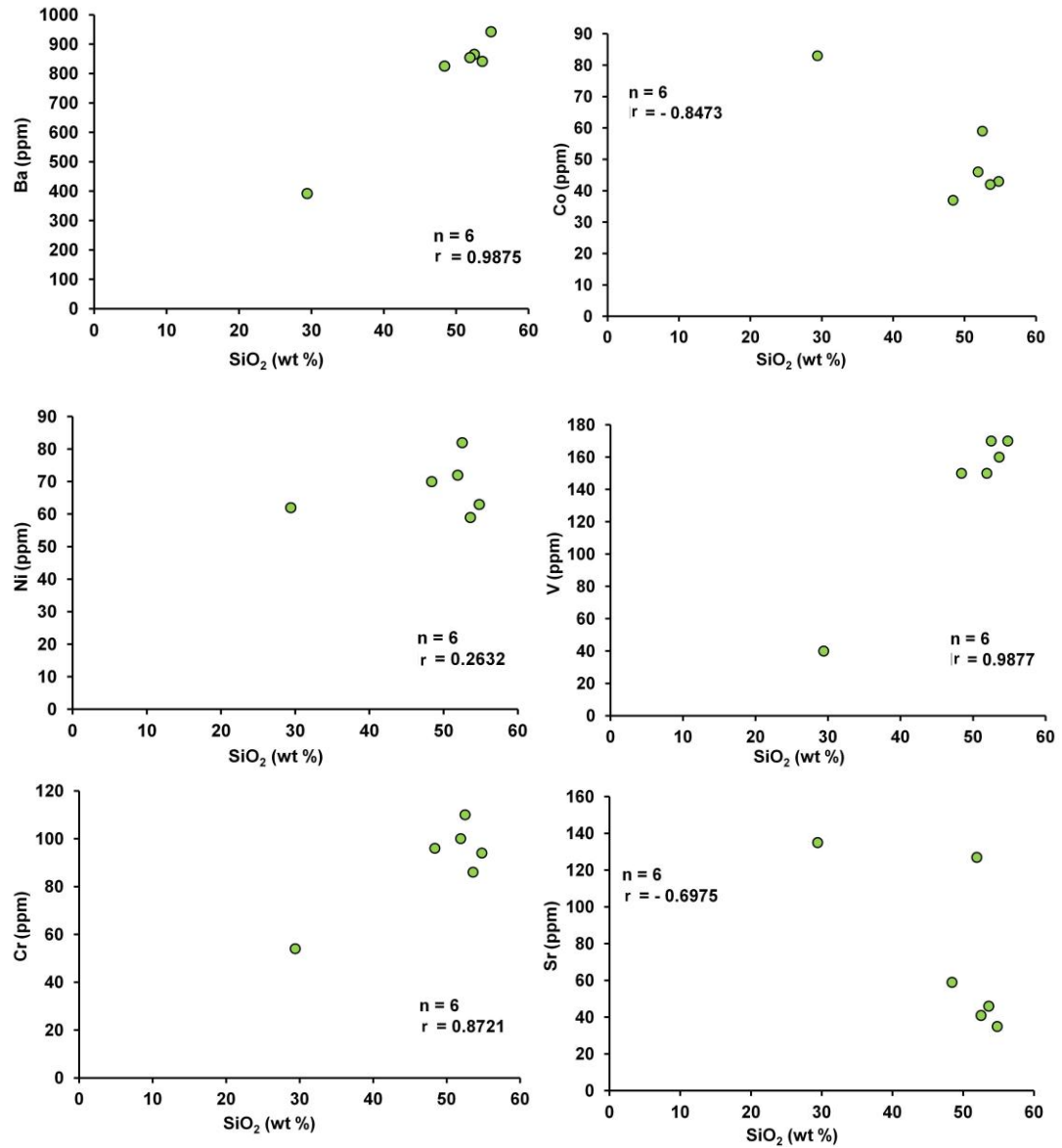
Fig. 5.2: (continued).

Fig. 5.2: (continued).

5.2.3. LITHOFACIES ASSOCIATION II (LOWER MEMBER SMYRNA MILLS FORMATION)

Seventy-two samples taken from DDH-87-2, DDH-87-3, DDH-87-4, DDH-87-5, Trench 1, and Trench 2 are from Lithofacies Association II (Fig. 5.3). This association has mean Fe_2O_3 content of $21 \pm 7\%$ and a MnO content of $12 \pm 6\%$, which are considerably higher than in the aforementioned associations, and demonstrative of the presence of the Fe-Mn mineralized lithofacies *Fgnz* (Fe-Mn oxide-silicate-carbonate) and minor lithofacies *Frmz* (Fe-Mn oxide-carbonate) within the Plymouth deposit (Fig. 5.4). Samples collected are representative of lithofacies *Fgnl, Fgygn*, and *Fgnz*. The major oxides Al_2O_3, TiO_2, and K_2O display strong positive linear trends with increasing SiO_2 content, whereas CaO, Fe_2O_3, MnO, and P_2O_5 exhibit strong negative trends (Fig. 5.4). Mean $\pm$ stdev values of major oxides such as K_2O ($2 \pm 1\%$), Al_2O_3 ($10 \pm 4\%$), MgO ($2.5 \pm 0.9\%$) and TiO_2 ($0.5 \pm 0.2\%$) are slightly lower in comparison to Lithofacies Association I whereas CaO contents ($2 \pm 1\%$) and Na_2O ($1.1 \pm 0.8\%$) are slightly higher.

Trace elements such as Cu, Zn, Pb, Ba, Zr, Ni, Cr, and V display positive linear trends, and Co, As, and Sr negative linear trends, with increasing SiO_2 content (Fig. 5.4). Collectively, trace elements such as V (48 ± 39 ppm), S (1633 ± 1460 ppm), Cr (58 ± 24 ppm), As (9 ± 6 ppm), Cu (57 ± 27 ppm), Pb (13 ± 8 ppm), and Zn (84 ± 26) were found to have lower mean values in comparison to Lithofacies Association I. Lithofacies Association II also has a U concentration of 1.8 ± 0.9 ppm with a maximum value of 7 ppm, whereas Th has a concentration of 6 ± 3 ppm with a maximum value of 14 ppm.
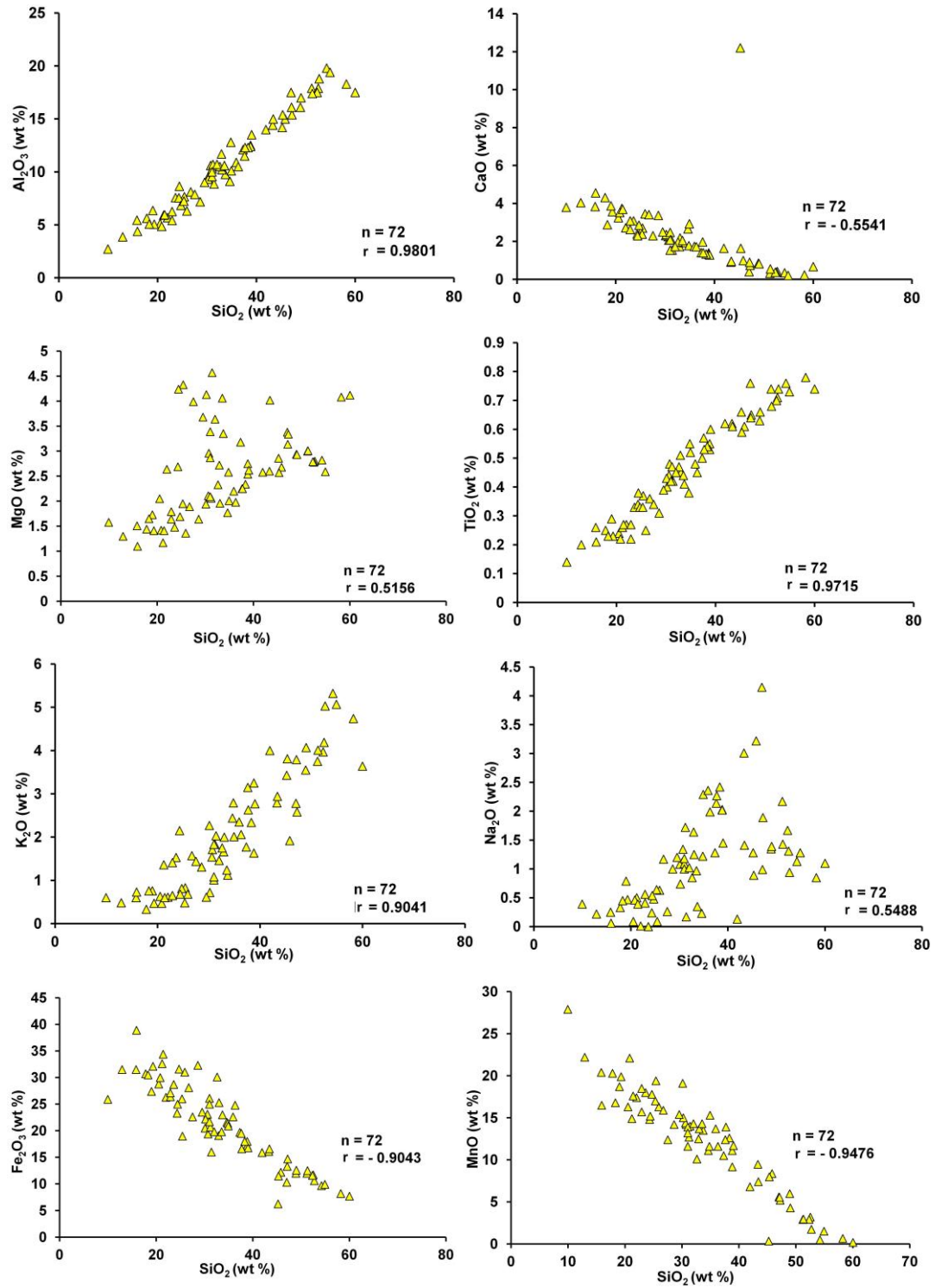
Fig. 5.3: Harker Diagrams for various major oxides and trace elements plotted against SiO_2 within Lithofacies Association II.

Fig. 5.3: (continued).

133

Fig. 5.3: (continued).

134
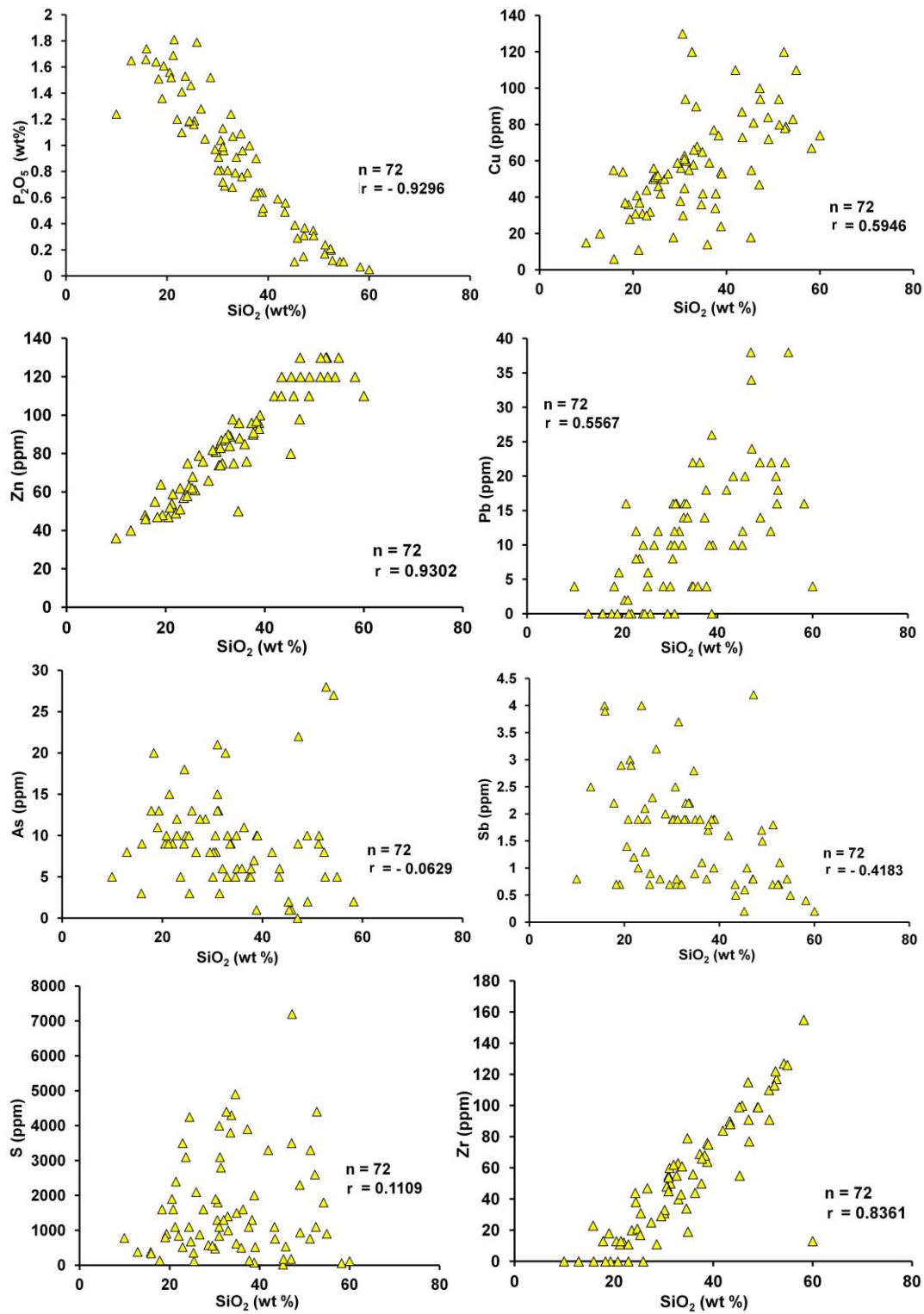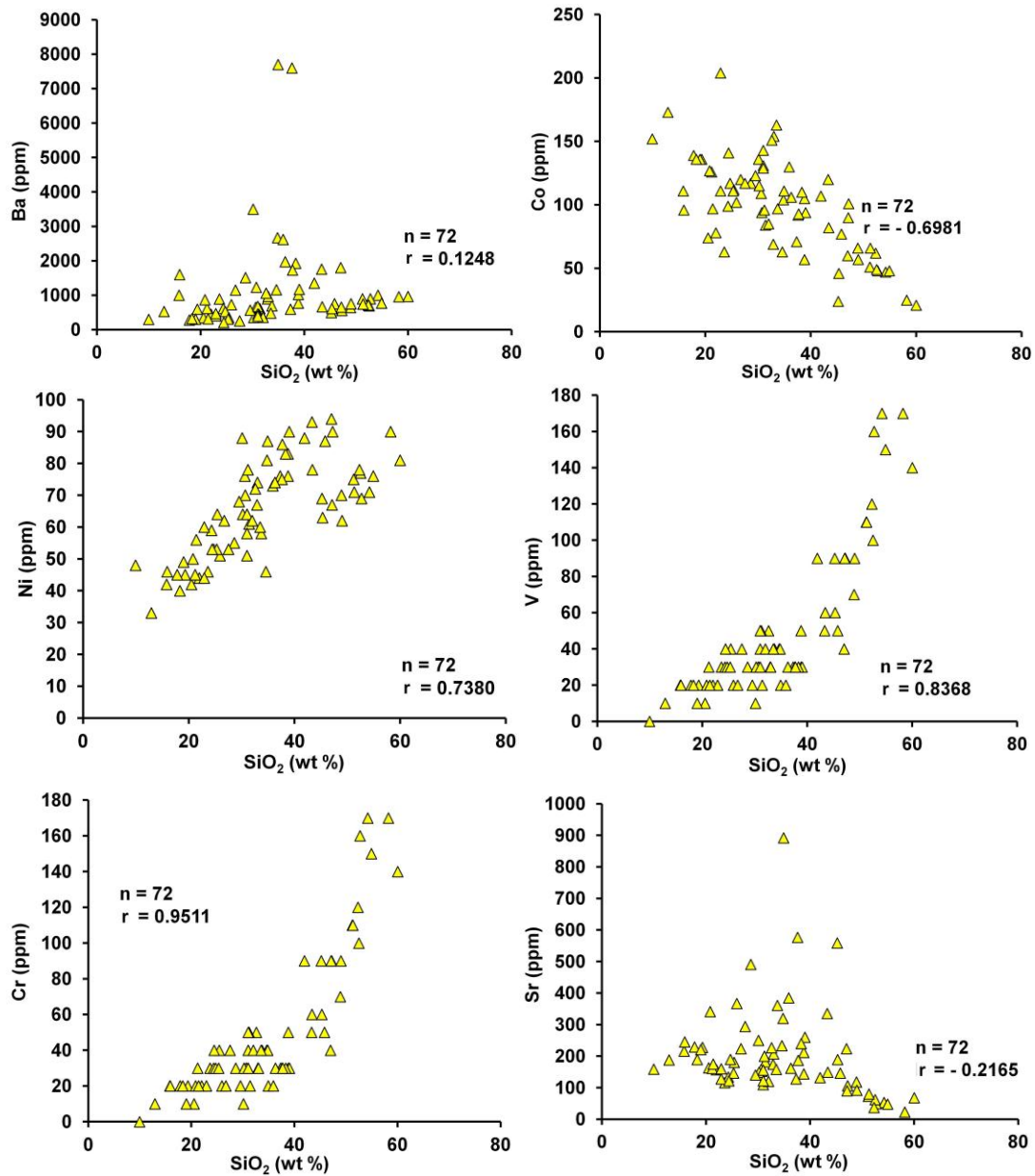
Fig. 5.4: A small outcropping of lithofacies *Fgnz* (Fe-Mn oxide-silicate-carbonate) in Lithofacies Association II in an outcrop near the Plymouth deposit.

5.2.4 LITHOFACIES ASSOCIATION III (LOWER MEMBER SMYRNA MILLS FORMATION)

Sixty-two samples were taken from the lithofacies *Frml* and *Frmz* that collectively make up Lithofacies Association III at the Plymouth deposit (Fig. 5.5). As previously noted, the highest mean $\pm$ stdev concentrations of both Fe_2O_3 ($24 \pm 8\%$), and MnO ($14 \pm 5\%$), correspond to this lithofacies association. Positive linear trends are present within Al_2O_3 ($9 \pm 4\%$), MgO ($2.2 \pm 0.9\%$), Na_2O ($1.1 \pm 0.8\%$), K_2O ($2 \pm 1\%$), and TiO_2 ($0.3 \pm 0.2\%$), in comparison to increasing SiO_2 content (Fig. 5.5). In contrast, Fe_2O_3 and MnO, together with CaO ($2 \pm 1\%$) and P_2O_5 ($1.0 \pm 0.5\%$), collectively display strong negative linear trends with increasing SiO_2 content.

The trace elements Cu, Zn, Pb, V, Cr, Ni, Ba, and Zr display positive linear trends with increasing SiO_2 content and negative trends are displayed for As, Sb, and Sr (Fig. 5.5). Slight decreases were seen in Cu (56 ± 55 ppm) and increases Co (122 ± 41 ppm), with no apparent lower values in trace elements in comparison to Lithofacies Association II. Lithofacies Association III has a U concentration of 2.0 ± 2 ppm with a maximum value of 14.3 ppm. Thorium has an average concentration of 5 ± 3 ppm with a maximum concentration of 12 ppm. Overall, Lithofacies Association III has higher mean values of P_2O_5 ($1.0 \pm 0.5\%$), Cu (56 ± 55 ppm), Co (122 ± 41 ppm), Pb (12 ± 8 ppm), As (10 ± 7 ppm), Sb (3 ± 2 ppm), Sr (288 ± 260 ppm), and Ba (1442 ± 1544 ppm) and lower K_2O ($2 \pm 1\%$), TiO_2 ($0.3 \pm 0.2\%$), MgO ($2.3 \pm 0.8\%$) in comparison to Lithofacies Association II (Fig. 5.5).
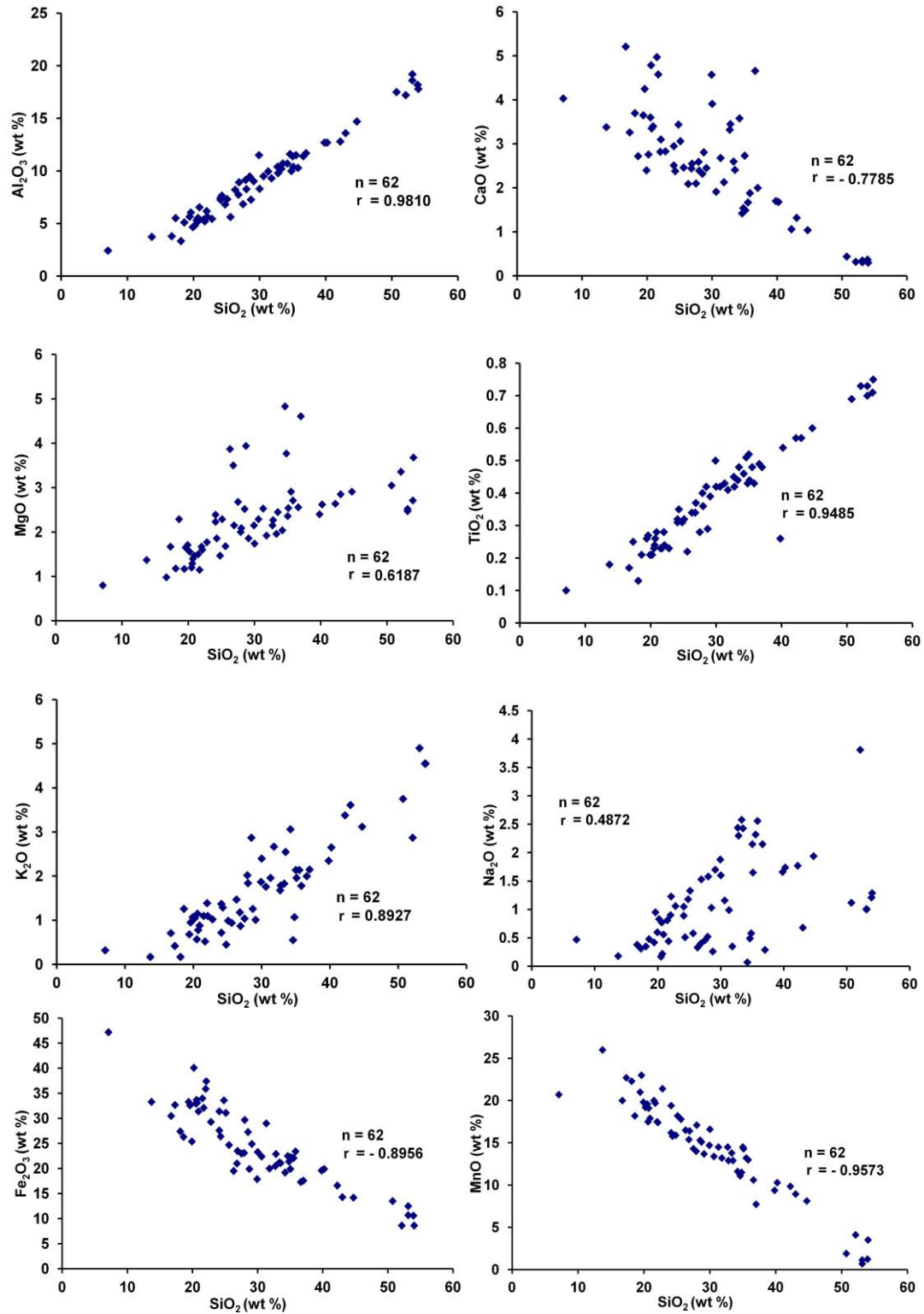
Fig. 5.5: Harker Diagrams for various major oxides and trace elements plotted against SiO_2 within Lithofacies Association III.

137
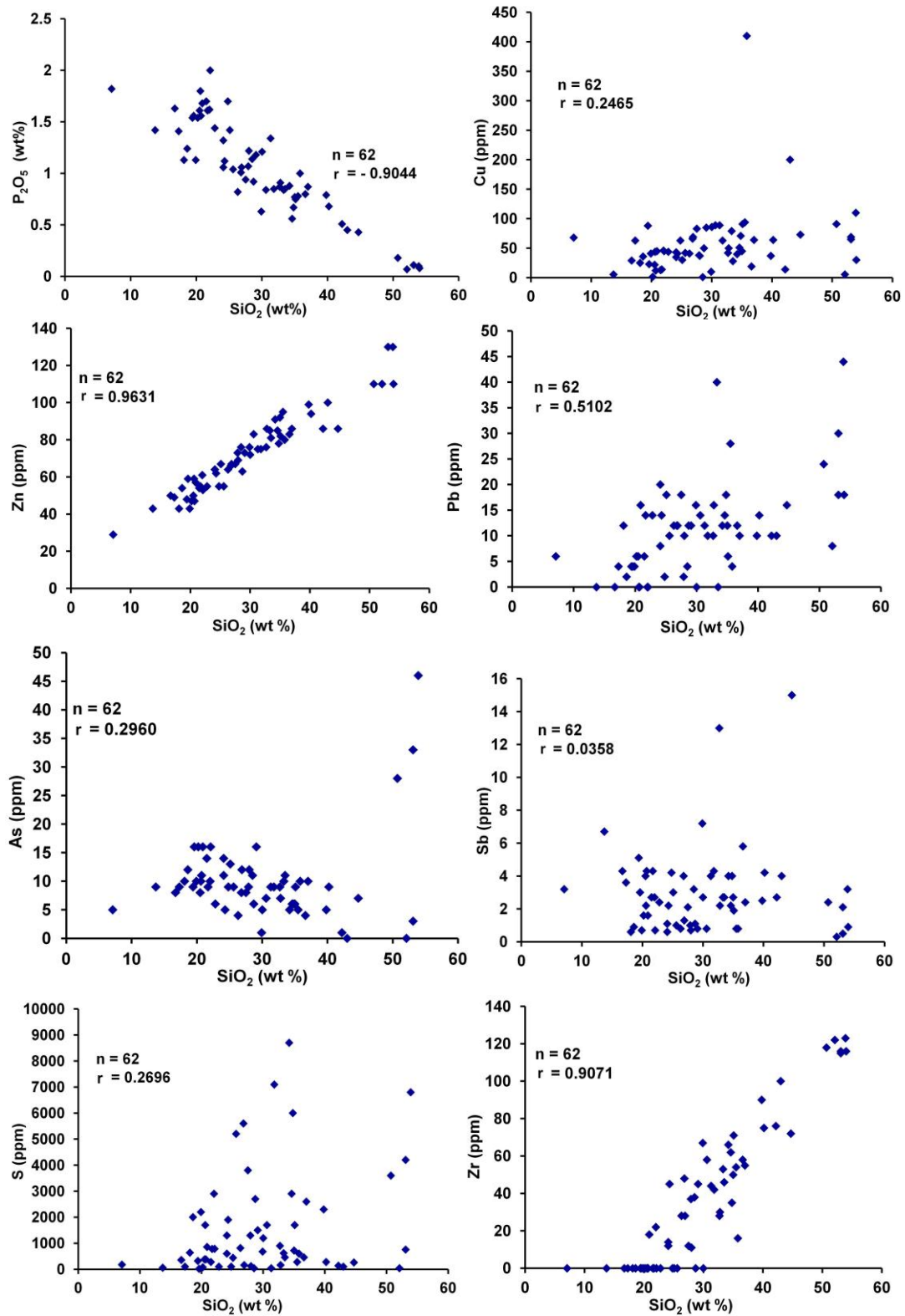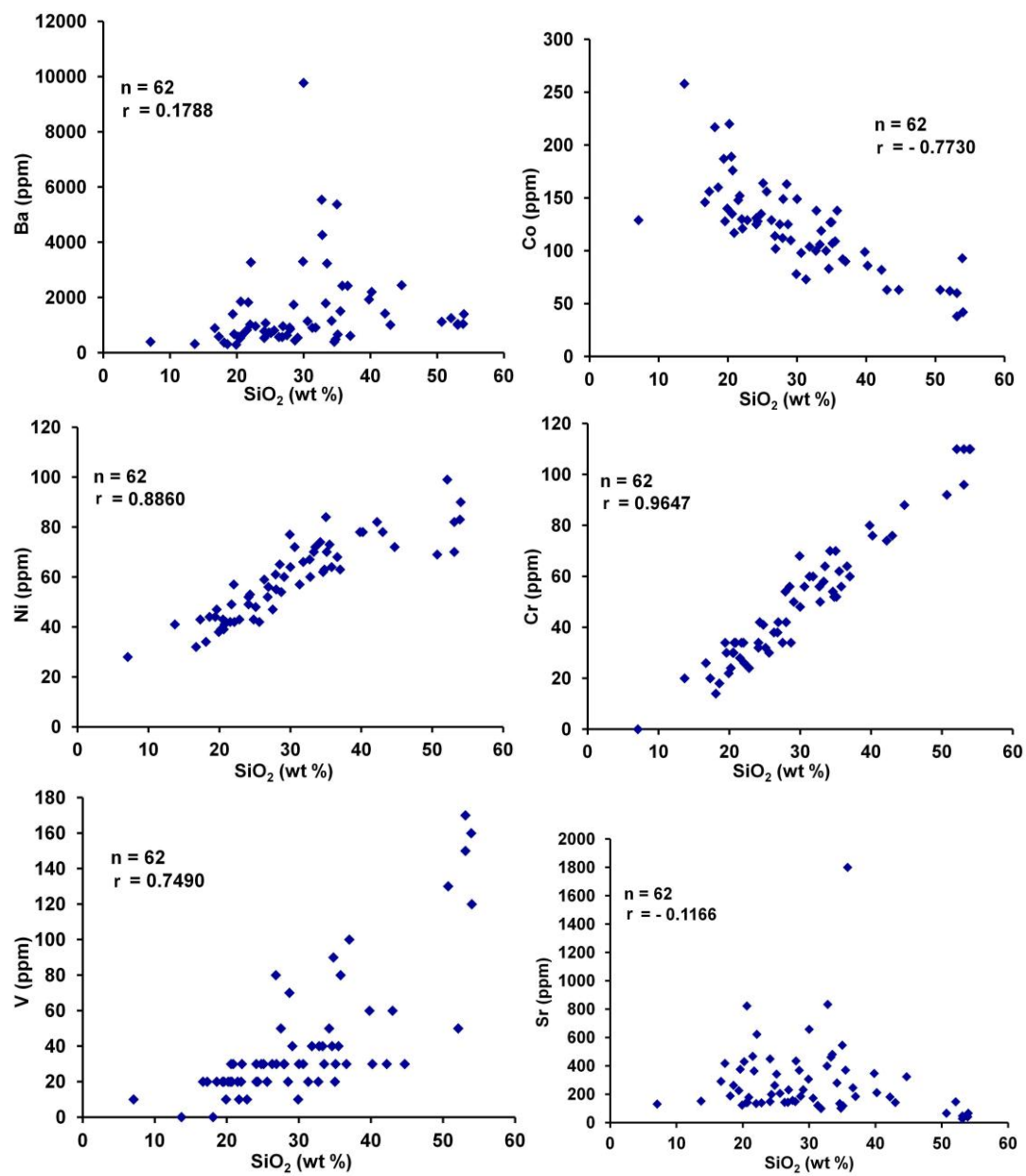
Fig. 5.5: (continued).

Fig. 5.5: (continued).

5.3   INTERPRETATION OF GEOCHEMISTRY

5.3.1 Major Oxides, Trace Elements, and REEs

Lithofacies Association O appears to be not only lithologically different, but also geochemically distinct in relation to Lithofacies Associations I, II, III as observed in downhole plots from the Plymouth deposit (Figs. 5.1 – 5.6). Spider plots display average CaO and Sr values higher than in other lithofacies associations, whereas other major oxides (Fe_2O_3, MnO, P_2O_5) and trace elements (Cu, Pb, S, As, Ba, Co, and V) are lower (Fig. 5.7).

The high CaO average ($12 \pm 7\%$) that is present in the Lithofacies Association O (White Head Formation) is attributed to the sampling of interbedded lithofacies *Lbu* within this unit. In comparison to Lithofacies Association O, Lithofacies Association I contains higher averages of other major elements Fe_2O_3, MnO, P_2O_5, K_2O, and Al_2O_3. The elevated values of these major elements are attributed to a higher abundance of in clay minerals, sulfides, with minor rhodochrosite and apatite. Lithofacies Associations II, and III have lower averages of K_2O ($2 \pm 1\%$, $2 \pm 1\%$) and Al_2O_3 ($10 \pm 4\%$, $9 \pm 4\%$) than Lithofacies Associations I ($4 \pm 2\%$, $16 \pm 5\%$) and O ($2.8 \pm 0.4\%$, $13 \pm 2\%$). This lower quantity is likely caused by a lower abundance in clay minerals and micas, consistent with the lack of clay minerals in thin section (Figs. 3.17, 3.18, 3.21). Geochemical values of Fe_2O_3, MnO, and P_2O_5, in contrast to Lithofacies Association O, increase consistently, stratigraphically upward within Lithofacies Association I, II, and III. This statement keeps in mind, that, in general, Lithofacies Association O forms the lowermost unit and is overlain successively by Lithofacies Associations I, II, III.

a)
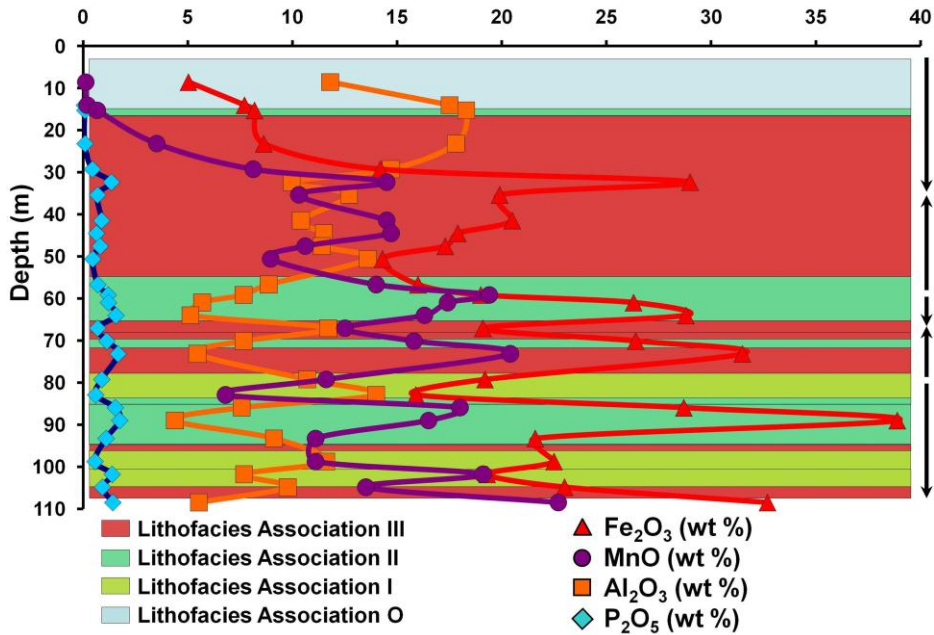
Fig. 5.6a: DDH 87-2 down hole plots of Fe_2O_3, MnO, Al_2O_3, and P_2O_5. Because the succession is extensively folded, the core penetrates the lithofacies associations several times. The arrows are indicating tops direction.

b)
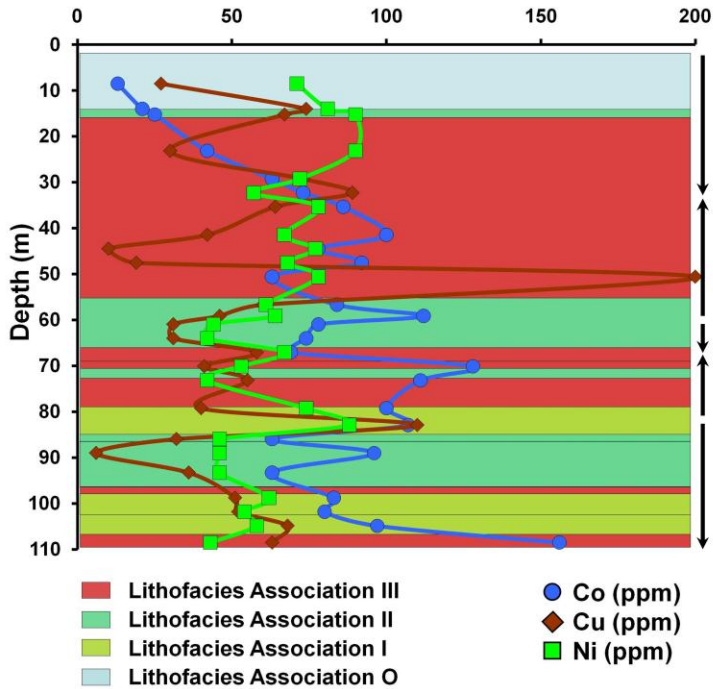
Fig. 5.6b: DDH 87-2 down hole plots of Co, Cu, and Ni. Because the succession is extensively folded, the core penetrates the lithofacies associations several times. The arrows are indicating tops direction.

141

c)
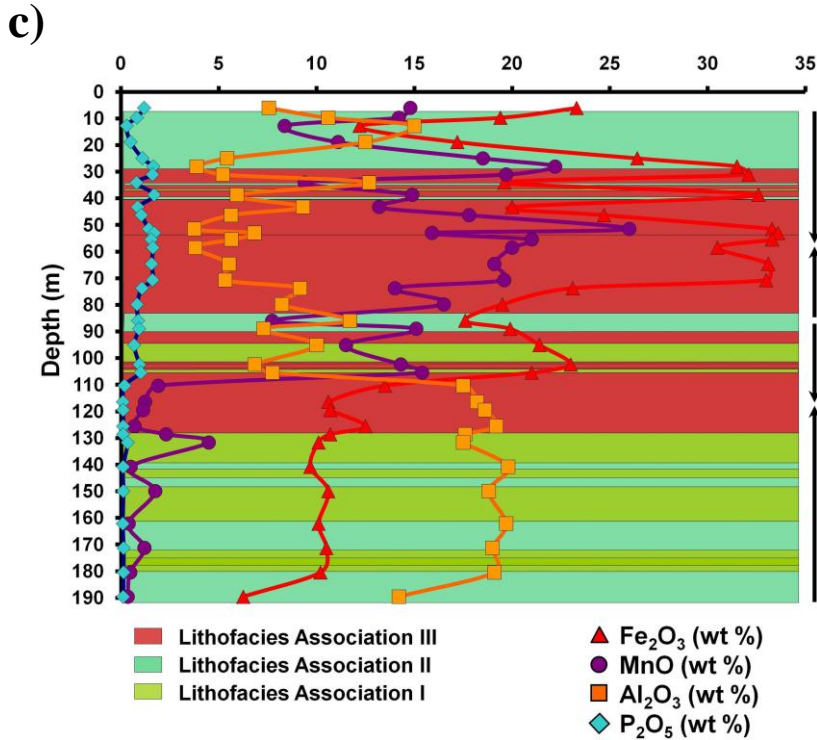
Fig. 5.6c: DDH 87-3 down hole plots of Fe$_2$O$_3$, MnO, Al$_2$O$_3$, and P$_2$O$_5$. Because the succession is extensively folded, the core penetrates the lithofacies associations several times. The arrows are indicating tops direction.

d)
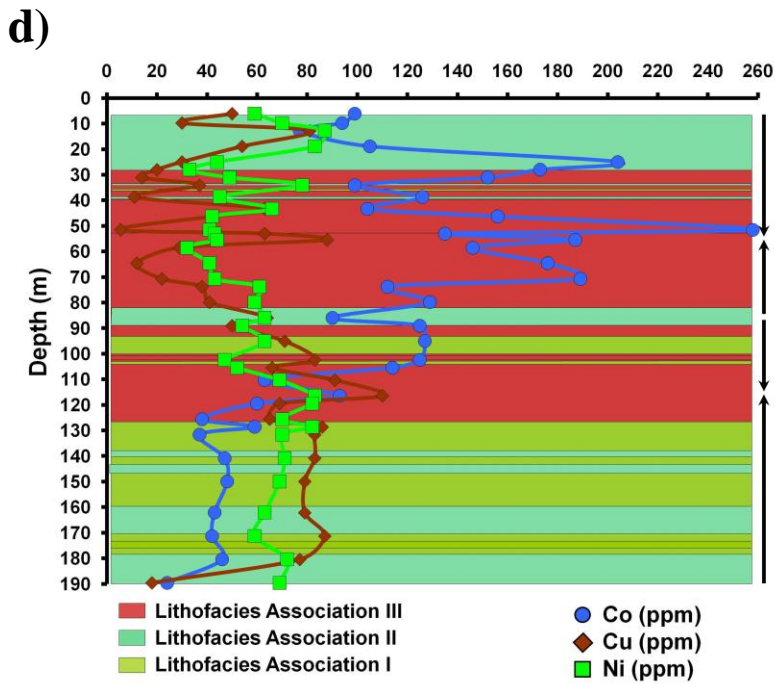
Fig. 5.6d: DDH 87-3 down hole plots of Co, Cu, and Ni. Because the succession is extensively folded, the core penetrates the lithofacies associations several times. The arrows are indicating tops direction.

e)
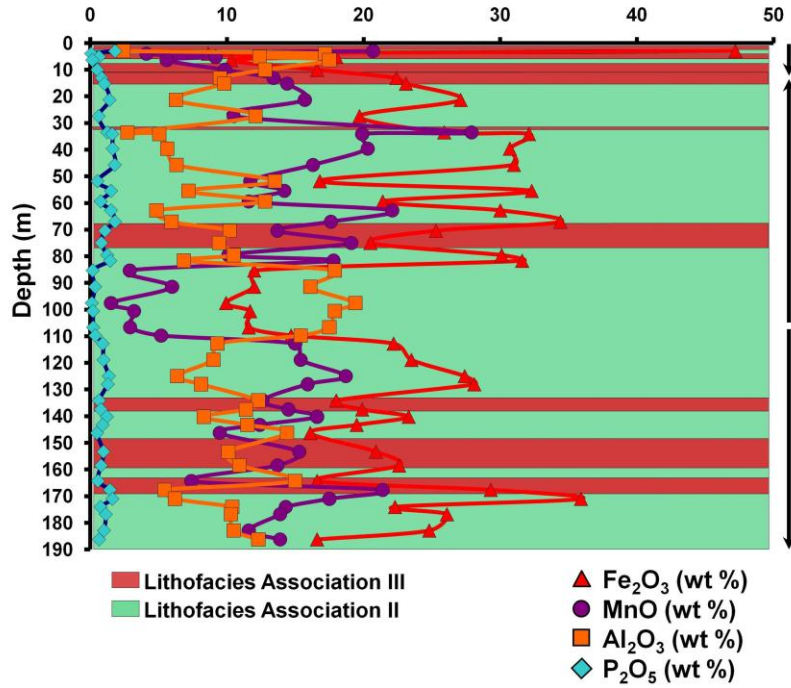
Fig. 5.6e: DDH 87-4 down hole plots of Fe_2O_3, MnO, Al_2O_3, and P_2O_5. Because the succession is extensively folded, the core penetrates the lithofacies associations several times. The arrows are indicating tops direction.

f)
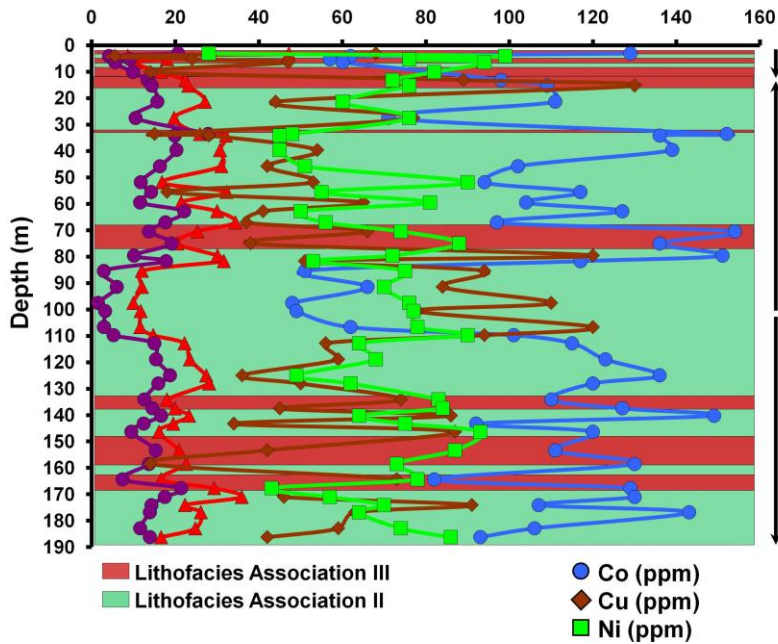
Fig. 5.6f: DDH 87-4 down hole plots of Co, Cu, and Ni. Because the succession is extensively folded, the core penetrates the lithofacies associations several times. The arrows are indicating tops direction.

g)
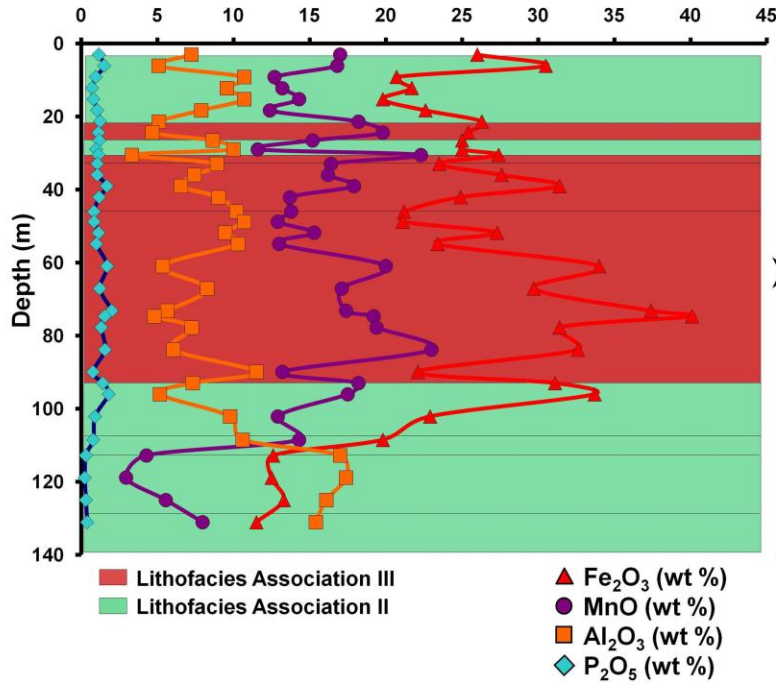
Fig. 5.6g: DDH 87-5 down hole plots of Fe_2O_3, MnO, Al_2O_3, and P_2O_5. Because the succession is extensively folded, the core penetrates the lithofacies associations several times. The arrows are indicating tops direction.

h)
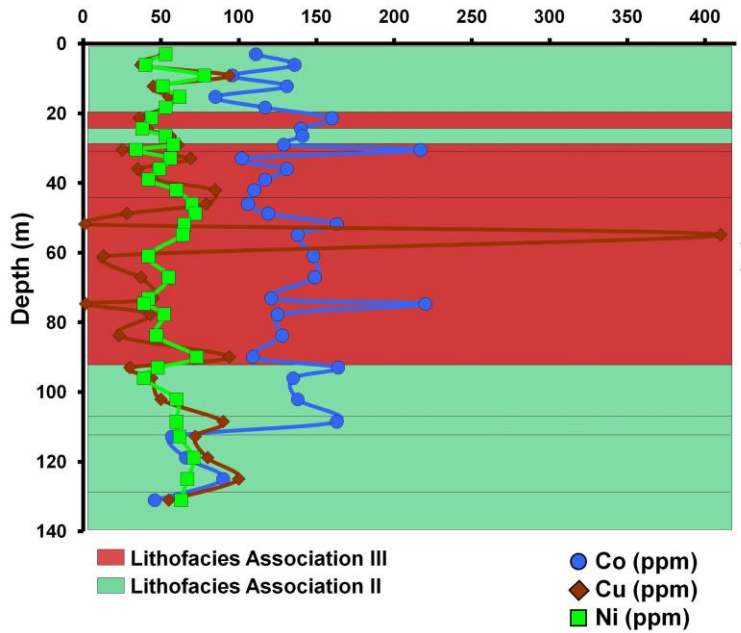
Fig. 5.6h: DDH 87-5 down hole plots of Co, Cu, and Ni. Because the succession is extensively folded, the core penetrates the lithofacies associations several times. The arrows are indicating tops direction.

144
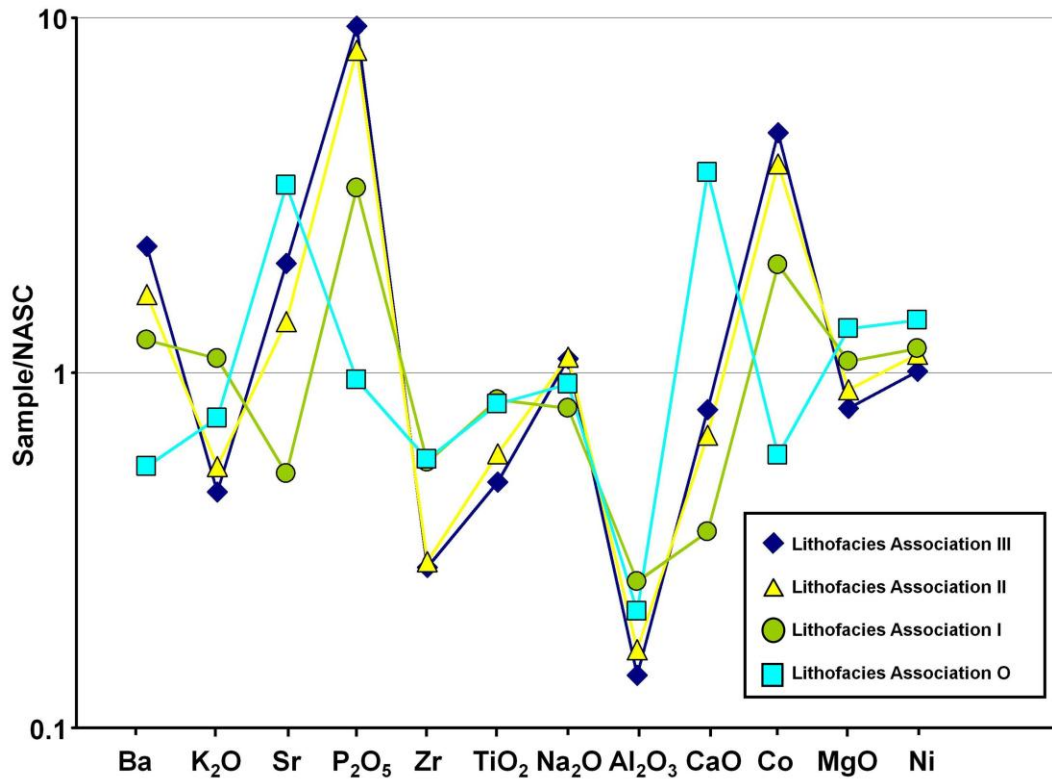
Fig. 5.7: NASC-normalized average major-oxide and trace-element plot of
Lithofacies Association O, I, II, III (Gromet et al., 1984).

This chemical variation is caused by the precipitation of pyrite and Fe-Mn carbonates in Lithofacies Associations I and II and increasing Fe-Mn hydroxide and oxyhydroxide precipitation in Lithofacies Association III. The increase in P_2O_5 may be associated with apatite that formed following reduction of the precursor Fe-oxides onto which phosphate had absorbed. Fe_2O_3, MnO, and P_2O_5 often have strong inverse correlations with K_2O and Al_2O_3 that are observable in downhole plots (Figs. 5.6a - h), a relationship often associated with chemical sediments that lack a detrital input (Beukes and Gutzmer, 2008). The Fe_2O_3 and MnO values would be associated with chemical precipitates and P_2O_5 is associated with phosphates that chelate with the hydrated Fe-oxide complexes (Jones and Bowser, 1978; Beukes and Gutzmer, 2008).

The increase in Fe_2O_3 content upsection reflects the presence of three main groups of iron-rich minerals within Lithofacies Associations I, II, III. In Lithofacies Association I, the higher average Fe_2O_3 ($12 \pm 4\%$), MnO ($4 \pm 1\%$) and S (3683 ± 2916 ppm) (Fig. 5.2), in comparison to Lithofacies Association O ($6.0 \pm 0.9\%$, $0.13 \pm 0.01\%$) is caused by an increase in diagenetic framboidal pyrite and overprinting euhedral pyrite (Fig. 3.9). In Lithofacies Association II, the higher average Fe_2O_3 and MnO content ($21 \pm 7\%$, $12 \pm 6\%$) is interpreted to be largely associated with magnetite, rhodochrosite, siderite, and minor hematite. In Lithofacies Association III, the still higher average Fe_2O_3 and MnO content ($24 \pm 8\%$, $14 \pm 5\%$) in relation to the Lithofacies Association O ($6.0 \pm 0.9\%$, $0.13 \pm 0.01\%$) is related to an abundance of hematite, rhodochrosite, Fe-Mn silicate, with minor magnetite and siderite. This major change of Fe-mineralogy upsection suggests: a decrease in

146

sulfur content in the sediment and an increase in ocean oxidation during the time of deposition.

As previously noted, high phosphorus content is particularly common in the Woodstock Fe-Mn deposits and was one of several factors that caused production of mining the Fe-Mn deposits to cease in 1864 (Sidwell, 1957). The phosphorous content is related to the presence of alternating layers of both amorphous and subhedral apatite that are conformable with the beds of hematite, magnetite, and Fe-Mn carbonate laminae. The high P content of the Plymouth deposit (Figs. 5.8, and 5.9) is correlated to high Fe_2O_3 (r = 0.947 for Fe_2O_3/P_2O_5 in Lithofacies Association III, n = 62; r = 0.971 for Fe_2O_3/P_2O_5 in Lithofacies Association II, n = 72) and to a lesser extent with the MnO content (r = 0.863for MnO/P_2O_5 in Lithofacies Association III, n = 62; r = 0.860 for MnO/P_2O_5 in Lithofacies Association II, n = 72). This is explained by the relationship between phosphates and iron content where high amounts of dissolved iron are measured alongside high amounts of phosphate in the water column (Jones and Bowser, 1978). Phosphate will be adsorbed onto amorphous, hydrated, iron-oxide complexes formed during oxic redox conditions (often $Fe_2O_3 \cdot nH_2O$ or colloidal $Fe(OH_3)$) during deposition and forms as apatite during diagenesis (Jones and Bowser, 1978).

Trace elements [Cu (77 ± 13 ppm), Pb (18 ± 6 ppm), S (3683 ± 2916 ppm), As (13± 5 ppm), Ba (786 ± 197 ppm), Co (52 ± 17 ppm), and V (140 ± 50 ppm)] in Lithofacies Association I are higher compared to Lithofacies Association O, II, and III (Figs. 5.1, 5.2, 5.3) and are associated with sulfide and sulfate minerals, such as chalcopyrite, cobaltite, galena, and barite that are locally found in sulfide-rich black
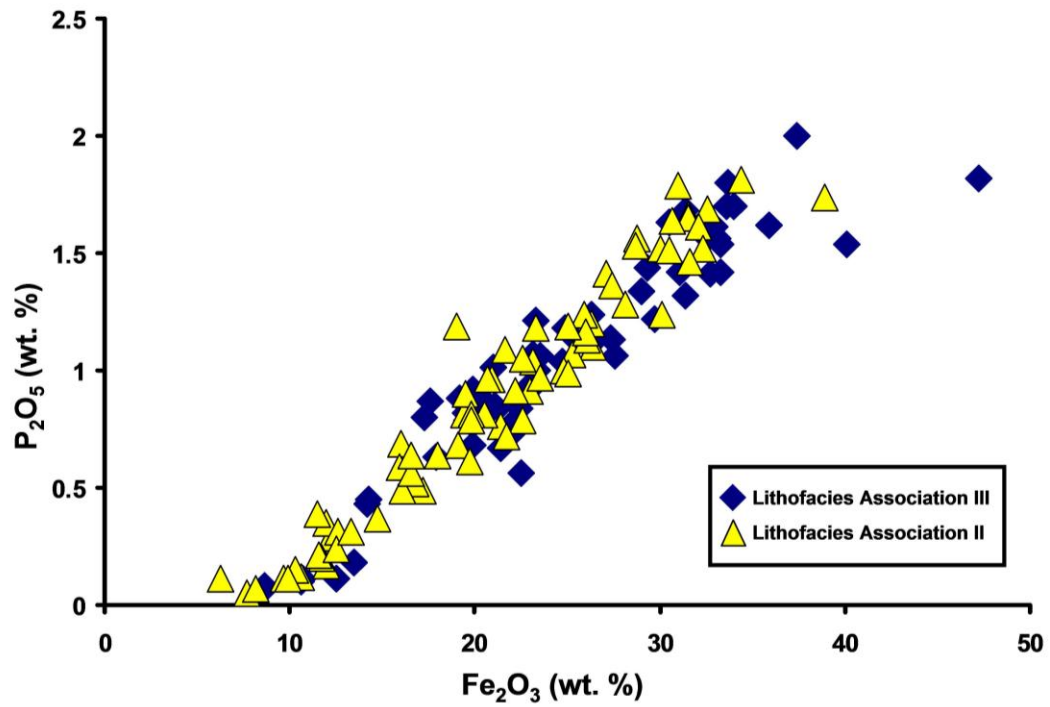
Fig. 5.8: Fe$_2$O$_3$ vs. P$_2$O$_5$ values from Lithofacies Associations II and III within the Plymouth Fe-Mn deposit.
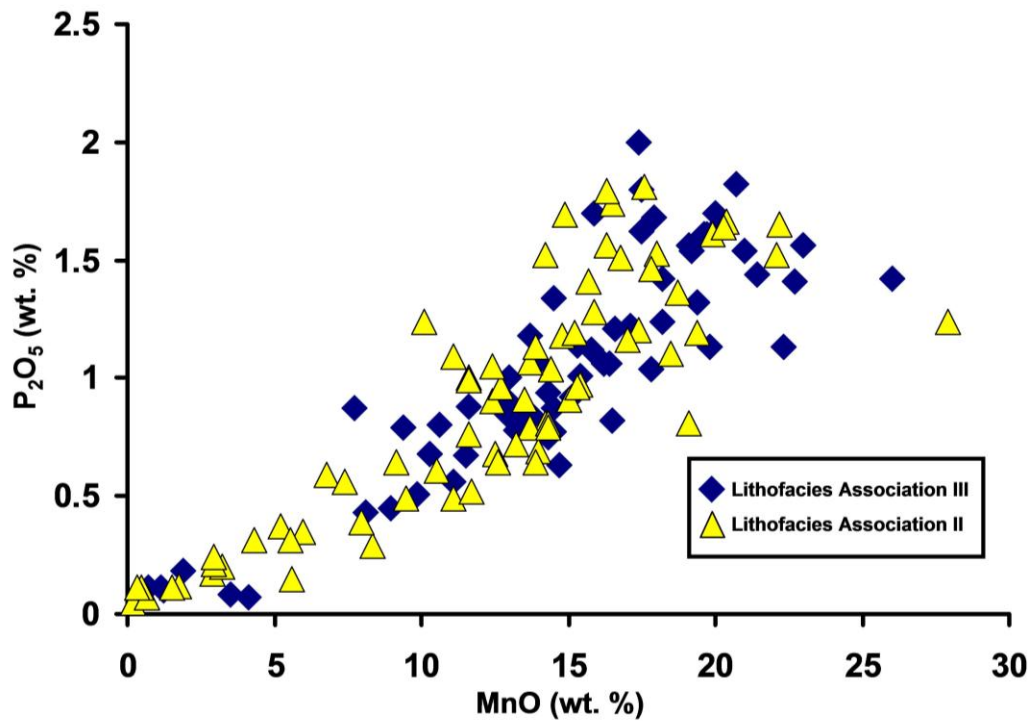
Fig. 5.9: MnO vs. P$_2$O$_5$ values from Lithofacies Associations II and III within the Plymouth Fe-Mn deposit.

148

mudstones (Fig. 3.8). These higher values compared to Lithofacies Association O are likely attributed to minor base-metal mineralization that is observable as euhedral sulfide crystals and in quartz-sulfide veinlets in Lithofacies Associations I, II, III. Copper and cobalt in particular appear to have sporadic high anomalies that are present in Lithofacies I, II, and III and will be discussed further later in the Chapter.

Lithofacies Associations II and III of the Plymouth deposit display vast differences in REE composition in comparison to Lithofacies I and O (Figs. 5.10, and 5.11). The higher amounts of REEs within lithofacies *Fgnz* associated with Lithofacies Association II are visible as trace monazite inclusions within the subhedral oligonite grains (Fig. 4.6) and may also be associated with diagenetic apatite in this lithofacies association. However, REEs may also be present within the apatite precipitates present in Lithofacies Association III.

Most REEs exist at a 3^+ oxidation state (except $Ce^{3+, 4+}$ and $Eu^{3+, 2+}$) and are a relatively immobile group of elements under sedimentary and most metamorphic conditions with exceptions being cerium and europium, which may be more mobile in their other valance states. The quantity of a cerium and (or) europium anomaly is measured by the ratio of that particular REE (Ce or Eu) in relation to where it would be if a straight line were drawn between the surrounding REEs. The Ce/Ce* values are calculated by Ce/Ce* = $2Ce_N/(La_N + Pr_N)$ and Eu/Eu* values are calculated by Eu/Eu* = $2Eu_N/(Sm_N + Gd_N)$, where the N value represents CI chondrite-normalized values. The most significant change is observable in the higher CI chondrite-normalized REE patterns of Lithofacies Associations II and III

149
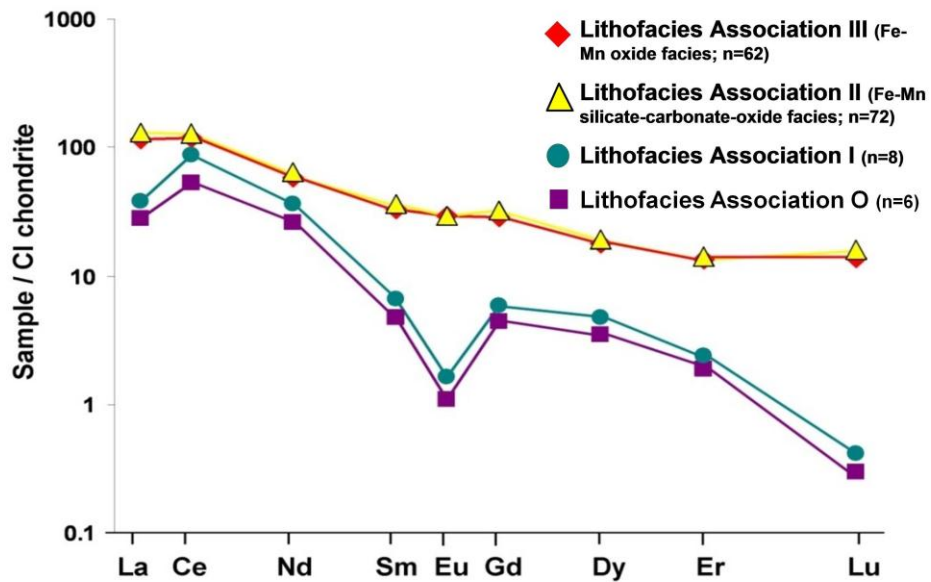
Fig. 5.10: CI chondrite-normalized average REE of Lithofacies Associations O, I, II, III (Sun and McDonough, 1989).
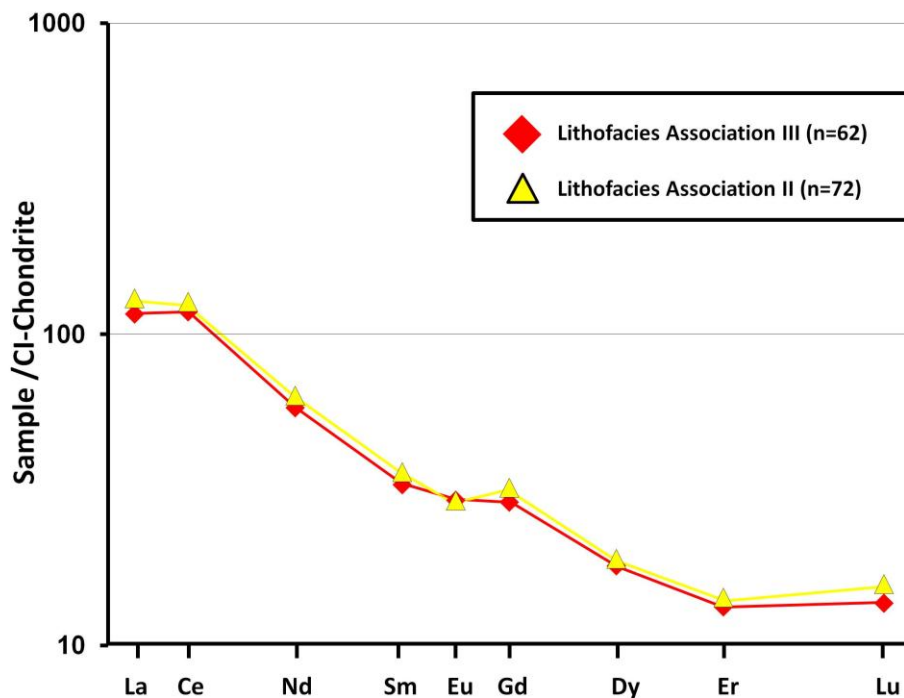
Fig. 5.11: Enlarged CI chondrite-normalized average REE of Lithofacies Associations II and III only. These lithofacies associations are observed to have higher average concentrations of Fe (13%) and Mn (9%) in comparison to the underlying Lithofacies Associations I and O (Sun and McDonough, 1989).

(Figs. 5.10, 5.11), notably the Ce and Eu anomalies (Ce/Ce* = 1.42; Eu/Eu* = 0.87) that can suggest a change in the environmental conditions present at the time of deposition.

The presence of positive Eh conditions would oxidize Ce^{+3} and remove it from the seawater as CeO_2 or $Ce(OH)_4$, to be deposited in the sediment, and would be observed as positive Ce anomalies. Shallow marine sediments present in oxidizing conditions of less than 200 m depth display smaller positive Ce anomalies(Ce/Ce* = 0.33 to 0.43) within chondrite-normalized REEs (Kato et al., 2006). Both Lithofacies Association III (lithofacies *Frml* and *Frmz*) (Ce/Ce* = 1.18) and Lithofacies Association II (*Fgnl, Fgygn,* and *Fgnz*) (Ce/Ce* = 1.14) display minor positive Ce anomalies within Lithofacies *Fgnl, Fgygn,* and *Fgnz* (Fig. 5.10), a characteristic of a shallow marine environment (<200 m) within an oxidizing environment (cf. Kato et al., 2006). The high Ce anomalies associated with Lithofacies Associations O (Ce/Ce* = 2.02) and I (Ce/Ce* = 2.33) (Fig. 5.10) may associated with depletions in Lanthanum and Neodymium.

Strong positive Eu anomalies (Eu/Eu* = 7.2 to 15.1) are typically seen in hydrothermal Fe-Mn deposits associated with black smoker systems and are evidence of high-temperature fluids precipitating out dissolved Eu when it mixes with the colder seawater. In contrast small negative anomalies are observed in the Plymouth deposit (Figs. 5.10, 5.11). However, due to the mobility of Eu, negative anomalies cannot be used as a definitive indicator of a lack of volcanic and hydrothermal input associated with formation of the Fe-Mn deposits (Kato et al., 2006).

Chondrite-normalized REEs within the Plymouth deposit display a smaller

negative Eu anomaly within Lithofacies Association III (Eu/Eu* = 0.95) relative to

Lithofacies Association II (Eu/Eu* = 0.87). Lithofacies Association II (lithofacies

Fgnl, Fgygn, and *Fgnz*) contain a slightly greater HREE content compared to

Lithofacies Association III (lithofacies *Frml* and *Frmz*) of the Plymouth deposit

(Fig. 5.10). This enrichment of HREEs may be attributed to the deeper offshore

environment inferred for Lithofacies Association II. Slower rates of precipitation

for lithofacies *Fgnz, Fgnl*, and *Fgygn* would allow greater rates of chemical

scavenging of HREEs from the seawater onto the surfaces of Fe^{2+} hydroxides and

Fe-Mn carbonates and produce an enrichment of HREEs within this Fe-Mn

mineralized assemblage (Elderfield and Greaves, 1982; Byrne and Kim, 1990).

5.3.2 Anomalous Trace Elements in relation to Lithofacies Association O

The rare, higher Cu and Co anomalies associated with Lithofacies

Associations I [Cu (77± 13 ppm), Co (52 ± 17 ppm)], II [Cu (57 ± 27 ppm), Co

(100 ± 36 ppm)], and III [Cu (60 ± 55 ppm), Co (120 ± 41 ppm)] are associated

with two different mineralization events. Cobalt is found to have a maximum

concentration of 250 ppm within Lithofacies Association III and 200 ppm with

Lithofacies Association II, whereas Cu values have a maximum concentration of

410 ppm Lithofacies Association III and 130 ppm in Lithofacies Association II

(Roberts and Prince, 1990). Euhedral to subhedral magnetite grains associated with

the Plymouth deposit display inclusions and overprinting of cobaltite and (or)

chalcopyrite (Figs 4.15a & b). This relationship suggests that the base-metal

mineralization occurred synchronous to the magnetite mineralization in Units B, C, and D.

Cu-Fe-S and Co-As-S mineralization was also identified in thin section optically and by SEM-BSE (Figs. 4.20, 4.21, 4.23, and 4.24) within quartz-chlorite-sulfide, quartz-sulfide, and sulfide veinlets. These veinlets contain minor inclusions of overprinting euhedral to subhedral cobaltite and chalcopyrite crystals that crosscut the Fe-Mn laminae. This mineralizing fluid event could be attributed to regional subgreenschist-grade metamorphism generated during the Devonian Acadian Orogeny that also produced the folding that is visible in outcrops proximal to the Plymouth deposit (Roberts and Prince, 1990) and possibly responsible for the juxtaposition of Lithofacies Associations within outcrops and drill core.

Another potential explanation of the Co-As-S and Cu-Fe-S is a possible hydrothermal source. Nicholson (1992) described hydrothermally sourced Fe-Mn deposits as having high concentrations of As-Ba-Cu-Li-Mo-Pb-Sb-Sr-V-Zn. These elements would be deposited near the hydrothermal source as sulfides as observed in many SEDEX (SEDimentary EXhalative) deposits and Volcanic Massive Sulfide (VMS) deposits. High anomalous amounts of metals, such as As, Ba, Cu, Pb, and Zn are more commonly seen within the sulfide facies of Banded Iron Formations. In manganiferous BIFs, occurrences of Cu and Fe sulfides are present as overprinting and crosscutting minerals (Nicholson, 1992). In particular, rare-earth elements are depleted in hydrothermal BIFs. This is in contrast to the geochemistry of the Plymouth deposit suggests a non-hydrothermal source of Fe and Mn is associated with the Woodstock Fe-Mn deposits (German et al., 1990).

153

5.4   SUMMARY

Lithofacies Association O (White Head Formation) appears geochemically distinct in relation to Lithofacies Associations I, II, III (Smyrna Mills Formation); CaO and Sr values are higher whereas the major oxides (Fe_2O_3, MnO, P_2O_5) and trace elements (Cu, Pb, S, As, Ba, Co, and V) are lower in the White Head Formation. REE contents are slightly lower with Lithofacies Association O in comparison to the Lithofacies Association I, but display the same overall trends in CI chondrite-normalized REE plots (Fig. 5.9) and minor Ce and Eu anomalies (Ce/Ce* = 2.33; Eu/Eu* = -0.26). Cl-Chondrite normalized REE spider plots of Lithofacies Associations II and III display only minor changes in REE contents with increases in Ce anomalies and decreases in Eu anomalies and heavy rare earth elements (HREEs) (Fig. 5.9).

Geochemical values show only minor variations between Lithofacies Association II and Lithofacies Association III. However, the latter has higher concentrations of P_2O_5, Ba, Sr, Co, and Cu values and lower in K_2O, TiO_2, MgO, and Ni (see NASC-normalized plot Fig. 5.7). Lithofacies Association II is enriched in CaO, Na_2O and P_2O_5 and is depleted in K_2O, TiO_2, Al_2O_3, and MgO compared to Lithofacies Association I (Fig. 5.8). Highly anomalous phosphorus values within the Plymouth deposit, in relation to Lithofacies Association O, are directly associated with layers of amorphous to subhedral apatite visible in thin section (Figs. 4.9b, 4.10, 5.8). Trace elements (Zn, As, S, and Cr) are also found to lower in content in Lithofacies Association II (Fig. 5.7) when compared to Lithofacies Association I.

154

Anomalously high values of Co and Cu are present in Lithofacies Associations I, II, and III of the Plymouth deposit in comparison to the White Head Formation. These Co and Cu anomalies are associated with cobaltite and chalcopyrite mineralization hosted in bedded magnetite laminae, crosscutting quartz-sulfide veins and veinlets, and euhedral overprinting cobaltite crystals which are observable in drill core from the Plymouth deposit. It is also in the North Hartford deposit and the Union Corner occurrence in outcrop.

CHAPTER 6

ORIGIN OF THE WOODSTOCK FE-MN DEPOSITS

6.1   INTRODUCTION

Sedimentary ferromanganiferous deposits can form in a variety of marine environments as nodules, crusts, or sedimented layers. The purpose of this chapter is to review the processes by which they may have form and to identify which is the most likely genetic explanation for the origin of the Woodstock Fe-Mn deposits, based on the data presented in the earlier chapters.

6.2   PHYSIOCHEMICAL CONDITIONS FOR PRECIPITATING FE AND MN

Iron exists in nature as Fe^{2+} and Fe^{3+}, whereas manganese can exist as Mn^{2+}, Mn^{3+}, and Mn^{4+}. Similarities in atomic size, mass, and thermodynamic properties allow iron and manganese to often form simultaneously in mineral complexes, such as in the minerals oligonite, jacobsite ($MnFe_2O_4$), and bixbyite. Under oxidizing conditions both metals may precipitate out from solution as oxides and (or) hydroxides (Roy, 1981; Maynard, 1983). Ions of ferric iron (Fe^{3+}) are almost completely insoluble except under highly oxidizing and acidic conditions. Ferrous iron (Fe^{2+}) and Mn^{2+} are readily soluble within most aqueous systems and can be oxidized to Fe^{3+} and Mn^{4+}. The Fe^{3+} and Mn^{4+} ions may precipitate out as a series of ferric oxides and Fe-Mn carbonates under oxidizing conditions. Under reducing conditions, the Fe^{2+} and Mn^{2+} may precipitate out as reduced carbonates and sulfides under reducing conditions (Fig. 6.1). Manganese content in seawater is
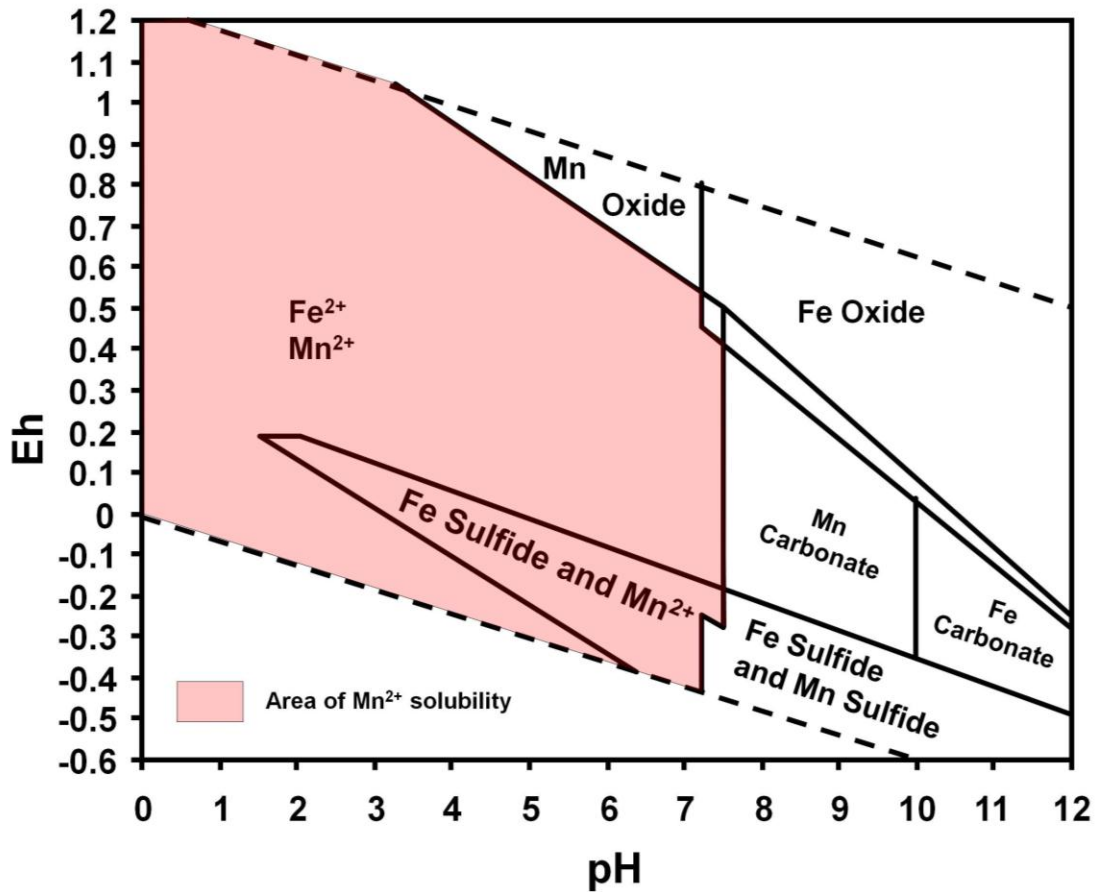
Fig. 6.1: Superimposed thermodynamic stability diagrams at 25° C and 1 atm for Fe^{2+} and Mn^{2+} displaying the solubility contrasts that occur with the presence of S and C. The pink section of the diagram shows the area of Mn^{2+} solubility. At certain Eh and pH conditions, Fe^{2+} will precipitate out as pyrite (FeS_2). At this stage Mn^{2+} is near the saturation point of alabandite (MnS), but still remains soluble as observable in the pink region of the diagram (Hem, 1972; Force and Cannon, 1988; Force and Maynard, 1991).

generally in the range of 0.1 to 8 ppb and will precipitate out of seawater when in excess of 450 ppb. Iron generally has a content of 3.4 ppb in seawater and will usually precipitate out when in excess of 200 ppb (Roy, 1981; Frakes and Bolton, 1984).

An increase in the abundance of dissolved Fe^{2+} and Mn^{2+} ions is often aided by the weathering of continents and by the development of hydrothermal vents that can enrich the seawater with excessive amounts of Fe^{2+} and Mn^{2+}. The fractionation of Fe by the precipitation of pyrite within the environment in general also assists in the formation of a dilute Fe-Mn ore-forming solution, a process that takes place under anoxic and alkaline conditions (Force and Cannon, 1988).

The presence of Fe^{2+} and Mn^{2+} within seawater is also a function of the amount of dissolved O_2, organic matter, salinity, pH, and other dissolved ions, such as SO_4^{2-} (Frakes and Bolton, 1984). Detrital minerals and organic matter introduced into the paleo-water column will immediately be oxidized and (or) deposited on the ocean floor. Organic matter and already dissolved O_2 is converted to CO_2 so that oxygen content in the seawater decreases. In areas where stagnant water conditions are present alongside a high organic content often led to the formation of an anoxic basin (Frakes and Bolton, 1984). This occurs most commonly in deep water sheltered from ocean currents that circulate and replenish O_2, but can occur on sheltered continental shelves most particularly during sea-level highstands (i.e. , late transgression and early regression).

Within these settings, chelation of Fe^{2+} to organic complexes is common. Sulfate ions (SO_4^{2-}) which are often more common within the water column than Fe^{2+}, will fixate with Fe^{2+}, precipitating pyrite (FeS_2) and resulting in the deposition

of black pyritic mudstone. Mn^{2+} will often remain in solution within the reduced settings except under highly anoxic or euxinic conditions (Fig. 6.1), such as observed in the present-day Black Sea and Baltic Sea. Euxinic redox settings will precipitate out Mn^{2+} with SO_4^{2-} to form alabandite (MnS) simultaneously with pyrite in the water column (Roy, 1981; Force and Cannon, 1988; Force and Maynard, 1991).

If the redox conditions within the anoxic environment change to highly oxic, the once soluble Fe^{2+} and Mn^{2+} will oxidize to form Fe^{3+} and Mn^{4+} and precipitate out and form Fe and Mn oxides and hydroxides in the water column (Equation 6.1), a process that is often hastened by the existence of algae (Braterman et al., 1983; Posth et al., 2008).

The ratio of Fe to Mn within the precipitated sediments is directly a function of the redox conditions present at the time of deposition (Roy, 1981; Force and Cannon, 1988). Seasonal fluctuations of Fe and Mn alongside differential rates of evaporation in shallow marine environments frequently results in microbanding of the Fe-Mn deposits during the process of Fe-Mn precipitation. During warmer months when anoxygenic phototrophic bacteria would flourish, Fe and Mn would precipitate out Fe and Mn oxides and hydroxides. The colder months would allow the precipitation of amorphous silica since microbial populations would not be able to oxidize significant amounts of Fe and Mn (Maynard, 1983; Force and Maynard, 1991; Posth et al., 2008).

$$2Fe^{+2} (aq) + 2H^+ \rightarrow 2Fe^{+3} (aq) + H_2$$

$$Fe^{+3} (aq) \leftrightarrow Fe(OH)^{+2} (aq) + H^+ \leftrightarrow 2Fe(OH)_2^+ (aq) + 2H^+ \leftrightarrow Fe(OH)_3 (aq) + 3H^+$$

$$Fe(OH)_3 (aq) \rightarrow FeOOH (s) + H_2O$$
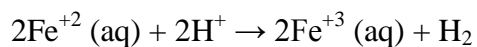
Equation 6.1: Fixation of soluble ferrous iron species to insoluble ferric oxyhydroxides (Braterman et al., 1983).

Hydrogenous (Slow precipitation from seawater or freshwater in oxidized environments)	Microparticles dispersed in sediments Nodules and concretions in abyssal plains Solid pavements on topographic highs.
Hydrothermal (Precipitation from hydrothermal solutions in areas of volcanism and/or high heat flow)	Along active oceanic ridges and rifts. Associated with central submarine volcanics.
Halmyrolitic (Supplied by submarine weathering of basaltic debris)	Important in some limited areas of the Pacific ocean.
Diagenetic (Precipitation resulting from diagenetic remobilization of Mn in the sediment column)	In helmipelagic regions of the oceans, and marginal and enclosed areas.

Table 6.1: Different types of modern-day ferromanganiferous deposits on the ocean floor (from Bonatti et al., 1972).

6.3 **FORMATION OF FE AND MN DEPOSITS WITHIN MARINE ENVIRONMENTS**

Fe-Mn precipitates that eventually become sedimentary Fe-Mn deposits may form by four potential models of Fe and Mn enrichment as described by Bonatti et al. (1972) within modern marine settings. The first two listed in Table 6.1 and below form the largest enrichments of Fe and Mn and are known as Hydrogenous and Hydrothermal Fe-Mn Deposits. Hydrogenous and Hydrothermal deposits form during deposition and are formed by precipitation and deposition of Fe and Mn minerals. The source of Fe^{+2} and Mn^{2+} is supplied from continental weathering for Hydrogenous deposits or from tectonically active centres for Hydrothermal deposits.

Halmyrolytic and Diagenetic deposits (Table 6.1) in contrast, are formed by the remobilization of Fe and Mn minerals after deposition of hydrogenous and (or) hydrothermal Fe and Mn has occurred. The eventual lithification of the Fe-Mn deposits from post-depositional processes (including diagenesis) forms the Fe-Mn layers into iron formations or ironstones described later in this chapter.

6.3.1 *HYDROGENOUS DEPOSITS*

Hydrogenous Fe-Mn deposits form in both shallow and deep-marine environments by the precipitation of Fe^{3+} and Mn^{4+} from Fe^{2+} and Mn^{2+} due to changes in ocean redox. Seawater generally has a concentration of both Fe^{2+} and Mn^{2+} ions ranging from 0.001 to 0.01 ppm with a Mn/Fe ratio of 5 to 0.5. Much of the Fe in the seawater is thought to exist largely as colloidal ferric hydroxide that can settle out of seawater without changes in ocean redox, and also as soluble Fe^{2+} complexes that can precipitate out of seawater under oxidizing conditions as oxides and hydroxides and some reducing conditions as carbonates and sulfides (Fig. 6.1;

Hem, 1972; Force and Cannon, 1988; Force and Maynard, 1991). Manganese

occurs as divalent colloidal compounds that can settle out of seawater or as

dissolved ion complexes in the seawater that can precipitate out under oxidizing

conditions as oxides and hydroxides and some reducing conditions as carbonates

and sulfides (Fig. 6.1; Bonatti et al., 1972; Hem, 1972; Bonatti, 1975; Force and

Cannon, 1988; Force and Maynard, 1991).

Within the deep sea, the adsorption of amorphous Fe^{3+} hydroxides onto the

surfaces of clastic or biogenic nuclei is the precondition for the precipitation of the

Mn hydroxides and oxides, such as manganite (MnO(OH) and manganese dioxide

with the latter precipitating out of the seawater at highly oxidizing conditions (Fig.

6.1; Equation 6.2). The Fe and Mn precipitates will often form as Fe-Mn nodules on

the ocean floor at the sediment-water interface. Other Fe-Mn deposits such as Fe-

Mn crusts, form only in hydrothermally active areas, whereas Fe-Mn sediment

layers form in shallower marine environments (Burns and Burns, 1972; Roy, 1981;

Equation 6.2, Fig. 6.2).

Nodules of Fe-Mn minerals can also contain relatively high concentrations

of Ni, Co, and Cu in areas of the oceans where sedimentation is on the order of

$1mm/10^3$ years, such as is observed within the abyssal plains (Bonatti et al., 1972).

The slow rates of precipitation allow Fe-Mn deep-sea nodules in the North Pacific

formed in radiolarian ooze to have significant enrichments of Mn, Ni, and Cu,

where the metals are supplied from both biochemical cycles of organisms and from

organometallic complexes formed by the degradation of biochemical compounds

(Roy, 1981). This high concentration of base metals with Fe-Mn nodules is a

step 1) Palagonite (montmorillonite, illite, etc.) + biogenic silica → phillipsite

(step 2a) Biogenic matter + limonite → oxidized organics + soluble Fe^{+2}

(step 2b) Biogenic matter + amorphous δ-MnO_2 oxidized organics + Mn^{+2}-MnO_2 (todorokite)

(step 3) Soluble Fe^{+2} + amorphous δ-MnO_2 or aerated seawater → $FeO \cdot OH \cdot H_2O$ + Mn^{+2}- MnO_2

(step 4a) Ni^{+2}, Cu^{+2} organic complexes + $Fe^{+3}OOH$ x nH_2O (adsorbed on montmorillonite) → soluble Ni^{+2} + Cu^{+2} (+ Fe^{+2} oxidized to $FeOOH$ x H_2O coating phillipsite)

(step 4b) (Ni^{+2}, Cu^{+2}) organic complexes + amorphous δ-MnO_2 → soluble Ni^{+2} + Cu^{+2} + Mn^{+2}-MnO_2(s)

(step 5) Soluble Ni^{+2} + Cu^{+2} + Mn^{+2}-MnO_2(s) → (Ni^{+2}, Cu^{+2}, Mn^{+2})$_2$$Mn_5O_{10}$ x nH_2O (todorokite) → deposited on $FeOOH$ x H_2O substrate on phillipsite

Equation 6.2: Formation of Fe and Mn layers within deep-sea Fe-Mn nodules in radiolarian siliceous oozes and the fixation of Ni and Cu-rich organometallic complexes onto Fe and Mn precipitates (Burns and Burns, 1978).
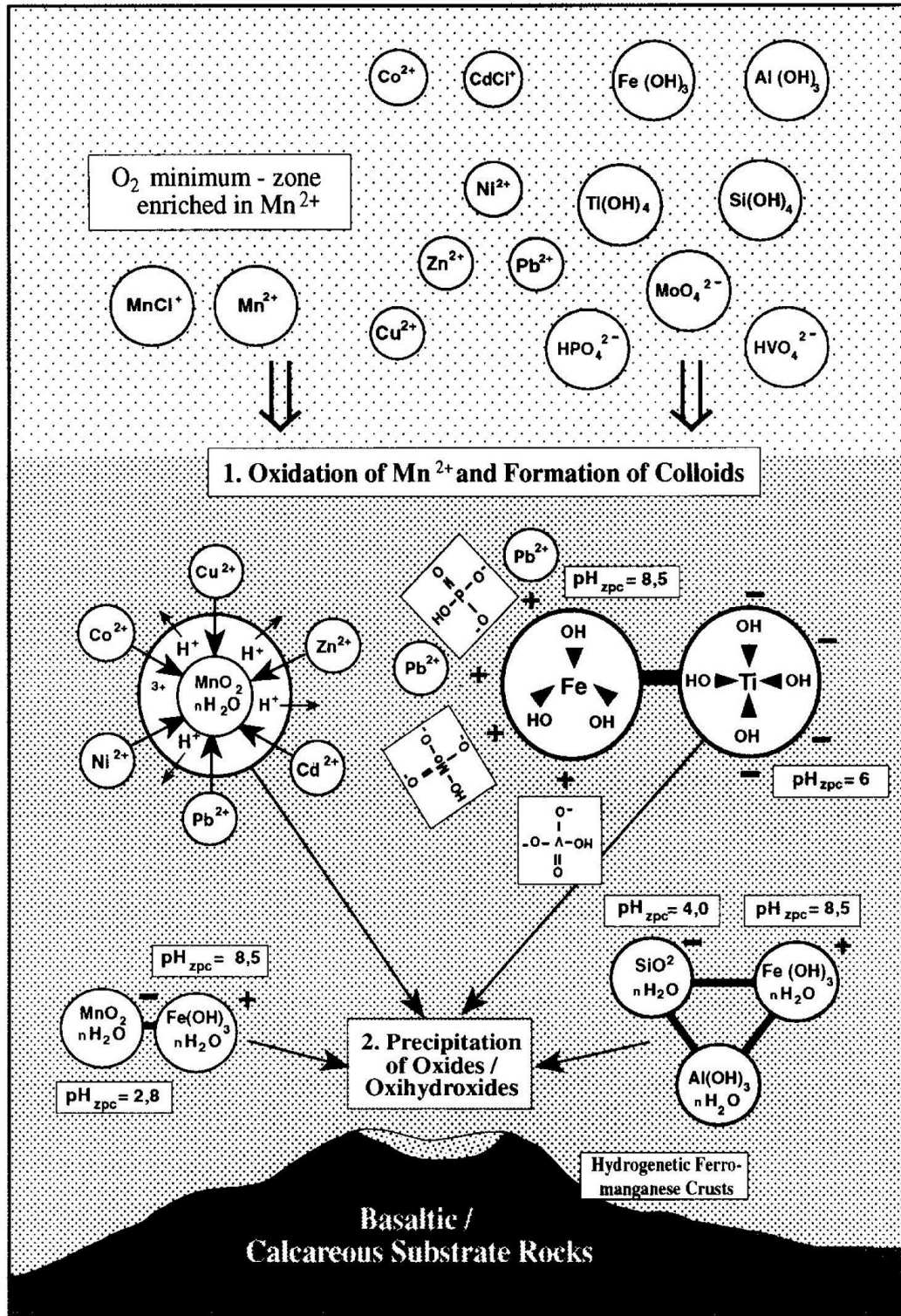
Fig. 6.2: Model for modern formation of hydrogeneous Fe-Mn crusts on seamounts (modified from Koschinsky and Halbach, 1995).

characteristic specific to deep sea Fe-Mn deposits formed in radiolarian oozes and is not usually observed in shallow marine Fe-Mn deposits that generally have lower concentrations of Ni, Co, and Cu due to more rapid rates of sedimentation (Ku and Glasby, 1972) allowing less time for chemical scavenging.

6.3.2   HYDROTHERMAL DEPOSITS

Some Fe-Mn deposits are the result of submarine hydrothermal activity that is often proximal to areas of undersea volcanism. These areas of metal enrichment are often the result of localized addition of metals from hydrothermal vents, a process which is actively observable in areas such as the submerged caldera within the island of Thera in the Mediterranean Sea and the submarine volcano of Banu Wuhu in Indonesia (Bonatti et al., 1972; Bonatti, 1975). These deposits also precipitate from hot metalliferous seawater that has circulated through parts of the igneous lithosphere and reacted to the colder surrounding seawater (Fleet, 1983) and can occasionally contain areas of base-metal mineralization within the Fe-Mn deposit. These Fe-Mn deposits are commonly a SEDimentary EXhalative (SEDEX) origin (Nicholson, 1992a) and form as Algoma-type iron formations. The Fe/Mn ratios for hydrothermal Fe-Mn deposits, unlike those of hydrogenous Fe-Mn deposits vary depending on the distance from the source of metals. The Fe/Mn ratios are higher in early precipitates proximal to the source and gradually decrease as the distance increases from the source (Fleet, 1983).

6.3.3   HALMYROLYTIC DEPOSITS

This Fe-Mn mineralization is formed following deposition in contrast to hydrogenous and hydrothermal deposits. Halmyrolytic Fe-Mn deposits are

produced by the reaction of fine-grained debris composed of basaltic glass slowly reacting to the surrounding seawater to form Fe- and Mn-rich zeolites and clays, such as phillipsite ($[Ca,Na_2,K_2]3Al_6Si_{10}O_{32}\cdot12H_2O$) and Fe-smectite ($Ca_{0.17}(Fe)_2(Si, Al)_4O_{10}(OH)_2\cdot nH_2O$). This process is enhanced in tectonically active areas where heat and hydrothermal fluids cause rapid alteration of the original mineralogy. During these reactions some Mn is first leached out of the basaltic glass and then precipitated out as MnO_2. Many of the zeolites contain MnO_2 in the form of microparticles and concretions (Bonatti et al., 1972; Bonatti, 1975).

6.3.4 DIAGENETIC DEPOSITS

Diagenetic deposits are formed by the post-depositional remobilization of Fe and Mn during burial that subsequently become concentrated into Fe-Mn deposits. This commonly happens in hemipelagic sediment where Mn and Fe oxyhydroxides and hydroxides have been deposited within organic-rich sedimentary basins in a lacustrine or marine setting. As the organic matter decomposes, Fe^{3+} and Mn^{4+} that were deposited near the organic matter are reduced to form Fe^{2+} and Mn^{2+} by sulfur-reducing bacteria, such as *Bacillus circulans* and *B*. 29. The Fe^{2+} and Mn^{2+} are then remobilized and dissolved within interstitial water to be transported upward and precipitated out as Mn^{4+} and Fe^{3+} oxides upon contact with areas of overlying oxidized pore-, lake-, sea-water sediments. These precipitates are typically observed as hard compact crusts of Fe-Mn oxides. This process is locally restricted to sediments in areas where the sediment-water interface is proximal to the oxic-anoxic boundary (Bonatti et al., 1972; Bonatti, 1975; Roy, 1981).

6.4   CONTINENTAL SHELF FE-MN DEPOSITS VS. DEEP-SEA NODULES

The four listed models of Fe-Mn enrichment can form in both continental-shelf and deep-marine settings. As indicated earlier in this chapter, continental shelf Fe-Mn deposits and deep-sea Fe-Mn nodules form at different rates and have geochemical differences that reflect their rates of formation. The rates of deposition within continental shelf settings are generally faster than precipitation of hydrogenous deep-sea nodules. Continental-shelf Fe-Mn deposits also have lower concentrations of Co, Ni, Cu, and Mo (Roy, 1981; Kim et al., 2005). Exceptions can occur for continental-shelf and (or) deeper marine Fe-Mn deposits that form proximal to a source of hydrothermal activity and can have high concentrations of As-Ba-Cu-Li-Mo-Pb-Sb-Sr-V-Zn (Nicholson, 1992a). The elements As, Ba, Cu, Pb, and Zn, in particular are sourced from hydrothermal vents and would also occur in nearby SEDEX deposits and Volcanic Massive Sulfide (VMS) deposits. Hydrothermal SEDEX and hydrothermal banded iron formations (BIFs) typically have enrichments in sulfides and depletions in other metals Co, Ni, U, and REEs that are more common in diagenetic and hydrogenous deposits associated with deep sea Fe-Mn nodules.

Deep-sea Fe-Mn nodules generally precipitate at a rate of 0.2 – 2.1 mg Mn cm^{-2} ka^{-1} (Marchig et al., 1982) and are formed in areas of the ocean where sedimentation rates are on the order of less than 5mm per 1000 years. This slow rate of precipitation allows time for absorption of other metals (Co, Cu, Ni, U, and REEs) from solution to form mineral complexes on the nodule surface in the displayed reactions (Equation 6.2; steps 4a - 5).

Radiolarian siliceous oozes that have high pore volume and open pore structure allow several reactions to occur that promote the concentration of Fe-Mn mineralization on the surfaces of the nodules. Biogenic silica and palagonite (a stable glass alteration product with a composition similar to basalt; Stroncik and Schmincke, 2002) associated with clay minerals such as montmorillonite ((Na,Ca)(Al, Mg)$_6$(Si$_4$O$_{10}$)$_3$(OH)$_6 \cdot$ nH$_2$O) and illite (K$_{0.8}$Al$_2$(Al$_{0.8}$Si$_{3.2}$)(OH)$_2$) within the sediment react to form phillipsite. Contemporary to these processes, interbedded organic matter is oxidized by local limonite (FeO(OH) $\cdot$ nH$_2$O) from the nodules and reduces solid Fe^{3+} to aqueous Fe^{2+}, CO$_2$, and H$_2$O. At the same time the limonite also oxidizes the amorphous δ-MnO$_2$ to form todorokite ((Na,Ca,K,Ba,Sr)(Mn,Mg,Al)$_6$O$_{12}\cdot$3H$_2$O). The soluble Fe^{2+} and remaining amorphous δ-MnO$_2$ in oxidized seawater then form limonite and todorokite. The limonite is first deposited on the phillipsite then coated with a layer of todorokite (Roy, 1981).

6.5   IRON FORMATIONS AND IRONSTONES

Although the aforementioned four models have been proposed for the origin of Fe-Mn mineralization, once the layers are lithified to form sedimentary Fe and Mn deposits, they are typically subdivided into two groups: banded iron formations (BIFs) and ironstones (Fig. 6.3). BIFs are defined as layered, iron-rich sedimentary rocks of a restricted chemical lithology consisting of layers of hematite and (or) magnetite separated by beds of chert, and containing at least 15% Fe (James, 1954; Gross, 1983; Pufahl and Fralick, 2004). BIFs, which can be subdivided into Lake
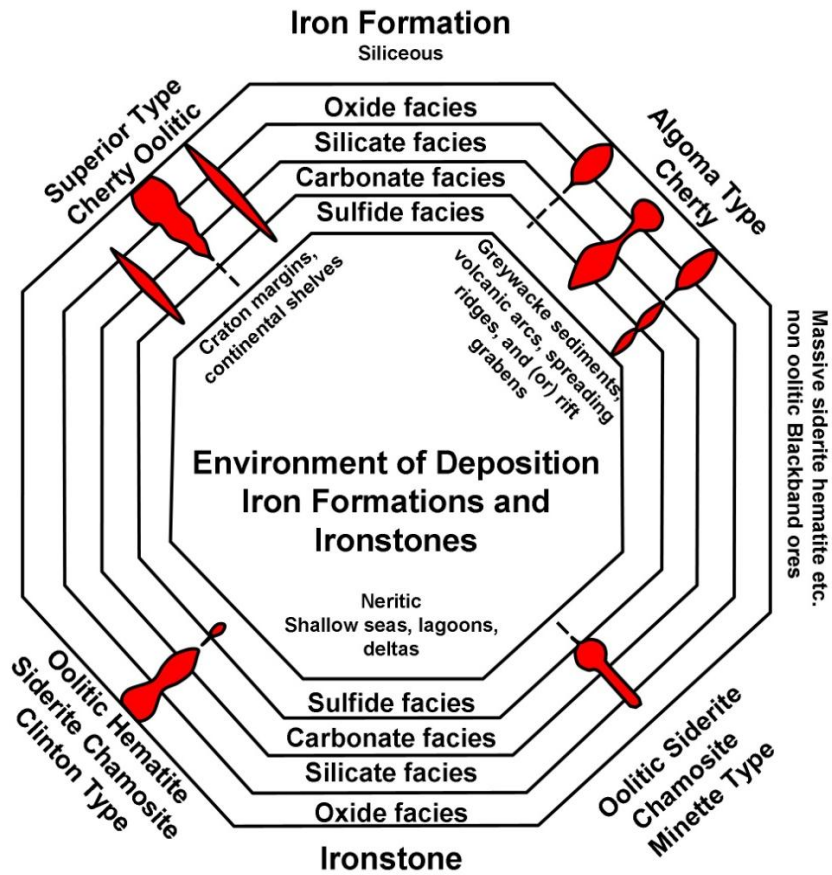
Fig. 6.3: Classification of Iron Formations and Ironstones as described by Gross (1965; 1980; 1996a). They are divided into two subcategories of iron formations that consist of Lake Superior BIFs, and Algoma BIFs (Gross, 1965; 1980; 1996a). The ironstone members can be subdivided into Clinton- and Minette- types.

Superior- and Algoma-types, are found in a variety of locations around the world and are interpreted to have been deposited in a variety of geologic environments.

In contrast, ironstones are defined by Gross (1996) to be lithified marine or lacustrine-based sedimentary rocks composed of yellow to brown and (or) red iron oxides, clay minerals, fine-grained clastics and fossil debris. They often exhibit oolitic textures and are considered to have formed by the precipitation and replacement of Fe-oxides and hydroxides on the surfaces of clastic sediment along the edge of the continental shelf to approximately 200m depth). They can be subdivided into Clinton-type and Minette-type ironstones.

6.5.1 *LAKE SUPERIOR-TYPE BIFS*

Lake Superior-type BIFs (Fig. 6.3) are the largest and most extensive type of BIF and account for most of the world's supply of iron (Braterman et al., 1983). They are named after the Precambrian BIFs localities discovered in the 1830's surrounding Lake Superior in northern Minnesota and southern Ontario (Minnesota Historical Society, 2009). Lake Superior BIFs in general are found commonly with quartz, dolomite, black shale, and minor tuffaceous sedimentary rock, and are interpreted to have formed along the edges of cratonic basins in shallow marine environments (Gross, 1965; 1980). The iron within these BIFs is initially supplied from both hydrogenous and hydrothermal sources during deposition. All known Lake Superior-type BIFs formed between 3800 and 1700 Ma (Maynard, 1983; Page, 2001; Kappler et al., 2005) and those of around 2200 to 1800 Ma are particularly common (Klein, 2005). All Lake Superior-type BIFs formed as a result of the

particular atmospheric conditions present within the Late Archean and Early Proterozoic periods and did not occur anywhere else on the geologic time scale.

The process of precipitation of Fe^{2+} to insoluble Fe^{3+} oxyhydroxides that occurred during deposition of Lake Superior BIFs is largely controversial. Evidence of stromatolite intergrowths within the Lake Superior BIFs suggest biogeochemical oxidation of soluble Fe^{2+} to insoluble Fe^{3+} in the seawater by anoxic phototrophic Fe^{2+} oxidizing bacteria. The soluble Fe^{2+} would be initially derived from hydrogenous and (or) hydrothermal sources (Kappler et al., 2005). Posth et al. (2008) explored the possibly of Fe being precipitated out of seawater by anoxic phototrophs and suggested that if the Precambrian BIFs were precipitated by micro-organisms that would be directly affected by the temperature in the surrounding seawater. It is likely that this process of Fe^{2+} to Fe^{3+} oxidation would occur for other types of iron formations, if anoxic phototrophs were present during the time of deposition (Braterman, 1983; Posth et al., 2008).

The formation of these deposits is interpreted to occur along the edges of stable cratonic basins within continental-shelf environments by changing ocean redox conditions caused by transgression and regression cycles (Force and Cannon, 1988; Force and Maynard, 1991). Lake Superior BIFs are interpreted as beds of finely laminated Fe-Mn strata formed below the tidal range at approximately 200 m depth (Fig. 6.4).

6.5.2 *ALGOMA-TYPE BIFS*

Algoma-type BIFs are hydrothermal BIFs that are found deposited with volcanic, greywacke, turbidite, and pelitic rocks and hosted in volcanic arcs, rift

171
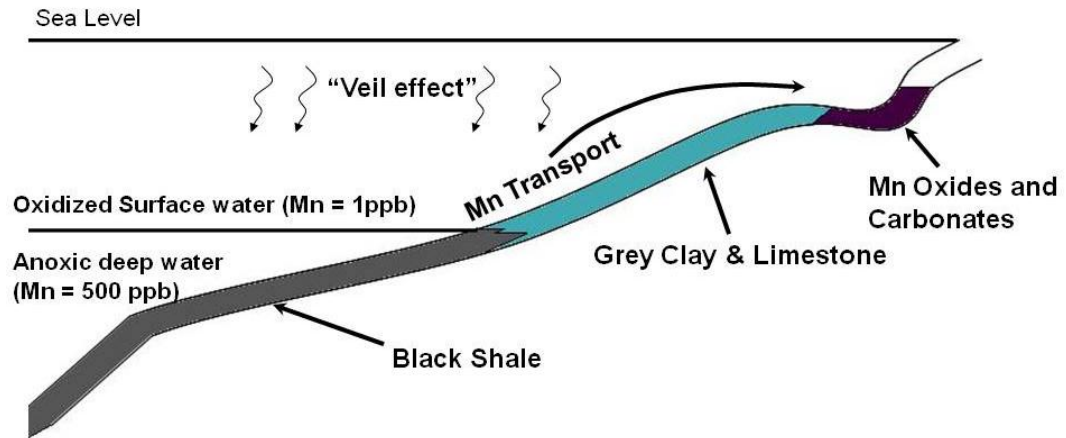
Fig. 6.4: Depositional model of shallow marine Fe and Mn along a stable cratonic margin. The "veil effect" is the flocculant fallout of manganese particulates from river water (Force and Cannon, 1988; Force and Maynard, 1991).

172

zones, and deep-seated fracture and fault systems forming both proximal and distal to a volcanic center (Gross, 1980; 1996a; 1996b). The Algoma-type BIFs are often associated with deeper water sediment and can often surround barren pyritic massive sulfide deposits and rare base-metal massive sulfides. Examples of Precambrian Algoma-type BIFs are noted for often having less than 2% Mn (Gross, 1996a), but many Paleozoic examples host a widespread Mn lithofacies and occasionally anomalous base-metals and precious metals (particularly in the sulfide facies), such as Cu, Zn, Sn, and Au. Both oxide and carbonate lithofacies within Algoma BIFs are noted for containing REEs and various lithofacies can host syngenetic and epigenetic Au within Precambrian Algoma BIFs (Gross, 1996a).

6.5.3   CLINTON-TYPE IRONSTONES

Clinton-type ironstones are predominantly hematite with very little siderite. This type of ironstone deposit occurs as red and purple Fe-rich siltstone and often formed in marine foreland basins along stable cratonic margins (Van Houten, 1991; VanCotter and Link, 1993; Gross, 1996). Many of the Phanerozoic Clinton-type ironstones are distinguishable by the presence of ferric oxide coatings on ooliths, replacement minerals, and cements, and often have plentiful with bioclasts (Van Houten, 1991). These ironstones are often high in Al_2O_3 and P_2O_5 and can contain high base-metal and REE concentrations.

6.5.4   MINETTE-TYPE IRONSTONES

Minette-type ironstones typically host goethite, siderite, and chamosite as the primary Fe minerals and contain more clay-rich material compared to the more cherty BIFs. As with the other type of ironstone, the Minette-type also host oolitic

textures and locally abundant bioclasts. The Minette-type ironstones are found to occur in a shallow marine to deltaic environments. They can also be found in lacustrine, fluviatile, and pedogenic environments (Siehl and Thein, 1989). These are typically very aluminum-rich in composition.

6.6   DEPOSITIONAL ENVIRONMENT OF LITHOFACIES ASSOCIATIONS O, I, II, AND III IN THE WOODSTOCK AREA

6.6.1 INTRODUCTION

The Woodstock Fe-Mn deposit contains four depositional Lithofacies Associations that differ in sedimentology and stratigraphic position as described in Chapter 3. Lithofacies Association O appears to be devoid of Fe-Mn mineralization and other high anomalous metals, whereas Lithofacies Association I is generally devoid of Fe-Mn mineralization, but contains rare, anomalously high Cu and Co concentrations. Lithofacies Association II contains more abundant lenticular beds of magnetite, Fe-Mn carbonates, and Fe-Mn silicates alongside rare, anomalously high Cu and Co concentrations in Lithofacies *Fgnz* and some minor occurrences of Lithofacies *Frmz*. Lithofacies Association III contains beds of hematite, Fe-Mn carbonates, Fe-Mn silicates, and rare, high anomalous Cu, Co, and P concentrations Fe-Mn mineralization in Lithofacies *Frmz* and some minor occurrences of Lithofacies *Fgnz*.

6.6.2   FE-MN LITHOFACIES RELATIONSHIPS

Depending on the redox conditions occurring at time of deposition, different Fe and Mn minerals can be deposited to form different mineralized lithofacies

174

associated with an iron formation or ironstone. Force and Cannon (1991)

determined there are three possible Fe-Mn mineralized lithofacies that may result

from deposition: oxide, oxide-carbonate, and reduced carbonate. Sediment beneath

a highly oxic water column, generally a shallow-marine environment,

characteristically comprises Fe and Mn oxides (Fig. 6.5). The Fe-Mn oxide-

carbonate lithofacies forms at slightly lower redox potential (Eh) and, or, partial

pressures of CO_2 (pCO_2). The pCO_2 may also be responsible for controlling the

precipitation of Fe-Mn carbonates. This lithofacies often contains layers of Fe-Mn

oxide, Fe-Mn silicate, and Fe-Mn carbonate minerals as observed in lithofacies

Frmz (Roy, 1981; Roberts and Prince, 1990). The reduced carbonate lithofacies has

a low redox potential and often minerals, such as siderite and rhodochrosite,

precipitate out of the water column (Force and Maynard, 1991; Gross, 1996a), as

observed in Lithofacies *Fgnz*. The Fe and Mn in those deposits are typically derived

from a variety of sources (Bonatti et al., 1972).

      During the deposition of the Matapédia basin, in which the Woodstock Fe-

Mn deposits preside, there were four regression events that occurred from the Upper

Ordovician to the Lower Devonian (1. Late Ordovician - late Taconic regression, 2.

Early to Middle Silurian – early Salinic regression, 3. Late Silurian - late Salinic

regression, and 4. late Early Devonian - Acadian regression). Each regression

interval within this time relates to the chronological accretion of a terrane upon the

Laurentian margin (Fyffe et al., 2011). At the time of the Early to Middle Silurian –

early Salinic regression sediments of Lithofacies Association O were deposited

which is consistent with the general
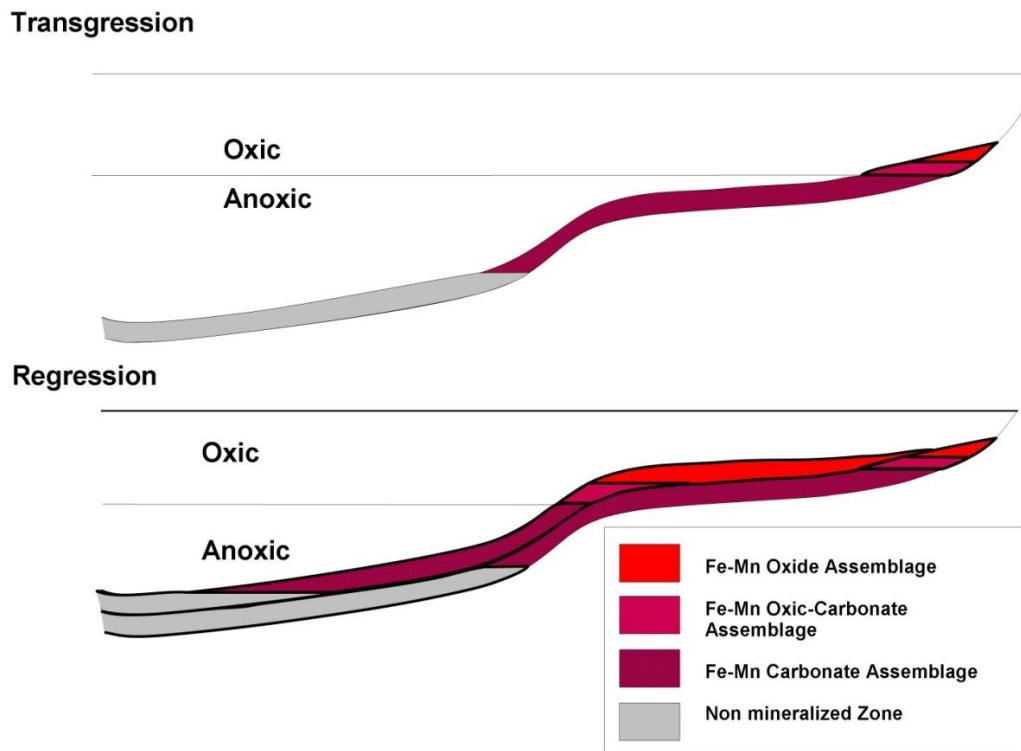
Fig. 6.5: Diagram displaying the distribution of the different Fe-Mn assemblages during transgression and regression cycles (modified from Frakes and Bolton, 1984; DesRoches, 2004).

coarsening upward of the lithofacies association. Then Lithofacies Associations I, II, III would have been deposited along a continental margin within areas of poor ocean circulation that would result in several anoxic basins. As the seawater continued to regress the depositional environment would undergo changes in redox potential and allow the precipitation of Fe and Mn oxides and carbonates. The final Lithofacies Associations IV and V were deposited during the Late Silurian - late Salinic regression where these Lithofacies Associations was deposited in the deeper southwest section of the basin (Fyffe et al., 2011).

As explained earlier in this chapter, Fe and Mn initially accumulate as Fe and Mn hydroxides and carbonates (Figs. 4.15 and 4.16) in sediments, by deposition, either by hydrogenous processes whereby the Fe and Mn are derived from weathering of continental bedrock, or by hydrothermal activity associated with active-ridge volcanism. Several geochemical plots were used in attempts to determine the source of Fe and Mn and further determine the depositional environment of the Fe-Mn mineralization.

Currently there are two contradicting hypotheses that suggest the genesis of the Woodstock Deposits. The high chlorite content within Units A, B, C of Lithofacies *Fgnz,* (Lithofacies Association II), cross-cutting veinlets, overall high Mn content (11.3% Mn in Lithofacies *Frmz*; 9.5% Mn in Lithofacies *Fgnz*), and anomalous Cu, Co, Au, Ge, Ga values of Lithofacies *Fgnz* and *Frmz* have led to the hypothesis by Roberts and Prince (1990) that the Woodstock Fe-Mn Deposits are Algoma-type BIFs, in which the Mn and base-metal mineralization are initially

derived from a hydrothermal source and could suggest a potential exhalative origin for the Woodstock Fe-Mn Deposits (i.e. Wonder et al., 1988).

In contrast, the general lack of volcanic rocks within the Smyrna Mills Formation, except for minor mafic flows and felsic tuffs (Fig. 2.1), suggest that much of the Fe and Mn could also be derived from alternative sources (hydrogenous-detrital, or diagenetic). The rare microspheriodal textures and higher Al_2O_3 and P_2O_5 contents within the Plymouth Fe-Mn deposit suggest the Woodstock Fe-Mn deposits may be a series of manganiferous Clinton-type ironstones as described by Baldwin (1954) and not Algoma-type BIFs.

6.6.3 LITHOFACIES ASSOCIATION O

The sedimentology of Lithofacies Association O (White Head Formation) is composed of Lithofacies *Fbuc, Sbuc*, with interbedded Lithofacies *Lbu* with increasing Lithofacies *Sbuc* upsection that are observable as turbidite beds that coarsen upwards and are observable in several outcrops (Sites 5, 10, 11) and interpreted have been deposited in a relatively deep marine environment. A plot of TiO_2 and Ni ratios of Lithofacies Association O samples (Fig. 6.6) confirms a submarine mudstone and sandstone clastic composition. This is consistent with the sand and silt-sized grains observed in outcrop (Sites 5 and 10). In particular, Lithofacies *Fbuc, Sbuc,* and *Lbu* that are restricted to this lithofacies association, the higher CaO content, and lack of anomalous Fe, Mn, and trace elements, suggest that this lithofacies association was formed in a distinctive depositional environment than the other lithofacies associations.
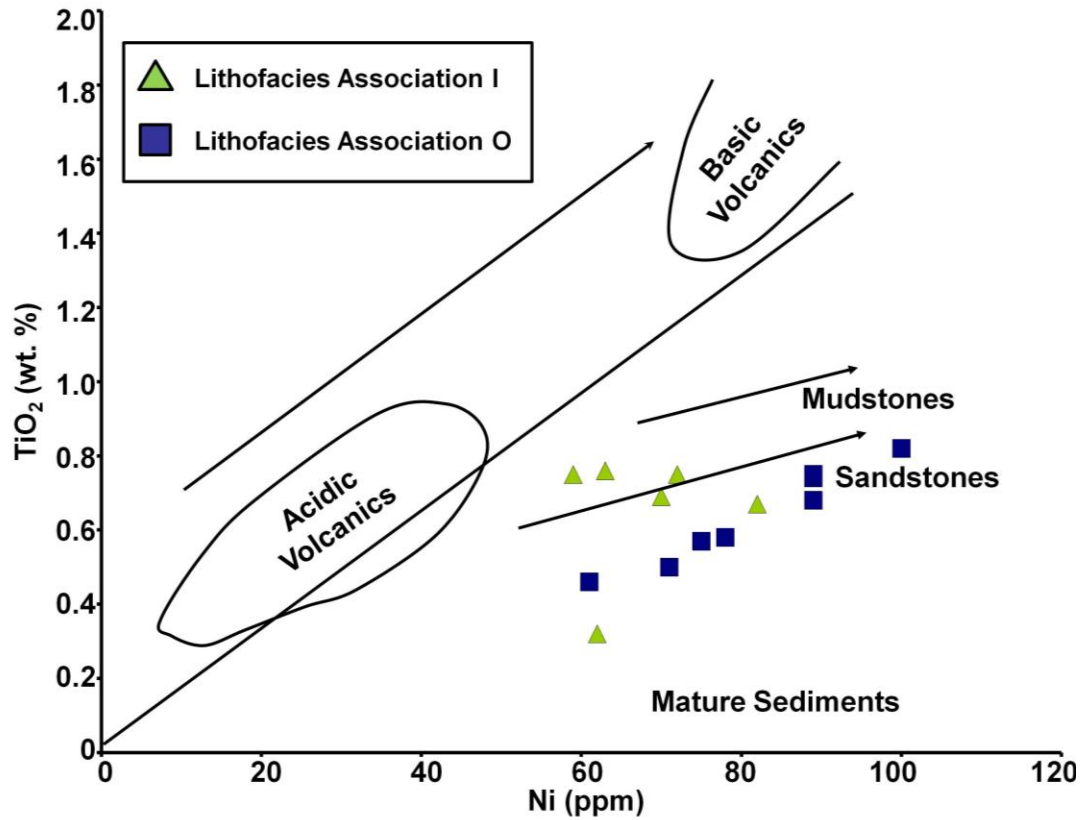
Fig. 6.6: TiO$_2$ (wt %) vs. Ni (ppm) contents of the Lithofacies Association O (White Head Formation) and unmineralized Lithofacies Association I (Smyrna Mills Formation) (diagram after Floyd et al., 1989; Gu, et al., 2002).

179

6.6.4 LITHOFACIES ASSOCIATION I

Lithofacies Association I (lower member, Smyrna Mills Formation) is interpreted to be deposited in a continental-shelf environment and in general is stratigraphically above Lithofacies Association O. Passive margins are a part of the ocean basin that can be subject to rapid changes in redox conditions (Frakes and Bolton, 1984) and so offer ideal settings for the precipitation and formation of continental-shelf Fe-Mn deposits. The TiO_2 and Ni ratios of Lithofacies Association I suggest a composition ranging from sandstone to mudstone. This can also be observed by the general siltstone composition of Lithofacies Association I as shown in Fig. 3.6. DF1 and DF2 ratios suggest that the unmineralized green and black siltstone of Lithofacies Association I are derived from an intermediate igneous provenance (Fig. 6.7).

6.6.5 LITHOFACIES ASSOCIATIONS II AND III

Lithofacies Associations II and III contain higher overall Fe_2O_3 and MnO contents and higher REE contents (Fig. 5.13) than the generally underlying Lithofacies Association I. These upper associations exclusively are associated with Fe-Mn mineralized lithofacies *Fgnz* and *Frmz*. The diagrams on the following pages are utilized in attempts to determine geochemical differences in the two lithofacies associations and the source of Fe and Mn that eventually was deposited to form the Fe-Mn-rich beds associated with the Woodstock Fe-Mn deposits. Nicholson (1992a) utilized Na/Mg ratios as a means to determine the depositional environment associated with Fe-Mn deposits (Fig. 6.8). Data from both Lithofacies Associations II and III indicate a range from the marine to, rarely for both, the shallow-marine.

180

Major-Element Provenance Discrimination
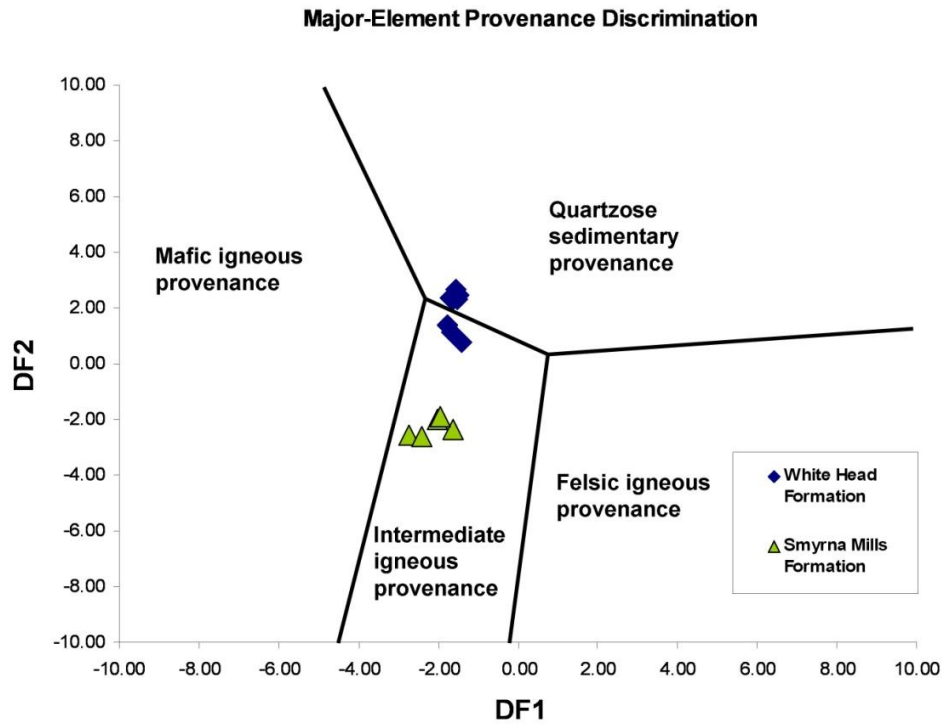
Fig. 6.7: Major-element provenance discrimination diagram of Lithofacies Associations O (White Head Formation) and I (Smyrna Mills Formation). DF1 $=30.6038TiO_2/Al_2O_3 - 12.541Fe_2O_3$ (total)$/Al_2O_3 + 7.329MgO/Al_2O_3 + 12.031Na_2O/Al_2O_3 + 35.42K_2O/Al_2O_3 - 6.382$. DF2 $= 56.500TiO_2/Al_2O_3 - 10.879$ Fe_2O_3 (total)$/Al_2O_3 + 30.875MgO/Al_2O_3 - 5.404Na_2O/Al_2O_3 + 11.112K_2O/Al_2O_3 - 3.89$ (modified from Roser and Korsch, 1988; Khider and McQueen, 2005).
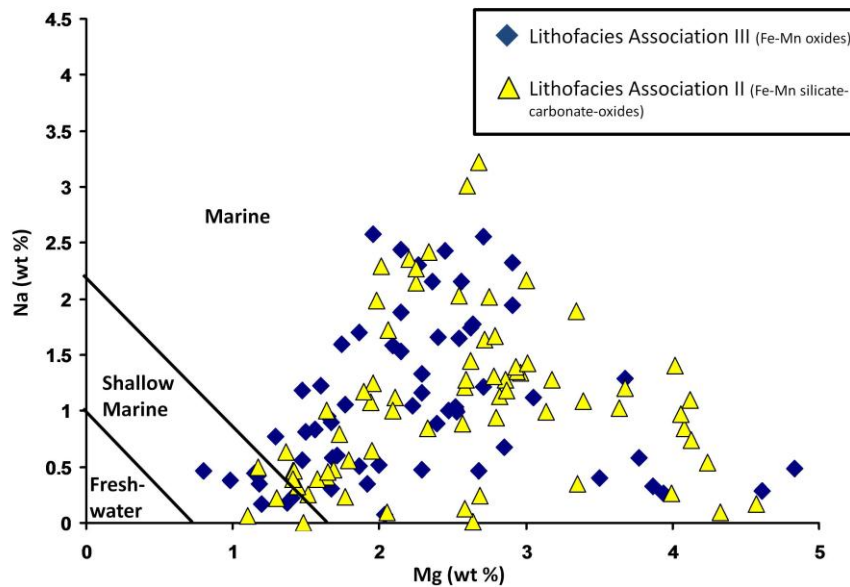
Fig. 6.8: Na versus Mg (wt %) with fields for freshwater to marine conditions for the depositional environment associated with lithofacies *Fgnz* and *Frmz* in the Plymouth Fe-Mn deposit (Nicholson, 1992a).

181

Boström (1973) developed a method to determine the relative contributions of common terrigenous elements (Al, Fe, Ti) and common hydrothermal elements (Fe, Mn) components within pelagic sediment by assessing the ratio of Fe/Ti against the ratio of Al/(Al+Fe+Mn) (Fig. 6.9). Almost all of the Al and Ti associated with marine sedimentary rocks are of continental derivation with no significant Al or Ti values from basaltic volcanism (Boström, 1973). The Fe/Ti ratio is ideal for determining hydrothermal (Fe) input verses terrigenous input (Ti) origin of sediments. Active-ridge volcanism at its maximum intensity will often produce vast quantities of Fe and Mn and some other elements (Ba, As) that are unsurpassed in other regions of the ocean and that result in Fe-Mn-rich metalliferous sediment similar to Fe-Mn deposits observed in the Red Sea and the East Pacific Rise (Fig. 6.9). However, regions of the ocean that are proximal to land, in particular continental-shelf environments often have sediments that are rich in Fe and Mn (Fig. 6.9) where the Fe and Mn are derived from weathering of the continental (terrestrial) bedrock (Boström, 1973). Hardly any of the data points associated with Lithofacies Associations II and III of the Plymouth deposit plot close to samples described as metalliferous and display the samples as being non-metalliferous with minor terrigenous components (Fig. 6.9). The minor terrigenous component may suggest some of the Fe and Mn are supplied from weathering terrestrial bedrock.

The relationship between Al_2O_3, Fe_2O_3, and MnO on a ternary plot has also been used to determine the origin of Fe and Mn deposits (Fig. 6.10). Active-ridge Fe-Mn deposits (hydrothermal) are found to have approximately 30% Fe, whereas
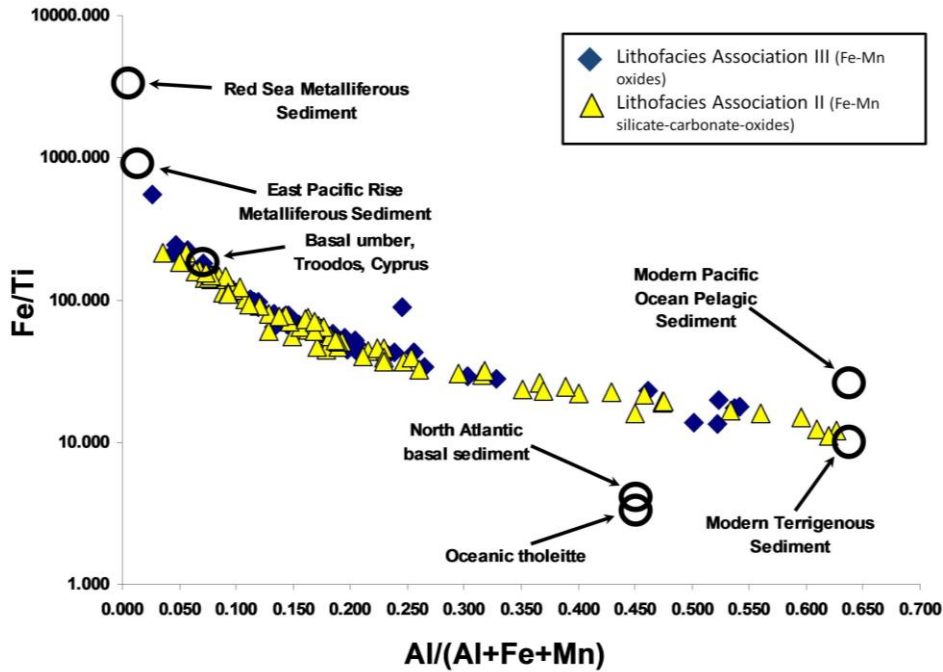
Fig. 6.9: Fe/Ti verses Al/(Al+Fe+Mn) ratios of the lithofacies *Fgnz* and *Frmz* within the Plymouth deposit in comparison to various modern volcanic rocks and sediments (plot devised by Boström, 1973; Peter, 2003).
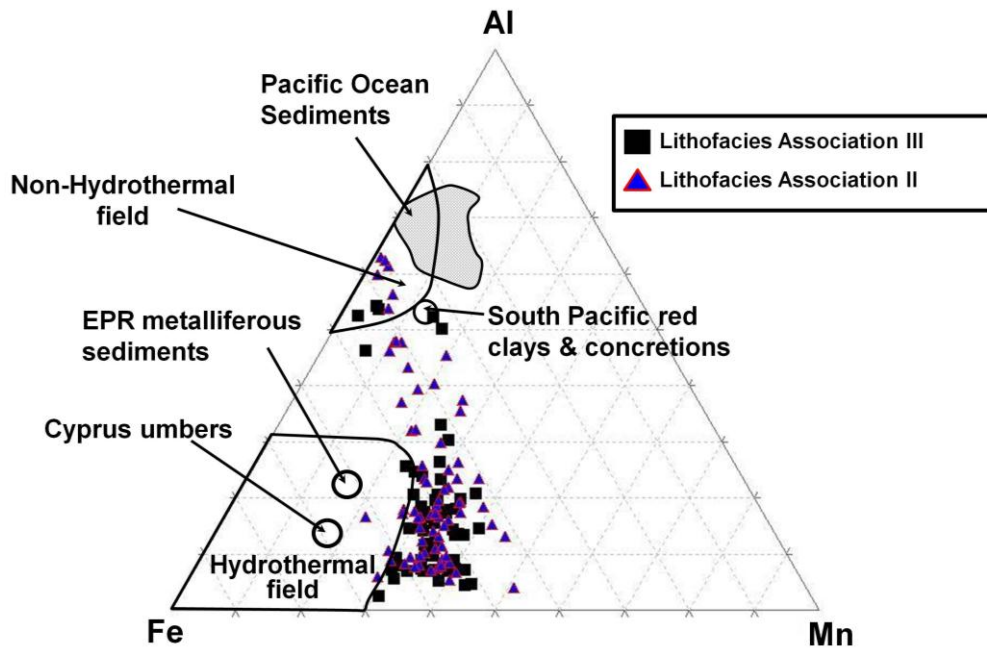
Fig. 6.10: Al-Fe-Mn ternary diagram in relation to the origin of precipitated Fe-Mn sediments. Most of the oxide-carbonate and oxide-silicate-carbonate lithofacies exhibit chemical signatures just outside of the hydrothermal field with minor occurrences in the non-hydrothermal field suggesting that the Fe and Mn was derived from a source other than hydrothermal (Boström, 1973; Peter, 2003).

183

ordinary pelagic sediments only contain about 5% Fe (Boström, 1973). Both

lithofacies *Fgnz* and *Frmz* exhibit chemical signatures just outside of the

hydrothermal field with minor occurrences in the non-hydrothermal field. This

suggests that the Fe and Mn were derived from a source other than hydrothermal

(Boström, 1973; Peter, 2003). The lithofacies associations are interpreted in Chapter

3 as being deposited in a continental-shelf environment where Fe and Mn could be

supplied from weathering terrestrial bedrock alongside other elements, such as Al,

Ti, and Si. Hydrothermal Fe-Mn deposits, in contrast derive Fe and Mn from active-

ridge volcanism with no significant input of Al and Ti (Boström, 1973).

Bonatti (1975) suggested that hydrogenous Fe-Mn deposits could be

distinguished from hydrothermal deposits by Si/Al ratios (Fig. 6.11), where the Si is

associated with quartz in hydrothermal sediment and both Si and Al are associated

with feldspars and clays in clastic sediment. The ratios within hydrothermal Fe-Mn

deposits are considered generally higher (>5) than hydrogenous Fe-Mn, which plot

at around 3, a ratio typically seen within average marine sediment. These ratios can

also be utilized to determine if the deposits are deep-sea sediments since deep-

marine Fe-Mn nodules plot in a very confined linear plot (Bonatti et al., 1972;

Crerar 1982). Both lithofacies *Fgnz* and *Frmz* of the Plymouth deposit plot within a

section of the hydrogenous-detrital field (Fig. 6.11) with only one sample associated

with the lithofacies *Frmz* plotting within the hydrothermal field. This anomalous

data point represents a potassic/silicic and chlorite-altered, red Fe-Mn mineralized

unit with epigenetic quartz-chlorite fracture fills similar to hydrothermally altered

sedimentary rocks (Roberts and Prince, 1990). Samples that plotted within the deep-
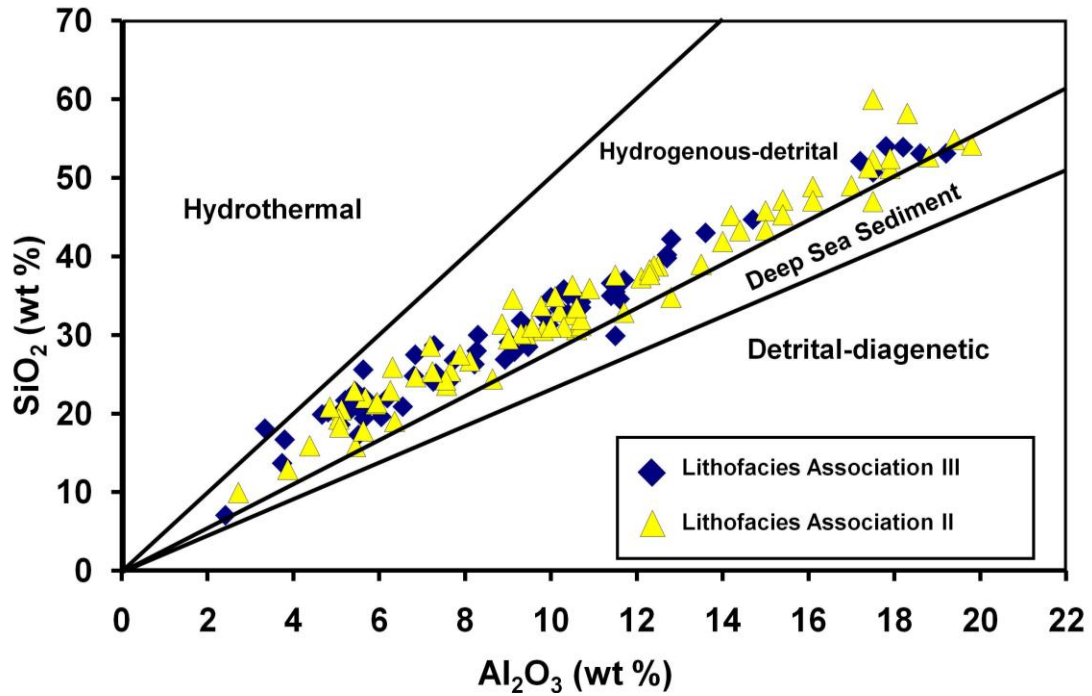
Fig. 6.11: SiO$_2$/Al$_2$O$_3$ ratios of the Fe-Mn oxide-carbonate and oxide-silicate-carbonate lithofacies within the Plymouth deposit suggestive that the Fe and Mn was mainly derived from hydrogenous-detrital sources (modified from Bonatti, 1975; Crerar et al., 1982; Wonder et. al., 1988).

sea sediment field represent lithofacies *Fgnz* (Unit A) that is largely dominated by phyllosilicates (particularly chlorite, epidote, and muscovite mica; Roberts and Prince, 1990). No samples for the SiO_2/Al_2O_3 ratios (Fig. 6.11) have suggested a diagenetic/detrital input for Fe and Mn from the Plymouth deposit where the Fe and Mn would be remobilized from another source during diagenesis. At the time of diagenesis, there was no remobilization of Fe and Mn. This is consistent with the prediagenetic rhodochrosite microspheroids and microbanding that were observed in thin section.

U-Th plots can also be utilized as a means to determine the origin of sediment in particular with deep sea Fe-Mn deposits (Bonatti et al., 1972; Fig. 6.12). Uranium concentrations within seawater on average are about 3.3×10^{-6} g/L. In contrast, thorium is generally absent in seawater due to its short residence time and insolubility. The slow rate of deep-sea Fe-Mn hydrogenous nodule growth allows Th to be scavenged from seawater and produces high anomalous Th values within nodules (Bonatti et al., 1972). A majority of the Fe-Mn mineralized samples plot within the pelagic field with lithofacies *Fgnz* having greater overall concentrations of Th than lithofacies *Frmz* (Fig. 6.12). The one anomalous sample from lithofacies *Frmz* occurring within the hydrothermal field (higher amounts of U) was not geochemically anomalous in any other element.

The concentration of REEs within hydrogeneous and hydrothermal Fe-Mn deposits varies significantly (Fleet, 1983). Although many major and minor elements are enriched within lithofacies *Frmz*, lithofacies *Fgnz* contains higher HREEs than those observed in lithofacies *Frmz*. This enrichment of HREEs may be

186
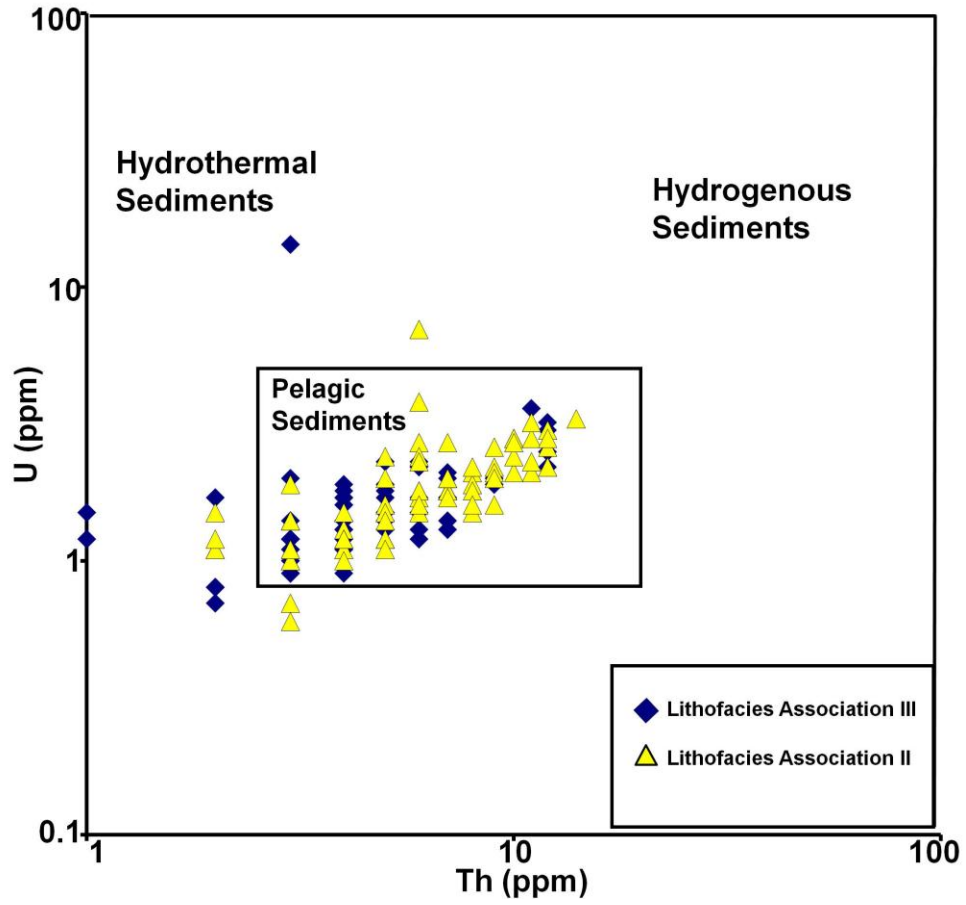
Fig. 6.12: U vs Th plot of Fe-Mn mineralized lithofacies *Frmz* and *Fgnz* within the Plymouth deposit (diagram's fields from Bonatti et al., 1972).

attributed to the deeper marine and more anoxic environment associated with lithofacies *Fgnz*. Slower rates of chemical precipitation and clastic deposition would allow greater rates of chemical scavenging of elements within the seawater and an enrichment of HREEs (Elderfield and Greaves, 1982; Byrne and Kim, 1990).

In contrast, continental-shelf Fe-Mn deposits precipitate at a faster rate than deep marine Fe-Mn nodules and generally have lower amounts of REEs (Wonder et al., 1988) as observable in Fig. 6.13. Monazite inclusions within the subhedral oligonite grains contribute to the higher REEs within lithofacies *Fgnz* (Fig. 5.12). REEs may also be present within the diagenetic apatite crystals and cements (see Fig. 4.10). In summary, the higher REE contents of lithofacies *Frmz* and *Fgnz* in the Woodstock Fe-Mn deposits are likely associated with apatite and trace inclusions of monazite. Within Lithofacies Association II and III of the Smyrna Mills Formation, REEs plot (Fig. 6.13) within both the hydrothermal and hydrogenous fields, but below average values.

A majority of REEs are relatively immobile, but the elements Ce and Eu exist within more than one oxidation state, therefore are affected by environmental redox changes during deposition and post-depositional weathering of the bedrock (Fig. 6.13). Both Lithofacies Association III (lithofacies *Frmz*) ($Ce/Ce^* = 1.18$) and Lithofacies Association II (lithofacies *Fgnz*) ($Ce/Ce^* = 1.14$) display minor positive Ce anomalies within NASC-normalized REEs, a characteristic of a shallow-marine environment (<200 m) within oxidizing conditions. In contrast, oxygenated deep marine environments (>2000 m), which have a very large positive Ce anomalies associated with high amounts of CeO_2 in deep marine carbonates (Kato et al., 2006).
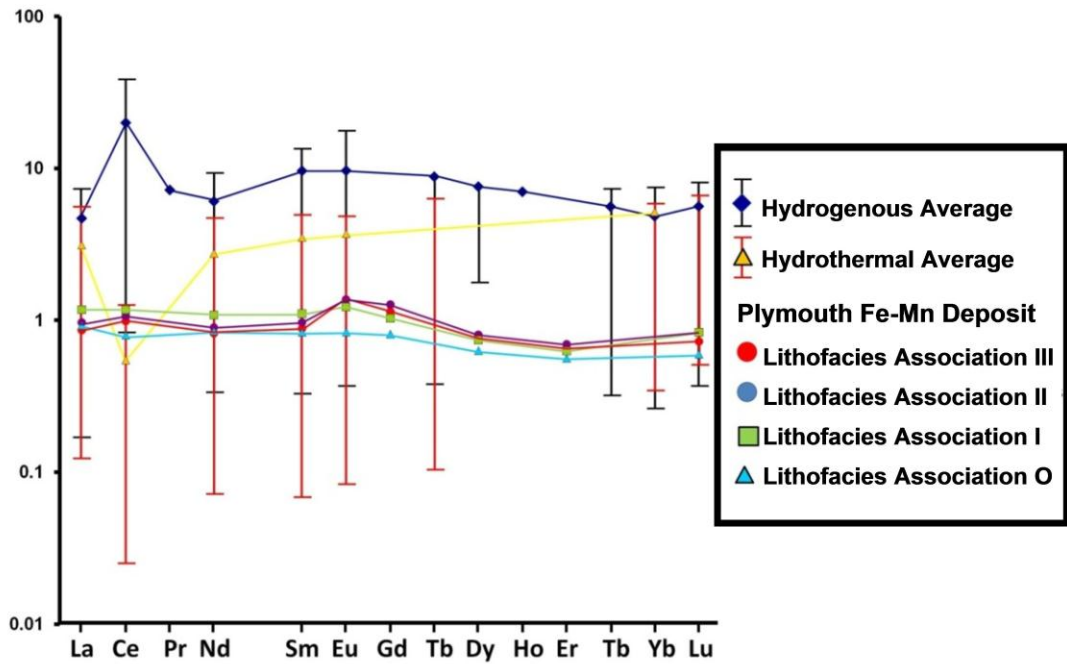
Fig. 6.13: NASC-normalized plot of modern hydrogenous and hydrothermal Fe-Mn deposits in relation to the average values of the four Lithofacies Associations within the Plymouth deposit. Hydrogenous Fe-Mn and hydrothermal Fe-Mn data from Fleet (1983), Plymouth Fe-Mn data from Roberts and Prince (1990).

In hydrothermal environments there is generally a very strong negative Ce anomaly. NASC-normalized REEs within the Plymouth deposit display slightly higher Eu anomalies within the Lithofacies Association III (lithofacies *Frmz*) (Eu/Eu* = 1.35) in relation to the Lithofacies Association II (lithofacies *Fgnz*) (Eu/Eu* = 1.22).

As previously explained no geochemical data from Lithofacies Association IV and V was available from the Plymouth deposit. This was due to the fact that neither Lithofacies Association IV nor V was present at this location.

6.7   SUMMARY

Geochemical plots of the Lithofacies Association II and III of the Smyrna Mills Formation suggest that the Woodstock Fe-Mn deposits were deposited in a relatively shallow-marine environment reflected in Na-Mg (wt. %) abundances (Fig. 6.8). Deep-sea hydrogenous sediment has lower U/Th ratios than hydrothermal sediment (Fig. 6.12). The Fe and Mn in the lithofacies was derived from hydrogenous-detrital sources (Fig. 6.11) where the Fe and Mn is sourced from the chemical weathering of continents and then precipitated out as Fe-Mn minerals in seawater similar to many shallow-marine Fe-Mn deposits that lack hydrothermal Fe-Mn input. Fig. 6.11 also indicates that the Fe-Mn mineralization in Lithofacies Association II and III are not associated with deep-sea Fe-Mn deposits. The small positive average Ce anomaly (Ce/Ce* = 1.18) present in Lithofacies Association III associated with NASC-normalized REEs suggests an oxygen-rich environment of deposition, whereas Lithofacies Association II is more oxygen-poor that is associated with a smaller average Ce anomaly Ce/Ce* = 1.14. The shallow-marine

190

to marine setting (Fig. 6.8) and lack of deep-sea sediment signatures from Si/Al ratios (Fig. 6.11) are consistent with initial Fe and Mn mineralization was formed by deposition within a continental-shelf environment. Figs. 6.9 and 6.10 display both Lithofacies Associations II and III to lie just outside of the hydrothermal (<30% Fe) and metalliferous active-ridge deposit regions of both diagrams. Since Fe and Mn from active ridge/hydrothermal Fe-Mn deposits is supplied exclusively from Fe and Mn, the close proximately to terrestrial bedrock may have caused an enrichment of Fe of Mn of greater than 30% since there would likely be Fe and Mn supplied from multiple sources. REE patterns from Fig. 6.13 fall into the hydrothermal average as opposed to the hydrogenous average for Fe-Mn. This lower level of REEs is a signature of hydrothermal Fe-Mn deposits and also continental-shelf Fe-Mn deposits. However the small positive Ce anomalies and negative Eu anomalies do not support a hydrothermal source of Fe and Mn.

Si/Al plots suggest that the initial Fe and Mn mineralization occurred during deposition and was not remobilized from another source during diagenesis (Fig. 6.11). During diagenesis is likely that deposited Fe-hydroxide gel, Fe-Mn clays and clastics, and microspheroidal Fe-Mn carbonates were compacted and altered to form hematite, magnetite, Fe-Mn silicates, and Fe-Mn carbonates (Figs. 4.16 and 4.17). Some fluid migration would have also occurred during diagenesis and may have caused minor quartz-carbonate and quartz-chlorite-sulfide veinlets. Then during subgreenschist grade metamorphism, fluids would have infiltrated the lithofacies with quartz veins (some of which contained sulfides) and folded the Fe-Mn mineralized lithofacies *Fgnz* and *Frmz* to there present shape.

In summary, Gross (1983) described earlier that there were four types of sedimentary iron deposit types: Lake Superior-type, Algoma-type, Clinton-type, and Minette-type (Fig. 6.3). Lake Superior-type BIFs are formed in shallow-marine basins and associated with black mudstone, dolomite, chert, and banded iron-rich sediments. These Fe deposits are restricted solely to the Precambrian due to the atmospheric conditions needed to produce the widespread Fe deposits. Stratigraphic and graptolite data indicates that the Woodstock Fe-Mn deposits are Silurian and not Precambrian, and therefore these are not Lake Superior-type BIFs.

Algoma-type BIFs, which were initially suggested as type of iron deposit for the Woodstock Fe-Mn deposits, are generally associated with volcanic rocks, deep seated fracture systems, turbidite sequences, and hydrothermally altered Fe-Mn-rich sedimentary rocks that are cherty in composition (Gross, 1983; Fig. 6.3). The only evidence of turbidite beds appears in Lithofacies Association O of the White Head Formation. Geochemically, Algoma-type BIFs are often rich in base metals, low in REEs, have a strong positive Eu anomaly, and a strong negative Ce anomaly (Kato, et al., 2006). Although there are Cu and Co anomalies associated with the Woodstock Fe-Mn deposits, there was no outcrop or drill core evidence of volcanic rocks or hydrothermally altered rocks. All of the geochemical plots give no indication of a hydrothermal input associated with the Fe-Mn mineralization. REE data also displays a minor positive Ce anomaly and minor negative Eu anomaly in contrast to the strong positive Eu anomaly and a strong negative Ce anomaly associated with Algoma-type BIFs. Both stratigraphic and geochemical data suggests that the Woodstock Fe-Mn deposits are not Algoma-type BIFs.

192

Clinton-type ironstones as previously explained occur along the edges of stable cratonic margins and are composed largely of hematite-rich red and purple siltstone and are locally abundant with bioclasts. Geochemically, these are often Al_2O_3 and P_2O_5 in contrast to the cherty Lake Superior- and Algoma-type BIFs. Outcrop and drill core data from the Woodstock Fe-Mn deposits suggests a marine environment of deposition subject to changes in redox similar to the edge of a cratonic basin. Although generally devoid of bioclasts, the Fe-Mn mineralized lithofacies *Frmz* and F*gnz* are composed of largely of Fe oxides (hematite and magnetite, Fe-Mn carbonates (rhodochrosite and oligonite), and chlorite. These Fe-Mn deposits are also rich in Al_2O_3 and P_2O_5, and REEs, which suggests that these are a Clinton-type ironstone.

Minette-type ironstones are formed in a shallow-marine to deltaic environments and can also form in lacustrine, fluviatile, and pedogenic environments and are locally abundant with bioclasts. In contrast to the Clinton-type ironstone, these are typically composed of goethite, siderite, and chamosite and are less oxide-rich and more clay-rich. Although Minette-type ironstones can form in shallow-marine environments the Woodstock Fe-Mn deposits are found to have a mineralogy composed of more oxide- and carbonate-rich (hematite, magnetite, and rhodochrosite) minerals in contrast to goethite, siderite, and chamosite that occur in Minette-type ironstones. This suggests that the Woodstock Fe-Mn deposits are not a Minette-type ironstone and are a Clinton-type ironstone. Alternatively, since the Woodstock Fe-Mn Deposits do not completely fit the description of a Clinton-type

193

ironstone it is possible that they in fact a different subdivision of an ironstone all

together which is currently not shown in Fig. 6.3.

CHAPTER 7

CONCLUSIONS AND RECOMMENDATIONS

7.1   CONCLUSIONS

In western New Brunswick, conformably and stratigraphically above the Upper Ordovician to Lower Silurian White Head Formation is the Silurian Smyrna Mills Formation that hosts six significant Fe-Mn deposits (Plymouth, North Hartford, South Hartford, Sharpe Farm, Iron Ore Hill, and Moody Hill) collectively estimated at 194,000,000 tonnes (with 13% Fe and 9% Mn). The latter two deposits were utilized as a source of iron from 1848 to 1884.

Six lithofacies associations are identified within the study area, that, in general, stratigraphically overlie each other in a conformable succession, but in many areas have been folded resulting in a juxtaposition and complication of lithofacies associations that are not always in stratigraphic order. Lithofacies Association O is collectively composed of lithofacies *Sbuc* (Blue-grey laminated calcareous sandstone)*, Fbuc* (Blue-grey laminated calcareous siltstone), and with minor interbedded *Lbu* (Blue-grey limestone). This lithofacies association contains abundant turbidite beds and forms the uppermost section of the White Head Formation and is interpreted as forming in a deep marine environment. This lithofacies association has elevated amounts of CaO and Sr that are not present in the other lithofacies associations.

Lithofacies Association I is collectively composed of lithiofacies *Fgnc* (Green calcareous siltstone)*, Fgngyib* (Green and grey interbedded siltstone), *Fbkpl*

195

(Black to grey laminated mudstone with authigenic pyrite), *Fgyl* (Grey and minor greenish laminated siltstone), *Fgygn* (Greyish green siltstone), and *Fgnl* (Green laminated siltstone with rare white microspheroidal limestone). Petrographically the lithofacies are composed of a groundmass of muscovite, quartz, calcite and framboidal pyrite, with minor coarse silt-sized quartz and feldspar clasts have been observed, locally with overprinting euhedral pyrite. Lithofacies *Fgnc* is observed to be the only calcite-rich lithofacies in Lithofacies Association I and is interpreted to be the transitional layer between the White Head Formation and the Smyrna Mills Formation. The presence of lithofacies *Fbkpl* suggests an anoxic and organic-rich environment at the time of deposition where much of the Fe in solution was precipitated out as framboidal pyrite that later recrystallized to euhedral pyrite during diagenesis. Although this Lithofacies Association contains abundant pyrite, it contains no visible areas of Mn mineralization. Harker diagrams of Lithofacies Association I display enrichments in Al_2O_3, K_2O, Fe_2O_3, MnO, and P_2O_5 and decreases of CaO in comparison the conformably underlying White Head Formation. Increases of Cu, Pb, S, As, Ba, Co, and V with decreases in Sr relative to SiO_2 in comparison to the Lithofacies Association O are also present in this unit.

Lithofacies Association II is collectively comprised of lithofacies *Fgygn* (Greyish green siltstone), *Fgnl* (Green laminated siltstone with rare white microspheroidal limestone), *Sgnl* (Green to grayish green and tan calcareous and noncalcareous sandstone), and *Fgnz* (Dark green to black laminated Fe-Mn mineralized siltstone) with rare interbedded *Frmz* (maroon to red laminated Fe-Mn mineralized siltstone). Lithofacies *Fgnz* is composed is Fe-Mn oxide-silicate-

196

carbonate and petrographically contains silt-sized magnetite, chlorite, rhodochrosite, oligonite, Mn-clays, with minor acicular hematite laminae, and trace chalcopyrite and cobaltite. The abundance of ferrous minerals, such as magnetite and lack of pyrite, suggests that these were precipitated within a region of lower dissolved oxygen and sulfur content.

Lithofacies *Fgnz* is divided up into three mineralized units (A, B, and C) that are generally in stratigraphic order, but can occur out of order due to folding and interbedding. Unit A is composed of dark green very fine crystalline unit composed of chlorite, Fe-Mn silicates, and Fe-Mn carbonates. Unit B that is comprised of a weakly magnetic, dark green, very fine crystalline unit that is composed of chlorite, magnetite, Fe-Mn silicates, and Fe-Mn carbonates. Unit C that is composed of a strongly magnetic, dark green to black, very fine crystalline unit composed of magnetite, chlorite, Fe-Mn silicates, and Fe-Mn carbonates. Gradational changes in mineralogy could suggest these lithofacies are depositional or diagenetic in origin.

Lithofacies Association II collectively displays decreased K_2O, TiO_2, V, S, Cr, As, Zn, and Cu abundance, and increased REEs in relation to Lithofacies Association I. The overall increase in grain size in relation to Lithofacies Association I and presence of bedded magnetite and Fe-Mn carbonates suggest that the environment of deposition was shallower, but with a lower redox potential than the overlying Lithofacies Association III. Beds of Fe-Mn mineralization within Lithofacies Association II also contain rare occurrences of Fe-Mn-rich concretions composed of rhodochrosite, Mn-silicates, or hematite that likely formed during

197

diagenesis. Microspheroidal carbonate laminae within layers of zoned pyrite stratigraphically beneath beds of Fe-Mn carbonate mineralization and occasional Fe-Mn microspheroids suggest biogenic activity could be associated with changes in ocean redox. This increase in Eh conditions would have eventually caused the precipitation of Fe-Mn carbonates, a characteristic that is similar to many Precambrian continental-shelf Fe-Mn deposits.

Lithofacies Association III is collectively composed of lithofacies *Frml, Frmz, Sgnl,* and *Fgnl.* Lithofacies *Frmz* is composed of very fine crystalline bands of silt-sized acicular crystals of hematite and minor cryptocrystalline hematite interbedded with laminae of anhedral grains of rhodochrosite, minor euhedral magnetite, subhedral apatite, chlorite, Mn-silicates, with trace stilpnomelane, and Mn-clinochlore.

Lithofacies *Frmz* (Fe-Mn oxide-carbonate) is divided into three stratigraphic mineralized units (D, E, and F) that are generally in stratigraphic order but can occur out of order due to folding and interbedding. Unit D is composed of strongly magnetic, maroon, very fine crystalline unit composed of magnetite, rhodochrosite, and hematite. Units E is composed of a laminated maroon very fine crystalline unit of hematite and rhodochrosite. Unit F is composed of a red very, finely crystalline unit of hematite and Fe-Mn carbonates.

In contrast to Lithofacies Association II, the shallower Lithofacies Association III display bands that are typically of cryptocrystalline hematite with inclusions of Mn-silicates. Petrographic and SEM analysis of the magnetite-rich Units B, C, and D among all sampled areas of Fe-Mn mineralization contain coarse

silt-sized euhedral magnetite with inclusions and overprinting crystals of chalcopyrite and cobaltite. This mineralization overprints acicular hematite, subhedral rhodochrosite, and chlorite that suggests final magnetite crystallization formed after the advent of hematite and rhodochrosite mineralization. The higher abundance of depositional microspheroidal ferric minerals with prediagenetic features, and ghost structures of rhodochrosite microspheroids within lithofacies *Frmz* suggest that the Fe and Mn were precipitated within a marine environment that was higher in dissolved oxygen. This conclusion is observable by the presence of surrounding red siltstones that suggests a highly oxic environment of deposition.

The upper member of the Silurian Smyrna Mills Formation is composed of Lithofacies Associations IV and V that is collectively composed of lithofacies *Sgyce* (Grey laminated, bedded, bioturbated, and massive sandstone)*, Sgnl* (Green to greyish green and tan calcareous and non calcareous sandstone)*, Fgnl* (Green laminated siltstone with rare white microspheroidal limestone)*, Fgyl* (Grey and minor greenish laminated siltstone)*, and *Fgygn* (Greyish-green siltstone). These are devoid of any Fe-Mn mineralization. This member of the Smyrna Mills Formation is represented by beds of massive green quartz-chlorite-carbonate sandstone, which contains rare occurrences of crinoidal debris, and overlying beds of grey quartz-carbonate siltstone.

Stratigraphic and petrographic relationships suggest that the Fe-Mn mineralization, confined to the lower member of the Smyrna Mills Formation is depositional in origin. The Fe-Mn mineralization is interpreted as being precipitated from seawater by changes in ocean redox conditions. The Fe-Mn oxide-carbonate

lithofacies *Frmz* is commonly associated with red siltstone, which is indicative of a more oxic environment associated with deposition. Lithofacies *Fgnz* that is commonly associated with green siltstone is indicative of an anoxic depositional environment. The depositional environment for the Smyrna Mills Formation was on the continental shelf in the offshore zone (~200 m depth), on a stable cratonic margin at the oxic/anoxic interface.

Several of the Woodstock Fe-Mn deposits contain minor chalcopyrite and cobaltite mineralization that accounts for Cu and Co anomalies identified. This Cu-Fe-S and Co-As-S mineralization occurs as inclusions and crystals within the magnetite-rich Units B, C, and D, but also within minor cross-cutting quartz-chlorite-sulfide, quartz-sulfide, and sulfide veinlets. By observation it is apparent that there were two episodes of base-metal mineralization. The first occurred during deposition of the magnetite beds within a marine anoxic and anoxic/oxic environment where the base-metal mineralization formed at the same time as the magnetite. The second base-metal mineralization episode hosted in the overprinting and cross-cutting veinlets is interpreted to be late epigenetic in origin. It is possible that some of the original, depositional, base-metal mineralization was remobilized during this second base-metal mineralization event. This late epigenetic mineralization is present within the Plymouth, North Hartford, and Iron Ore Hill deposits. Locally the Plymouth deposit contains several areas of minor sericite, and chloritic alteration with minor quartz-chlorite-sulfide mineralization.

Veinlets and overprinting Cu-Fe-S and Co-As-S mineralization appear to be minor in all areas of observed Fe-Mn mineralization with an exception of the Unit

200

B associated with an 4.3 m wide outcrop of continuous Fe-Mn present at Union Corner, NB where cross-cutting veinlets of quartz-chlorite-sulfide, quartz-sulfide, and sulfide veinlets that host minor chalcopyrite are abundant and increase in density towards the southwest in the rhodochrosite-rich mineralized Unit B. This outcrop is largely composed of oligonite with minor bands of rhodochrosite, but also contains micro-inclusions of Mn-ilmenite and monazite that are only present in the subhedral oligonite crystals.

Geochemical discrimination diagrams suggest the depositional Fe-Mn mineralization of lithofacies *Frmz* and *Fgnz* is derived from hydrogenous-detrital sources and not from hydrothermal sources. This model of hydrogenous-detrital based Fe-Mn mineralization is consistent with the stratigraphy and general lack of Silurian volcanic rocks in the lower Smyrna Mills Formation. The mafic flows and tuffs within this formation appear to be confined to the upper member of the Smyrna Mills Formation and are not associated with the Fe-Mn mineralization. Minor silicic and potassic alteration of both mineralized lithofacies are interpreted as an interaction of unmineralized silicates and Fe-Mn carbonates related to the regional subgreenschist grade metamorphism during the Devonian Acadian Orogeny. In conclusion, stratigraphic, petrographic, and geochemical evidence suggests that the Woodstock Fe-Mn Deposits are a series of Clinton-type ironstones with no observed hydrothermal input and were geochemically controlled largely by the initial weathered source material and the redox conditions present at the time of deposition. However since the Woodstock Fe-Mn deposits do not completely fit the

description of a Clinton-type ironstone it is also possible that these fall into their own separate ironstone subdivision that is not currently shown on Fig. 6.3.

7.2   RECOMMENDATIONS FOR FURTHER RESEARCH ON THE WOODSTOCK FE-MN DEPOSITS

Mining of the Woodstock Fe-Mn deposits, although profitable during the mid-19th century as a source of iron, could now be a potential source of manganese, if cost-effective and high-recovery methods were adopted in its extraction (Wark, 1970; Gliders, 1976). The mineralogy of the two Fe-Mn mineralized lithofacies is consistent over all of the Fe-Mn mineralized areas. This assemblage of Fe-Mn mineralization is dominated by 40 – 80% Fe-Mn carbonate minerals chiefly rhodochrosite, Mn-calcite, and Mn-siderite (Roberts and Prince, 1990). The South Hartford deposit in particular contains a consistent mineralogy composed of interbedded acicular hematite and rhodochrosite with minor chlorite and Mn-silicate laminae over the span of the Fe-Mn mineralized lithofacies with no observed sulfides present. The main concern regarding the extraction of the Fe-Mn deposits is the silt-sized crystals, interbedded nature of the Fe and Mn minerals, and geochemical and thermodynamically similarities of both Fe and Mn. The silt-sized attributes of these Fe-Mn deposits, which are consistent in all areas of Fe-Mn mineralization within the Woodstock area, could lead to difficulty in extraction of the Fe and Mn ore and development of concentrates (Wark, 1970). If cost-effective methods of Mn and Fe recovery are utilized, it is possible that Cu and Co could be extracted from the waste material as valuable byproducts.

REFERENCES

Anderson, F.D., 1968, Woodstock, Millville, and Coldstream Map-Areas, Carleton and York Counties, New Brunswick: Geological Survey of Canada Memoir 353, 69 p.

Appel, P.W.U., Fedo, C.M., Moorbath, S., and Myers, J.S., 1998, Early Archaean Isua supracrustal belt,West Greenland: pilot study of the Isua Multidisciplinary Research Project: Geology of Greenland Survey Bulletin, v. 180, p. 94 – 99.

Atkinson, E.C., 1960, Final Report of the Commissioner of Mines in New Brunswick Mining Act and Mining Tax Act, Fredericton, p. 14 – 18.

Bailey, L.W., 1864, Report on the Mines and Minerals of New Brunswick, Queen's Printer, Fredericton, p. 158.

Bailey, L.W., 1898, The mineral resources of the province of New Brunswick: Geological Survey of Canada, Summary Report 1897, v. 10, part. M, p. 128.

Baldwin, A.B., 1954, The Nature and Genesis of the Iron Ores of the Hayot Lake Area, Labrador-New Quebec in Comparison with those of New Brunswick: unpublished MSc. Thesis, University of New Brunswick, Fredericton, NB, 92 p.

Barbarand, J., and Pagel, M., 2001, Cathodoluminescence study of apatite crystals: American Mineralogist, v. 86, p. 473 – 484.

Barrett, T.J., 1981, Chemistry and Mineralogy of Jurassic bedded chert overlying ophiolites in the North Apennines, Italy: Chemical Geology, v. 34, p. 289 – 317.

Berner, R.A., 1974, Kinetic models for the early diagenesis of nitrogen, sulfur, phosphorus, and silicon in anoxic marinc sediments, *in* Goldberg, E.D. ed., The Sea – v. 5, p. 427 – 449.

Beukes, N.J., and Gutzmer, J., 2008, Origin and Paleoenvironmental Significance of Major Iron Formations at the Archean-Paleoproterozoic Boundary, *in* Hagemann S., Rosière C., Gutzmer J., Beukes N.J., eds., Banded Iron Formation – related high – grade iron ore: Reviews in Economic Geology – v. 15, Society of Economic Geologists, p. 5 – 47.

Boggs, S., Jr., and Krinsley, D., 2006, Application of Cathodoluminescence Imaging to the Study of Sedimentary Rocks: New York, Cambridge University Press, 165 p.

Bonatti, E., Kraemer, T., and Rydell, H., 1972, Classification and genesis of iron-manganese deposits, *in* Horn, D.R., ed., Ferro-manganese deposits on the ocean floor, Washington, National. Sci. Foundation, p. 149 – 166.

Bonatti, E., 1975, Metallogenesis at Oceanic Spreading Centers: Annual Review of Earth and Planetary Sciences, v. 3, p. 401 – 431.

Boström, K., 1973, The origin and fate of ferromanganoan active ridge sediments: Stockholm Contributions to Geology, v. 27, p. 147 – 243.

Boström, K., 1983, Genesis of Ferromanganese Deposits – Diagnostic criteria for recent and old deposits, *in* Rona, P.A., Boström, K., Laubier, L., Smith, K.L., Jr., eds., Hydrothermal Processes at Seafloor spreading centers: Plenum Press, New York and London, p. 473 – 490.

Braterman, P.S., Cairns-Smith, A.G., and Sloper, R.W., 1983, Photo-oxidation of hydrated Fe^{2+} – significance for banded iron formations: Nature, v. 303, p. 163 – 164.

Burdige, D.J., 2006, Geochemistry of Marine Sediments: Princeton, Princeton University Press, 609 p.

Burns, V. M., and Burns, R.G., 1978, Post-depositional metal enrichment processes inside manganese nodules from the north equatorial Pacific: Earth and Planetary Science Letters, v. 39, p. 341 – 348.

Burns, R.G., and Brown, B.A., 1972, Nucleation and mineralogical on the composition of manganese nodules, *in* Horn, D.R., ed., Ferro-manganese deposits on the ocean floor, Washington, National. Sci. Foundation, p. 51 – 61.

Caley, J. F., 1936, Geology of the Woodstock Area, Carleton and York Counties, New Brunswick: Geological Survey of Canada Memoir 198, 21 p.

Cannon, W.F., and Force, E.R., 1986, Descriptive model of sedimentary Mn: U.S. Geological Survey Bulletin 1693, 231 p.

Carr, D.D., ed., 1994, Industrial Minerals and Rocks: Bloomington, Indiana, Indiana Geological Survey, 1196 p.

Chalmin, Y., Osuga, Y., Harada, M., Hirata, T., Koga, K., Morimoto, C., Hirota, Y., Yoshino, O., et al. 2006, Minerals discovered in paleolithic black pigments by transmission electron microscopy and micro-X-ray absorption near-edge structure: Applied Physics A, v. 83, p. 213 – 218.

Crerar, D.A., Namson, J., Chyl, M.S., Williams, L., and Feigenson, M.D., 1982, Manganiferous cherts of the Franciscan assemblage: I. General geology, ancient and modern analogues, and implications for hydrothermal convection at oceanic spreading centers: Economic Geology, v. 77, p. 519 – 540.

Corliss, J.B., Dymond, J., Gordon, L.I., Edmond, J.M., von Herzen, R.P., Ballard, R.D., Green, K., Williams, D., Bainbridge, A., Crane, K., and van Andel, T.H., 1979, Submarine Thermal Springs on the Galápagos Rift: Science, v. 203, no. 4385, p. 1073 – 1083.

Cotter, E., and Link, J.E., 1993, Deposition and diagenesis of Clinton ironstones (Silurian) in the Appalachian Foreland Basin of Pennsylvania: GSA Bulletin, v. 105, p. 911 – 922.

de Villiers, P.R., 1971, The geology and mineralogy of the Kalahari manganese-field north of Sishem, Cape Province: South Africa Geological Survey, Dept. of Mines, Memoir 59, 84 p.

DesRoches, A.J., 2004, Sedimentology and Geochemistry of Plymouth Iron Manganese Deposits, Woodstock, New Brunswick: Unpublished manuscript, Dept. of Geology, University of New Brunswick, 10 p.

Eckel, E.B., and Milton, C., 1953, Reconnaissance of Superficial Phosphate Deposit near Minas, Uruguay: Economic Geology, v. 48, no. 6, p. 437 – 446.

Ells, R.W., 1876, Report on the Iron Ore Deposits of Carleton County, New Brunswick: Geological Survey of Canada, Report on Progress 1874-1875, part 7, p. 97 – 104.

Fan, D., and Yang, P., 1999, Introduction to and Classification of Manganese deposits of China: Ore Geology Reviews, v. 15, p. 1 – 13.

Filippelli, G.M., and Delaney, M.L., 1993, The effects of manganese(II) and iron(II) on the cathodoluminescence signal in synthetic apatite: Journal of Sedimentary Petrology, v. 63, p. 167 – 173.

Fleet, A.J., 1983, Hydrothermal and Hydrogenous Ferro-Manganese deposits: Do they form a continuum? The rare earth element evidence, *in* Rona, P.A., Boström, K., Laubier, L., Smith, K.L., Jr., eds., Hydrothermal Processes at Seafloor spreading centers: Plenum Press, New York and London, p. 535 – 555.

Floyd, P.A., Winchester, J.A., and Park, R.G., 1989, Geochemistry and tectonic setting of Lewisian clastic metasediments from the early Proterozoic Loch Maree Group of Gairloch, N.W. Scotland: Precambrian Research, v. 45, p. 203 – 214.

Force, E.R., and Cannon, W.F., 1988, Depositional model for shallow-marine manganese deposits around black-shale basins: Economic Geology, v. 83, p. 93 – 117 .

Force, E.R., and Maynard, J. B., 1991, Manganese: Syngenetic Deposits on the Margins of Anoxic Basins, *in* Force, E.R., Eidel, J.J., and Maynard, J. B., eds.,

Sedimentary and Diagenetic Mineral Deposits: A Basin Analysis Approach to Exploration: Reviews in Economic Geology, Society of Economic Geologists, v. 5., p. 147 – 157.

Frakes, L.A., and Bolton, B.R., 1984, Origin of manganese giants: Sea-level change and anoxic-oxic history: Geology, v. 12, p. 83 – 86.

Fryer, B.J., 1977, Rare Earth evidence in iron-formations for changing Precambrian oxidation states: Geochimica et Cosmochimica Acta, v. 41, p. 361 – 367.

Fyffe, L.R., 1982, Geology of Woodstock (sheet 21 J): New Brunswick Department of Natural Resources, Map NR-4.

Fyffe, L.R., 2001, Stratigraphy and geochemistry of the Ordovician volcanic rocks of the Eel River area, west-central New Brunswick: Atlantic Geology, v. 37, p. 81 – 101.

Fyffe, L.R., Johnson, S.C., and van Staal, C.R., 2011, A review of Proterozoic to Early Paleozoic lithotectonic terranes in the northeastern Appalachian orogen of New Brunswick, Canada, and their tectonic evolution during Penobscot, Taconic, Salinic, and Acadian orogenesis: Atlantic Geology, v. 47, p. 211 – 248.

Garcia, D., Fonteilles M., and Moutte J., 1994, Sedimentary fractionations between Al, Ti, and Zr and the genesis of strongly peraluminous granites: Journal of Geology, v. 102, p. 411 – 322.

Gardiner, W.W., 2003, Compliation of historical data on geology, mineral exploration, and mining in New Brunswick: Department of Natural Resources; Minerals, Policy, and Planning Division, Open File Report 2003-17, 2126 p.

Garver J.I., Royce, P.R., and Smick, T.A., 1996, Chromium and Nickel in Shale of the Tectonic Foreland: A case study for the provenance of fine grained sediments with an Ultramafic Source: Journal of Sedimentary Research, v. 66, p. 100 – 106.

German, C.R., Klinkhammer, G.P., Edmond, J.M., Mitra, A., and Elderheld, H., 1990, Hydrothermal scavenging of rare-earth elements in the ocean: Nature v. 345, p. 516 – 518.

Glasby, G.P. ed., 1977, Marine Manganese Deposits: Amsterdam, Elsevier Sci. Publishing Comp., 523 p.

Gliders, R., 1976, Geology of the Woodstock Manganese Claim Group for R.S. Boorman, Assessment Report #470389, Open File Report, New Brunswick Department of Natural Resources, Mineral Development Branch, 17 p.

Goldberg, E.G., 1954, Marine Geochemistry 1. Chemical scavengers of the sea: Journal of Geology, v. 62, p. 249 – 265.

Goldschmidt, V.M., 1954, Geochemistry: Oxford, Clarendon Press, 730 p.

Grigsby, J.D., 1990, Detrital Magnetite as a Providence Indicator: Journal of Sedimentary Petrology, v. 60, no. 6, p. 940 – 951.

Grigsby, J.D., 2001, Origin and Growth Mechanism of Authigenic Chlorite in Sandstones of the Lower Vicksburg Formation, South Texas: Journal of Sedimentary Research, v. 71, p. 27 – 36.

Gromet, L.P., Dymek, R.F., Haskin, L.A., and Korotev, R.L., 1984, The "North American shale composite": It's compilation, major and trace element characteristics: Geochimica et Cosmochimica Acta, v. 48, p. 2469 – 2482.

Gross, G.A., 1972, Primary features in cherty iron-formations: Sedimentary Geology, v. 7, p. 241 – 261.

Gross, G.A., 1980, A Classification of Iron Formations based on Depositional Environments: Canadian Mineralogist, v. 18, p. 215 – 222.

Gross, G.A., 1983, Tectonic systems and the deposition of iron formations: Precambrian Research, v. 20, p. 171 – 187.

Gross, G.A., 1996a, Stratiform iron, *in* Eckstrand, O.R., Sinclair, W.D., Thorpe, R.I., eds., Geology of Canadian Mineral Deposit Types, Geological Survey of Canada, no. 8, p. 41 – 54.

Gross, G.A., 1996b, Algoma-type Iron-formations, *in* Selected British Columbia Mineral Deposit Profiles. v. 2: British Columbia Ministry of Energy, Mines, and Petroleum Resources, p. 25 – 27.

Gu, X.X., Liu, J.M., Zheng, M.H., Tang, J.X., and Qi, L., 2002, Provenance and tectonic setting of the Proterozoic turbidites in Hunan, South China: Geochemical Evidence: Journal of Sedimentary Research, v. 72, p. 393 – 407.

Gutzmer, J., Chisonga, B.C., and Beukes, N.J., 2008, The Geochemistry of Banded Iron Formation-Hosted High-Grade Hematite-Martite Iron Ores *in* Hagemann, S., Rosière, C., Gutzmer, J., Beukes, N.J., eds., Banded Iron Formation-related High-Grade Iron Ore: Reviews in Economic Geology, v. 15, Society of Economic Geologists, p. 157 – 184.

Hale, W.E., and Chrzanowski, N., 1976, Manganese occurrences in Atlantic Canada. New Brunswick Department of Natural Resources, Open File Report 82-7, 25 p.

Hamilton-Smith, T., 1972, Stratigraphy and structure of Silurian rocks of the McKenzie Corner area New Brunswick. New Brunswick Department of Natural Resources, Mineral Development Branch, Report of Investigation 15, 26 p.

Heinrich, E.W., 1962, Sursassite from New Brunswick: Canadian Mineralogist, v. 7, p. 291 – 300.

Hem, J. D., 1972, Chemical Factors that Influence the Availability of Iron and Manganese in Aqueous Systems: GSA Bulletin, v. 83, p. 443 – 450.

Herron, M.M., 1988, Geochemical classification of terrigenous sands and shales from core or log data: Journal of Sedimentary Petrology, v. 58, p. 820–829.

Hind, H.Y., 1865, A preliminary report of the Geology of New Brunswick, Queen's Printer, Fredericton, p. 161 – 165.

Hoffman P.F. et. al., 1998, A Neoproterozoic Snowball Earth: Science, v. 281, p. 1342 – 1346.

Holland, H.D., 1979, Metals in Black Shales – A Reassessment: Economic Geology, v. 74, p. 1676 – 1680.

Howard, J.D., 1978, Sedimentology and Trace Fossils, *in* Basan, P.B., ed., Trace Fossil concepts: SEPM Short Course no. 5, Society of Econ. Paleontologists and Mineralogists, p. 13 – 47.

Jackson, C.T., 1837, First report on the geology of the State of Maine: Augusta, Smith and Robinson, 128 p.

James, H.L., 1954, Sedimentary facies of iron formation: Economic Geology, v. 49, p. 235 – 293.

Jiancheng, X., Yang, X., Jianguo, D., and Wei, X., 2006, Geochemical Characteristics of Sedimentary Manganese Deposit of Guichi, Anhui Province, China: Journal of Rare Earths, v. 24, p. 374 – 380.

Johnsson, M.J., 1993, The system controlling the composition of clastic sediment, *in* Johnsson, M.J. and Basu, A., eds., Processes Controlling the Composition of Clastic Sediments: Geological Society of America Special Paper 284, p. 1 – 19.

Kappler, A., Pasquero, C., Konhauser, K.O., and Newman, D. K., 2005, Deposition of banded iron formations by anoxygenic phototrophic Fe(II)-oxidizing bacteria: Geology, v. 33, p. 865 – 868.

Kato, Y., Yamaguchi, K.E., and Ohmoto, H., 2006, Rare earth elements in Precambrian banded iron formations: Secular changes of Ce and Eu anomalies and

evolution of atmospheric oxygen, *in* Kesler, S.E., Ohmoto, H., eds., Evolution of the Early Earth's Atmosphere, Hydrosphere, and Biosphere – Constraints from Ore Deposits: Geological Society of America – Memoir 198, Geological Society of America, p. 269 – 289.

Khider, K., and McQueen, K. G., 2005, Geochemical discrimination of weathered bedrock in the Hermidale-Byrock region of Western NSW, *in* Roach I.C., ed., Regolith 2005 – Ten Years of CRC LEME: CRC LEME, p. 170 – 175.

Kim, J., Hyeong, K., Yoo, C.M. et al., 2005, Textural and geochemical characteristics of Fe-Mn crusts from four seamounts near the Marshall Islands, western Pacific: Geosciences Journal, v. 9, p. 331 – 338.

Klein, C., and Beukes, N.J., 1993, Sedimentology and Geochemistry of Glaciogenic Late Proterozoic Iron-Formation in Canada: Economic Geology, v. 88, p. 545 – 565.

Klein, C., 2005, Some Precambrian banded iron-formations (BIFs) from around the world: Their age, geologic setting, mineralogy, metamorphism, geochemistry, and origin: American Mineralogist, v. 90, p. 1473 – 1499.

Koschinsky, A., and Halbach, P., 1995, Sequential leaching of marine ferromanganese precipitates: Genetic implications: Geochimica et Cosmochimica Acta, v. 59, p. 5113 – 5132.

Ku, T.L., and Glasby, G.P., 1972, Radiometric evidence for rapid growth rate of shallow-water continental margin manganese nodules: Geochimica et Cosmochimica Acta, v. 36, p. 699 – 704.

Kuhn, T., Bau, M., Blum, N., and Halbach, P., 1998, Origin of negative Ce anomalies in mixed hydrothermal–hydrogenetic Fe–Mn crusts from the Central Indian Ridge: Earth and Planetary Science Letters, v. 163, p. 207 – 220.

Laznicka, P., 1992, Manganese deposits in the global lithogenetic system: Quantitative approach: Ore Geology Reviews, v. 7, p. 279 – 356.

Lo, W., and Waite, T.D., 2000, Structure of Hydrous Ferric Oxide Aggregates: Journal of Colloid and Interface Science, v. 222, p. 83 – 89.

Lougheed, M.S., 1983, Origin of Precambrian iron-formations in the Lake Superior region: Geological Society of America Bulletin, v. 94, p. 325 – 340.

Lovering, T.S., 1963, Epigenetic, Diplogenetic, Syngenetic, and Lithogene Deposits: Economic Geology, v. 58, p. 315 – 331.

Ludman, A., 1988, Revised bedrock geology of central-eastern and southeastern Maine: Maine Geological Survey, Open File Report, 36 p.

Ludman, A., Hopeck, J.T., and Brock, P.C., 1993, Nature of the Acadian orogeny in eastern Maine. *in* Roy D.C., and Skehan, J.S., eds., The Acadian Orogeny. Recent Studies in New England, Maritime Canada, and the Autochthonous Foreland: Geological Society of America, Special Paper 275, p. 67 – 84.

Maine, M.A., Hammerly, J.A., Leguizamon, M.S., and Pizarro, M.J., 1992, Influence of the pH and redox potential on phosphate activity in the Parana Medio system: Hydrobiologia, v. 228, p. 83 – 90.

Maine Geological Survey, 2005, The Iron Age of Maine - 1800's - Katahdin Iron Works, Maine Geological Survey website: <http://www.maine.gov/doc/nrimc/mgs/mgs.htm>.

Marchig, V., Gundlach, H., Moller, P., and Schley, F., 1982, Some geochemical indicators for discrimination between diagenetic and hydrothermal metalliferous sediments: Marine Geology, v. 50, p. 241 – 256.

Mariano, A.N., and Ring, P.J., 1975, Europium-activated cathodoluminescence in minerals: Geochimica et Cosmochimica Acta, v. 39, p. 649 – 660.

Marmontov, E.A., Chernyak, S.S., Nosyreva, E.S., Azhermacheva, S.M., and Nyurenberg, M.M., 1969, Effect of phosphorus and alloying elements on the properties of steel G13L: Metal Science and Heat Treatment, v. 10, no. 12, p. 998 – 1002.

Maynard, J.B., 1983, Geochemistry of Sedimentary Ore Deposits: New York, Springer-Verlag, 305 p.

McCombe, J.C., 1952, Memorandum on Manganese Deposits west of Woodstock: Providence of New Brunswick, Canada, Sault Ste. Marie, Ontario, Unpublished report, 8 p.

Miall, A.D., 1978, Lithofacies types and vertical profile models in braided river deposits: a summary, *in* Miall, A.D. ed, Fluvial Sedimentology, Canadian Society of Petrology: Geol. Memoir 5, p. 597 – 604.

Monture, G. C., 1957, Woodstock Manganese Ores (New Brunswick) occurrence and treatment: Canadian Mining Journal, v. 78, p. 117 – 120.

Nath, B.N., Plüger, W.L., Roelandts, I., 1997, Geochemical constraints on the hydrothermal origin of ferromanganese encrustations from the Rodriguez Triple Junction, Indian Ocean, *in* Nicholson, K., Hein, J. R., Bfihn, B. & Dasgupta, S. eds,

Manganese Mineralization: Geochemistry and Mineralogy of Terrestrial and Marine Deposit: Geological Society Special Publication 119, p. 199 – 211.

Nealson, K.H., 2006, The Manganese-Oxidizing Bacteria: Prokaryotes 3rd edition, v. 5, p. 222 – 231.

Newman, A.C.D., and Brown, G., 1987, The Chemical Constitution of Clays, *in* Newman, A.C.D., ed., Chemistry of clays and clay minerals: Mineralogical Society, Monograph no. 6, p. 1 – 128.

Nichols, G. 2009, Sedimentology and Stratigraphy 2nd ed.: West Sussex, Wiley-Blackwell, 432 p.

Nicholson, K., 1992a, Contrasting Mineralogical-Geochemical Signatures of Manganese Oxides: Guides to Metallogenesis: Economic Geology, v. 87, p. 1253 – 1264.

Nicholson, K., 1992b, Genetic Types of Manganese Oxide Deposits in Scotland: Indicators of Paleo-Ocean-Spreading Rate and a Devonian Geochemical Mobility Boundary: Economic Geology, v. 87, p. 1301 – 1309.

Page, D., 2001, Banded iron formations and paleoenvionment: a problem in petrogenesis: Geology Today, v. 17, p. 140 – 143.

Pavlides, L., 1962, Geology and manganese deposits of the Maple and Hovey Mountains area, Aroostook County, Maine: U.S. Geological Survey, Professional Paper 362, 116 p., map scale 1:48,000.

Pavlides, L., and Berry, W.B.N., 1966, Graptolite-bearing Silurian rocks of the Houlton-Smyrna Mills area, Aroostook County, Maine: United States Geological Survey, Professional Paper 550-B, p. B51 – B61.

Peter, J.M., 2003, Ancient iron formations: their genesis and use in the exploration for stratiform base metal sulphide deposits, with examples from the Bathurst Mining Camp, *in* Lentz, D.R., (ed.), Geochemistry of sediments and sedimentary rocks : evolutionary considerations to mineral deposit-forming environments, Geological Association of Canada, GEO text 4, p. 145 – 176.

Pickerill, R. K., 1980, Phanerozoic flysch trace fossil diversity-observations based on an Ordovician flysch ichnofauna from the Aroostook-Matapedia Carbonate Belt of northern New Brunswick: Canadian Journal of Earth Sciences, v. 17, p. 1259 – 1270.

Piper, D.Z., 1974, Rare earth elements in the Sedimentary cycle: A Summary: Chemical Geology, v. 14, p. 285 – 304.

Posth, N.R., Florian, H., Konhauser, K.O. and Kappler, A., 2008, Alternating Si and Fe deposition caused by temperature fluctuations in Precambrian oceans: Nature Geoscience, v. 1, p. 703 – 708.

Potter, R.R., 1983, The Woodstock iron works Carleton County, New Brunswick: CIM Bulletin, v. 76, p. 81 – 83.

Prince, J.D., 1987, Ground Magnetometer Survey no. 473394; Department of Natural Resources and Energy, Minerals, and Energy Division, p. 24.

Pufahl, P.K., and Fralick, P.W., 2004, Deposition controls on Paleoproterozoic iron formation accumulation, Gogebic Range, Lake Superior region, USA: Sedimentology, v. 51, p. 791 – 808.

Reed, J.C. Jr., Wheeler, J.O., and Tucholke, B.E., (Compilers), 2005, Geologic Map of North America, Continent-Scale-Map-001, Geological Society of America, Inc., 1:5,000,000.

Robb, C., 1870, Report on the geology of northwestern New Brunswick, Geological Survey of Canada, Report of Progress for 1866-1869, Part N, p. 173-209.

Roberts, G.C., 1985, Exploration Report of M.R.R.'s Woodstock Mn Property, Carleton County, New Brunswick: Assessment File #473168, New Brunswick Department of Natural Resources, Mineral Development Branch Open File Report, 28 p.

Roberts, G.C., and Prince, J.D., 1990, Further Characterization of Plymouth Mn Deposit: New Brunswick, Department of Natural Resources and Energy, Minerals, and Energy Division, Open File Report 90-4, 362 p.

Roser, B.P., and Korsch, R.J., 1988, Provenance signatures of sandstone-mudstone suites determined using discrimination function analysis of major element data: Chemical Geology, v. 67, p. 119 – 139.

Roy, S., 1976, Ancient Manganese Deposits, *in* Wolf, K.H. (ed.), Handbook of Stratabound and Stratiform Ore Deposits, v. 7: Elsevier Scientific Publishing Company, p. 376 – 476.

Roy, S., 1981, Manganese Deposits: London, Academic Press Inc., 458 p.

Roy, S., 1992, Environments and Processes of Manganese Deposits: Economic Geology, v. 87, p. 1218 – 1236.

Sayre, E.V., and Smith, R.W., 1961, Compositional Categories of Ancient Glass: Science, v. 133, p. 1824 – 1826.

Schoen, R., 1964, Clay Minerals of the Silurian Clinton ironstones, New York State: Journal of Sedimentary Petrology, v. 34, p. 855 – 863.

Sharma, R., 1994, Technological challenges Manganese nodule mining, *in* Distribution of manganese nodules, rocks and sediments in the Central Indian Ocean Basin: Factors influencing performance of mining system, DRS at National Institute of Oceanography, India, p. 307 – 316.

Sidwell, K.O.J., 1951, Iron Ore Occurrences in New Brunswick: New Brunswick Resources Development Board, Fredericton, 76 p.

Sidwell, K.O.J., 1954, Preliminary report on the National Management Ltd. Property (N.B. Group 24), Woodstock, N.B.: New Brunswick Department of Natural Resources, Mineral Development Branch, Open file report, 10 p.

Sidwell, K.O.J., 1957, The Woodstock, N.B., Iron – Manganese Deposits: Transactions of the Canadian Institute of Mining & Metallurgy, v. 50, p. 411 – 416.

Sidwell, K.O.J., 1959, The Woodstock, New Brunswick, iron-manganese deposits, *in* W.R. Trost, ed., The Chemistry of Manganese Deposits, Canada Department of Lands and Mines, Mines Branch, Research Report R-8, 98 – 109.

Sidwell, K.O.J., 1960, Plymouth Deposit Proposed Mining Plan, 1:200 scale.

Sidwell, K.O.J., 1964, Manganese ore occurrences in New Brunswick: New Brunswick Resources Development Board, New Brunswick Department of Natural Resources, Minerals Division, Reference 26, 172 p.

Siehl A. and Thein J., 1989, Minette-type ironstones: Geological Society, Special Publications, v. 46, p. 175 – 193.

Smith, E.A., and Fyffe, L.R., (Compilers) 2006, Bedrock Geology of the Woodstock Area (NTS 21 J/04) Carleton county, New Brunswick, New Brunswick Department of Natural Resources, Minerals, Policy and Planning Division, Plate 2006 – 5.

Stroncik, N. A., and Schmincke, H., 2002, Palagonite – a review: Int. Journal of Earth Sci (Geol Rundsch) ,v. 91, p. 680 – 697.

St. Peter, C., 1982, Geology of Juniper-Knowlesville-Carlisle area, map-areas I-16, I-17, I-18 (Parts of 21 J/11 and 21 J/06): New Brunswick Department of Natural Resources, Geological Surveys Branch, Map Report 82-1, 82 p.

Sun, S.S., and McDonough, W.F., 1989, Chemical and isotopic systematics of oceanic basalts: implications for mantle composition and processes, *in* Saunders, A.D., and Norry, M.J., (eds.), Magmatism in the Ocean Basins, Geological Society Special Publication, 42, p. 313 – 345.

Taylor, R.M, 1987, Non-Silicate Oxide and Hydroxides, *in* Newman, A.C.D., ed., Chemistry of clays and clay minerals: Mineralogical Society, Monograph 6, p. 129 – 201.

Torres-Ruiz, J., 1983, Genesis of the Marquesado and Adjacent Iron Ore Deposits, Granada, Spain: Economic Geology, v. 78, p. 1657 – 1673.

Twenhofel, W.H., 1941, The Silurian of Aroostook County, Northern Maine: Journal of Paleontology, v. 15, p. 166 – 174.

van der Weijden, C.H., 1992, Early Diagenesis and marine water, *in* Wolf, K.H. and Chilinger, G.V., eds., Diagenesis III, Elsevier Science Publishers B.V., p. 13 – 134.

Van Houton, F.B., 1991, Interpreting Silurian Clinton Oolitic Ironstones – 1850-1975: Journal of Geological Education, v. 39, p. 19 – 22.

Van Houton, F.B., and Arthur, M.A., 1989, Temporal patterns among Phanerozoic oolitic ironstones and ocean anoxia, *in* Young, T.P. and Taylor, W.E.G., eds., Phanerozoic ironstones, Geological Society Special Publication, 46, p. 33 – 49.

van Staal, C.R., and Fyffe, L.R., 1991, Dunnage and Gander zones; New Brunswick. Canadian Appalachian Region: New Brunswick Department of Natural Resources and Energy, Mineral Resources, Geoscience Report 91-2, 39 p.

van Staal, C.R., and Fyffe, L.R. 1995, Dunnage Zone-New Brunswick, *in* Williams, H., ed., Chapter 3 of Geology of the Appalachian-Caledonian Orogen in Canada and Greenland: Geology Survey of Canada, Geology of Canada, 6, p. 166 – 178.

Venugopal, D.V., 1981, Geology of Hartland-Woodstock-Nortondale region, map-areas H-19, H-20, 1-20 (Parts of 21 J/03, 21 J/04, 21 J/05, 21 J/06): New Brunswick Department of Natural Resources, Mineral Resources Branch, Map Report 81-6, 37 p.

Wark, W.J., 1970, The Mandate Project, Woodstock, N.B.: New Brunswick Department of Natural Resources, Mineral Development Branch, Assessment Report #470245, Open File Report, 68 p.

Wedepohl, K.H., 1995, The composition of the continental crust: Geochimica et Cosmochimica Acta, v. 59, 7, p. 1217 – 1232.

White, W.S., 1943, Occurrence of manganese in eastern Aroostook County, Maine: U.S. Geological Survey Bulletin, 940 – E, p. 125 – 161.

Wilde, P., and Quinby-Hunt, M. S., 2007, Paradoxes and perceptions in color identification of paleo-redox conditions in pelitic rocks: Unpublished Report, p. 1 - 12.

Wilkin, R.T., and Barnes, H.L., 1997, Formation processes of framboidal pyrite: Geochimica et Cosmochimica Acta, v. 61, p. 323 – 339.

Wonder, J.D., Spry, P.G., and Windom K.E., 1988, Geochemistry and Origin of manganese-rich rocks related to iron-formation and sulfide deposits, western Georgia: Economic Geology, v. 83, p. 1070 – 1081.

Young, R.S., 1970, Mineral Exploration and Development in Maine, *in* Ridge, J.D., ed., Ore Deposits of the United States, 1933 – 1967 the Grafton-Sales Volume, Vol. 1., The American Institute of Mining, Metallurgical, and Petroleum Engineers, Inc., p. 125 – 139.

Zyryanov, G.A., 1960, A Canadian plant for the direct reduction of iron: Metallurgist, v. 4, 3, p. 38.

GLOSSARY OF MINERALS

MINERAL NAME:	CHEMICAL FORMULA	ABBREVIATION
Axinite	$Ca_2MgAl_2BO_3Si_4O_{12}[OH]$	ax
Apatite	$(Ca_5[PO_4]_3[OH,F,Cl]$	ap
Barite	$BaSO_4$	ba
Bixbyite	$(Mn,Fe)_2O_3$	n/a
Braunite	$MnMn_6[O_8SiO_4]$	n/a
Calcite	$CaCO_3$	cal
Chalcopyrite	$CuFeS_2$	cp
Chlorite	$(Fe,Mg_5Al)(AlSi_3)O_{10}(OH)_8$	chl
Cobaltite	$CoAsS$	cob
Covellite	CuS	cv
Epidote	$(Ca_2)(Al_2Fe)(Si_2O_7)(SiO_4)O(OH)$	ep
Feldspar	$NaAlSi_3O_8$	fsp
Galena	PbS	gn
Hematite	Fe_2O_3	hem
Illite	$K_{0.8}Al_2(Al_{0.8}Si_{3.2})(OH)_2$	ill
Ilmenite	$FeTiO_3$	ilm
Jacobsite	$MnFe_2O_4$	n/a
Knebelite	$(Fe,Mn)_2SiO_4$	n/a
Limonite	$FeO(OH) \cdot nH_2O$	lm
Magnetite	Fe_3O_4	mag
Manganite	$MnO(OH)$	n/a

216

Montmorillonite	$(Na,Ca)(Al, Mg)_6(Si_4O_{10})_3(OH)_6 \cdot nH_2O$	mnt
Monazite	$(La,Ce,Nd)(PO_4)$	mnz
Mn-calcite	$(Ca,Mn)CO_3$	Mn-cal
Mn-chlorite	$(Mn,Mg_5Al)(AlSi_3)O_{10}(OH)_8$	Mn-chl
Mn-mica	$KMnAl(AlSi_3O_{10})(OH,F,Cl)_2$	Mn-mca
Mn-clinochlore	$Mg_3Mn_2AlSi_3AlO_{10}(OH)_8$	Mn-clc
Mn-siderite	$(Mn,Fe)CO_3$	Mn-sd
Muscovite	$(KAl_2(AlSi_3O_{10})(OH)_2$	mus
Oligonite	$(Fe,Mn)CO_3$	n/a
Palagonite	n/a	n/a
Phillipsite	$KCaAl_3Si_5O_{16} \cdot 6H_2O$	n/a
Pyroxmangite	$(Fe,Mn)SiO_3$	n/a
Pyrite	FeS_2	py
Pyrolusite	MnO_2	pyl
Quartz	SiO_2	qtz
Rhodochrosite	$(Ca,Fe,Mn)CO_3$	rdc
Rhodonite	$(Mn,Fe,Ca)SiO_3$	rdn
Sursassite	$Mn_2Al_3[(OH)_3(SiO_4)Si_2O_7]$	n/a
Stilpnomelane	$K(Fe,Mg,Fe)_8(Si,Al)_{12}(O,OH)_{27} \cdot n(H_2O)$	stp
Tephroite	$Mn_2(SiO_4)$	n/a
Todorokite	$(Na,Ca,K,Ba,Sr)(Mn,Mg,Al)_6O_{12}\cdot3H_2O$	n/a

Sample #	Strike (true north)	Dip	Latitude	Longitude	Description
4-8-S4	54	82E	n/a	n/a	Grey laminated siltstone
4-8-S5	57	50E	n/a	n/a	Grey laminated siltstone and minor grey sandstone
5-9-S3	72	80E	n/a	n/a	Weathered dark grey siltstone (highly fractured).
5-9-S5	63	81E	n/a	n/a	Black pyritic mudstone
5-12-S1	n/a	n/a	n/a	n/a	Siliceous concretion in weathered grey siltstone
5-13-S1	106	56E	46°09'27.5" N	67°41'25.5" W	Folded interbedded green and dark grey siltstone
5-13-S3	61	72E	46°09'27.1" N	67°41'30.5" W	Blue-grey calcareous siltstone
5-13-S5	82	61W	46°09'27.1" N	67°41'31.0" W	Blue-grey calcareous siltstone with laminated bedding
5-13-S6	55	70E	46°09'27.0" N	67°41'31.5" W	Dark grey pyritic siliceous siltstone
5-14-S1	60	89W	46°09'26.9" N	67°41'32.3" W	Black pyritic mudstone
5-14-S3	65	80E	46°09'27.5" N	67°41'25.5" W	Black pyritic mudstone (foliated)
5X-1	235	80W	46°09'23.3" N	67°41'52.6" W	Laminated, dark green, concretion-rich, Fe-Mn silicates
5X-2	247	85W	46°09'23.6" N	67°41'52.3" W	Laminated red Fe-Mn silicates in sharp contact with grey siltstone
6-10-S1	56	82W	46°09'18.8" N	67°42'22.2" W	Tan laminated siltstone
6-10-S3	67	83W	46°09'18.9" N	67°41'29.6" W	Red siltstone with possible cross-bedding present
6-10-S4	60	90	46°09'18.9" N	67°42'20.5" W	Concretion rich red chert
6-10-S5	62	70E	46°09'18.9" N	67°42'20.4" W	Red siltstone with concretions
6-10-S6	42	81E	46°09'18.9" N	67°42'20.2" W	Red siltstone
7-12-S1	61	68E	46°07'45.6" N	67°42'45.0" W	Grey laminated siltstone with minor veinlets of Fe-Mn hydroxide
8-15-S2	73	89E	46°09'24.5" N	67°41'21.8" W	Grey green laminated siltstone with possible ripple marks
8-S23	n/a	n/a	46°09'27.3" N	67°44'08.3" W	Crinoid stems in green sandstone
9-15-S1	110	83W	46°11'09.4" N	67°38'33.9" W	Banded hematite with minor rhodochrosite and green siltstone
9-15-S2	96	83W	46°11'09.3" N	67°38'33.8" W	Banded hematite with rhodochrosite and Fe-Mn silicates
9-16-S2	81	87W	46°11'07.0" N	67°38'29.7" W	Laminated red siltstone
9-16-S3	n/a	n/a	46°11'06.8" N	67°38'29.5" W	Red chert with quartz chlorite vein
9-16-S4	71	82W	46°11'06.8" N	67°38'29.4" W	Red chert with cross-cutting veinlets of Fe-Mn hydroxide
9-NH-S1	n/a	n/a	46°09'18.2" N	67°38'33.8" W	Banded concretion-rich rhodochrosite with chlorite and minor hematite
10-17-S2	111	78	46°09'27.6" N	67°38'29.0" W	Laminated calcareous siltstone with cross-cutting veins of calcite
11-19-S2	82	61	46°09'24.0" N	67°39'56.9" W	Laminated and folded grey siltstone and sandstone
11-20-S2	58	87	46°11'22.4" N	67°39'58.1" W	Grey calcareous siltstone with fine disseminated pyrite
1-SH-1	50	63W	46°11'23.1" N	67°38'16.7" W	Finely laminated banded hem, and rhc with perpendicular qtz-chl veinlet
1-SH-2	60	65W	46°11'23.7" N	67°38'16.3" W	Finely laminated banded hem, and rhc with perpendicular qtz-chl veinlet

Sample #	Strike (true north)	Dip	Latitude	Longitude	Description
1-2-S1	58	80E	46°05'45.4" N	67°46'05.4" W	Green siltstone with Mn-rich crust
1-2-S3	63	40E	46°08'46" N	67°46'00.9" W	Interbedded green and grey siltstone with parallel quartz veins
1-2-S5	81	46E	46°08'47.6" N	67°45'59.0" W	Pale green brecciated siltstone with quartz clasts
1-2-S6	87	83E	46°08'48.2" N	67°45'58.6" W	Dark Grey laminated siltstone
1-3-S3	36	46E	46°08'48.9" N	67°45'57.8" W	Pale green brecciated siltstone with quartz clasts
1-3-S7	100	22E	46°08'49.8" N	67°45'56.5" W	Folded grey siltstone
1-4-S1	n/a	n/a	46°08'51.6" N	67°45'54.8" W	Dark grey shear zone breccia
1-4-S2	82	50E	46°08'52.8" N	67°45'53.6" W	Dark grey fault bound breccia with quartz clasts
1-4-S7	87	82E	46°08'55.2" N	67°45'51.7" W	Green siltstone
1-4-S8	84	86E	46°08'55.3" N	67°45'51.9" W	Highly folded green/grey siltstone with minor white carbonate layers
1-4-S9	82	88E	46°08'55.3" N	67°45'51.9" W	Interbedded green siltstone and white carbonate
1-4-S10	49	70W	46°08'55.7" N	67°45'52.5" W	Banded Fe-Mn siltstone
1-4-S11	55	78E	46°08'56.0" N	67°45'52.7" W	Slump folded Fe-Mn siltstone
1-4-S12	33	88W	46°08'55.9" N	67°45'52.8" W	Dark green laminated siltstone
S1-015	88	78E	46°08'55.2" N	67°45'52.2" W	White carbonate with quartz veins and minor pyritic green shale
S1-025	n/a	n/a	46°08'55.2" N	67°45'52.2" W	White carbonate with quartz veins
2-5-S5	61	65E	46°09'27.6" N	67°44'15.5" W	Tan crossbedded calcareous sandstone
2-5-S9	76	70E	46°09'27.3" N	67°44'10.0" W	Grey, grey-green ripple marked cal sandstone and siltstone
2-5-S10	86	66E	46°09'27.5" N	67°44'8.9" W	Grey siltstone with minor quartz veins
2-5-S11	41	78W	46°09'27.0" N	67°44'7.9" W	Greyish-green siltstone with minor Mn-hydroxide dendrites
2-5-S12	22	52W	46°09'26.8" N	67°44'5.2" W	Grey laminated siltstone with minor pyrite
3-6-S3	47	85W	46°09'25.2" N	67°43'47.0" W	Green calcareous fine grained sandstone
4-6-S1	61	69E	46°09'25.2" N	67°43'47.0" W	Green and tan calcareous ripple marked siltstone
4-6-S2	61	67E	46°09'20.6" N	67°41'35.3" W	Green and tan calcareous ripple marked siltstone
4-6-S3	61	67E	46°09'20.6" N	67°41'35.3" W	Tan ripple marked calcareous sandstone
4-6-S4	55	56E	46°09'20.8" N	67°41'32.8" W	Tan cross-bedded calcareous sandstone and green siltstone
4-6-S8	57	70E	46°09'20.7" N	67°41'31.2" W	Green sandstone with Mn-hydroxide dendrites
4-6-S11	59	81E	46°09'20.8" N	67°41'31.2" W	Green sandstone
4-7-S2	66	83E	n/a	n/a	Green ripple marked siltstone
4-7-S3	66	83E	n/a	n/a	Green siltstone with interbedded calcareous layers
4-7-S5	63	77E	n/a	n/a	Grey laminated siltstone
4-8-S1	57	90	n/a	n/a	Green siltstone pyrite clusters

Sample #	Strike (true north)	Dip	Latitude	Longitude	Description
1-SH-3	68	75W	46°11'23.1" N	67°38'16.1" W	Banded hematite and rhodochrosite in contact with red siltstone
1-SH-4	50	85W	46°11'22.7" N	67°38'16.8" W	Finely laminated banded hem, and rhc with perpendicular qtz-chl veinlet
1-SH-5	30	85W	46°11'22.8" N	67°38'16.6" W	Light tan microspheroidal carbonate with cross cutting qtz chl veinlets
2-SH-1	100	70E	46°11'22.1" N	67°38'17.6" W	Folded laminated hem and rhc with red chert and minor hem concretions
3-SH-1	n/a	n/a	46°11'20.8" N	67°38'29.6" W	Brecciated banded hematite and rhodochrosite
PLY-001	n/a	n/a	46°09'53.7" N	67°39'44.1" W	Finely laminated banded hem and rhc with folded qtz-chl veinlets
PLY-002	n/a	n/a	46°09'53.7" N	67°39'44.1" W	Banded magnetite siltstone with Fe-Mn silicates
IR-S13-02	14	61W	46°12'20.9" N	67°37'45.9" W	Fractured red chert
IRH-01	n/a	n/a	n/a	n/a	Folded banded hematite and Fe-Mn silicates
IRH-001	n/a	n/a	46°12'22.8" N	67°37'43.3" W	Concretions in finely laminated hem and rhc
IRH-TH1	n/a	n/a	46°09'20.8" N	67°41'29.6" W	Banded hematite and chert
IRH-2	n/a	n/a	n/a	n/a	Laminated hematite and Fe-Mn silicates
IHR-03	172	79E	46°12'19.4" N	67°37'41.5" W	Banded manganiferous Magnetite and chlorite
GR-S13-01	309	70W	46°04'35.4" N	67°45'37.5" W	Banded microspheroidal rhodochrosite and crystalline oligonite
GR-S13-02	315	58W	46°04'35.4" N	67°45'37.4" W	Banded microspheroidal rhc and crystalline oligonite with cross-cutting qtz-chl-sulfide veinlets
GR-S13-03	316	58W	46°04'35.4" N	67°45'37.4" W	Banded microspheroidal rhodochrosite and crystalline oligonite with cross-cutting qtz-chl-sulfide veinlets
S1-1R	52	79E	46°15'24.2" N	67°37'22.1" W	Red siltstone
2-S1-1R	74	80E	46°09'20.8" N	67°41'29.6" W	Red siltstone

Sample	87-2-76	87-2-96	87-2-106	87-2-116	87-2-136	87-2-146	87-2-156	87-2-166	87-2-230	87-2-260
Major Oxides (wt%)										
SiO2	54	44.7	31.3	40.2	32.7	29.9	36.6	43	24.3	34.2
Al2O3	17.8	14.7	9.95	12.7	10.4	11.5	11.4	13.6	7.66	10.7
CaO	0.3	1.04	2.68	1.68	3.32	4.57	4.66	1.32	2.38	3.58
MgO	3.68	2.91	2.53	2.62	2.15	2.15	2.56	2.85	1.86	2.04
NaO	1.29	1.94	0.99	1.74	2.44	1.88	2.15	0.68	0.51	0.07
K2O	4.55	3.12	1.96	2.65	1.68	1.87	2	3.61	1.29	3.06
Fe2O3	8.63	14.2	29	19.9	20.5	17.9	17.3	14.3	26.4	19.2
MnO	3.51	8.12	14.5	10.3	14.5	14.7	10.6	8.95	15.8	11.6
TiO2	0.75	0.6	0.43	0.54	0.45	0.5	0.49	0.57	0.35	0.46
P2O5	0.08	0.43	1.34	0.68	0.87	0.63	0.8	0.45	1.12	0.88
LOI	4.85	6.46	5.31	5.16	9.24	12.5	10.9	9.7	18.2	12.9
SUM	99.6	98.5	100.1	98.5	98.9	98.5	99.8	99.2	100	98.9
Trace Metals (ppm)										
Au (ppb)	<1	<1	<1	<1	<1	12	17	<1	6	30
Li	30	30	20	30	40	30	20	40	100	20
Be	5	5	10	5	5	5	<5	<5	10	5
B	100	70	70	60	60	70	40	60	40	90
S	<20	260	40	280	900	680	460	100	1900	8700
V	120	30	20	30	20	10	30	60	20	50
Cr	110	88	60	76	56	68	64	76	42	70
Co	42	63	73	86	100	78	92	63	128	100
Ni	90	72	57	78	67	77	68	78	53	74
Cu	30	73	89	64	42	10	19	200	41	40
Zn	110	86	75	94	76	76	83	100	62	91
Ga	18	17	17	17	17	17	15	18	14	16
Ge	10	<10	10	<10	<10	<10	<10	<10	<10	<10
As	<1	7	9	9	9	1	4	<1	5	5
Se	<3	<3	<3	<3	<3	<3	<3	<3	<3	<3
Mo	2	5	10	7	10	10	7	8	11	9
Pd (ppb)	<2	<2	3	3	3	4	2	4	4	2
Ag	<0.5	<0.5	<0.5	<0.5	<0.5	<0.5	<0.5	<0.5	<0.5	<0.5
Cd	1	<1	1	1	1	1	2	1	<1	<1
In	<1	<1	<1	<1	<1	<1	<1	<1	<1	<1
Sn	<10	<10	<10	<10	<10	<10	<10	<10	<10	<10
Sb	0.9	15	4	4.2	13	7.2	5.8	4	2.2	4
Cs	7	6	4	5	5	8	4	6	6	6
U	2.1	1.3	1.4	1.5	1.3	1.1	1.2	2.3	1.7	2
Th	7	6	3	5	4	4	4	5	2	3
Bi	<0.5	<0.5	<0.5	<0.5	<0.5	<0.5	<0.5	<0.5	<0.5	<0.5
Pb	18	16	12	14	10	16	12	10	14	12
Zr	116	72	44	75	28	67	58	100	45	66
Y	11	<10	<10	<10	<10	<10	<10	<10	<10	<10
Ba	1400	2440	899	2200	5540	3300	2420	1010	1070	1150
Rb	175	<10	<10	<10	<10	<10	<10	<10	<10	<10
Sr	66	324	121	211	399	307	245	142	199	280
Nb	24	21	19	30	14	<10	24	30	27	18
Ba	1400	2440	899	2200	5540	3300	2420	1010	1070	1150
Ta	1	1	<1	<1	<1	<1	<1	<1	<1	<1
W	<3	3	4	<3	4	<3	5	<3	6	6
Pt (ppb)	<10	<10	<10	<10	<10	<10	<10	<10	<10	<10
Tl	<1	<1	<1	<1	<1	<1	<1	<1	<1	<1

Sample	87-2-76	87-2-96	87-2-106	87-2-116	87-2-136	87-2-146	87-2-156	87-2-166	87-2-230	87-2-260
REEs (ppm)										
La	36	23	23	30	26	27	25	29	30	29
Ce	78	51	68	77	67	67	64	72	81	80
Nd	33	19.6	26.3	31.7	27.2	24	25.3	27.7	29.5	30.6
Sm	5.8	4	5.5	5.9	5.3	4.5	5.5	5.8	6.1	6.6
Eu	1.3	1	1.3	1.4	1.8	1.1	1.4	1.3	1.4	1.5
Gd	4.8	4	5.7	5.6	5.3	4.3	5.1	5.5	7	6.6
Dy	3.9	3.2	4.7	4.5	4.4	3.6	4.1	3.9	5.8	5.5
Er	2.3	2.1	2.7	2.6	2.3	2	2.3	2.1	2.8	3.2
Lu	0.4	0.3	0.3	0.3	0.3	0.3	0.3	0.3	0.4	0.6

Sample	87-2-324	87-2-356	87-3-102	87-3-112	87-3-142	87-3-152	87-3-169	87-3-174	87-3-182	87-3-192
Major Oxides (wt%)										
SiO2	34.6	17.3	21.7	39.8	31.8	25.6	13.7	24.8	19.4	16.7
Al2O3	11.6	5.52	5.21	12.7	9.3	5.63	3.74	6.81	5.65	3.8
CaO	1.42	3.26	4.58	1.7	2.13	2.46	3.38	3.44	3.65	5.21
MgO	4.83	1.67	1.15	2.4	1.92	1.68	1.37	1.47	1.17	0.98
NaO	0.49	0.31	0.44	1.66	0.35	0.58	0.18	1.18	0.42	0.38
K2O	0.55	0.42	0.52	2.35	2.67	0.94	0.17	0.45	0.68	0.71
Fe2O3	22.5	32.7	32.1	19.6	20	24.7	33.3	33.6	33.3	30.5
MnO	11.1	22.7	19.7	9.38	13.2	17.8	26	15.9	21	20
TiO2	0.51	0.25	0.23	0.26	0.41	0.22	0.18	0.31	0.26	0.17
P2O5	0.56	1.41	1.61	0.79	0.85	1.04	1.42	1.7	1.54	1.63
LOI	12	14.5	12.5	7.16	17.3	19.5	16.5	10.2	12.8	19.8
SUM	100.2	100.2	100	98.4	100.1	100.3	100	100	100.1	100
Trace Metals (ppm)										
Au (ppb)	2	<1	<1	<1	20	5	<1	6	8	3
Li	70	10	30	50	20	40	20	40	30	50
Be	5	10	10	5	5	5	10	10	10	10
B	20	10	60	60	90	40	60	60	120	50
S	2900	100	780	2300	7100	5200	60	100	320	360
V	40	20	10	60	40	20	<10	30	20	20
Cr	54	20	34	80	60	30	20	41	34	26
Co	83	156	152	99	104	156	258	135	187	146
Ni	62	43	49	78	66	42	41	43	44	32
Cu	51	63	14	37	63	42	5.5	63	88	29
Zn	85	49	55	99	75	55	43	55	48	50
Ga	15	14	28	30	20	24	31	22	30	27
Ge	<10	<10	<10	<10	<10	<10	10	<10	10	<10
As	6	9	9	5	9	9	9	9	9	8
Se	<3	<3	<3	<3	<3	<3	<3	<3	<3	<3
Mo	7	13	9	7	7	18	12	7	9	9
Pd (ppb)	5	<2	3	3	2	3	2	2	2	2
Ag	<0.5	<0.5	<0.5	<0.5	<0.5	<0.5	<0.5	<0.5	<0.5	<0.5
Cd	<1	<1	2	2	1	1	2	2	1	1
In	<1	<1	<1	<1	<1	<1	<1	<1	<1	<1
Sn	<10	<10	<10	<10	<10	<10	<10	<10	<10	<10
Sb	2.2	3.6	4.3	2.5	4.3	1	6.7	4.2	5.1	4.3
Cs	4	11	13	10	5	4	5	6	6	3
U	1.9	1.2	0.9	2	1.5	1	0.8	1.6	0.9	0.8
Th	4	1	3	9	6	3	2	4	4	2
Bi	<0.5	<0.5	<0.5	0.6	<0.5	0.5	<0.5	<0.5	<0.5	<0.5
Pb	14	4	14	10	10	10	<2	2	4	<2
Zr	62	<10	<10	90	42	<10	<10	<10	<10	<10
Y	<10	19	11	30	<10	<10	<10	18	<10	11
Ba	392	580	1820	1930	908	807	314	725	1400	891
Rb	10	<10	51	94	88	49	29	33	<10	45
Sr	135	417	364	347	99	206	152	263	226	291
Nb	19	17	24	25	15	11	25	31	15	14
Ba	392	580	1820	1930	908	807	314	725	1400	891
Ta	<1	<1	<1	<1	<1	<1	<1	<1	<1	<1
W	<3	9	6	6	6	3	6	11	10	8
Pt (ppb)	<10	<10	10	<10	10	10	10	10	10	10
Tl	<1	<1	<1	<1	<1	<1	<1	<1	<1	<1

Sample	87-2-324	87-2-356	87-3-102	87-3-112	87-3-142	87-3-152	87-3-169	87-3-174	87-3-182	87-3-192
REEs (ppm)										
La	29	24	26	34	23	18	21	33	25	21
Ce	71	66	75	88	60	52	60	91	73	57
Nd	26	22.9	22.5	33.1	23	20.2	19.8	32.4	26	20.5
Sm	4.6	4.3	5.5	6.3	5	3.8	4.1	6.4	5.1	4
Eu	1	1.1	1.2	1.4	1	1	1	1.5	1.3	1
Gd	4.5	5.1	5.9	6.6	5.1	4.1	4.7	6.5	5.6	5
Dy	3.8	4.5	4.9	4.9	3.2	3.5	3.4	6.1	4.4	3.8
Er	1.9	2.1	2.6	2.7	2.1	1.6	1.7	2.7	2.3	2.3
Lu	0.3	0.2	0.4	0.3	0.2	0.2	0.2	0.4	0.4	0.3

Sample	87-3-212	87-3-232	87-3-242	87-3-262	87-3-282	87-3-292	87-3-312	87-3-336	87-3-346	87-3-362
Major Oxides (wt%)										
SiO2	20.7	20.5	27.9	26.3	37	28.7	34.8	27.5	26.8	50.7
Al2O3	5.53	5.33	9.15	8.22	11.7	7.28	10	6.84	7.74	17.5
CaO	3.35	3.6	2.59	2.09	2	2.81	1.54	2.1	2.44	0.44
MgO	1.4	1.2	2	3.87	4.61	3.94	3.77	2.68	3.5	3.05
NaO	0.22	0.17	0.52	0.33	0.29	0.26	0.58	0.46	0.4	1.12
K2O	0.78	0.57	2.02	1.47	2.15	1.26	1.07	1.04	1.18	3.75
Fe2O3	33.1	33	23.1	19.5	17.6	19.9	21.4	23	21	13.5
MnO	19.1	19.6	14	16.5	7.73	15.1	11.5	14.3	15.4	1.9
TiO2	0.26	0.23	0.4	0.34	0.48	0.29	0.43	0.28	0.34	0.69
P2O5	1.56	1.61	1.07	0.82	0.87	0.92	0.67	0.94	1.01	0.18
LOI	14.1	14.4	17	20.5	15.3	19.5	14.4	21	20.3	6.47
SUM	100.2	100.3	99.9	100	99.8	100	100.2	100.2	100.2	99.5
Trace Metals (ppm)										
Au (ppb)	<1	2	25	5	10	2	7	4	6	1
Li	30	30	70	100	280	100	90	140	170	60
Be	10	5	5	<5	5	5	5	5	5	5
B	40	60	60	70	90	60	40	90	60	40
S	380	380	1300	820	2600	2700	6000	3800	5600	3600
V	20	20	30	30	100	70	90	50	80	130
Cr	34	30	54	38	60	34	52	34	38	92
Co	176	189	112	129	90	125	127	125	114	63
Ni	41	43	61	59	63	54	63	47	52	69
Cu	12	22	38	41	64	50	71	83	66	91
Zn	47	50	73	64	86	63	78	67	66	110
Ga	29	31	29	26	24	27	25	25	27	23
Ge	10	10	10	<10	<10	10	10	<10	10	<10
As	11	8	9	4	10	6	6	8	8	28
Se	<3	<3	<3	<3	<3	<3	<3	<3	<3	<3
Mo	9	9	7	8	4	14	8	8	29	<2
Pd (ppb)	2	2	<2	<2	2	2	4	2	3	3
Ag	<0.5	<0.5	<0.5	<0.5	<0.5	<0.5	<0.5	<0.5	<0.5	<0.5
Cd	1	1	1	1	<1	1	1	1	<1	<1
In	<1	<1	<1	<1	<1	<1	<1	<1	<1	<1
Sn	<10	<10	<10	<10	<10	<10	<10	<10	<10	<10
Sb	4.3	4	1	0.8	2.4	1.1	4	2.1	4	2.4
Cs	4	5	4	3	7	5	3	4	4	7
U	0.9	1	1.2	1.3	2	1.3	2.2	1.4	1.7	3
Th	3	3	6	5	7	4	6	4	4	12
Bi	<0.5	<0.5	<0.5	<0.5	<0.5	<0.5	<0.5	0.6	<0.5	0.6
Pb	<2	6	2	12	10	12	18	18	12	24
Zr	<10	<10	37	28	55	<10	35	12	48	118
Y	<10	<10	13	12	26	<10	17	<10	12	28
Ba	611	527	909	571	607	443	481	628	567	1120
Rb	43	<10	81	57	89	42	46	33	54	162
Sr	142	140	148	143	184	186	101	156	143	66
Nb	16	35	18	28	16	14	28	20	15	17
Ba	611	527	909	571	607	443	481	628	567	1120
Ta	<1	<1	<1	<1	<1	<1	<1	<1	<1	1
W	8	8	6	9	<3	<3	<3	3	<3	<3
Pt (ppb)	<10	<10	<10	10	<10	<10	<10	10	<10	<10
TI	<1	<1	<1	<1	<1	<1	<1	<1	<1	<1

Sample	87-3-212	87-3-232	87-3-242	87-3-262	87-3-282	87-3-292	87-3-312	87-3-336	87-3-346	87-3-362
REEs (ppm)										
La	26	25	28	22	31	21	27	20	28	36
Ce	75	73	73	59	78	59	70	52	69	84
Nd	26.1	24.7	26.8	23.4	32.7	23.1	27.2	20	28	36.3
Sm	4.7	4.9	4.9	4.2	6.5	5.5	5.1	4	5.8	5.8
Eu	1.3	1.2	1.2	1.1	1.7	1.2	1.2	1.2	1.5	1.6
Gd	4.7	5.1	5.2	4.4	7.2	4.7	5.3	4.7	5.9	5.4
Dy	4.3	4.6	4.4	4.4	5.2	4.6	4.3	3.5	4.5	4.2
Er	2.1	2.3	2.1	1.8	2.5	1.7	2	2.1	2.2	2
Lu	0.4	0.4	0.3	0.3	0.3	0.3	0.4	0.3	0.4	0.4

Sample	87-3-382	87-3-392	87-3-412	87-4-10	87-4-13	87-4-33	87-4-43	87-4-451	87-4-460	87-4-550
Major Oxides (wt%)										
SiO2	53.9	53.1	53.1	7.08	52.1	42.2	30.6	35	30	22.8
Al2O3	18.2	18.6	19.2	2.42	17.2	12.8	9.5	11.4	8.3	5.45
CaO	0.37	0.35	0.31	4.03	0.32	1.06	1.91	2.73	3.91	2.83
MgO	2.71	2.52	2.47	0.8	3.36	2.64	2.29	2.36	1.74	1.77
NaO	1.21	1.01	1	0.47	3.81	1.77	1.16	2.15	1.6	1.06
K2O	4.55	4.9	4.9	0.32	2.87	3.38	1.76	2.14	2.4	1.02
Fe2O3	10.6	10.7	12.5	47.2	8.63	16.6	22.4	19.9	23.3	29.3
MnO	1.23	1.13	0.69	20.7	4.1	9.85	13.4	14.5	16.6	21.4
TiO2	0.71	0.7	0.73	0.1	0.73	0.57	0.42	0.52	0.42	0.23
P2O5	0.1	0.11	0.11	1.82	0.07	0.51	0.84	0.77	1.21	1.44
LOI	5.08	5.39	4.31	15.2	5.23	8.47	15.6	7.31	9.93	12.2
SUM	98.8	98.7	99.5	100.2	98.6	100.1	100	99.5	100.6	99.6
Trace Metals (ppm)										
Au (ppb)	1	<1	<1	6	<1	2	4	<1	<1	2
Li	60	70	60	20	50	40	70	30	40	20
Be	5	5	5	10	<5	5	5	<5	5	5
B	90	70	80	10	40	50	50	110	110	40
S	6800	4200	760	180	40	140	1700	720	1200	100
V	160	170	150	10	50	30	30	20	30	10
Cr	110	110	96	<2	110	74	56	70	48	24
Co	93	60	38	129	62	82	98	127	149	129
Ni	83	82	70	28	99	82	72	84	64	43
Cu	110	69	65	68	5.5	14	89	45	86	44
Zn	130	130	130	29	110	86	83	92	72	55
Ga	25	22	24	16	20	21	22	26	25	18
Ge	<10	<10	<10	<10	<10	<10	<10	<10	<10	<10
As	46	33	3	5	<1	1	7	6	5	6
Se	<3	<3	<3	<3	<3	<3	<3	<3	<3	<3
Mo	<2	<2	<2	15	3	7	10	10	11	11
Pd (ppb)	3	2	<2	2	<2	2	2	2	<2	3
Ag	<0.5	<0.5	<0.5	<0.5	<0.5	<0.5	<0.5	<0.5	<0.5	<0.5
Cd	1	<1	1	<1	<1	<1	<1	<1	<1	<1
In	<1	<1	<1	<1	<1	<1	<1	<1	<1	<1
Sn	<10	<10	<10	<10	<10	<10	<10	<10	<10	<10
Sb	3.2	2.1	0.5	3.2	0.3	2.7	0.8	2.7	2.7	2.4
Cs	7	8	9	3	4	9	5	23	29	43
U	3.6	3.2	2.2	1.5	2.5	1.9	1.7	1.3	1.7	1.2
Th	11	12	12	1	12	9	7	7	5	3
Bi	0.5	<0.5	1	<0.5	<0.5	<0.5	<0.5	<0.5	0.7	<0.5
Pb	44	30	18	6	8	10	14	12	<2	14
Zr	123	116	115	<10	122	76	58	50	<10	<10
Y	<10	25	18	<10	26	15	29	<10	13	<10
Ba	1040	1010	1040	394	1250	1420	1140	5370	9770	959
Rb	167	188	198	<10	124	136	71	80	84	62
Sr	41	46	27	131	146	181	172	546	658	139
Nb	34	25	31	18	13	20	15	<10	19	29
Ba	1040	1010	1040	394	1250	1420	1140	5370	9770	959
Ta	<1	1	1	<1	1	1	1	1	<1	<1
W	<3	<3	<3	14	3	4	5	6	10	8
Pt (ppb)	<10	<10	10	<10	<10	2	<10	<10	<10	10
Tl	<1	1	<1	<1	<1	<1	<1	<1	<1	<1

Sample	87-3-382	87-3-392	87-3-412	87-4-10	87-4-13	87-4-33	87-4-43	87-4-451	87-4-460	87-4-550
REEs (ppm)										
La	37	40	28	23	38	29	29	34	29	27
Ce	82	88	82	66	83	69	76	85	74	72
Nd	38.2	37.5	35.4	20.9	31.8	26.6	28	31	26.5	24.7
Sm	6.3	6.2	5.7	3.7	4.7	4.9	5.7	5.6	3.9	4.9
Eu	1.4	1.4	1.3	1	1.5	1.7	1.8	4.3	5.6	1.8
Gd	4.6	5.3	4.6	5.2	4.3	5.3	6.3	6.7	5.7	6.9
Dy	3.7	3.7	3.4	4.5	3.7	3.6	5.1	4.9	4.2	4.8
Er	1.8	2	1.5	2	2.1	1.9	2.2	2.4	1.6	2.5
Lu	0.4	0.5	0.4	0.4	0.4	0.4	0.4	0.5	0.4	0.4

Sample	87-4-561	87-4-571	87-5-70	87-5-80	87-5-100	87-5-108	87-5-118	87-5-128	87-5-138	87-5-151
Major Oxides (wt%)										
SiO2	22	35.1	18.6	19.9	18.1	26.9	24.1	20.9	29.1	33.3
Al2O3	6.19	10.4	5.1	4.67	3.34	8.93	7.44	6.55	9.02	10.2
CaO	2.82	1.49	2.72	2.4	3.7	2.55	2.51	3.4	2.45	2.6
MgO	1.67	2.54	2.29	1.71	1.18	2.15	2.39	1.47	1.86	1.96
NaO	0.9	1.65	0.48	0.6	0.35	1.53	0.89	0.56	1.7	2.58
K2O	1.39	1.96	1.26	1.07	0.17	0.87	0.72	0.88	1.01	1.83
Fe2O3	35.9	22.3	26.3	25.4	27.4	23.5	27.6	31.4	24.9	21.2
MnO	17.5	14.3	18.2	19.8	22.3	16.4	16.2	17.9	13.7	13.8
TiO2	0.28	0.44	0.21	0.21	0.13	0.37	0.32	0.28	0.39	0.44
P2O5	1.62	0.75	1.24	1.13	1.13	1.06	1.06	1.68	1.18	0.84
LOI	9.7	9.31	24	23.2	21.7	15.5	16.2	15	14.5	10.3
SUM	100.1	100.4	100.5	100.1	99.6	99.9	99.5	100.1	99.9	99.3
Trace Metals (ppm)										
Au (ppb)	4	<1	2	6	4	<1	2	6	3	2
Li	10	20	90	30	20	40	40	20	40	20
Be	5	5	<5	<5	<5	<5	5	10	5	5
B	50	60	70	40	<10	20	40	80	30	50
S	2900	1700	2000	2200	640	160	1300	860	1500	620
V	20	30	20	10	<10	30	30	30	40	40
Cr	34	52	18	22	14	42	32	34	50	58
Co	130	107	160	140	217	102	131	117	110	106
Ni	57	70	44	38	34	56	49	42	60	70
Cu	46	91	36	41	25	69	35	45	85	79
Zn	61	82	54	43	43	67	64	57	73	85
Ga	18	18	20	19	21	20	15	17	20	21
Ge	<10	<10	<10	<10	<10	<10	<10	<10	<10	<10
As	10	9	12	10	10	12	14	16	16	10
Se	<3	<3	<3	<3	<3	<3	<3	<3	<3	<3
Mo	11	9	13	15	16	11	13	15	14	10
Pd (ppb)	<2	3	3	2	2	<2	<2	<2	<2	<2
Ag	<0.5	<0.5	<0.5	<0.5	<0.5	<0.5	<0.5	<0.5	<0.5	<0.5
Cd	<1	<1	<1	<1	<1	<1	<1	<1	<1	<1
In	<1	<1	<1	<1	<1	<1	<1	<1	<1	<1
Sn	<10	<10	<10	<10	<10	<10	<10	<10	<10	<10
Sb	2.7	1.9	0.9	0.7	0.6	1.3	0.6	1.6	0.8	2.7
Cs	41	31	8	5	2	9	5	11	6	16
U	1.2	1.8	14.3	0.9	0.7	1.9	1.8	1.1	1.5	1.7
Th	3	5	3	3	2	5	4	4	5	7
Bi	<0.5	<0.5	<0.5	<0.5	<0.5	<0.5	<0.5	<0.5	<0.5	0.5
Pb	<2	6	2	4	12	12	8	16	12	40
Zr	22	71	<10	<10	<10	28	12	18	45	53
Y	<10	13	18	<10	<10	20	10	<10	19	12
Ba	1020	661	311	292	368	960	530	674	543	1790
Rb	71	94	57	51	12	43	50	70	40	90
Sr	134	119	262	124	188	231	148	178	232	461
Nb	<10	22	22	13	<10	16	13	12	31	14
Ba	1020	661	311	292	368	960	530	674	543	1790
Ta	<1	<1	<1	<1	<1	<1	<1	<1	<1	<1
W	8	4	<3	<3	<3	3	4	6	4	6
Pt (ppb)	<10	<10	<10	<10	10	<10	<10	<10	<10	<10
Tl	<1	<1	<1	<1	<1	<1	<1	<1	<1	<1

Sample	87-4-561	87-4-571	87-5-70	87-5-80	87-5-100	87-5-108	87-5-118	87-5-128	87-5-138	87-5-151
REEs (ppm)										
La	27	26	21	21	16	32	27	33	29	29
Ce	77	68	57	59	46	86	72	93	78	73
Nd	29	27.7	22.1	21.9	16.2	28.6	24.2	34.2	29.6	27
Sm	5.8	4.7	4.7	4.2	2.7	5.2	4.2	5.7	4.9	4.4
Eu	2.2	1.5	1.3	1.4	1.1	1.3	1.2	2	1.5	2.3
Gd	7.9	6.6	6.4	5.7	4.7	5.5	6.2	9.1	7.2	6.5
Dy	5.2	4.7	4.4	4.3	3.5	4.8	3.8	5.1	5	3.9
Er	3.1	2.3	2.1	2	1.5	2.4	1.8	2.7	2.3	2
Lu	0.4	0.4	0.3	0.3	0.3	0.3	0.4	0.4	0.4	0.4

Sample	87-5-160	87-5-170	87-5-180	87-5-200	87-5-220	87-5-240	87-5-245	87-5-255	87-5-275	87-5-295
Major Oxides (wt%)										
SiO2	33.5	28.5	35.8	21.5	28	22.1	20.2	24.1	19.6	35.5
Al2O3	10.7	9.47	10.3	5.37	8.27	5.65	4.81	7.26	6.05	11.5
CaO	2.41	2.32	1.88	4.97	2.39	3.1	2.76	2.95	4.25	1.67
MgO	2.45	2.52	2.71	1.5	2.09	1.6	1.56	2.23	1.65	2.91
NaO	2.43	1.03	2.56	0.81	1.58	1.23	0.83	1.05	0.95	2.32
K2O	2.55	2.87	1.78	1.1	1.84	1.1	1.05	1.37	0.95	2.14
Fe2O3	21.1	27.3	23.4	34	29.7	37.4	40.1	31.4	32.6	22.1
MnO	12.9	15.3	13	20	17.1	17.4	19.2	19.4	23	13.2
TiO2	0.48	0.42	0.43	0.23	0.36	0.24	0.21	0.31	0.27	0.48
P2O5	0.85	1.14	1	1.7	1.22	2	1.54	1.32	1.56	0.78
LOI	8.62	9.08	6.93	9	7.47	7.62	7.08	8.54	8.62	7.31
SUM	98.4	100.2	100.3	100.3	100.2	99.9	99.5	100.1	99.6	100.1
Trace Metals (ppm)										
Au (ppb)	<1	<1	<1	<1	<1	1	<1	<1	10	<1
Li	20	20	30	10	20	20	20	10	<10	20
Be	5	5	5	5	5	10	10	5	5	5
B	60	90	60	80	80	40	70	110	180	60
S	460	40	600	280	120	790	80	600	20	280
V	30	20	80	20	30	30	20	20	20	40
Cr	64	56	56	28	42	26	24	34	30	62
Co	119	163	138	148	149	121	220	125	128	109
Ni	72	65	64	42	55	42	39	52	47	73
Cu	28	1	410	13	37	45	1.5	43	23	94
Zn	81	76	80	54	69	53	47	64	59	95
Ga	22	21	21	19	22	18	18	21	17	21
Ge	<10	<10	<10	<10	<10	<10	<10	<10	<10	<10
As	11	11	10	14	12	16	16	11	16	5
Se	<3	<3	<3	<3	<3	<3	<3	<3	<3	<3
Mo	10	11	11	16	14	14	15	14	13	9
Pd (ppb)	<2	<2	<2	<2	2	<2	<2	<2	<2	<2
Ag	<0.5	<0.5	<0.5	<0.5	<0.5	<0.5	<0.5	<0.5	<0.5	<0.5
Cd	<1	<1	<1	<1	<1	<1	<1	<1	<1	<1
In	<1	<1	<1	<1	<1	<1	<1	<1	<1	<1
Sn	<10	<10	<10	<10	<10	<10	<10	<10	<10	<10
Sb	2.7	3.2	0.8	2.7	0.7	0.7	1.6	1.1	3	0.8
Cs	21	34	24	50	42	49	59	31	25	27
U	1.4	1.4	2.3	1.1	1.3	1.2	0.8	1.3	1.1	1.6
Th	7	5	6	3	5	3	2	4	3	4
Bi	<0.5	<0.5	<0.5	<0.5	<0.5	<0.5	<0.5	<0.5	<0.5	0.5
Pb	<2	4	4	6	10	<2	6	20	4	28
Zr	46	38	16	<10	11	<10	<10	14	<10	54
Y	18	15	12	<10	24	26	<10	14	<10	<10
Ba	3230	1740	2420	816	855	3270	582	779	675	1500
Rb	111	112	89	68	88	68	85	55	<10	22
Sr	481	369	1800	468	435	623	430	449	376	370
Nb	13	23	16	11	23	<10	24	20	10	29
Ba	3230	1740	2420	816	855	3270	582	779	675	1500
Ta	<1	<1	<1	<1	<1	<1	<1	<1	<1	<1
W	5	5	5	7	6	8	8	6	8	5
Pt (ppb)	<10	<10	<10	<10	<10	<10	<10	<10	<10	<10
Tl	<1	<1	<1	<1	<1	<1	<1	<1	<1	<1

Sample	87-5-160	87-5-170	87-5-180	87-5-200	87-5-220	87-5-240	87-5-245	87-5-255	87-5-275	87-5-295
REEs (ppm)										
La	27	27	31	26	28	27	22	29	27	30
Ce	66	67	79	71	74	77	66	78	76	78
Nd	25.4	26.2	31	24.7	27.9	27.6	22.4	28.5	26.6	28.7
Sm	4.7	5.3	6.2	5.1	5.1	5.2	3.8	4.5	4.5	4.3
Eu	2.8	1.9	2.7	3.2	1.8	3.6	1.3	1.6	1.5	1.8
Gd	6.1	6.5	7	7.4	7.3	7.6	6.6	7.3	7.4	6.8
Dy	4.2	4.3	4.7	5.5	5.1	5.3	4.3	4.8	4.5	4.8
Er	2	2.3	2.6	2.7	2.3	2.3	2	2.4	2	2.1
Lu	0.3	0.3	0.3	0.3	0.4	0.4	0.3	0.3	0.3	0.3

Sample	87-5-305	87-5-315	87-5-335
Major Oxides (wt%)			
SiO2	25.1	20.6	32.8
Al2O3	7.32	5.17	9.79
CaO	3.06	4.79	3.45
MgO	2.29	1.29	2.27
NaO	1.33	0.77	2.3
K2O	0.99	1.15	1.79
Fe2O3	31.1	33.7	22.9
MnO	18.2	17.5	12.9
TiO2	0.32	0.24	0.42
P2O5	1.42	1.8	0.91
LOI	8.7	12.5	9.77
SUM	100	99.8	99.9
Trace Metals (ppm)			
Au (ppb)	17	<1	<1
Li	30	20	20
Be	5	5	5
B	90	10	50
S	440	1700	160
V	30	30	40
Cr	32	30	50
Co	164	135	138
Ni	48	39	60
Cu	30	44	50
Zn	67	59	86
Ga	20	19	24
Ge	<10	<10	<10
As	13	10	7
Se	<3	<3	<3
Mo	13	13	11
Pd (ppb)	<2	<2	<2
Ag	<0.5	<0.5	<0.5
Cd	<1	<1	<1
In	<1	<1	<1
Sn	<10	<10	<10
Sb	3	2.2	2.2
Cs	22	18	21
U	1.7	1.2	1.7
Th	4	3	6
Bi	<0.5	<0.5	<0.5
Pb	18	<2	16
Zr	<10	<10	30
Y	14	17	13
Ba	713	1850	4260
Rb	50	48	53
Sr	342	822	834
Nb	11	<10	10
Ba	713	1850	4260
Ta	<1	<1	<1
W	10	17	5
Pt (ppb)	<10	<10	<10
Tl	<1	<1	<1

Sample	87-5-305	87-5-315	87-5-335
REEs (ppm)			
La	31	31	29
Ce	82	90	75
Nd	29.7	29.7	30.4
Sm	4.9	5.2	4.6
Eu	1.8	2.9	4.4
Gd	8.4	8.3	7.3
Dy	5.2	5.1	4.4
Er	2.4	2.3	2.1
Lu	0.3	0.3	0.4

Sample	87-2-46	87-2-50	87-2-186	87-2-194	87-2-200	87-2-210	87-2-220	87-2-240	87-2-272	87-2-282
Major Oxides (wt%)										
SiO2	60	58.2	31.4	25.4	22	20.5	32.9	15.8	41.9	23.6
Al2O3	17.5	18.3	8.86	7.66	5.68	5.12	11.7	5.45	14	7.57
CaO	0.67	0.23	1.54	2.7	2.72	3.25	1.73	3.84	1.64	3.09
MgO	4.12	4.08	4.57	4.33	2.64	2.05	2.72	1.51	2.58	1.48
NaO	1.1	0.85	0.17	0.09	0.01	0.09	1.64	0.25	0.13	<0.01
K2O	3.64	4.74	2.03	0.83	0.61	0.63	1.66	0.6	4	1.53
Fe2O3	7.71	8.19	16	19	26.3	28.8	19.1	31.5	15.9	28.7
MnO	0.19	0.66	14	19.4	17.4	16.3	12.5	20.4	6.8	18
TiO2	0.74	0.78	0.42	0.37	0.27	0.24	0.51	0.26	0.62	0.33
P2O5	0.05	0.07	0.69	1.19	1.2	1.56	0.68	1.66	0.59	1.53
LOI	4.23	4.23	20.2	19.2	21.1	21.7	14.7	18.3	11.6	14.2
SUM	100.1	100.5	100	100.2	100	100.3	100	99.7	99.9	100.1
Trace Metals (ppm)										
Au (ppb)	<1	<1	30	3	2	1	3	14	6	5
Li	50	40	100	90	110	90	80	100	30	30
Be	<5	5	<5	5	5	5	5	10	5	10
B	90	90	70	40	30	30	50	20	80	30
S	120	60	2800	120	840	1900	1400	380	3300	3100
V	140	170	20	40	20	10	30	20	90	30
Cr	120	120	50	44	30	32	64	28	92	40
Co	21	25	84	112	78	74	69	111	107	63
Ni	81	90	61	64	44	42	67	42	88	46
Cu	74	67	60	46	31	31	58	55	110	32
Zn	110	120	75	68	49	47	84	48	110	57
Ga	16	17	14	16	15	14	18	15	17	16
Ge	10	<10	<10	<10	<10	<10	<10	<10	<10	<10
As	<1	2	3	3	9	9	5	3	8	5
Se	<3	<3	<3	<3	<3	<3	<3	<3	<3	<3
Mo	<2	<2	11	12	13	11	8	13	7	12
Pd (ppb)	<2	<2	2	3	3	4	3	5	5	4
Ag	<0.5	<0.5	<0.5	<0.5	<0.5	<0.5	<0.5	<0.5	<0.5	<0.5
Cd	<1	<1	1	<1	<1	<1	<1	<1	<1	<1
In	<1	<1	<1	<1	<1	<1	<1	<1	<1	<1
Sn	<10	<10	<10	<10	<10	<10	<10	<10	<10	<10
Sb	0.2	0.4	3.7	0.9	1.2	1.4	2.2	4	1.6	4
Cs	5	7	5	6	3	3	6	3	6	3
U	1.8	2.1	1.1	1.1	0.8	0.7	1.3	0.8	2.4	1.5
Th	7	8	2	2	0	0	4	0	5	2
Bi	<0.5	<0.5	<0.5	<0.5	<0.5	<0.5	<0.5	<0.5	<0.5	<0.5
Pb	4	16	16	6	<2	2	14	<2	18	8
Zr	13	155	50	31	12	13	63	23	84	20
Y	13	29	<10	<10	<10	<10	<10	<10	<10	<10
Ba	960	957	613	350	444	348	898	1000	1350	891
Rb	164	208	<10	<10	<10	<10	<10	<10	<10	<10
Sr	68	23	182	180	157	163	174	216	132	116
Nb	34	27	<10	19	27	41	18	29	13	24
Ba	960	957	613	350	444	348	898	1000	1350	891
Ta	1	1	<1	<1	<1	<1	<1	<1	<1	<1
W	<3	<3	<3	<3	<3	6	4	9	4	16
Pt (ppb)	<10	<10	<10	<10	<10	<10	<10	<10	<10	<10
Tl	<1	<1	<1	<1	<1	<1	<1	<1	<1	<1

Sample	87-2-46	87-2-50	87-2-186	87-2-194	87-2-200	87-2-210	87-2-220	87-2-240	87-2-272	87-2-282
REEs (ppm)										
La	33	38	23	23	25	23	27	28	39	24
Ce	66	79	62	63	66	66	67	84	110	71
Nd	28.6	34.4	21.5	21.8	23.6	23.1	25.6	28	36.2	23.4
Sm	5	5.8	4.7	4.3	4.5	4.7	5.1	6.1	7.7	4.5
Eu	1	1.2	1	1	1.2	1.2	1.2	1.6	1.7	1.3
Gd	3.9	5.3	4.3	4.4	5.3	5.8	5.4	6.5	7.1	5.1
Dy	3.2	3.6	3.4	3.7	4.5	5	4.5	5.4	5.2	4.4
Er	2	2.1	2.1	2.1	2.5	2.6	2.3	2.9	3.2	2
Lu	0.3	0.4	0.3	0.3	0.3	0.3	0.3	0.4	0.5	0.3

Sample	87-2-292	87-2-306	87-2-344	87-3-20	87-3-32	87-3-42	87-3-62	87-3-82	87-3-92	87-3-127
Major Oxides (wt%)										
SiO2	15.9	34.6	33.7	24.3	30.7	45.8	38.8	22.9	12.9	21.2
Al2O3	4.38	9.11	9.77	7.55	10.6	15	12.5	5.42	3.87	5.92
CaO	4.56	2.66	1.94	2.39	2.07	0.99	1.39	2.63	4.04	3.74
MgO	1.1	1.77	3.35	2.69	2.96	2.68	2.54	1.64	1.3	1.17
NaO	0.06	0.23	0.35	0.24	1.34	3.22	2.03	0.41	0.22	0.5
K2O	0.73	2.44	1.12	2.15	1.71	1.92	1.63	0.65	0.48	1.36
Fe2O3	38.9	21.6	23	23.3	19.4	12.2	17.2	26.4	31.5	32.6
MnO	16.5	11.1	13.5	14.8	14.2	8.36	11.1	18.5	22.2	14.9
TiO2	0.21	0.38	0.41	0.34	0.48	0.61	0.55	0.22	0.2	0.26
P2O5	1.74	1.09	0.91	1.18	0.81	0.29	0.49	1.1	1.65	1.69
LOI	16.1	15.1	12.1	21.2	15.5	7.7	11.3	20.2	21.3	16.9
SUM	100.3	100.2	100.3	100.2	99.9	98.9	99.7	100.1	99.7	100.3
Trace Metals (ppm)										
Au (ppb)	<1	6	<1	2	3	2	3	2	<1	3
Li	50	<10	30	60	140	60	80	50	20	40
Be	10	5	5	5	5	5	5	5	5	10
B	30	70	30	80	70	50	50	30	30	50
S	340	4900	4300	1100	1800	540	2000	520	380	1100
V	20	40	40	30	30	50	50	20	10	30
Cr	20	52	40	51	68	94	82	26	24	36
Co	96	63	97	99	94	77	105	204	173	126
Ni	46	46	58	59	70	87	83	44	33	45
Cu	6	36	68	50	30	81	54	30	20	11
Zn	46	50	75	58	74	110	96	51	40	54
Ga	11	13	16	19	24	27	28	27	29	25
Ge	<10	<10	<10	<10	<10	<10	<10	<10	<10	<10
As	9	5	9	9	8	1	10	12	8	9
Se	<3	<3	<3	<3	<3	<3	<3	<3	<3	<3
Mo	10	7	8	6	19	4	5	9	10	14
Pd (ppb)	2	4	<2	2	<2	2	<2	2	2	6
Ag	<0.5	<0.5	<0.5	<0.5	<0.5	<0.5	<0.5	<0.5	<0.5	<0.5
Cd	<1	<1	<1	2	1	1	1	1	2	2
In	<1	<1	<1	<1	<1	<1	<1	<1	<1	<1
Sn	<10	<10	<10	<10	<10	<10	<10	<10	<10	<10
Sb	3.9	2.8	2.2	2.1	2.5	1	1	1	2.5	3
Cs	2	4	13	5	7	8	5	3	2	4
U	0.7	1.2	1.9	1.2	1.8	2.1	1.9	1	0.7	1.1
Th	0	2	3	5	7	11	8	3	3	3
Bi	<0.5	<0.5	<0.5	0.6	6.4	0.5	3.7	<0.5	<0.5	0.6
Pb	<2	4	14	<2	16	20	26	8	<2	2
Zr	<10	34	61	44	48	100	64	11	<10	11
Y	<10	<10	17	11	16	17	22	<10	12	<10
Ba	1600	1160	695	616	1230	752	770	399	526	616
Rb	<10	<10	18	101	57	79	78	38	26	63
Sr	245	233	361	134	152	146	144	128	188	161
Nb	<10	35	25	17	22	17	10	21	17	15
Ba	1600	1160	695	616	1230	752	770	399	526	616
Ta	<1	<1	<1	<1	<1	<1	<1	<1	<1	<1
W	15	5	3	4	5	4	4	<3	8	7
Pt (ppb)	<10	<10	<10	<10	<10	<10	<10	10	10	10
Tl	<1	<1	<1	<1	<1	<1	<1	<1	<1	<1

238

Sample	87-2-292	87-2-306	87-2-344	87-3-20	87-3-32	87-3-42	87-3-62	87-3-82	87-3-92	87-3-127
REEs (ppm)										
La	<2	22	29	26	27	36	30	22	24	27
Ce	0	63	75	70	69	86	73	60	70	77
Nd	<0.5	22.2	27.6	26.4	25.3	33.5	29.7	20.6	22.8	27.7
Sm	<0.5	4.1	5.1	6.4	4.8	7	5.1	3.8	4.8	5.6
Eu	0	1.2	1.2	1.4	1	1.2	1.2	1.1	1.3	1.1
Gd	<0.5	4.9	5.6	5.5	5.1	5.2	5.3	4.8	5.9	6.3
Dy	<0.5	3.8	4.5	5	3.8	4.2	4.2	4.2	4.2	4.7
Er	<0.5	1.9	2.1	2.4	2	2	2	2.2	2	2.3
Lu	<0.1	0.2	0.3	0.3	0.3	0.4	0.4	0.3	0.3	0.3

Sample	87-3-462	87-3-492	87-3-622	87-4-17	87-4-21	87-4-50	87-4-70	87-4-90	87-4-110	87-4-112
Major Oxides (wt%)										
SiO2	54.2	52.7	45.2	38.8	47	30.6	22.9	37.3	9.94	19.3
Al2O3	19.8	18.8	14.2	12.4	17.5	9.82	6.26	12.1	2.72	5.06
CaO	0.35	0.41	12.2	1.32	0.4	2.26	3.09	1.41	3.8	3.57
MgO	2.82	2.8	2.86	2.75	3.38	2.11	1.79	3.18	1.58	1.41
NaO	1.13	0.94	1.28	2.02	4.15	1.12	0.56	1.28	0.39	0.47
K2O	5.32	5.03	3.43	3.25	2.78	1.54	1.41	1.77	0.6	0.47
Fe2O3	9.68	10.6	6.25	18	10.3	23.1	27.1	19.7	25.9	32.1
MnO	0.49	1.74	0.34	9.17	5.6	14.4	15.7	10.5	27.9	19.9
TiO2	0.76	0.74	0.66	0.53	0.76	0.44	0.27	0.5	0.14	0.23
P2O5	0.11	0.12	0.11	0.64	0.15	1.04	1.41	0.61	1.24	1.61
LOI	4.31	5.16	13.1	10.8	6.47	13.8	19.8	11.8	25.6	16.2
SUM	99.1	99.2	99.8	99.8	98.7	100.3	100.4	100.3	99.9	100.4
Trace Metals (ppm)										
Au (ppb)	3	<1	4	<1	<1	3	5	3	2	1
Li	50	60	50	30	30	30	50	60	20	20
Be	<5	<5	<5	5	<5	5	5	5	5	10
B	100	80	50	70	50	50	60	50	20	90
S	1800	4400	20	80	180	1300	3500	3900	780	900
V	170	160	90	30	40	30	20	30	<10	20
Cr	94	96	100	80	96	60	36	66	16	28
Co	47	48	24	57	60	109	111	71	152	136
Ni	71	69	69	76	94	76	60	76	48	45
Cu	83	79	18	24	47	130	44	77	15	28
Zn	120	120	80	93	98	83	62	96	36	48
Ga	25	26	18	20	20	20	18	21	22	20
Ge	<10	<10	<10	<10	<10	<10	<10	<10	<10	<10
As	27	28	2	1	<1	10	10	5	5	13
Se	<3	<3	<3	<3	<3	<3	<3	<3	<3	<3
Mo	<2	<2	<2	6	4	11	16	12	20	15
Pd (ppb)	3	4	<2	<2	3	<2	3	3	<2	<2
Ag	<0.5	<0.5	<0.5	<0.5	<0.5	<0.5	<0.5	<0.5	<0.5	<0.5
Cd	<1	<1	<1	<1	<1	<1	<1	<1	<1	<1
In	<1	<1	<1	<1	<1	<1	<1	<1	<1	<1
Sn	<10	<10	<10	<10	<10	<10	<10	<10	<10	<10
Sb	0.8	1.1	0.2	1.9	0.8	1.9	1.9	0.8	0.8	2.9
Cs	10	9	4	8	7	7	5	5	1	13
U	3.3	3	1.6	1.8	2.2	1.8	1.2	2.2	0.6	1
Th	14	12	9	8	12	7	4	8	3	3
Bi	0.8	0.6	<0.5	<0.5	<0.5	<0.5	<0.5	<0.5	<0.5	<0.5
Pb	22	18	10	<2	38	8	12	14	4	6
Zr	127	117	99	76	115	48	<10	69	<10	<10
Y	23	37	18	32	11	12	17	24	<10	19
Ba	1000	895	494	1020	1800	646	465	594	295	596
Rb	207	196	138	121	108	71	57	62	19	14
Sr	53	49	559	212	224	158	160	128	159	228
Nb	27	17	25	14	14	15	<10	18	<10	35
Ba	1000	895	494	1020	1800	646	465	594	295	596
Ta	1	1	<1	1	1	<1	<1	<1	<1	<1
W	<3	<3	<3	4	4	5	4	<3	<3	4
Pt (ppb)	<10	<10	<10	<10	<10	<10	<10	<10	<10	<10
Tl	<1	<1	<1	<1	<1	<1	<1	<1	<1	<1

Sample	87-3-462	87-3-492	87-3-622	87-4-17	87-4-21	87-4-50	87-4-70	87-4-90	87-4-110	87-4-112
REEs (ppm)										
La	41	38	33	29	38	29	24	33	19	27
Ce	93	86	64	76	83	77	68	83	54	77
Nd	39.9	36.8	29.7	31.4	33.1	28.9	23.7	33	18.4	26.1
Sm	7.2	5.5	4.8	5.7	5	4.9	4.7	6.4	3.3	5
Eu	1.4	1.5	1.5	2	1.8	1.6	1.5	1.8	1	1.5
Gd	5.2	5.3	4.4	6.9	5.8	6.5	7	7.7	5.1	7.5
Dy	4.3	4	3.8	5.2	3.8	4.8	4.8	5.2	3.8	4.8
Er	2.1	2	1.7	2.4	1.9	2.2	2	2.5	2.1	2.3
Lu	0.5	0.4	0.4	0.4	0.5	0.4	0.3	0.5	0.3	0.4

Sample	87-4-130	87-4-150	87-4-170	87-4-182	87-4-195	87-4-206	87-4-220	87-4-231	87-4-246	87-4-261
Major Oxides (wt%)										
SiO2	17.8	25.9	39	28.6	34.8	20.8	21.4	33	30.1	32.6
Al2O3	5.63	6.31	13.5	7.19	12.8	4.85	5.95	10.2	9.42	10.5
CaO	4.31	3.45	1.29	3.37	1.78	3.53	3.69	2.19	2.31	1.97
MgO	1.44	1.36	2.62	1.64	2.58	1.42	1.41	1.96	1.94	2.33
NaO	0.33	0.63	1.45	1	1.22	0.46	0.39	1.25	1.08	0.85
K2O	0.33	0.68	2.77	1.31	2.79	0.47	0.6	2	2.27	1.75
Fe2O3	30.7	31	16.8	32.3	21.4	30	34.4	25.3	20.5	30.1
MnO	20.3	16.3	11.7	14.2	11.6	22.1	17.6	13.7	19.1	10.1
TiO2	0.25	0.25	0.6	0.31	0.55	0.22	0.27	0.45	0.43	0.47
P2O5	1.64	1.79	0.52	1.52	0.76	1.52	1.81	1.07	0.81	1.24
LOI	17.2	12	9.23	8.7	8.77	14.2	12.5	8.7	10.7	8
SUM	100	99.8	99.7	100.4	99.4	99.7	100.1	100	99.1	100.1
Trace Metals (ppm)										
Au (ppb)	<1	<2	<1	2	5	3	<1	<2	<1	6
Li	30	<10	50	20	40	10	20	10	30	50
Be	5	5	5	5	5	5	10	5	5	5
B	90	90	60	70	70	100	160	90	120	120
S	140	2100	520	580	620	1600	2400	1000	480	4400
V	20	20	30	30	40	20	20	30	10	50
Cr	34	38	82	44	70	32	38	60	56	62
Co	139	102	94	117	104	127	97	154	136	151
Ni	45	51	90	55	81	50	56	74	88	72
Cu	54	42	53	18	65	41	37	66	38	120
Zn	55	61	100	66	96	52	59	89	81	90
Ga	20	20	24	19	24	24	22	22	27	20
Ge	<10	<10	<10	<10	<10	<10	<10	<10	<10	<10
As	13	13	10	12	10	10	15	10	5	20
Se	<3	<3	<3	<3	<3	<3	<3	<3	<3	<3
Mo	14	12	12	10	9	18	11	16	15	10
Pd (ppb)	<2	2	<2	<2	<2	<2	3	3	<2	3
Ag	<0.5	<0.5	<0.5	<0.5	<0.5	<0.5	<0.5	<0.5	<0.5	<0.5
Cd	<1	<1	<1	<1	<1	<1	<1	<1	<1	<1
In	<1	<1	<1	<1	<1	<1	<1	<1	<1	<1
Sn	<10	<10	<10	<10	<10	<10	<10	<10	<10	<10
Sb	2.2	2.3	1.9	2	0.9	1.9	2.9	1.9	1.9	1.9
Cs	6	27	23	48	28	29	32	17	32	28
U	1.5	1.1	2.1	1.6	2.6	1.1	1.8	1.4	2.7	2
Th	4	4	10	5	9	3	6	3	6	7
Bi	<0.5	<0.5	<0.5	<0.5	<0.5	<0.5	<0.5	<0.5	<0.5	<0.5
Pb	<2	<2	10	4	22	16	<2	16	4	10
Zr	13	<10	75	11	79	<10	13	40	31	55
Y	24	15	<10	16	12	<10	19	24	<10	20
Ba	283	723	1170	1510	2670	870	313	965	3500	1060
Rb	13	28	103	68	103	61	44	81	72	83
Sr	229	367	260	491	320	341	175	207	250	227
Nb	27	35	28	21	<10	21	22	17	<10	11
Ba	283	723	1170	1510	2670	870	313	965	3500	1060
Ta	<1	<1	1	<1		<1	<1	<1	<1	<1
W	5	<3	5	6	5	3	4	5	5	5
Pt (ppb)	10	<10	<10	<10	<10	<10	<10	<10	<10	<10
Tl	<1	<1	<1	<1	<1	<1	<1	<1	<1	<1

Sample	87-4-130	87-4-150	87-4-170	87-4-182	87-4-195	87-4-206	87-4-220	87-4-231	87-4-246	87-4-261
REEs (ppm)										
La	29	33	35	29	34	24	31	30	27	43
Ce	85	90	87	76	87	66	82	85	73	113
Nd	29.5	29.6	32.9	29.3	31.3	22.4	29.8	30.6	26.4	40.9
Sm	5.9	5.3	5.5	6.1	6.4	4.7	5.6	6.1	4.7	6.8
Eu	1.4	1.9	2	2.3	2.5	1.6	2	1.7	2.8	2.4
Gd	6.2	8.1	7.5	7	7.5	6.6	7.6	8.1	5.8	10.1
Dy	5.4	6.1	5.3	5.5	5.1	4.6	5.4	5.8	4.3	6.5
Er	2.5	2.9	2.5	3.1	3.1	2.4	2.9	2.8	1.9	2.8
Lu	0.4	0.5	0.5	0.5	0.4	0.4	0.5	0.5	0.5	0.4

Sample	87-4-268	87-4-280	87-4-300	87-4-320	87-4-330	87-4-350	87-4-360	87-4-370	87-4-390	87-4-410
Major Oxides (wt%)										
SiO2	24.7	51.2	48.9	54.9	52.5	52.3	47.2	30.2	29.5	19
Al2O3	6.85	17.9	16.1	19.4	17.9	17.5	15.4	9.3	9.01	6.36
CaO	2.86	0.32	0.85	0.21	0.38	0.37	0.74	2.37	2.5	3.88
MgO	1.69	3	2.94	2.59	2.78	2.79	3.34	4.13	3.68	1.73
NaO	0.48	2.17	1.35	1.28	1.31	1.67	1.89	0.74	1.2	0.79
K2O	0.81	3.75	3.55	5.07	4.19	3.97	2.58	0.72	0.61	0.76
Fe2O3	31.6	12	12	9.94	11.7	11.6	14.7	22.2	23.5	27.4
MnO	17.8	2.89	5.99	1.52	3.2	2.92	5.19	15	15.4	18.7
TiO2	0.33	0.74	0.63	0.73	0.71	0.7	0.65	0.4	0.39	0.29
P2O5	1.46	0.17	0.35	0.11	0.2	0.21	0.37	0.91	0.97	1.36
LOI	11.5	4.85	6.93	4.31	5.16	5.16	6.85	14.4	13.5	19.9
SUM	100.2	99.1	99.7	100.2	100.2	99.3	99	100.4	100.4	100.2
Trace Metals (ppm)										
Au (ppb)	<1	<1	4	3	2	1	4	2	1	7
Li	40	50	60	60	50	40	50	30	10	20
Be	5	5	<5	<5	<5	<5	<5	<5	<5	5
B	140	60	60	80	80	60	40	20	<10	10
S	680	760	2300	900	1100	2600	7200	1900	560	800
V	30	110	70	150	100	120	90	30	20	10
Cr	40	92	76	100	94	94	92	50	50	34
Co	117	51	66	48	49	62	101	115	123	136
Ni	53	75	70	76	77	78	90	64	68	49
Cu	51	94	84	110	78	120	94	56	59	36
Zn	63	120	110	130	130	130	120	81	82	64
Ga	21	22	21	23	24	25	24	24	23	22
Ge	<10	<10	<10	<10	<10	<10	<10	<10	<10	<10
As	10	9	10	5	5	8	22	8	8	11
Se	<3	<3	<3	<3	<3	<3	<3	<3	<3	<3
Mo	11	2	4	<2	2	10	8	11	9	11
Pd (ppb)	3	2	3	<2	2	<2	2	2	2	2
Ag	<0.5	<0.5	<0.5	<0.5	<0.5	<0.5	<0.5	<0.5	<0.5	<0.5
Cd	<1	<1	<1	<1	<1	<1	<1	<1	<1	<1
In	<1	<1	<1	<1	<1	<1	<1	<1	<1	<1
Sn	<10	<10	<10	<10	<10	<10	<10	<10	<10	<10
Sb	1.9	0.7	1.7	0.5	0.7	0.7	4.2	1.9	0.7	0.7
Cs	29	7	7	11	8	8	6	4	11	2
U	1.2	2.6	2.8	2.8	2.3	3.2	2.8	1.7	1.5	1
Th	4	12	11	12	11	11	10	6	5	4
Bi	<0.5	<0.5	<0.5	0.6	1.3	<0.5	<0.5	<0.5	<0.5	<0.5
Pb	<2	12	22	38	16	20	24	10	<2	<2
Zr	21	110	99	126	122	113	77	33	29	18
Y	18	32	24	13	29	21	22	15	15	<10
Ba	528	894	645	769	692	715	557	350	565	304
Rb	47	142	134	206	158	156	110	25	40	40
Sr	190	73	118	48	62	37	106	149	140	221
Nb	21	40	12	<10	27	26	11	22	23	25
Ba	528	894	645	769	692	715	557	350	565	304
Ta	<1	1	1	1	1	1	1	<1	<1	<1
W	5	<3	<3	<3	4	4	<3	3	4	5
Pt (ppb)	10	10	<10	<10	<10	<10	<10	<10	<10	<10
Tl	<1	<1	<1	<1	<1	<1	<1	<1	<1	<1

Sample	87-4-268	87-4-280	87-4-300	87-4-320	87-4-330	87-4-350	87-4-360	87-4-370	87-4-390	87-4-410
REEs (ppm)										
La	30	42	35	41	36	36	37	27	27	30
Ce	85	98	84	95	83	84	85	73	71	80
Nd	30.6	38.9	36	40	34.5	36.4	35.6	28.1	26.5	29.5
Sm	5.4	6.4	6.6	6.7	6	6.4	5.9	6.1	4.8	5.2
Eu	1.7	2	1.8	2	1.8	1.5	1.6	1.4	1.6	1.7
Gd	7.6	7.8	5.2	7.3	6.8	7	7.2	6.8	6.4	7.2
Dy	5.3	4.4	4.7	4.3	4.5	3.9	4.7	4.9	4.5	5.1
Er	2.7	2.3	2	1.9	2.1	2.2	2.3	3.3	2.4	2
Lu	0.6	0.4	0.4	0.4	0.3	0.4	0.5	0.4	0.5	0.4

Sample	87-4-420	87-4-440	87-4-470	87-4-480	87-4-503	87-4-520	87-4-539	87-4-580	87-4-600	87-4-611
Major Oxides (wt%)										
SiO2	26.7	38.3	37.6	43.3	34.9	35.9	43.4	31	36.3	37.7
Al2O3	8.11	12.3	11.5	14.4	10.1	10.9	15	10.3	10.5	12.3
CaO	3.41	1.34	1.97	0.91	2.93	1.74	0.95	2.47	1.72	1.4
MgO	1.89	2.34	2.25	2.6	2.01	2.2	4.02	3.39	1.98	2.25
NaO	1.17	2.42	2.14	3.01	2.29	2.36	1.41	1.09	1.99	2.27
K2O	1.57	2.34	3.15	2.79	2.01	2.35	2.94	1.01	2.06	2.63
Fe2O3	28.1	18	19.5	16.1	20.9	22.6	16.6	26.1	24.8	16.6
MnO	15.9	12.6	12.4	9.47	15.3	13.7	7.4	13.9	11.6	13.9
TiO2	0.36	0.54	0.57	0.62	0.52	0.48	0.61	0.42	0.45	0.53
P2O5	1.28	0.64	0.9	0.49	0.96	0.79	0.56	1.13	1	0.64
LOI	11.2	8.54	7	5.23	6.08	5.85	6.62	9.08	7.31	9.16
SUM	99.9	99.6	99.9	99.2	99	99.2	99.6	100	100	99.6
Trace Metals (ppm)										
Au (ppb)	1	3	1	<1	<1	<1	7	2	<1	5
Li	<10	20	30	40	<10	10	50	30	30	20
Be	5	<5	5	<5	<5	5	5	5	5	5
B	90	70	90	70	130	110	50	80	60	80
S	880	1300	1100	1100	1500	500	760	840	1600	140
V	20	30	30	50	20	20	60	30	30	30
Cr	52	70	65	82	62	62	72	46	56	66
Co	120	110	92	120	111	130	82	143	106	93
Ni	62	83	75	93	87	73	78	64	74	86
Cu	50	74	34	87	42	14	73	63	59	42
Zn	79	97	90	110	88	85	120	83	76	91
Ga	23	25	24	25	23	24	21	21	20	21
Ge	<10	<10	<10	<10	<10	<10	<10	<10	<10	<10
As	8	7	5	5	6	6	6	15	11	6
Se	<3	<3	<3	<3	<3	<3	<3	<3	<3	<3
Mo	10	8	9	6	9	9	4	14	8	6
Pd (ppb)	2	2	2	2	<2	2	2	<2	5	<2
Ag	<0.5	<0.5	<0.5	<0.5	<0.5	<0.5	<0.5	<0.5	<0.5	<0.5
Cd	<1	<1	<1	<1	<1	<1	<1	<1	<1	<1
In	<1	<1	<1	<1	<1	<1	<1	<1	<1	<1
Sn	<10	<10	<10	<10	<10	<10	<10	<10	<10	<10
Sb	3.2	1.9	1.7	0.7	1.9	1.9	0.5	0.7	1.1	1.8
Cs	20	21	40	24	20	28	16	17	35	30
U	1.2	1.7	1.5	2.2	1.1	1.5	2.1	1.8	1.6	1.6
Th	5	7	8	9	5	6	9	6	6	8
Bi	<0.5	<0.5	<0.5	<0.5	<0.5	<0.5	<0.5	<0.5	<0.5	<0.5
Pb	10	10	18	20	4	4	10	10	22	4
Zr	47	68	50	90	19	56	88	55	44	66
Y	16	28	24	15	23	<10	30	12	29	14
Ba	1150	1930	7600	1760	7700	2620	666	674	1970	1730
Rb	73	79	122	113	66	103	122	61	81	109
Sr	224	240	577	335	892	385	149	156	162	187
Nb	<10	21	<10	32	27	31	28	26	26	<10
Ba	1150	1930	7600	1760	7700	2620	666	674	1970	1730
Ta	<1	<1	<1	1	<1	<1	1	<1	<1	<1
W	<3	4	5	<3	3	4	3	5	4	4
Pt (ppb)	<10	<10	<10	<10	<10	<10	<10	<10	10	<10
Tl	<1	<1	<1	<1	<1	<1	<1	<1	<1	<1

Sample	87-4-420	87-4-440	87-4-470	87-4-480	87-4-503	87-4-520	87-4-539	87-4-580	87-4-600	87-4-611
REEs (ppm)										
La	29	31	32	38	28	27	36	34	30	31
Ce	81	79	80	94	70	68	89	88	78	76
Nd	27.8	29.5	28.9	36.5	25.1	26.6	36.5	35.1	29.5	31.1
Sm	5.7	5.4	5.3	5.5	3.9	5.3	6.8	6.7	5.2	5.2
Eu	2	2.3	5.5	2.4	4.3	2.3	1.8	1.9	2.3	1.5
Gd	6.8	6.2	6.7	7.1	5.5	5.9	8.7	8.2	6.7	5
Dy	4.9	4.5	4.8	5.7	3.5	4.2	5.3	5.8	5	4.6
Er	2.9	2.4	2.6	2.3	2.1	2.5	3.5	3.1	2.9	2.1
Lu	0.5	0.5	0.4	0.5	0.5	0.3	0.5	0.5	0.5	0.4

Sample	87-5-10	87-5-20	87-5-30	87-5-40	87-5-50	87-5-60	87-5-87	87-5-95	87-5-356	87-5-370
Major Oxides (wt%)										
SiO2	25.3	18.3	31.2	31	32	27.5	24.4	31	33.5	49
Al2O3	7.24	5.08	10.7	9.56	10.7	7.88	8.64	10	10.6	17
CaO	2.38	2.88	2.09	1.54	1.73	2.3	2.3	2.08	2.05	0.82
MgO	1.95	1.65	2.06	2.09	3.64	3.99	4.24	2.87	4.06	2.93
NaO	0.64	0.45	1.72	1	1.02	0.26	0.54	1.18	0.97	1.39
K2O	0.48	0.76	1.83	1.83	1.46	1.44	0.68	1.08	1.24	4.07
Fe2O3	26	30.5	20.7	21.7	19.8	22.6	25	25	19.8	12.6
MnO	17	16.8	12.7	13.2	14.3	12.4	15.2	11.6	14.3	4.29
TiO2	0.33	0.23	0.47	0.42	0.45	0.34	0.38	0.42	0.44	0.66
P2O5	1.16	1.51	0.96	0.72	0.81	1.05	1.19	0.99	0.79	0.31
LOI	17	21.4	15.9	16.7	14.4	20.2	16.8	14	12.1	6.08
SUM	99.9	99.8	100.4	99.8	100.4	100	99.4	100.3	99.9	99.3
Trace Metals (ppm)										
Au (ppb)	<1	1	2	<1	1	3	8	6	<1	<1
Li	70	100	80	60	60	230	80	30	40	50
Be	5	5	5	5	5	<5	<5	5	5	5
B	20	40	80	70	50	110	30	10	30	70
S	360	1600	3100	1100	1300	1600	4250	4000	3800	940
V	30	20	50	40	40	40	40	50	40	90
Cr	38	24	62	50	52	34	42	50	48	76
Co	111	136	96	131	85	117	141	129	163	57
Ni	53	40	78	51	62	53	53	58	60	62
Cu	52	37	94	45	55	53	56	61	90	72
Zn	62	47	87	74	88	76	75	83	98	120
Ga	14	15	21	19	21	19	26	21	28	27
Ge	<10	<10	<10	<10	<10	<10	<10	<10	<10	<10
As	10	20	13	13	6	12	18	21	9	2
Se	<3	<3	<3	<3	<3	<3	<3	<3	<3	<3
Mo	8	10	8	11	13	19	13	9	13	3
Pd (ppb)	<2	3	2	<2	<2	2	3	3	<2	<2
Ag	<0.5	<0.5	<0.5	<0.5	<0.5	<0.5	<0.5	<0.5	<0.5	<0.5
Cd	<1	<1	<1	<1	<1	<1	<1	<1	<1	<1
In	<1	<1	<1	<1	<1	<1	<1	<1	<1	<1
Sn	<10	<10	<10	<10	<10	<10	<10	<10	<10	<10
Sb	0.7	0.7	1.9	0.8	0.7	0.8	1.3	0.8	2.2	1.5
Cs	2	2	5	5	5	10	5	4	8	11
U	1.4	1.4	2	7	3.8	2	2.4	2.3	2.7	2.4
Th	5	3	7	6	6	5	6	6	7	10
Bi	<0.5	<0.5	<0.5	<0.5	<0.5	<0.5	<0.5	<0.5	0.5	<0.5
Pb	4	4	16	<2	12	12	10	12	16	14
Zr	17	<10	60	45	62	25	38	54	43	99
Y	13	<10	24	16	21	<10	19	20	15	18
Ba	309	322	448	455	359	252	212	388	479	751
Rb	33	52	84	68	41	49	33	52	47	162
Sr	146	189	200	110	120	294	122	122	158	92
Nb	26	13	25	19	29	33	29	23	19	17
Ba	309	322	448	455	359	252	212	388	479	751
Ta	<1	<1	<1	<1	<1	<1	<1	<1	<1	1
W	<3	4	4	4	4	<3	4	4	3	<3
Pt (ppb)	<10	10	<10	<10	<10	10	10	<10	<10	<10
Tl	<1	<1	<1	<1	<1	<1	<1	<1	<1	<1

Sample	87-5-10	87-5-20	87-5-30	87-5-40	87-5-50	87-5-60	87-5-87	87-5-95	87-5-356	87-5-370
REEs (ppm)										
La	25	26	33	27	29	27	38	33	31	41
Ce	67	74	89	69	72	71	99	84	80	97
Nd	24.4	25.9	35.5	26.3	27.8	28.7	22.1	21.9	31.3	40.6
Sm	4.3	5.1	6.7	4.2	5.6	5.3	7.3	5.9	5.1	6.2
Eu	1.2	1.5	1.8	1.4	1.4	1.5	2	1.5	1.7	2.1
Gd	5.6	7.9	8.6	5.5	7.4	7.3	10.2	8.8	8.3	9.4
Dy	3.6	5	5.6	3.9	4.6	5	6.1	5.2	4.7	4.9
Er	2	2.2	2.7	2	2.3	2.6	3	2.8	1.8	2
Lu	0.3	0.4	0.5	0.4	0.4	0.4	0.5	0.4	0.3	0.4

Sample	87-5-390	87-5-410	87-5-430
Major Oxides (wt%)			
SiO2	51.3	47.1	45.3
Al2O3	17.4	16.1	15.4
CaO	0.55	0.9	1.64
MgO	3.01	3.14	2.57
NaO	1.43	0.99	0.89
K2O	4.01	3.79	3.81
Fe2O3	12.5	13.3	11.5
MnO	2.95	5.55	7.98
TiO2	0.68	0.64	0.59
P2O5	0.24	0.31	0.39
LOI	5.31	7.47	9
SUM	99.5	99.4	99.2
Trace Metals (ppm)			
Au (ppb)	<1	1	8
Li	60	50	30
Be	5	5	5
B	60	70	80
S	3300	3500	180
V	110	90	60
Cr	90	80	68
Co	66	90	46
Ni	71	67	63
Cu	80	100	55
Zn	130	130	120
Ga	24	24	23
Ge	<10	<10	<10
As	10	9	1
Se	<3	<3	<3
Mo	3	5	5
Pd (ppb)	<2	3	<3
Ag	<0.5	<0.5	<0.5
Cd	<1	<1	<1
In	<1	<1	<1
Sn	<10	<10	<10
Sb	1.8	0.8	0.6
Cs	9	9	8
U	2.8	2.7	2
Th	10	10	9
Bi	0.5	<0.5	<0.5
Pb	22	34	12
Zr	91	91	55
Y	28	<10	19
Ba	744	653	609
Rb	168	142	140
Sr	80	90	189
Nb	<10	24	19
Ba	744	653	609
Ta	1	1	<1
W	<3	<3	<3
Pt (ppb)	<10	<10	<10
Tl	<1	<1	<1

Sample	87-5-390	87-5-410	87-5-430
REEs (ppm)			
La	36	36	35
Ce	87	83	81
Nd	35.5	32.7	33.5
Sm	6.9	6.1	5.3
Eu	1.7	1.6	1.6
Gd	7.8	7.6	7.3
Dy	3.8	3.9	3.9
Er	2.3	2.3	1.5
Lu	0.4	0.3	0.3

Trench 1

DDH 87-2

Calcareous Blue-Gray Slate Siltstone

Gray-Green Siltstone

Interbedded Brick-red to Maroon-red siltstone

Highly Altered Sericitzed Chloritic Gray-Green Siltstone
Gray-Green Siltstone with Minor Interbedded Brick-Red Siltstone
Interbedded Gray-Green and Maroon-Red Siltstone
Maroon-Red Siltstone
Interbedded Gray-Green and Maroon-Red Siltstone (quartz and chlorite alteration present)
Interbedded Maroon-Red and green chloritic Siltstone minor sulfides present
Sericite Maroon-Red siltstone with abundant pyrite
Green-Black Siltstone
Green-Black Blue Siltstone with Minor Interbedded Maroon-Red Siltstone
Maroon-Red Blue Siltstone with minor quartz and pyrite

- 1.5 m
- 14 m
- 17.1 m
- 56.7 m
- 67.1 m
- 70.1 m
- 71.3 m
- 73.2 m
- 79.3 m
- 98.8 m
- 103.6 m
- 108.5 m
- 111.3 m

252

DDH 87-3

Highly Altered Interbedded Maroon-red & Gray-Green Slate Sericite-rich

Maroon-Red Siltstone
Gray-Green Siltstone
Gray-Green Siltstone
Interbedded Brick-red and Maroon-red siltstone
Interbedded Maroon-red and Black siltstone
Maroon-Red Siltstone
Hematitic Iron Formation
Hematitic Iron Formation
Interbedded Maroon-Red & Black Siltstone
Red Siltstone with potassic silic alteration
Dark Green to Black Siltstone
Altered Red Siltstone
Green-Black Siltstone with sericite alteration
Interbedded Maroon-Red & Black Siltstone
Red Siltstone with potassic silic alteration (?)
Red Siltstone with pyrite, possibly silted. The Red Siltstone with potassic silic alteration
Interbedded Maroon-Red & Black Siltstone Faulting present
Gray-Green Siltstone
Green-Black Siltstone
Gray-Green Siltstone
Green-Black Siltstone
Pyritic Green-Black Siltstone
Gray-Green Siltstone
Green-Black Siltstone
Gray-Green Siltstone (calcareous)

- 6.1 m
- 28 m
- 38.7 m
- 53 m
- 95.1 m
- 102.4 m
- 140.2 m
- 149.4 m
- 179.2 m
- 182.9 m
- 193.6 m

Trench 2

DDH 87-4

Maroon-Red Siltstone
Gray-Green and minor Red Siltstone
Maroon-Red Siltstone
Green Siltstone with minor Red Siltstone
Tan Siltstone with potassic-silic alteration
Interbedded Brick-Red and Maroon-Red Siltstone
Red Siltstone
Interbedded Gray-Green and Maroon-Red Siltstone
Interbedded brown-red and green-black Siltstone
Interbedded green-black and red siltstone
Interbedded red and minor red-black Siltstone
Interbedded green-black and red black Siltstone
Interbedded gray-green and Maroon-red Siltstone
Gray-green with minor Maroon-red Siltstone
Maroon-red and brick-red siltstone
Interbedded Maroon-red and black Siltstone
Interbedded Gray-green and Maroon-red Siltstone

- 0.3 m
- 13 m
- 137.2 m
- 140.2 m
- 153.3 m
- 167.6 m
- 174 m
- 192.6 m

DDH 87-5

Interbedded Gray-Green and Minor Red Siltstone, with heavy chloritic and potassic silic alteration with minor sulfide
Heavymetamorphic silic alteration with up to 5% sulfide
Clinified fault breccia with clasts of sericitized siltstone and quartz veins
Red Siltstone with minor fault-hosted breccia
Interbedded Gray-green and Red Siltstone with potassic-silic- and chloritic alteration with half quartz chlorite fracture fills
Interbedded Maroon-red and Brick-Red Siltstone with minor Gray-green Siltstone 5% sulfide in potassic altered sections
Fault Zone with brecciated red and green siltstone fragments
Band of green and red siltstone with secondary bismuth and possibly galena
Gray-green siltstone with minor red siltstone beds
Brecciated siltstone with quartz, chlorite, and minor carbonates
Chlorite filled slickensided fault
Interbedded Green, Gray-Green and Green-Black Siltstone
Interbedded Gray-Green and Brown-Red Siltstone
Fault zone
Interbedded Gray-Green and Green-Black Siltstone

- 3 m
- 21.3 m
- 26.5 m
- 30.5 m
- 32.9 m
- 46 m
- 108 m
- 140 m

Bryan C. Way

10 Frederick St.
Lincoln, ME 04457
USA
Email: bryan.way1@gmail.com

Education

University of New Brunswick	MSc. in Geology
	Expected Graduation: 2012
University of Maine at Farmington	BA. in Geology
Farmington, ME	Graduated: 2007

Publications

- Reusch, D.N., Choquette, J., Hansen, J., Way, B., 2010, Stratigraphic, Structural, and contact relationships of the Rumford outlier near Farmington, Maine. *In* Yates, M. (editor) NEIGC 2010 guidebook, NEIGC, 102nd meeting of the New England Intercollegiate Geological Conference 102nd meeting, p. C3-1 − C3-19.

- Way, B.C., Lentz, D.R., Keighley, D.G. 2009, Origin of the Syngenetic Fe-Mn and late Epigenetic Cu-Fe-S Mineralization, Woodstock, New Brunswick. *In* Merlini, S.A.A., (editor), Abstracts 2009: Exploration, Mining and Petroleum New Brunswick / Résumés 2009: Exploration et exploitation miniére et pétrolieré au Nouveau-Brunswick, New Brunswick Department of Natural Resources; Minerals, Policy and Planning Division, Information Circular 2009-1, p. 41-42. Poster and Oral Presentation.

- Way, B.C., Lentz, D.R., Keighley, D.G., 2009. Stratigraphic and Geochemical interpretation of the Early Silurian Woodstock ferromanganese deposits, New Brunswick, Canada. In: Lentz, D.R., Thorne, K.G., and Beal, K-L., (editors), Proceedings of the 24th IAGS, Fredericton, Canada, 335-338 p. Poster Presentation.

- Way, B.C., Lentz, D.R., Keighley, D.G., 2009. Detailed lithogeochemical analysis of the Plymouth Fe-Mn Deposit, New Brunswick, Canada. In: Lentz, D.R., Thorne, K.G., and Beal, K-L., (editors), Proceedings of the 24th IAGS, Fredericton, Canada. Poster Presentation.

- Way, B.C., Lentz, D.R., Keighley, D.G. 2009. The Early Silurian Woodstock Ferromanganese Deposits, New Brunswick, Canada: A Stratigraphic, Depositional, and Paleoenvironmental Analysis *In* GSA Abstracts with Programs, vol. 41, no. 3, p. 28. Poster Presentation.

- Way, B.C., Lentz, D.R., Keighley, D.G. 2008. Geology and Geochemistry of the Sedimentary Ferromanganese Ore Deposits, Woodstock, New Brunswick, Canada. *In* Merlini, S.A.A., (editor), Abstracts 2008: Exploration, Mining and Petroleum New Brunswick / Résumés 2008: Exploration et exploitation miniére et pétrolieré au Nouveau-Brunswick, New Brunswick Department of Natural Resources; Minerals, Policy and Planning Division, Information Circular 2008-1, p. 71. Poster Presentation.

- Way, B.C., Reusch, D.N. 2007. The Temple Stream Formation, West-Central Maine: Devonian or Silurian? *In* GSA Abstracts with Programs, vol. 39, no. 1, p. 60. Poster Presentation.

- Reusch, D.N., Choquette, J., Gregg, T., O'Brien, W., Powers, J., and Way, B.C. 2007, A Maritime Perspective on Maine's Gander Zone, including a few thoughts on Tectonic-Climate Linkages. GAC-AGC Abstracts. Oral Presentation.